DISSERTATION

LEVERAGING BIO-BASED MONOMERS, CHEMICAL RECYCLABILITY, AND SUSTAINABLE POLYMERIZATION TECHNIQUES FOR SUSTAINABLE POLYMER SYNTHESIS

Submitted by

Simone Noelle Bernsten

Department of Chemistry

In partial fulfillment of the requirements

For the Degree of Doctor of Philosophy

Colorado State University

Fort Collins, Colorado

Summer 2024

Doctoral Committee:

Advisor: Garret Miyake

Andy McNally
Melissa Reynolds
Brad Reisfeld

ABSTRACT

LEVERAGING BIO-BASED MONOMERS, CHEMICAL RECYCLABILITY, AND SUSTAINABLE POLYMERIZATION TECHNIQUES FOR SUSTAINABLE POLYMER SYNTHESIS

Polymeric materials have become vital to everyday life since their commercialization. Although polymers are integral to many industries and consumers, their synthesis and use brings with them a myriad of environmental concerns. Unsustainability can arise even before polymer synthesis in that many synthetic polymers are made from petroleum-derived monomers which are inherently nonrenewable. Next, many polymers are synthesized using one or more unsustainable components such as precious metals including iridium and ruthenium. Finally, at the end of a polymer's useful life, options for recycling are limited by the inability to make virgin-quality materials that can be used for the same application as the original polymer. The work described in this thesis aims to address each of these issues. The polymerizations of several bio-based monomers are described. The use of organic photoredox catalysis to enable polymerization represents sustainable synthesis of polymers. Polymers exhibiting chemical recyclability are also investigated, wherein end-of-life materials can be depolymerized and used to produce virgin-quality materials. Ultimately, this work represents a diverse array of methodologies for increasing the overall sustainability of polymeric materials.

ACKNOWLEDGEMENTS

General Acknowledgements

I would first like to thank my committee – Prof. Garret Miyake, Prof. Andy McNally, Prof. Melissa Reynolds, and Prof. Brad Reisfeld – for their guidance through the preparation and defense of this dissertation.

I would also like to thank Prof. Melissa Denler for her advice and guidance and for reigniting my love for teaching. I simply adored working with you.

I would not have made it to where I am today without the guidance of my undergraduate research advisor, Prof. Eric Kantorowski. You taught me so many valuable lab techniques but more importantly you taught me how to think like a scientist. You are an excellent role model and are by far one of the best educators I have ever had the pleasure of being in class with.

I am incredibly grateful to my fellow graduate students and the postdoctoral researchers who were part of the Miyake Lab while I was at CSU. You were all immensely helpful during my pursuit of knowledge. Going to work every day and seeing all of you was the greatest gift of my graduate studies. I believe that I would not have made it this far without you all by my side. I sincerely hope that I have been even a fraction of the friend to all of you that you were to me. I am a better scientist for having worked with you, and a better person for having been your friend. I will miss you all so much.

Thank you to Dr. Zhitao Hu for mentoring me during my final years of graduate school; I am forever grateful for your guidance as it shaped me into the scientist I am today. Furthermore, you always made me feel like my ideas were valuable – I cannot thank you enough for this.

To my dear friends Emma Rettner, Ethan Quinn, Katrina Puffer, Katherine Harry, and Anna Wolff: you were all instrumental in my success when learning about polymer chemistry and O-ATRP. You always took the time to help me and share with me your immense knowledge. I would not have been able to succeed without the five of you, and I hope that one day I can come close to returning the favor.

I am so grateful for the love and support of my family and friends during graduate school. I would not be here without all of you. I would especially like to thank my parents who have always pushed me to do my best and have made me feel like the possibilities in this life are limitless. The parts of myself that I take the most pride in are the parts that remind me of you.

Finally, I would of course like to thank my advisor, Garret. Despite the trials and tribulations of graduate school, I have truly loved being in your group. You have shaped me into someone who thinks critically about everything I do, plans thoroughly, and would bet my life on the work that I do. Thank you for all the support you have given me over the years and for encouraging me to push myself. You have always made me feel smart and full of potential.

Acknowledgements of Co-author Contributions and Funding Agencies

Chapter 2: This dissertation chapter contains the manuscript of an article [Chen, D.-F.; Bernsten, S.; Miyake, G.M. "Organocatalyzed Photoredox Radical Ring-Opening Polymerization of Functionalized Vinylcyclopropanes" *Macromolecules*, **2020**, *53*, 8352–8359.]. D.-F.C. performed polymerization experiments and polymer characterization. NMR analysis was performed in the Colorado State University Analytical Resources Core.

The work described in this chapter was supported by Colorado State University and the National Institute of General Medical Sciences of the National Institutes of Health under Award

No. R35GM119702. The content is solely the responsibility of the authors and does not necessarily represent the official views of the National Institutes of Health.

Chapter 3: This dissertation chapter contains the manuscript of an article [Hu, Z.*; Bernsten, S.N.*; Shi, C.; Sangroniz, A.; Chen, E. Y.-X.; Miyake, G.M. "Terpenoid-Based High-Performance Polyester with Tacticity-Independent Crystallinity and Chemical Circularity" *Chem,* **2024**, *XX*, XX-YY. *these authors contributed equally]. Z.H. spearheaded this project and designed initial experiments. Z.H. performed monomer synthesis and thermal and mechanical analysis of polymers. A.S. assisted with polymer characterization. C.S. and E.Y.-X.C. contributed intellectually and provided guidance throughout this work.

This work was supported by RePLACE (Redesigning Polymers to Leverage a Circular Economy) funded by the Office of Science of the US Department of Energy through award no. DE-SC0022290, the National Institutes of Health under award no. R35GM144356, Basque Country Government (GC IT 1667-22), and Colorado State University. The authors thank the Analytical Resources Core (RRID: SCR_021759) at Colorado State University for instrument access and training, and thank Jason Boes and Alan Kennan for assistance with CD experimentation. GMM acknowledges support from The Camille & Henry Dreyfus Foundation through a Camille Dreyfus Teacher-Scholar Award.

Chapter 4: This dissertation chapter contains the manuscript of an article [Bernsten, S.N.; Wolff, A.M.; Hu, Z.; Miyake, G.M. "Photoinduced Organocatalyzed Controlled Radical Vinyl Addition Polymerization of α-Methylene-δ-Valerolactone and α-Methylene-γ-Butyrolactone" *Journal of Polymer Science,* **2024**, *X*, XX-YY.]. A.M.W. aided in monomer synthesis, manuscript editing, and follow up experiments post review. Z.H. provided guidance throughout experimentation and preparation of the manuscript.

This work was supported by RePLACE (Redesigning Polymers to Leverage a Circular Economy) funded by the Office of Science of the US Department of Energy through award no. DE-SC0022290, the National Institutes of Health under award no. R35GM144356, Basque Country Government (GC IT 1667-22), and Colorado State University. The authors thank the Analytical Resources Core (RRID: SCR_021759) at Colorado State University for instrument access and training, and thank Jason Boes and Alan Kennan for assistance with CD experimentation. GMM acknowledges support from The Camille & Henry Dreyfus Foundation through a Camille Dreyfus Teacher-Scholar Award.

DEDICATION

This dissertation is dedicated to my family:

To my parents, Sally and Jim Bernsten, for your unrelenting support and for being my biggest cheerleaders since the day I was born.

To my sister, Camille Bernsten, for being my best friend and the greatest role model I could ever dream of.

To my brother, August Bernsten, for always believing in me and for being an incarnation of all the goodness in this world.

And to my brother, Harry Bernsten, for being my guardian angel.

TABLE OF CONTENTS

ABSTRACT ..... *ii*

DEDICATION ..... *vii*

CHAPTER 1 – INTRODUCTION *1*

Thesis Structure 1

Motivations 2

REFERENCES *5*

CHAPTER 2 – ORGANOCATALYZED PHOTOREDOX RADICAL RING-OPENING POLYMERIZATION OF FUNCTIONALIZED VINYLCYCLOPROPANES *6*

Overview 6

Introduction 6

Results and Discussion 8

Conclusion 23

REFERENCES *25*

CHAPTER 3 – TERPENOID-BASED HIGH-PERFORMANCE POLYESTER WITH TACTICITY-INDEPENDENT CRYSTALLINITY AND CHEMICAL CIRCULARITTY *28*

Overview 28

Introduction 28

Results and Discussion 33

Conclusion 51

REFERENCES *53*

CHAPTER 4 – PHOTOINDUCED ORGANOCATALYZED CONTROLLED RADICAL VINYL ADDITION POLYMERIZATION OF α-METHYLENE-δ-VALEROLACTONE AND α-METHYLENE-γ-BUTYROLACTONE *57*

Overview 57

Introduction 58

Results and Discussion 60

Conclusion 71

REFERENCES *72*

CHAPTER 5 – SUMMARY *74*

APPENDIX A – SUPPLEMENTARY INFORMATION FOR CHAPTER 2 ..... *75*

REFERENCES *122*

APPENDIX B – SUPPLEMENTARY INFORMATION FOR CHAPTER 3 ..... *123*

REFERENCES *174*
APPENDIX C – SUPPLEMENTARY INFORMATION FOR CHAPTER 4 ..... *175*
REFERENCES *215*

CHAPTER 1 – INTRODUCTION

Thesis Structure

The author of this dissertation conducted research covering a wide range of topics including photocatalyst design and use for small-molecule transformations, synthesis of novel monomers, organocatalyzed atom transfer radical polymerization (O-ATRP), and study of chemically recyclable polymers. This dissertation is focused on progress made in the area of sustainable polymers, encompassing sustainably-sourced monomers, sustainable polymerization techniques, and chemically recyclable polymers. First, radical ring opening polymerization (rROP) of a series of functionalized vinylcyclopropaes driven by an organic photoredox catalyst is described. Next, a terpenoid-based lactone is presented as an example of a bio-based monomer used to produce chemically recyclable polymers. Finally, photoinduced organocatalyzed polymerization of two additional bio-based lactones with reported chemical recyclability is reported.

The overall structure of this thesis follows a journal-format style based on selected publications, with each chapter being modeled off of one published research article or unpublished manuscript. The chapters include two unpublished first-author works, as well as one supporting-author manuscript published in *Macromolecules*. The topics covered in this thesis are presented in three chapters (Chapter 2 – Chapter 4) with the following titles:

1. Organocatalyzed Photoredox Radical Ring-Opening Polymerization of Functionalized Vinylcyclopropanes

2. Terpenoid-Based High-Performance Polymester with Tacticity-Independent Crystallinity and Chemical Circularity
3. Photoinduced Organocatalyzed Controlled Radical Vinyl Addition Polymerization of Bio-Based Lactones

Motivations

Over the last 50-75 years, polymers have become integral to modern society because of their low cost, processability, and diverse material properties. While there are many desirable things about using plastics, their use has brought about significant environmental concerns that arise during every step of a polymer's life cycle. The current scale of polymer production is enormous and is projected to continue increasing in the coming years,[1] thereby creating a dire need for the development of polymers with minimized environmental impact. Environmental concerns arise even before polymers are synthesized in that monomers used to produce many commodity plastics are derived from non-renewable resources including fossil fuels.[2] During polymerization, additional layers of environmental concern can arise. For example, syntheses of many polymers involve the use of precious metals,[3] toxic reagents,[4] or energetically intensive synthetic conditions. At the end of a polymer's useful life, incredibly prominent environmental issues arise due to poor end-of-life options. It is important to consider all of the ways in which

environmental issues can arise before, during, and after polymer synthesis in order to transition to more sustainable versions of these indispensable materials.

In the realm of monomer synthesis, the use of bio-based monomers is desirable for sustainability in that they are derived from renewable resources as opposed to non-renewable resources. The use of bio-based monomers has become increasingly popular in recent years due to concerns over the environmental impact of fossil fuel utilization.[5] Bio-based monomers have sustainability advantages over existing petroleum-based monomers, but they are much newer and therefore their syntheses and polymerizations are not nearly as well-established as petroleum-based monomers that have existed for decades. Therefore, in order to effectively make use of bio-based monomers, synthesis and polymerization methods must be investigated. To address these challenges, bio-based monomer synthesis and polymerization are investigated herein (Chapter 3 and Chapter 4).

In addition to using monomers derived from renewable resources, overall polymer sustainability can be bolstered by the use of sustainable polymerization techniques. The 12 principles of green chemistry are a useful benchmark for evaluating the sustainability of polymer syntheses. Among these principles are considerations of atom economy, reagent toxicity, energy consumption, use of catalysis, and renewability of reagent sources.[6] The use of organic photoredox catalysis (Chapter 2 and Chapter 4) is a promising method for sustainable synthesis of polymers due to increased adherence to the principles of green chemistry relative to other polymerization techniques.[7] Organic photoredox catalysis effectively enables harnessing of low-

energy visible light to drive polymerizations without the use of added heat. In addition, organic photoredox catalysts (OPCs) do not contain metal, which demonstrates twofold adherence to the principles of green chemistry in that they are not made from precious metals and are lacking in toxicity arising from the use of metal catalysis.

Once a polymer has been synthesized, the next sustainability challenge arises from the fact that many polymeric materials have poor end-of-life options. The fates for end-of-life polymeric materials most frequently include landfilling, incineration, and pollution. Pollution of polymers into the natural environment has given rise to the presence of plastics and microplastics both on land and in the ocean. In order to combat the presence of plastics and microplastics in the environment, polymers with better end-of-life options must be developed.

Even when consumers practice recycling, a large majority of polymeric materials that undergo recycling are mechanically recycled.[8] Mechanical recycling causes shear degradation of polymers resulting in materials with less desirable properties after recycling. As a result, even plastics that go through a recycling stream typically end up as waste. One avenue for decreasing plastic waste is to develop polymers that are chemically recyclable, meaning that an end-of-life plastic can be broken down into its constituent monomers and re-polymerized to yield virgin-quality material (Chapter 3 and Chapter 4).

REFERENCES

1. Polymers Market - Global Industry Analysis, Size, Share, Growth, Trends, Regional Outlook, and Forecast 2023-2032; https://www.precedenceresearch.com/polymers-market
2. P.T. Anastas and M.M. Kirchhoff, *Acc. Chem. Res.* **2002**, *35*, 686–694.
3. M. Ouchi, T. Terashima, M. Sawamoto, *Chem. Rev.* **2009**, *109*, 4963–5050.
4. A. Llevot, P.-K. Dannecker, M. von Czapiewski, L. C. Over, Z. Söyler, M. A. R. Meier, *Chem. Eur. J.* **2016**, *22*, 11510.
5. Ciardelli, C.; Maffei, A.; Di Natale, F.; D'Angelo, A.; *Sustain. Chem. Pharm.* **2019**, *14*, 100181.
6. Erythropel, H. C.; Birkett, J. W.; Andrady, O. M.; Halden, R. U. *Science*, **2020**, *367,* 1396–1398.
7. D. A. Corbin, G. M. Miyake, *Chem. Rev.* **2022**, *122*, 1830–1874.
8. Z. O. G. Schyns, M. P. Shaver, *Macromol. Rapid Commun.* **2021**, *42*, 2000415.

CHAPTER 2 – ORGANOCATALYZED PHOTOREDOX RADICAL RING-OPENING POLYMERIZATION OF FUNCTIONALIZED VINYLCYCLOPROPANES

Overview

Organocatalyzed photoredox radical ring-opening polymerization (rROP) of vinylcyclopropanes (VCPs) is employed for the synthesis of polymers with controlled molecular weight (MW), dispersity, and composition. Herein, we report the study on the rROP of a variety of VCP monomers bearing diverse functional groups (such as amide, alkene, ketal, urea, hemiaminal ether, and so on) under organocatalyzed conditions with varying light sources and temperature. Notably, VCP monomers bearing natural product functionality or their derivatives can be polymerized in a controlled manner to produce poly(VCPs) with predictable MW, low dispersity, tunable composition, as well as high thermal stability and tailored glass transition temperature (T_g), ranging 39 to 107 °C. Lastly, successful "grafting through" synthesis of molecular brush copolymers containing 1.0 or 5.0 kDa polydimethylsiloxane (PDMS) side chains from readily accessible EtVCP-PDMS macromonomers further demonstrates the robustness of this organocatalyzed photoredox rROP.

Introduction

Radical ring-opening polymerization (rROP) of strained 1,1-disubstituted vinylcyclopropanes (VCPs) is an interesting and useful polymerization methodology that often

exhibits low volume shrinkage, or even volume expansion, which has application potential in modeling and restorative materials.[1-2] In early studies, two radical polymerization pathways were proposed after the initial ring-opening event to deliver poly(VCPs) containing distinct unsaturated linear (*l*) and saturated cyclic (*c*) repeat units.[3] However, control over the molecular weight and dispersity of the resulting polymer remained a challenge. To tailor the molecular weight (MW) and l/c selectivity within the polymer, Cu(I)-catalyzed atom transfer radical polymerization (ATRP) was successfully applied to the polymerization of 1,1-diethoxycarboxyl-2-vinylcyclopropane (EtVCP), producing poly(EtVCP) with 98.7% linear repeat units and low dispersity (Đ) of 1.12.[4] However, the monomer conversion was low (< 50%), presumably due to the Cu(I) catalyst poisoning by coordination of EtVCP or poly(EtVCP).[5-6]

Recently, our group demonstrated a photocontrolled rROP of VCP monomers using an organic photocatalyst (PC), N,N′-di-2-naphthyl dihydrophenazine,[7] that allowed high monomer conversion to produce poly(VCPs) with predictable MW and low Đ (**Figure 2.1A**),[8] while the photoredox controlled polymerization mechanism[9-11] enabled temporal control over the polymerization was achieved.[12-26] Moreover, the high Br chain-end group fidelity allowed an unexpected polymer-chain modification of an isolated poly(EtVCP) that converted l repeat units into c repeat units, which inspired de novo regulation on the polymer structure, as well as further investigations into the mechanism of c repeat unit formation and structure-property relationships of the thermal/viscoelastic characteristics of the obtained polymers. However, our previous report

focused on VCP monomers bearing simple alkyl esters and the compatibility of functional groups on the cyclopropane ring with this organocatalyzed photoredox polymerization conditions remains unknown. Given the importance of functional polymers in both academia and industry,[27] we became interested in exploring the polymerization of diversely functionalized VCP monomers to prepare well-defined poly(VCPs) with tailored composition and properties (**Figure 2.1B**).

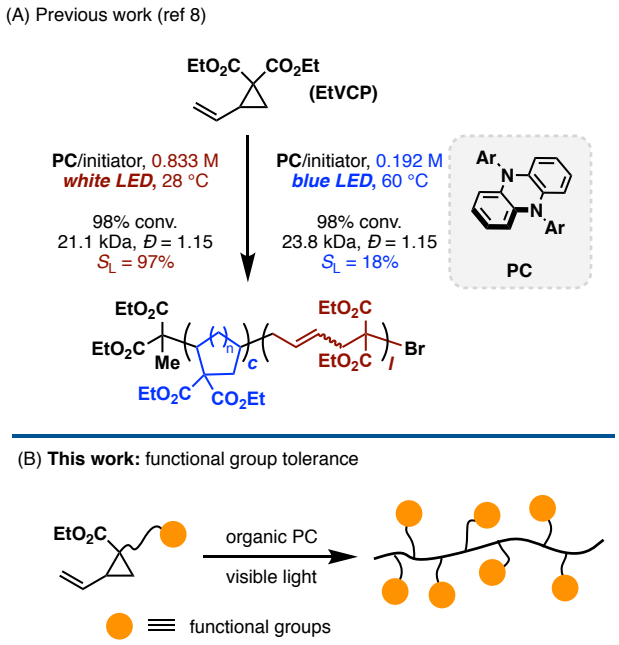

***Figure 2.1**. Organocatalyzed Photoredox Radical Ring-Opening polymerization of VCPs.*

Results and Discussion

To gain preliminary insights into the functional group tolerance under our organocatalyzed photoredox polymerization conditions, 20 small molecule additives were selected for the rROP of EtVCP. Specifically, MeOH and 2,2,2-trifluoroethanol led to slightly lower monomer conversions, while excellent control over polymerizations retained. Brønsted acids, such as benzoic acid and

benzamide, significantly slowed down the polymerizations probably due to decreased stability of PC **1** under acidic conditions. Lewis bases, including triethylamine and triphenylphosphine, may interfere with the deactivation step by quenching [$PC^{\bullet+}Br^{-}$], resulting the loss of control over polymerization. The addition of electrophilic propagating carbon radicals to electron-rich heteroarenes (e.g., indole and furan) could be considered as a potential termination pathway. Other additives, such as electron-deficient benzene derivatives, aldehyde, ketone, alkyne, epoxide, alkyl bromide, carbodiimide, and even phenol, were well-tolerated to achieve high monomer conversions, producing poly(EtVCP) with predictable MWs, low dispersities, and high S_L values (also see **Figure S2.17** for details).

Encouraged by discovering a variety of additive functional groups being tolerated in the rROP of EtVCP, we began our exploration of functionalized VCP monomers with varying the substituents at the C1 position. Three monomers, CNVCP, EtVCP-CN, and EtVCP-NHPh, were prepared and polymerized under previously optimized conditions ([monomer]:[DBMM]:[PC **1**] = [1000]:[10]:[1] with irradiation by white LED at ~28 °C) (**Table 2.1**).[8] Unfortunately, no monomer conversion was observed in the polymerization of CNVCP (**Table 2.1, entries 1–2**), while the polymerization of EtVCP-CN achieved 90% monomer conversion within 12 h achieving an initiator efficiency ($I^* = M_{n,theo}/M_{n,measured} \times 100\%$) of 86%, to produce highly linear poly(EtVCP-CN) (S_L = 99%) with a number average molecular weight (M_n) of 17.6 kDa, and low $Đ$ of 1.22 (**Table 2.1, entry 3**). Modulation of the monomer feed ratio allowed for synthesis of poly(EtVCP-CN)

with predictable MWs (from 11.2 to 25.4 kDa) and low dispersities ($Đ$ < 1.19) (**Table 2.1, entries 4–5**). Polymerization of EtVCP-NHPh was faster than EtVCP-CN and reached 96% monomer conversion within 6 h, exhibiting excellent control over polymer composition (S_L = 99%), molecular weight (M_n = 25.9 kDa, I* = 97%), and dispersity ($Đ$ = 1.19) (**Table 2.1, entries 6–7**). It has been demonstrated that increased stability of the C1-C2 bond of vinylcyclopropanes would result in lower monomer conversion in free radical polymerization. Calculated two-center energy suggested that the C1-C2 bond of CNVCP is more stable than that of EtVCP by 0.17 eV (i.e. 3.9 kcal/mol).[3] Given the radical polymerization mechanism under this organocatalyzed photoredox conditions, the ring-opening polymerizability approximately increases in the order EtVCP-NHPh ≈ EtVCP > EtVCP-CN >>> CNVCP. Interestingly, compared to EtVCP, the presence of the cyano and amide groups led to preferential formation of linear polymer composition (S_L = 86%, 60% respectively) under conditions of 34 W blue LED and 60 °C (**Table 2.1, entries 6** and **8**).

rROP of Natural Product-Derived Vinylcyclopropanes.

Due to the efficient and controlled polymerization of EtVCP, this parent monomer was selected for incorporation of further functional groups. A two-step synthetic route was developed which consisted of: (1) selective hydrolysis of EtVCP to provide major *cis* EtVCP-CO_2H (cis:trans = 10:1); and (2) high yielding coupling reactions of EtVCP-CO_2H with a few natural products or their derivatives (e.g., vitamin E, uridine, dehydroabietic acid, and cholesterol)[28-29] to afford a series of the targeted monomers with diverse functionalities, such as phenyl ether, hemiaminal

ether, ketal, urea, and alkene (**Figure 2.2**). The investigation into the polymerization of natural product-derived vinycyclopropane monomers was initially performed in EtOAc, with a [500]:[10]:[1] ratio of EtVCP-VE: DBMM: PC **1** and white LED at 28 °C (**Table 2.2, entry 1**), which achieved 96% monomer conversion and produced

Table 2.1. *Results of Polymerization of Monomers with Variable C1-Substituents*[a].

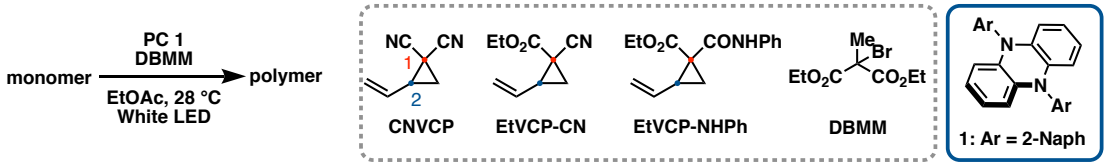

Entry	Monomer	[M]/[I]/[PC]	Time (h)	Conv. (%)[b]	M_n (kDa)[c]	$Đ$ (M_w/M_n)[c]	I^* (%)[d]	S_L (%)[b]
1	CNVCP	1000/10/1	12	0	-	-	-	-
2	CNVCP	1000/10/1	12	0	-	-	-	-
3	EtVCP-CN	1000/10/1	12	90	17.6	1.22	86	99
4	EtVCP-CN	500/10/1	12	84	11.2	1.18	64	92
5	EtVCP-CN	2000/10/1	12	70	25.4	1.19	92	95
6[e]	EtVCP-CN	1000/10/1	12	99	28.0	1.13	60	87
7	EtVCP-NHPh	1000/10/1	6	96	25.9	1.19	97	99
8[e]	EtVCP-NHPh	1000/10/1	6	99	30.9	1.11	85	60

[a]Polymerizations performed using 1.0 mmol of monomer, DBMM as the initiator, 1.0 mL of anhydrous EtOAc, and irradiated by 1.6 W white LEDs at 28 °C. [b]Measured by crude ^{1}H-NMR. S_L = $l/(l + c)$. [c]Measured by gel-permeation chromatography (GPC). [d]Initiator efficiency (I^*) =

$M_{n,theo}/M_{n,measured}$ × 100%, where $M_{n,theo}$ = MW(initiator) + MW(monomer) × conversion × ([monomer]/[initiator]). [e]Polymerizations performed in 5.0 mL of EtOAc and with irradiated by 34 W blue LED at 60 °C.

poly(EtVCP-VE) 31.6 kDa, and with good control over the chain-growth as indicated by a low *Đ* of 1.29, high *I** of 91%, as well as high S_L of 96%. This success suggested high compatibility of the vitamin E moiety with the organocatalyzed photoredox polymerization protocol, which

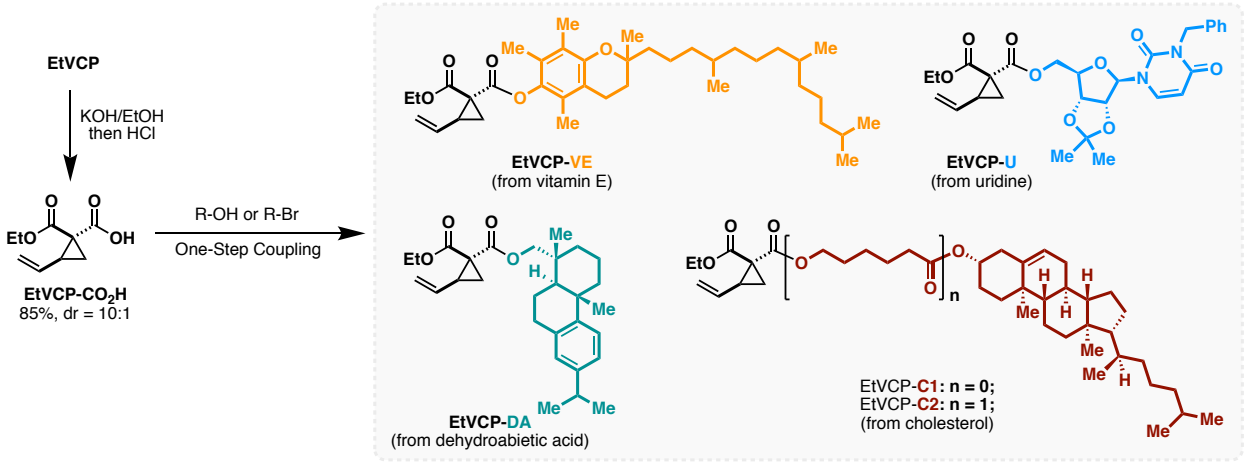

Figure 2.2. *Divergent Synthesis of Natural Product Derived VCP Monomers.*

encouraged further optimization and study of other natural product-derived vinylcyclopropane monomers.The effect of PC (**Table 2.2, entries 1–3**), initiator, and solvent (**Tables S2.5–S2.6**) on the polymerization of EtVCP-VE revealed that **1** was superior to other PCs while the use of chlorobenzene (PhCl) as the solvent resulted in the lowest *Đ* of 1.23 (**Table 2.2, entry 4**). Lower loadings of PC **1** were still able to drive the polymerization and achieved high monomer conversions, however, at the cost of less control over the chain-growth as the *Đ* value increased from 1.23 to 1.65 (**Table 2.2, entries 5–6**). Importantly, varying the loading of EtVCP-VE or DBMM allowed tuning of the MW of poly(EtVCP-VE) (**Table 2.2, entries 8–10**).

The polymerization of EtVCP-VE was monitored over time, and first-order kinetics was observed for the monomer consumption (**Figure 2.3A**). Analysis of poly(EtVCP-VE) produced at different time points indicated a linear increase of polymer MW with respect to monomer conversion, while low to moderate dispersity ($Đ$ = 1.21–1.34) was achieved during the entire course of polymerization (**Figure 2.3B**). Temporal control was also investigated using a pulsed-irradiation experiment and the polymerization proceeded only under light

Table 2.2. *Results of Polymerization of Natural Product-Based VCP Monomers at 28 °C Irradiated with a White LED*[a].

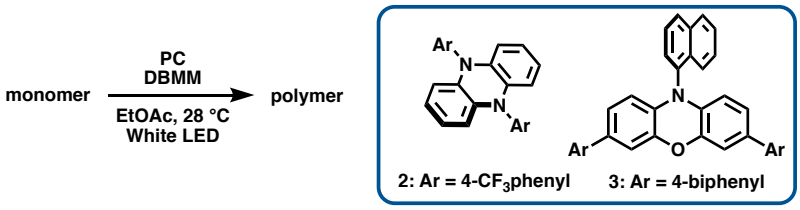

Entry	Monomer	PC	[M]/[I]/[PC]	Time (h)	Conv. (%)[b]	M_n (kDa)[c]	$Đ$ (M_w/M_n)[c]	I^* (%)[d]	S_L (%)[b]
1	EtVCP-VE	**1**	500/10/1	6	96	31.6	1.29	91	96
2	EtVCP-VE	**2**	500/10/1	6	98	30.8	1.54	96	96
3	EtVCP-VE	**3**	500/10/1	6	91	27.2	1.62	101	95
4[e]	EtVCP-VE	**1**	500/10/1	6	94	27.6	1.23	103	96
5[e]	EtVCP-VE	**1**	500/10/0.5	6	99	31.6	1.35	94	96
6[e]	EtVCP-VE	**1**	500/10/0.1	6	95	28.8	1.61	99	96
7[e]	EtVCP-VE	**1**	500/10/2	6	91	30.4	1.45	81	95
8[e]	EtVCP-VE	**1**	250/10/1	6	73	13.9	1.15	81	92
9[e]	EtVCP-VE	**1**	500/20/1	6	84	15.7	1.15	82	92

10[e]	EtVCP-VE	**1**	1000/10/1	6	90	42.2	1.59	128	95
11	EtVCP-U	**1**	500/10/1	6	90	29.4	1.77	84	95
12[e]	EtVCP-U	**1**	500/10/1	6	99	33.7	1.67	81	93
13[f]	EtVCP-U	**3**	500/10/1	6	99	33.9	1.35	81	95
14	EtVCP-DA	**1**	500/10/1	6	90	21.6	1.51	94	81
15	EtVCP-DA	**2**	500/10/1	6	82	12.3	1.57	153	76
16	EtVCP-DA	**3**	500/10/1	12	61	14.9	1.48	95	75
17[e]	EtVCP-C1	**1**	500/10/1	12	96	28.5	1.21	94	94
18[e]	EtVCP-C2	**1**	500/10/1	12	90	30.9	1.32	97	78

[a]Polymerizations performed using 0.5 mmol of monomer, DBMM as the initiator, 0.5 mL of anhydrous EtOAc, and irradiated by 1.6 W white LED at 28 °C. [b]Measured by crude ^{1}H-NMR. $S_L = l/(l + c)$. [c]Measured by GPC. [d]Initiator efficiency (I^*) = $M_{n,theo}/M_{n,measured} \times 100\%$, where $M_{n,theo}$ = MW(initiator) + MW(monomer) × conversion × ([monomer]/[initiator]). [e]PhCl was used as the solvent. [f]1,2-Dichloroethane (DCE) was used as the solvent.

irradiation, paused upon removal of light source (as long as 12 h), and could be resumed with continued irradiation (**Figure 2.3C**). The temporal control supported a light-driven reversible activation-deactivation polymerization mechanism, as well as the presence of the Br chain-end groups, which allowed the synthesis of advanced polymer architecture. As such, chain-extension could be used from the synthesized poly(EtVCP-VE) as a macroinitiator for the rROP of cholesterol-derived monomer EtVCP-C2 under photoredox conditions. ^{1}H-NMR characterization (**Figure S2.33**) and the observation of shorter retention time of the GPC trace of the chain-extended poly(EtVCP-VE)—although a low molecular shoulder presented, which probably due to the loss of some Br chain-end groups in poly(EtVCP-VE) macroinitiator or the radical termination during

chain extension—indicated success in synthesizing a block copolymer poly(EtVCP-VE)-*b*-poly(EtVCP-C2) (**Figure 2.3D**).

We next explored the polymerization behavior of the other natural product-derived vinylcyclopropane monomers. Under previously optimized conditions ([monomer]:[DBMM]:[**1**] = 500:10:1 in EtOAc at 28 °C, with white LED),[8] the polymerization of the uridine-derived monomer EtVCP-U was uncontrolled as indicated by a high $Đ$ of 1.77 (**Table 3.2, entry 11**). The use of PhCl as the solvent led to higher monomer conversion (99%) and slightly lower $Đ$ of 1.67 (**Table 2.3, entry 12**). The polymerization of EtVCP-U with 3,7-di(4-biphenyl)-*N*-naphthylphenoxazine **3**[30] as the PC in DCE achieved 99% conversion within

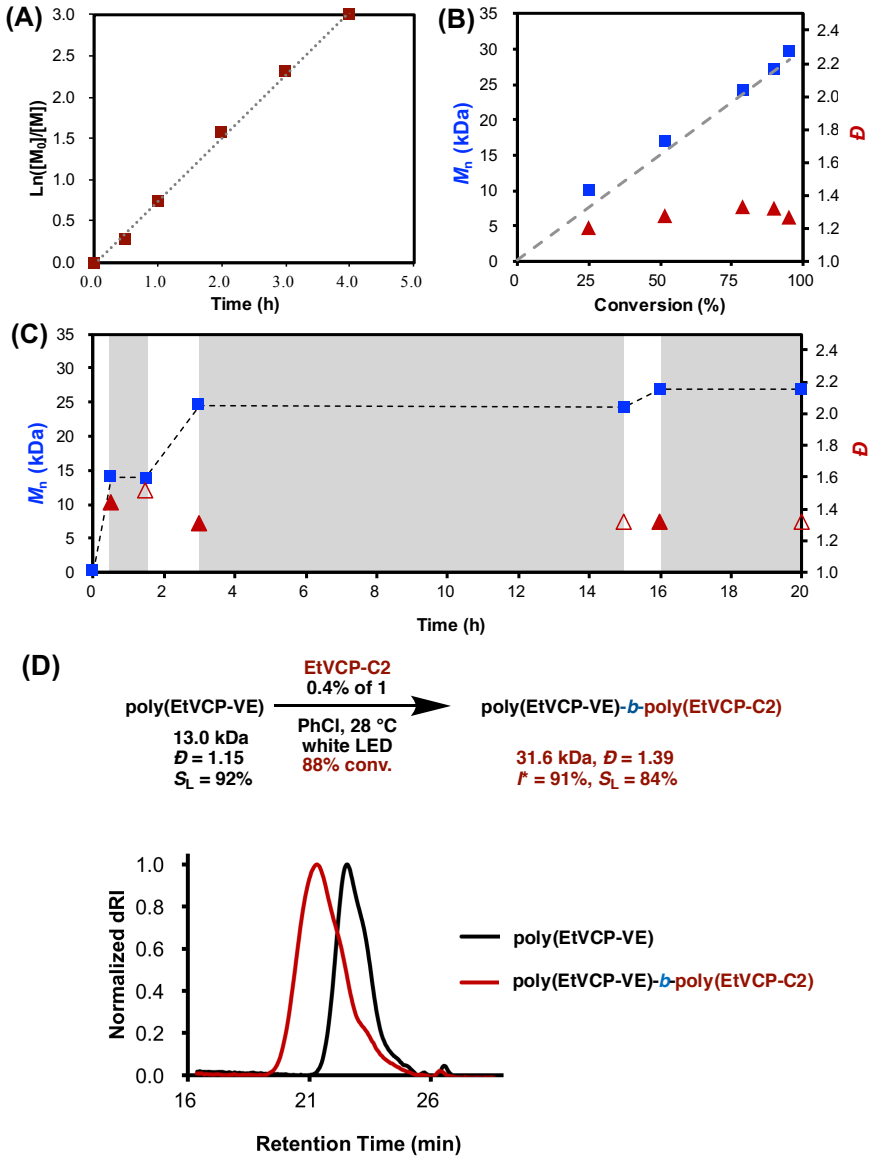

Figure 2.3: *Organocatalyzed photoredox rROP of EtVCP-VE: (A) plots of the natural log of monomer conversion as a function of time; (B) plots of experimentally measured M_n and dispersity as a function of monomer conversion; (C) plots of experimentally measured M_n and dispersity as a function of time for a pulsed irradiation experiment. (D) chain-extension polymerization from a poly(EtVCP-VE) macroinitiator with EtVCP-C2, and GPC traces before and after the polymerization.*

6 hours, and afforded the best control over the chain growth to product poly(EtVCP-U) of 33.9 kDa, with a lower $Đ$ of 1.35, I* of 81% and S_L of 95% (**Table 2.3, entry 13**).Screening of PCs for

the polymerization of dehydroabietic acid-derived monomer EtVCP-DA (in EtOAc at 28 °C, with white LED) suggested that **1** was superior to **2** and **3** in terms of monomer conversion and the S_L value (**Table 2.3, entries 14–16**). Lastly, polymerizations of cholesterol-derived monomer EtVCP-C1 with PC **1** in PhCl reached 96% monomer conversion to produce poly(EtVCP-C1) of 28.5 kDa, with $Đ$ of 1.21, I^* of 94%, and S_L of 94% (**Table 2.3, entry 17**). Polymerization of EtVCP-C2 was a little bit slower than that of EtVCP-C1, reaching 90% monomer conversion within 12 hours (**Table 2.3, entry 18**). The presence of an alkyl linker in EtVCP-C2 results in less steric hindrance on the cyclopropane motif, which may lower the ring strain and slow down the ring-opening process for propagation. The overall control over the polymerization of EtVCP-C2 was good (low $Đ$ of 1.32 and high I^* of 97%) except that significant amount of cyclic polymer composition was formed (S_L = 77%).

The impact of the monomer functionality on the *l*/*c* selectivity under varying conditions was also explored. In general, regardless the nature of the functional group, poly(VCPs) synthesized at 60 °C and with high power blue LED exhibited higher degree of cyclic composition than those prepared at 28 °C and with white LED (**Table 2.2** vs **Table 2.3**). In the polymerization of EtVCP-VE, the S_L decreased from 96% to 60% while the overall control over the chain-growth remained excellent ($Đ$ = 1.06, I^* = 77%; **Table 2.3, entry 1**). Lower polymerization concentration led to decreased S_L value (**Table 2.3, entry 2**) while polymerization with increased monomer feed ([EtVCP-VE]:[DBMM]:[1] = 1000:10:1) achieved 72% conversion to give poly(EtVCP-VE) of

29.2 kDa, with $Đ$ = 1.20, I^* = 147%, and S_L = 42% (**Table 2.3, entry 3**). When 1.0 mL solvent was used, polymerizations of EtVCP-U with PC **3** in DCE, EtVCP-DA with PC **1** in EtOAc, and EtVCP-C2 with PC **1**in PhCl all reached high monomer conversion (85–99%) to afford polymers with low to moderate $Đ$ (1.05–1.57), moderate to high I^* (72–92%), and moderate S_L (41-60%) (**Table 2.3, entries 4, 6,** and **10**). Polymerizations of EtVCP-U, EtVCP-DA, and EtVCP-C2 in 2.5 mL of indicated solvents generally achieved lower monomer conversion (65–90%), while the polymers synthesized exhibited low $Đ$, with an exception that the $Đ$ of poly(EtVCP-DA) was 1.96, high I^*, and further decreased S_L (**Table 2.3, entries, 5, 7**, and **11**). It is noteworthy that, due to the bulky steric hindrance of the cholesterol motif, polymerization of EtVCP-C1 under conditions of 34 W blue LED and 60 °C still produced major linear polymer composition (S_L = 85–90%; **Table 2.3, entries 8–9**).

Table 2.3: *Results of Polymerization of Natural Product-Based VCP Monomers at 60 °C with Blue LED*[a].

Entry	Monomer	PC	Solvent	Time (h)	Conv. (%)[b]	M_n (kDa)[c]	$Đ$ (M_w/M_n)[c]	I^* (%)[d]	S_L (%)[b]
1	EtVCP-VE	**1**	EtOAc	6	82	32.0	1.06	77	60
2[e]	EtVCP-VE	**1**	EtOAc	6	70	29.6	1.03	72	55
3[e,f]	EtVCP-VE	**1**	EtOAc	6	72	29.2	1.20	147	42
4	EtVCP-U	**3**	DCE	6	99	29.7	1.16	92	41
5[e]	EtVCP-U	**3**	DCE	6	90	24.5	1.16	100	35
6	EtVCP-DA	**1**	EtOAc	6	90	28.6	1.57	72	52

7[e]	EtVCP-DA	**1**	EtOAc	6	72	19.8	1.96	82	50
8	EtVCP-C1	**1**	PhCl	12	87	27.7	1.08	88	90
9[e]	EtVCP-C1	**1**	PhCl	12	83	24.9	1.05	93	85
10	EtVCP-C2	**1**	PhCl	12	85	35.0	1.05	82	60
11[e]	EtVCP-C2	**1**	PhCl	12	65	20.4	1.08	107	45

*[a]Polymerizations performed using 0.5 mmol of monomer, DBMM as the initiator, 1.0 mL of anhydrous solvent, and irradiated by 34 W blue LED at 60 °C. [b]Measured by crude ^{1}H-NMR. $S_L = l/(l + c)$. [c]Measured by GPC. [d]Initiator efficiency (I^*) = $M_{n,theo}/M_{n,measured} \times 100\%$, where $M_{n,theo}$ = MW(DBMM) + MW(monomer) × conversion × ([monomer]/[DBMM]). [e]2.5 mL of solvent was used. [f][monomer]:[DBMM]:[PC **1**] = 1000:10:1.*

Thermal Property of Natural Product-Derived Poly(VCPs).

Thermal properties of the synthesized natural product-derived polymers [poly(NPVCPs)] containing either high degree of linear composition [*l*-poly(NPVCPs)] or cyclic composition [*c*-poly(NPVCPs)] were examined by thermogravimetric analysis (TGA) and differential scanning calorimetry (DSC). Generally, regardless of the polymer composition, poly(EtVCP-VE), poly(EtVCP-U), and poly(EtVCP-DA) exhibited a much higher decomposition temperature (T_d, defined by the temperature at 10% weight loss) than poly(EtVCP-C2) (**Figure 2.4A** and **2.4B**), while increased cyclic composition led to higher thermal stability and higher T_d of 339–385 °C (**Figure 2.4A** vs **2.4B**). Compared to poly(EtVCP) (glass transition temperature, T_g = 32 °C), higher T_gs were observed for both *l*-poly(NPVCPs) and *c*-poly(NPVCPs), indicating that the presence of all four natural products in the side chain reduced the free volume (**Figure 2.4C** and **2.4D**). It is worth noting that T_g values of poly(NPVCPs) were drastically influenced by the nature of the natural product installed in the side chains. For example, *l*-poly(EtVCP-U) and *l*-

poly(EtVCP-DA) exhibited high T_gs (94 °C and 86 °C), while T_gs of *l*-poly(EtVCP-VE) and *l*-poly(EtVCP-C2) decreased to 39 °C and 44 °C, respectively (**Figure 2.4**C). Moreover, the composition of the polymer main-chain might also substantially change the T_g values. For instance, T_g of *c*-poly(EtVCP-U) was 13 °C higher than that of *l*-poly(EtVCP-U).

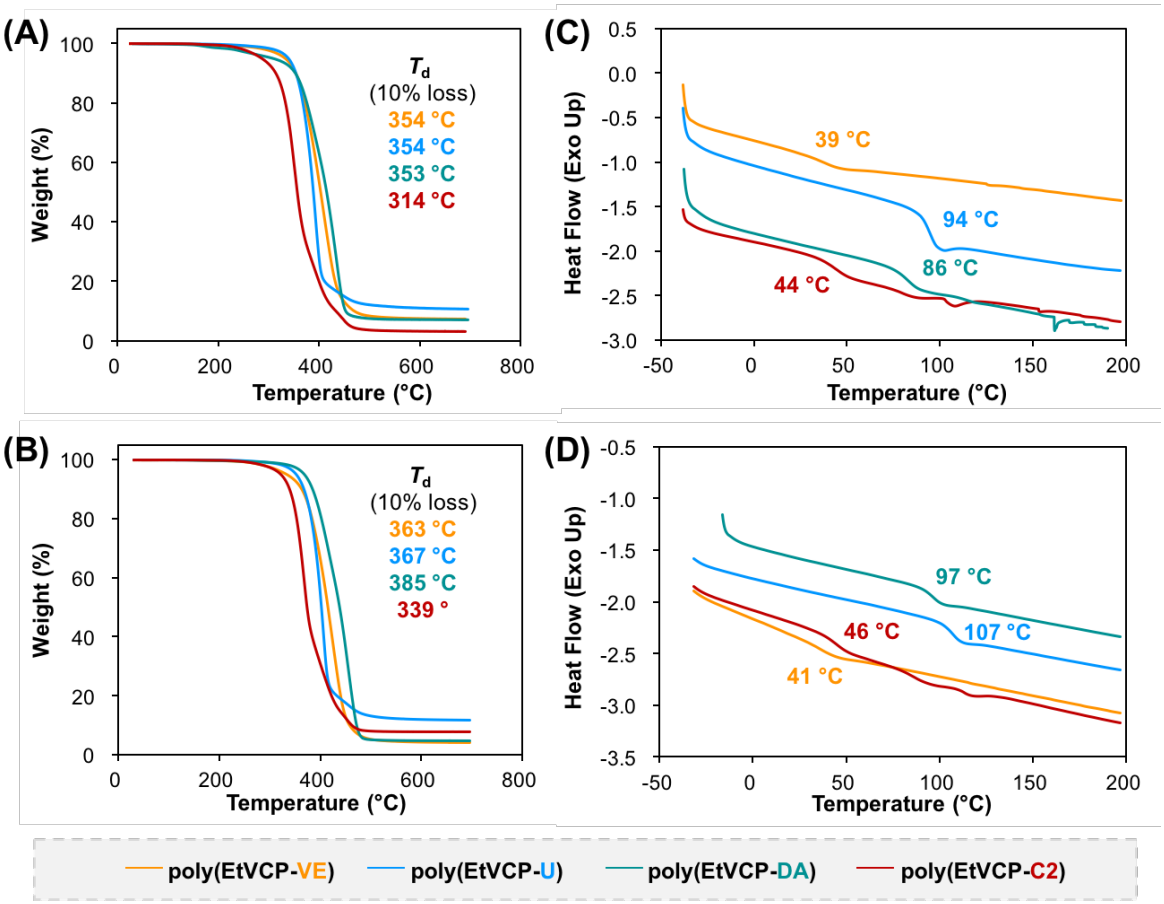

***Figure 2.4**: TGA curves of l-poly(NPVCPs) (A) and c-poly(NPVCPs) (B). DSC curves of l-poly(NPVCPs) (C) and c-poly(NPVCPs) (D). l-poly(NPVCPs) were l-poly(EtVCP-VE) (M_n = 27.6 kDa, Đ = 1.23, S_L = 96%), l-poly(EtVCP-U) (M_n = 33.9 kDa, Đ = 1.35, S_L = 95%), l-poly(EtVCP-DA) (M_n = 21.6 kDa, Đ = 1.51, S_L = 81%), and l-poly(EtVCP-C2) (M_n = 30.9 kDa, Đ = 1.32, S_L = 78%). c-poly(NPVCPs) were c-poly(EtVCP-VE) (M_n = 29.2 kDa, Đ = 1.20, S_L = 42%), c-poly(EtVCP-U) (M_n = 29.7 kDa, Đ = 1.16, S_L = 41%), c-poly(EtVCP-DA) (M_n = 28.6 kDa, Đ = 1.57, S_L = 52%), and c-poly(EtVCP-C2) (M_n = 20.4 kDa, Đ = 1.08, S_L = 45%).*

Synthesis of Molecular Brush Polymers through rROP.

Given the steric interactions of the side chains tethered to a linear backbone, densely grafted brush polymers often bond with compact conformation/dimension and unique material properties, thus holding a vast potential for applications in catalysis, medical diagnosis, drug delivery, and so on.[31-33] It is noteworthy that the "grafting through" method, i.e. the direct polymerization from macromonomers (MMs), has been one of the simplest ways to synthesize densely grafted brush polymer with well-defined side chains.[34-38] Although tremendous advances have been made, the diversity of the polymer backbone where side chains are covalently bonded to remains limited, which piqued our curiosity about synthesizing a novel type of brush polymers through organocatalyzed photoredox rROP of VCP-derived MMs. Commercially available monocarbinol terminated polydimethylsiloxanes (PDMS) of 1.0 and 5.0 kDa were chosen for dicyclohexylcarbodiimide-mediated coupling reaction with EtVCP-CO_2H, affording two EtVCP-PDMS macromonomers (i.e. **MM-1** of 1.4 kDa and **MM-2** of 5.0 kDa; see supporting information). Polymerization with a [500]:[10]:[1] ratio of **MM-1**:DBMM:PC **1** under optimized conditions and irradiated with a white LED at 28 °C successfully achieved 95% conversion within 12 hours, producing molecular brush poly(EtVCP-PDMS) with M_n 67.4 kDa, low $Đ$ of 1.09, high I^* of 99%, and moderate S_L value of 77% (**Table 2.4, entry 1**). Increasing the macromonomer feed ratio to [1000]:[10]:[1] of **MM-1**:DBMM:PC **1** provided brush poly(EtVCP-PDMS) of 111 kDa, while good control over the polymerization was retained ($Đ$ = 1.26, I^* = 116%, entry 2). However, when targeting a higher degree of polymerization (200 or 400) in rROP of **MM-1**, the macromonomer conversions decreased (71–90%) while $Đ$ values increased (1.41–1.47), and it

became challenging to predictably tune the MW of the synthesized poly(EtVCP-PDMS) as the experimental MWs appreciably deviated from the theoretical values as indicated by I^* greater than 100 % (**Table 2.4, entries 3–5**). The side chain length also influenced the polymerization behavior in that the rROP of **MM-2** under optimized conditions with white LED irradiation at 28 °C generally achieved lower conversions and exhibited less control in terms of $Đ$, I^*, and S_L than the rROP of **MM-1** (**Table 2.4, entries 6–7** vs **1–2**). Interestingly, rROP of **MM-1** and **MM-2** with blue LED at 60 °C resulted in polymers possessing lower dispersities ($Đ$ = 1.06–1.10) and major cyclic compositions (S_L = 30–33%), affording brush poly(EtVCP-PDMS) with M_n of up to 308.7 kDa (**Table 2.4, entries 8–10**).

Table 2.4: *Synthesis of Molecular Brush Poly(EtVCP-PDMS).*[a]

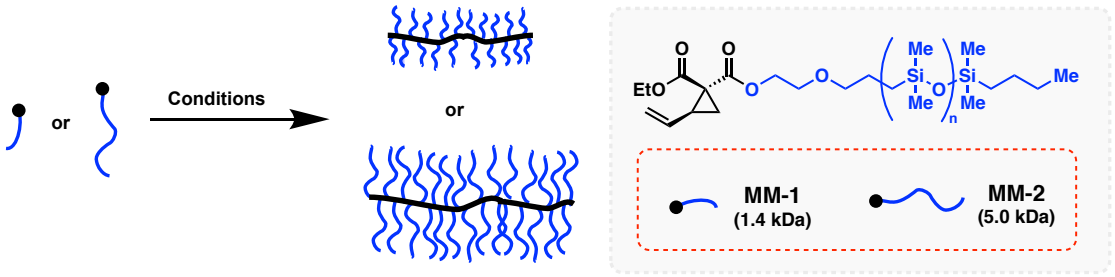

Entry	Macromonomer	[M]/[I]/[PC]	Time (h)	Conv. (%)[b]	M_n (kDa)[c]	$Đ$ (M_w/M_n)[c]	I^* (%)[d]	S_L (%)[b]
1	**MM-1**	500/10/1	12	95	67.4	1.09	99	77
2	**MM-1**	1000/10/1	12	95	111.0	1.26	116	66
3	**MM-1**	1000/5/1	12	90	102.7	1.47	245	63
4	**MM-1**	2000/10/1	12	78	141.7	1.41	149	60

5	**MM-1**	4000/10/1	12	71	208.8	1.41	184	60
6[e]	**MM-2**	500/10/1	12	84	84.5	1.14	160	74
7[e]	**MM-2**	1000/10/1	12	62	98.2	1.25	316	56
8[f,g]	**MM-1**	500/10/1	12	84	121.2	1.08	49	33
9[f,g]	**MM-1**	1000/10/1	12	82	165.0	1.10	70	31
10[f,h]	**MM-2**	500/10/1	12	75	308.7	1.06	61	30

[a]Polymerizations performed using 0.2 mmol of EtVCP-PDMS macromonomer, DBMM as the initiator, 0.5 mL of anhydrous EtOAc, and irradiated by white LED at 28 °C. [b]Measured by crude ^{1}H-NMR. $S_L = l/(l + c)$. [c]Measured by GPC. [d]Initiator efficiency (I^*) = $M_{n,theo}/M_{n,measured} \times 100\%$, where $M_{n,theo}$ = MW(DBMM) + MW(MM) × conversion × ([MM]/[DBMM]). [e]1.0 mL of EtOAc was used. [f]Polymerization was performed at 60 °C and with 34 W blue LED. [g]2.5 mL of anhydrous EtOAc was used. [h]5.0 mL of anhydrous EtOAc was used.

Conclusion

We have performed an study on the monomer scope for organocatalyzed photoredox radical ring-opening polymerization. The polymerizability of VCP monomers containing varying substituents at the C1 position was first evaluated, identifying that C1-ethoxycarbonyl resulted in the most efficient polymerization, which guided the subsequent incorporation of multiple functional natural products or their derivatives (such as vitamin E, uridine, dehydroabietic acid, and cholesterol) onto one ester group of EtVCP to expand the functional diversity of the monomers. The polymerization behavior of four natural product-derived VCP monomers was investigated using *N,N*-diaryldihydrophenzaines or 3,7-di(4-biphenyl)-*N*-naphthylphenoxazine as the photocatalyst. By varying the light sources (white LED or blue LED) and temperature (28 °C or 60 °C), natural product-derived poly(VCPs) with predictable MW, low dispersity, tunable linear or cyclic composition, and tailored thermal properties, were synthesized. Importantly, this

organocatalyzed photoredox protocol was also amenable to "grafting through" brush polymer synthesis through the polymerization of EtVCP-PDMS macromonomers with moderate to excellent control. These findings, demonstrated herein, improve the robustness of radical ring-opening polymerization of vinylcyclopropanes, and offer new opportunities for future design and preparation of structurally novel polymeric materials.

REFERENCES

1. Tardy, A.; Nicolas, J.; Gigmes, D.; Lefay, C.; Guillaneuf, Y. Radical Ring-Opening Polymerization: Scope, Limitations, and Application to (Bio)Degradable Materials. *Chem. Rev.* **2017**, *117*, 1319–1406.
2. Moszner, N.; Zeuner, F.; Völkel, T.; Rheinberger, V. Synthesis and Polymerization of Vinylcyclopropanes. *Macromol. Chem. Phys.* **1999**, *200*, 2173–2187.
3. Sanda, F.; Takata, T.; Endo, T. Radical Polymerization Behavior of 1,1-Disubstituted 2-Vinylcyclopropanes. *Macromolecules* **1993**, *26*, 1818–1824
4. Singha, N. K.; Kavitha, A.; Sarker, P.; Rimmer, S. Copper–Mediated Controlled Radical Ring-Opening Polymerization (RROP) of a Vinylcycloalkane. *Chem. Commun.* **2008**, 3049–3051.
5. Lad, J.; Harrisson, S.; Mantovani, G.; Haddleton, D. M. Copper Mediated Living Radical Polymerisation: Interactions Between Monomer and Catalyst. *Dalton Trans.* **2003**, 4175–4180.
6. Mittal, A.; Sivaram, S.; Baskaran, D. Unfavorable Coordination of Copper with Methyl Vinyl Ketone in Atom Transfer Radical Polymerization. *Macromolecules* **2006**, *39*, 5555–5558.
7. Theriot, J. C.; Lim, C.-H.; Yang, H.; Ryan, M. D.; Musgrave, C. B.; Miyake, G. M. Organocatalyzed Atom Transfer Radical Polymerization Driven by Visible Light. *Science* **2016**, *352*, 1082–1086.
8. Chen, D.-F; Boyle, B. M.; McCarthy, B. G.; Lim, C.-H.; Miyake, G. M. Controlling Polymer Composition in Organocatalyzed Photoredox Radical Ring-Opening Polymerization of Vinylcyclopropanes. *J. Am. Chem. Soc.* **2019**, *141*, 13268–3277.
9. Narayanam, J. M. R.; Stephenson, C. R. J. Visible Light Photoredox Catalysis: Applications in Organic Synthesis. *Chem. Soc. Rev.* **2011**, *40*, 102–113.
10. Prier, C. K.; Rankic, D. A.; MacMillan, D. W. C. Visible Light Photoredox Catalysis with Transition Metal Complexes: Applications in Organic Synthesis. *Chem. Rev.* **2013**, *113*, 5322–5363.
11. Schultz, D. M.; Yoon, T. P. Solar Synthesis: Prospects in Visible Light Photocatalysis. *Science* **2014**, *343*, 1239176.
12. Chen, M.; Zhong, M.; Johnson, J. A. Light-Controlled Radical Polymerization: Mechanisms, Methods, and Applications. *Chem. Rev.* **2016**, *116*, 10167–10211.
13. Corrigan, N.; Shanmugam, S.; Xu, J.; Boyer, C. Photocatalysis in Organic and Polymer Synthesis. *Chem. Soc. Rev.* **2016**, *45*, 6165–6212.
14. Corrigan, N.; Yeow, J.; Judzewitsch, P.; Xu, J.; Boyer, C. P Seeing the Light: Advancing Materials Chemistry through Photopolymerization. *Angew. Chem., Int. Ed.* **2019**, *58*, 5170−5189.

15. Discekici, E. H.; Anastasaki, A.; Read de Alaniz, J.; Hawker, C. J. Evolution and Future Directions of Metal-free Atom Transfer Radical Polymerization. *Macromolecules* **2018**, *51*, 7421–7434.
16. Fors, B. P.; Hawker, C. J. Control of a Living Radical Polymerization of Methacrylates by Light. *Angew. Chem., Int. Ed.* **2012**, *51*, 8850–8853.
17. Konkolewicz, D.; Schroder, K.; Buback, J.; Bernhard, S.; Matyjaszewski, K. Visible Light and Sunlight Photoinduced ATRP with ppm of Cu Catalyst. *ACS Macro Lett.* **2012**, *1*, 1219–1223.
18. Anastasaki, A.; Nikolaou, V.; Zhang, Q.; Burns, J.; Samanta, S. R.; Waldron, C.; Haddleton, A. J.; McHale, R.; Fox, D.; Percec, V.; Wilson, P.; Haddleton, D. M. Copper(II)/Tertiary Amine Synergy in Photoinduced Living Radical Polymerization: Accelerated Synthesis of ω-Functional and α,ω-Heterofunctional Poly(acrylates). *J. Am. Chem. Soc.* **2014**, *136*, 1141–1149.
19. Miyake, G. M.; Theriot, J. C. Perylene as an Organic Photocatalyst for the Radical Polymerization of Functionalized Vinyl Monomers through Oxidative Quenching with Alkyl Bromides and Visible Light. *Macromolecules* **2014**, *47*, 8255–8261.
20. Treat, N. J.; Sprafke, H.; Kramer, J. W.; Clark, P. G.; Barton, B. E.; Read de Alaniz, J.; Fors, B. P.; Hawker, C. J. Metal-Free Atom Transfer Radical Polymerization. *J. Am. Chem. Soc.* **2014**, *136*, 16096–16101.
21. Pan, X.; Malhotra, N.; Simakova, A.; Wang, Z.; Konkolewicz, D.; Matyjaszewski, K. Photoinduced Atom Transfer Radical Polymerization with ppm-Level Cu Catalyst by Visible Light in Aqueous Media. *J. Am. Chem. Soc.* **2015**, *137*, 15430–15433.
22. Xu, J.; Jung, K.; Atme, A.; Shanmugam, S.; Boyer, C. A Robust and Versatile Photoinduced Living Polymerization of Conjugated and Unconjugated Monomers and its Oxygen Tolerance. *J. Am. Chem. Soc.* **2014**, *136*, 5508–5519.
23. Shanmugam, S.; Xu, J.; Boyer, C. Exploiting Metalloporphyrins for Selective Living Radical Polymerization Tunable Over Visible Wavelengths. *J. Am. Chem. Soc.* **2015**, *137*, 9174–9185.
24. Kottisch, V.; Michaudel, Q.; Fors, B. P. Cationic Polymerization of Vinyl Ethers Controlled by Visible Light. *J. Am. Chem. Soc.* **2016**, *138*, 15535–15538.
25. Ogawa, K. A.; Goetz, A. E.; Boydston, A. J. Metal-Free Ring-Opening Metathesis Polymerization. *J. Am. Chem. Soc.* **2015**, *137*, 1400–1403.
26. Fu, C.; Xu, J.; Boyer, C. Photoacid-mediated ring opening polymerization driven by visible light. *Chem. Commun.* **2016**, *52*, 7126–7129.
27. Bruan, D., Cherdon, H., Rehahn, M., Ritter, H., Voit, B. *Polymer Synthesis: Theory and Practice; Fundamentals, Methods, Experiments*, 5th Eds.; Springer, Berlin, Heidelberg, **2013**.
28. Kristufek, S. L.; Wacker, K. T.; Tsao, Y.-Y. T.; Su, L.; Wooley, K. L. Monomer Design Strategies to Create Natural Product-Based Polymer Materials. *Nat. Prod. Rep.* **2017**, *34*, 433–459.
29. Ye, K.; Tang, C. Controlled Polymerization of Next-Generation Renewable Monomers and Beyond. *Macromolecules* **2013**, *46*, 1689–1712.

30. Pearson, R. M.; Lim, C.-H.; McCarthy, B. G.; Musgrave, C. B.; Miyake, G. M. Organocatalyzed Atom Transfer Radical Polymerization using N-Aryl Phenoxazines as Photoredox Catalysts. *J. Am. Chem. Soc.* **2016**, *138*, 11399–11407.
31. Milner, S. T. Polymer Brushers. *Science* **1991**, *251*, 905–914.
32. Advincula, R. C.; Brittain, W. J.; Caster, K. C.; Ruhe, J., Eds. *Polymer Brushes*; Wiley-VCH: Weinheim, Germany, **2004**.
33. Feng, C.; Li, Y. J.; Yang, D.; Hu, J. H.; Zhang, X. H.; Huang, X. Y. Well-Defined Graft Copolymers: from Controlled Synthesis to Multipurpose Applications. *Chem. Soc. Rev.* **2011**, *40*, 1282–1295.
34. Neugebauer, D.; Zhang, Y.; Pakula, T.; Sheiko, S. S.; Matyjaszewski, K. Densely-Grafted and Double-Grafted PEO Brushes via ATRP. A Route to Soft Elastomers. *Macromolecules* **2003**, *36*, 6746-6755.
35. Xie, M.; Dang, J.; Han, H.; Wang, W.; Liu, J.; He, X.; Zhang, Y. Well-Defined Brush Copolymers with High Grafting Density of Amphiphilic Side Chains by Combination of ROP, ROMP, and ATRR. *Macromolecules* **2008**, *41*, 9004-9010.
36. Xia, Y.; Kornfield, J. A.; Grubbs, R. H. Efficient Synthesis of Narrowly Dispersed Brush Polymers via Living Ring-Opening Metathesis Polymerization of Macromonomers. *Macromolecules* **2009**, *42*, 3761-3766.
37. Johnson, J. A.; Lu, Y. Y.; Burts, A. O.; Lim, Y.-H.; Finn, M. G.; Koberstein, J. T.; Turro, N. J.; Tirrell, D. A.; Grubbs, R. H. Core-Clickable PEG-Branch-Azide Bivalent-Bottle-Brush Polymers by ROMP: Grafting-Through and Clicking-To. *J. Am. Chem. Soc.* **2011**, *133*, 559-566.
38. Synthesis of Poly(OEOMA) Using Macromonomers via "Grafting-Through" ATRP. Cho, H. Y.; Krys, P.; Szcześniak, K.; Schroeder, H.; Park, S.; Jurga, S.; Buback, M.; Matyjaszewski, K. *Macromolecules* **2015**, *48*, 6385-6395.

CHAPTER 3 – TERPENOID-BASED HIGH-PERFORMANCE POLYESTER WITH TACTICITY-INDEPENDENT CRYSTALLINITY AND CHEMICAL CIRCULARITY

Overview

The development of chemically circular, bio-based polymers is an urgently needed solution to combat the plastic waste crisis. However, the most prominent, commercially implemented bio-based aliphatic polyester, poly(lactic acid) (PLA), is brittle, therefore largely limiting its broad applications. Herein, we introduce a class of aliphatic polyesters produced through the ring-opening polymerization (ROP) of (1R,5S)-8,8-dimethyl-3-oxabicyclo[3.2.1]octan-2-one (D-CamL) and the racemic mixture (rac-CamL), which exhibit superior materials properties relative to PLA. A metal-based or organic catalyst was used for the modulation of polymer tacticity. Notably, regardless of tacticity, poly(CamL) exhibits intrinsic crystallinity resulting in polyesters with high yield stress (24–39 MPa), high Young's modulus (1.36–2.00 GPa), tunable fracture strains (6–218%), and high melting temperatures (161–225 °C). Importantly, poly(CamL) can be chemically recycled to monomer in high yield and the virgin-quality poly(CamL) was obtained after repolymerization. Overall, poly(CamL) represents a new class of bio-derived and chemically circular high-performance polyesters.

Introduction

Plastic products have become ubiquitous and irreplaceable in modern life but linear life cycles and poor end-of-life options result in significant environmental issues such as waste accumulation and consumption of finite resources.[1,2] Plastic recycling is critical but traditional mechanical recycling methods yield materials with diminished properties and reduced value.[3,4] To address the shortcomings of mechanical recycling, alternative recycling strategies that enable the retention of material properties are needed.[5] Among these approaches, closed-loop chemical recycling is a desirable technology in which polymeric materials can be efficiently deconstructed into their starting monomers or oligomers and repolymerized into chemically identical, virgin-like polymer materials.[6-10]

In addition to chemical circularity, polymer sustainability can further be enhanced by the use of bio-derived monomers and feedstocks, especially those that do not come from food sources.[11] Among chemically recyclable bio-derived polymers, PLA has become particularly prevalent given its relatively low-cost,[12] processability,[13] chemical recyclability,[14,15] and generally desirable properties.[16,17] The crystalline and amorphous states of PLA are strongly dependent on the stereochemistry of the polymer backbone, with isotactic and syndiotactic PLA exhibiting crystallinity. Syndiotactic PLA has a lower glass transition temperature (T_g) and melting temperature (T_m) but a higher crystallization temperature (T_c) than isotactic PLA.[18] Regardless of being crystalline or amorphous, the low elongation at break ($\varepsilon B < 10\%$) of PLA and its high water and oxygen permeability limit the use of PLA materials in packaging applications.[17,19,20] In terms of the recycling of isotactic PLLA, the selective depolymerization to enantiopure monomer can be

challenging.[14,15] As such, the shortcomings of PLA inspired us to explore new bio-derived polymers that may have materials properties comparable to, or exceeding those of PLA.

Several notable innovations toward chemically recyclable plastics have been recently made. For example, 1,3-dioxolane (DXL), made from industrial feedstocks formaldehyde and ethylene glycol, is regarded as a green building block for recyclable plastic and can be polymerized by cationic ROP to yield high molecular weight poly(DXL) with potential for use as a packaging material. Poly(DXL) can be chemically recycled back to DXL, demonstrating an example of a successful circular plastic economy.[21,22] However, the low T_m of poly(DXL) (~60 °C) may limit its application in certain applications. Similarly, polymer made from the bio-derived monomer δ-valerolactone (VL) also has a low T_m (~57 °C). In order to make chemically recyclable, bio-based polymers that are tolerant to higher temperatures, structural modification of commercially available monomers can be a promising platform.[23] One example of such structural modification is the addition of geminal dialkyl (gem-dialkyl) functionality. In the case of VL, gem-disubstitution yields a gem-diakyl-substituted polymer, poly(VLR2) possessing a high T_m (~140 °C). Additionally, poly(VLR2) has good mechanical properties (ε_B could reach 322%) and a reduced ceiling temperature ($T_{ceiling}$, defined as equilibrium temperature between polymerization and depolymerization) from 298 °C for VL to 67 °C for VLR2 at 1 M.[24] The low ceiling temperature of poly(VLR2) makes it easier to thermally depolymerize than unsubstituted poly(VL) which can be explained by the fact that gem-dialkyl substitution enables harnessing of the Thorpe-Ingold effect[25,26] to promote ring closure during depolymerization, thereby enabling facile recovery of

monomer. Polyhydroxyalkanoates (PHAs) are another important class of bio-derived polyesters with potential to serve as analogues for PLA. However, their general thermal instability, and mechanical brittleness limit materials properties while their propensity for α-hydrogen elimination render them difficult to efficiently depolymerize back to their starting lactones.[27] Gem-dialkyl-substitution at the α-position of poly(3-hydroxybutyrate) (P3HB) produces poly(3-hydroxy-2,2-dialkylbutyrate) [P3H(alkyl)2B], which exhibits the unique property of intrinsic crystallinity, can undergo melt processing, and can be recycled back to the corresponding lactone by NaOH at 210 °C. The ε_B could reach 517% after gem-disubstitution, thus displaying significant improvement in mechanical properties relative to the unsubstituted polymer (ε_B, ~4%).[28] These reports demonstrate that gem-dialkyl-substitution can increase the materials properties and help realize the closed-loop recycling of bio-based polymers under mild conditions.

In addition to the gem-dialkyl-substitution strategy applied in monomer design, a recently developed hybrid monomer (or hybrid bicyclic monomer) strategy results in increased ease of chemical recycling as well as increased T_m and T_g.[29-32] Hybrid monomers combine the structures of monomers possessing a high ring-strain and low $T_{ceiling}$, where structural motifs imparting high ring-strain facilitate the facile polymerization of the hybrid monomer while motifs imparting a low $T_{ceiling}$ allow for efficient depolymerization. It is also noteworthy that the bridged bicyclic structure of the hybrid monomer facilitates depolymerization to selectively yield the cis-configuration monomer. With gem-dialkyl-substitution and hybrid monomer design strategies in mind, we hypothesized that terpenes or terpenoids would be suitable structures for constructing recyclable

polyesters merging natural hybrid and gem-dialkyl-substitution approaches.[33,34] Terpene- and terpenoid-based polymers are relatively well-studied with many polymers possessing high T_g (70 °C, 130 °C) or high strength at break (70 MPa), but most are amorphous even if the isotactic polymer is obtained.[35-41] As such, the structural modification of terpenes or terpenoids for developing high-performance polymer materials is warranted. In the realm of terpenes and terpenoids, camphor is widely used in daily life and organic synthesis.[42-44] Similar to lactide, the monomer unit of PLA (**Figure 3.1**), optically pure D-camphor ((1R,4R)-bornan-2-one) can be isolated from biomass while the racemic mixture of camphor can be obtained through chemical synthesis from α-pinene (obtained from turpentine).[45] The molecular weights of previously reported camphor-derived polymers by condensation polymerization have not exceeded 20 kDa and are brittle materials ($\varepsilon_B < 15\%$) which limits their application[46-48] while ROP is more successful for producing higher molecular weight polymers.[49,50] The presence of a methyl group on the bridgehead carbon in the backbone of these polymers impedes their ability to crystallize and only amorphous polymer is obtained while their T_g is higher than room temperature and polymers produced from camphor are rigid at room temperature.[46]

To broaden the application of terpene- or terpenoid-based polymers, we sought to use the structural modification strategy to design a camphor-based polymer that exhibited crystallinity and high-performance materials properties. We realized that the hybrid and gem-dimethyl structural motifs naturally occurring in camphor should be retained but the monomethyl group on the bridgehead carbon should be removed to enable crystallization. Ultimately, the proposed lactone,

(1R,5S)-8,8-dimethyl-3-oxabicyclo[3.2.1]octan-2-one (D-CamL) and the racemic mixture (rac-CamL or DL-CamL) (**Figure 3.1** and **Figure S3.1**), were obtained. Both D-CamL and rac-CamL were polymerized via ROP to relatively high molecular weight. Thanks to the hybrid and gem-dimethyl structure in the CamL repeat unit, poly(CamL) has intrinsic crystallinity and exhibits similar thermal properties and yield stress to PLA but with higher ε_B, and lower water and oxygen permeability. Furthermore, the closed-loop recycling of poly(CamL) could be easily performed under mild conditions (**Figure 3.1**).

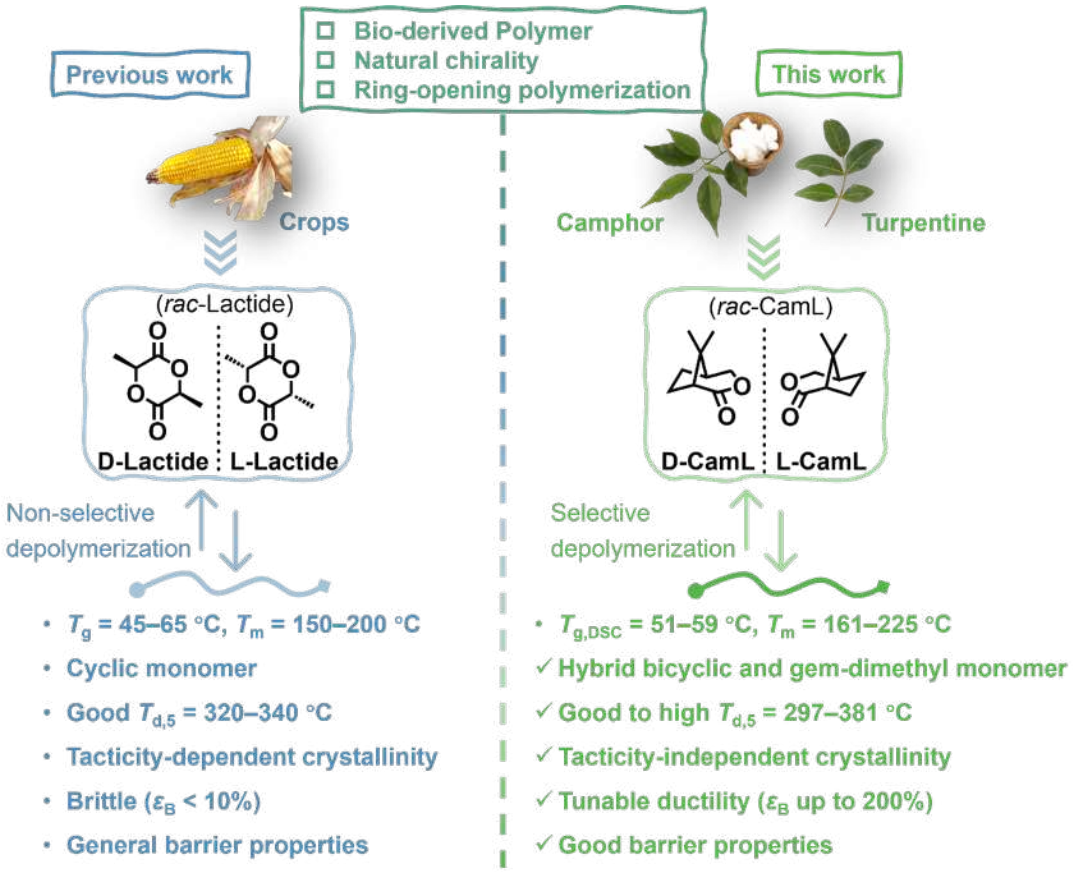

***Figure 3.1**: comparison between PLA and poly(CamL).*

Results and Discussion

Monomer design and polymerization

The D-camphor-derived lactone produced directly from the Baeyer-Villiger oxidation of D-camphor was not polymerizable under various conditions investigated (**Table S3.1**). We hypothesized that the a-methyl group inhibited the polymerization, presumably due to the steric hindrance of the methyl group in proximity to the carbonyl group. As such, we synthesized a D-camphor lactone derivative (D-CamL) devoid of the methyl group on the bridgehead carbon to investigate the polymerization of this monomer.

Initial attempts at the ROP of D-CamL used tris[N,N-bis(trimethylsilyl)amide]lanthanum [$La(N(SiMe_3)_2)_3$] as the catalyst, which has demonstrated success with benzyl alcohol as the initiator. Using $La(N(SiMe_3)_2)_3$ to catalyze the polymerization of D-CamL was only successful at elevated temperatures, achieving 68% conversion at 100 °C after 2.0 h (M_w = 9.80 kDa, **Table 3.1**, **Run 1**). Given that $La(N(SiMe_3)_2)_3$ is slightly expensive, tin octanoate [$Sn(Oct)_2$] was investigated as an alternative catalyst. However, when $Sn(Oct)_2$ was used for the polymerization of D-CamL at 100 °C, there was no monomer conversion after 8 hours (**Table S3.2**). Encouraged by the successful initial polymerization of D-CamL by $La(N(SiMe_3)_2)_3$, we explored organic catalysts. A series of common compounds (**Table 3.1, Run 2**) were investigated for the ROP of D-CamL, including 1,8-diazabicyclo(5.4.0)undec-7-ene (DBU), 1,5,7-triazabicyclo 4.4.0 dec-5-ene (TBD), and 1-tert-butyl-2,2,4,4,4-pentakis(dimethylamino)-2λ^5,4λ^5-catenadi(phosphazene) (^{t}BuP$_2$), but none of the initial attempts at the base-mediated ROP of D-CamL were successful. Given that all compounds investigated are basic enough to deprotonate the initiator, we hypothesized that the

polymerization of D-CamL could only proceed when the ion pair (formed through hydrogen (H)-bonding) between the protonated catalyst and propagating chain ends is sufficiently weak.[51-53]

To test this hypothesis, 1-tert-butyl-4,4,4-tris(dimethylamino)-2,2-bis[tris(dimethylamino)-phosphoranylidenamino]-2λ^5,4λ^5-catenadi(phosphazene)

***Table 3.1**: Polymerization Results of D-CamL*[a]

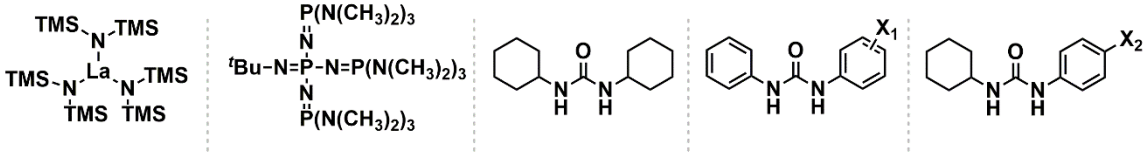

$La(N(SiMe_3)_2)_3$ | $^tBuP_4$ | urea 1 | urea 2: X_1 = H; urea 3: X_1 = CF_3 (*p*-); urea 4: X_1 = CF_3 (*m*-) | urea 5: X_2 = H; urea 6: X_2 = ^{t}Bu

Run	Catalyst	Time (h)	Conv. (%) [b]	M_w (kDa) [c]	$Đ$ [c]	T_g (ºC) [d]	T_m (ºC) [d]	ΔH_f (J/g) [d]	cis-/trans- (%/%) [e]
1	$La(N(SiMe_3)_2)_3$	2.0	68	9.80	1.30	/	186/216	29.0	100/0
2	Common bases[f]	24	/	/	/	/	/	/	/
3	$^tBuP_4$	1.0	88	34.5	1.50	58	169	30.6	61/39
4	$^tBuP_4$/urea	24	37	11.1	1.31	/	/	/	70/30
5	$^tBuP_4$/TU	24	/	/	/	/	/	/	/
6	$^tBuP_4$/urea 1	1.0	89	27.5	1.48	53	161	30.2	60/40
7	$^tBuP_4$/urea 2	20	55	16.0	2.06	59	171	21.9	77/23
8	$^tBuP_4$/urea 3	80	41	14.4	1.33	/	170/195	27.3	92/8

9	^{t}BuP$_4$/urea 4	80	48	17.8	1.60	51	164/199	26.0	88/12
10	^{t}BuP$_4$/urea 5	6.0	96	24.2	1.77	59	188	25.0	67/33
11	^{t}BuP$_4$/urea 6	3.5	91	28.6	1.80	58	174	25.3	64/36

*[a] Conditions: conducted in THF at room temperature except **Run 1** conducted in toluene at 100 °C, initiated by BnO$^-$, and monomer concentration was 100 mg D-CamL in 200 µL THF, [M]:[BnOH]:[Cat.] = 100:1:1 except **Run 1** [M]:[BnOH]:[Cat.] = 70:1:1. [b] Monomer conversions determined by ^{1}H NMR of the crude solution in $CDCl_3$ after quenching with benzoic acid. [c] Weight-average molecular weights (M_w), and dispersity ($Đ = M_w/M_n$) determined by gel-permeation chromatography (GPC) coupled with light scattering at 40 °C in $CHCl_3$. [d] T_g, T_m, and heat of fusion (ΔH_f) measured by differential scanning calorimetry (DSC) using the second heating scan at a rate of 10 °C min^{-1}. [e] Measured by the carbonyl region of ^{13}C NMR in $CDCl_3$. [f] Catalysts summarized in **Run 2**: DBU, TBD, and ^{t}BuP$_2$. [g] Reaction was stopped after 20 hours because the mixture solidified. Note: ^{1}H NMR spectra, ^{13}C NMR spectra, thermogravimetric analysis (TGA) results, and DSC results can be found in **Figures S3.8**-**S3.19**.*

was investigated and in 1.0 h successful conversion of monomer to polymer (88%) was observed (M_w = 34.5 kDa, **Table 3.1**, **Run 3**), supporting the hypothesis that the ion pair [^{t}BuP$_4$-H$^+$…O$^-$] must be weak enough for polymerization to proceed.

The polymerization solvent was subsequently investigated to achieve higher monomer conversion and greater polymerization control. In comparing poly(D-CamL) synthesized in acetonitrile (ACN), dimethylformamide (DMF), and toluene with poly(D-CamL) synthesized in tetrahydrofuran (THF), we found that there was no conversion of monomer in ACN, higher dispersity in DMF ($Đ$ = 1.96 in DMF, $Đ$ = 1.50 in THF), and much lower conversion of monomer in toluene (51% after 1 hour). Therefore, THF was selected as the polymerization solvent moving forward (**Table 3.1**, **Run 3** and **Table S3**). To assess the control over the polymerization of D-

CamL catalyzed by ^{t}BuP$_4$, monomer conversion and polymer molecular weight were monitored over reaction time. Pseudo-first-order kinetics with respect to monomer (R^2 = 0.990, **Figure S3.20A**) were observed and polymer molecular weight increased linearly as a function of conversion (R^2 = 0.973, **Figure S3.20B**). Matrix-assisted laser desorption/ionization time-of-flight (MALDI-TOF) of poly(D-CamL) (**Table 3.1**, **Run 3**) supported that the polymerization of D-CamL was initiated by BnO$^-$ (**Figure S3.20C**). However, a cyclic polymer chain could be seen with low molecular weight species in the MALDI-TOF mass spectrum (**Figures S3.20C and S3.20D**) of poly(D-CamL) indicating that intramolecular transesterification occurred during the polymerization process, thereby limiting polymerization control and resulting in increased polymer dispersity. When polymerization kinetics, molecular weight trends, and polymer structural analysis are considered collectively, the ROP of D-CamL catalyzed by ^{t}BuP$_4$ is not well-controlled. We conclude that control was limited by secondary transesterification reactions, where intramolecular transesterification could result in the formation of cyclic polymer chains.

Binary catalyst system

When comparing the ^{13}C NMR spectra of poly(D-CamL) synthesized using La(N(SiMe$_3$)$_2$)$_3$ and ^{t}BuP$_4$ (**Figure 3.2A**), it was deduced that the use of La(N(SiMe$_3$)$_2$)$_3$ resulted in isotactic poly(D-CamL) (**Table 3.1**, **Run 1**) with full cis-structure while the use of ^{t}BuP$_4$ resulted in atactic poly(D-CamL) (**Table 3.1**, **Run 3**) with a cis-/-trans ratio of 61/39. The carbonyl region of the ^{13}C NMR spectrum of poly(D-CamL) (**Table 3.1**, **Run 1**) showed only one peak indicating isotactic polymer while the ^{13}C NMR spectrum of poly(D-CamL) (**Table 3.1**, **Run 3**) showed two

separated peaks indicating non-uniformity in the stereoregularity. We hypothesized that the formation of atactic poly(D-CamL) resulted from epimerization of the bridgehead carbon near to the carbonyl group in the presence of the superbase ^{t}BuP$_4$ (**Figure S3.2**). To test this hypothesis, purified isotactic poly(D-CamL) (**Table 3.1**, **Run 1**) was treated with ^{t}BuP$_4$ in THF; after stirring for 2.0 h, atactic poly(D-CamL) with a cis-/trans- = 60/40 was produced (**Figure S3.21**).

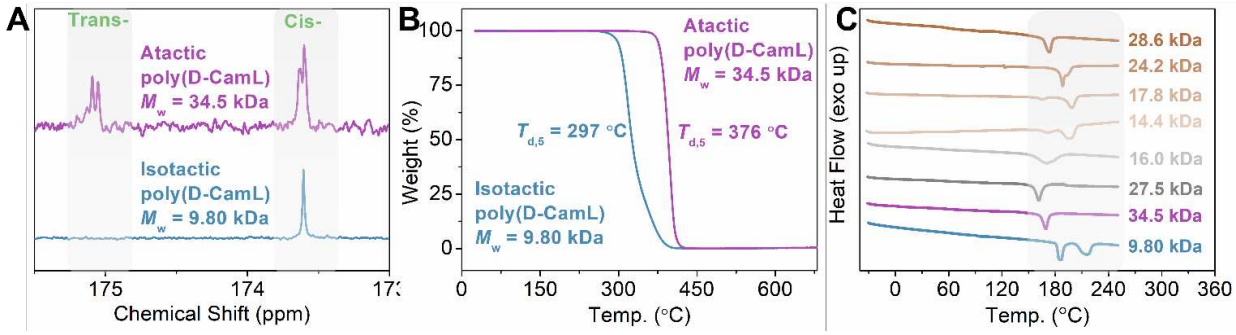

Figure 3.2: *Properties of poly(D-CamL) prepared with different catalysts reported in Table 3.1.* ***(A)*** *^{13}C NMR ($CDCl_3$, 23 °C) spectra of the* ***Run 1*** *(blue line, isotactic) and* ***Run 3*** *(purple line, atactic) in $CDCl_3$.* ***(B)*** *TGA curves of the* ***Run 1*** *(blue line, isotactic) and* ***Run 3*** *(purple line, atactic).* ***(C)*** *DSC profiles of the polymers came from* ***Runs 1, 3, 6-11****, showing the second heating scans at 10 °C/min.*

The thermal properties of the polymers possessing different tacticity were investigated. TGA of isotactic poly(D-CamL) (**Table 3.1**, **Run 1**) and atactic poly(D-CamL) (**Table 3.1**, **Run 3**) demonstrated that isotactic poly(D-CamL) ($T_{d,5}$ = 297 °C, defined by the temperature at 5% weight loss) decomposes at a much lower temperature than atactic poly(D-CamL) ($T_{d,5}$ = 376 °C). As such, the $T_{d,5}$ of the converted atactic poly(D-CamL) from isotactic poly(D-CamL) (**Table 3.1**, **Run 1**) is 370 °C (**Figure S3.21**). The TGA results may be attributed to the tendency of isotactic poly(D-CamL) to depolymerize to the cyclic monomer of D-CamL while the trans-structure

present in atactic poly(D-CamL) chains impedes the formation of monomer (**Figure S3.3**). The different thermal properties of the isotactic and atactic poly(D-CamL) further motivated us to investigate the stereocontrolled polymerization of D-CamL.

We next investigated the effects of adding an epimerization inhibitor to the polymerization with ^{t}BuP$_4$. Urea, thiourea, and their derivatives are commonly utilized as epimerization inhibitors.[54,55] We evaluated the effects of a series of these compounds on the polymerization of D-CamL catalyzed by ^{t}BuP$_4$. Upon polymerization, we found that the binary catalyst system, consisting of ^{t}BuP$_4$ and various urea derivatives allowed for the synthesis of poly(D-CamL) with varied tacticity (cis-/trans- ratio), where tacticity could be altered by changing the structure of the urea derivative added. Addition of commercially available carbonyl diamide (urea) and thiourea (TU) were investigated on the polymerization of D-CamL. Addition of urea resulted in a significant decrease in the polymerization rate (37% after 24 h) and a slight increase in the formation of cis- repeat units over trans- (cis-/trans- = 70/30), poly(D-CamL) (**Table 3.1**, **Run 4**). The improved cis-/trans- ratio indicated that urea slightly suppressed epimerization. Conversely, the addition of TU resulted in no conversion of D-CamL (**Table 3.1**, **Run 5**). We hypothesized that the lack of monomer conversion may be attributed to the formation of H-bonding. TU possessing a lower pK_a would form a stronger H-bond with O^- (active chain end) and -C=O (carbonyl group) in the monomer compared to urea (proposed mechanism in **Figure S3.4**). Furthermore, the use of TU combined with ^{t}BuP$_4$ results in significant steric hindrance which may

impede polymerization. Based on these results of using urea and thiourea additives, only urea derivatives were investigated further.

Two commercially available substituted ureas, N,N'-dicyclohexylurea (urea 1) and N,N'-diphenylurea (urea 2), were studied as additives in the polymerization of D-CamL catalyzed by ^{t}BuP$_4$. Upon addition of urea 1 (pK_a = 26.9, **Figure S3.5**), 89% conversion was achieved after 1.0 hour and poly(D-CamL) (M_w = 27.5 kDa, cis-/trans- = 60/40, T_m = 161 °C, **Table 3.1**, **Run 6**, **Figure 3.2C**) exhibited a lower cis-/trans- ratio and T_m compared to poly(D-CamL) (**Table 3.1**, **Run 3**). Upon utilizing urea 2 (pK_a = 20.8, **Figure S3.5**), the resulting poly(D-CamL) (M_w = 16.0 kDa, cis-/trans- = 77/23, T_m = 171 °C, **Table 3.1**, **Run 7**, **Figure 3.2C**) has higher tacticity compared to poly(D-CamL) produced using urea 1 (**Table 3.1**, **Run 6**), which suggested that the lower pK_a value of the substituted urea additive resulted in reduced epimerization. To test this hypothesis, we further decreased the pK_a of the urea additive by introducing strongly electron-withdrawing groups (-CF_3) at the para- (urea 3) and meta- (urea 4) positions. The poly(D-CamL)s obtained when adding either urea 3 or urea 4 (**Table 3.1**, **Run 8** and **Table 3.1**, **Run 9**, respectively) have a higher tacticity (cis-/trans- were around 90/10) but at the cost of monomer conversion as less than 50% conversion was observed after 80 h. The decreased monomer conversion and increased tacticity observed when lower pK_a urea derivatives were used may be explained by considering H-bonding between urea and both the O^- and -C=O in the monomer. The urea with lower pKa will have stronger H-bonding,[56] resulting in reduced reactivity and basicity of O^-. The proposed mechanism is depicted in **Figure S3.4**.

To achieve balance between tacticity and rate of monomer conversion, two asymmetric ureas, N-Cyclohexyl-N'-phenylurea (urea 5) and N-Cyclohexyl-N'-[4-(1,1-dimethylethyl)phenyl]urea (urea 6) were investigated as additives in the polymerization of D-CamL. Consistent with the pK_a value of urea 5 falling between that of urea 1 and urea 2 (**Figure S3.5**), the tacticity of the resulting poly(D-CamL) (M_w = 24.2 kDa, cis-/trans- = 67/33, **Table 3.1**, **Run 10**) was between that of poly(D-CamL) catalyzed by ^{t}BuP$_4$/urea 1 (**Table 3.1**, **Run 6**) and poly(D-CamL) catalyzed by ^{t}BuP$_4$/urea 2 (**Table 3.1**, **Run 7**). Additionally, the polymerization catalyzed by ^{t}BuP$_4$/urea 5 reached 96% conversion after 6.0 h which was also between that of the ^{t}BuP$_4$/urea 1 and ^{t}BuP$_4$/urea 2 catalyzed polymerization. To further decrease the time required to achieve high monomer conversion, an electron-donating group (tert-butyl group, -^{t}Bu) was introduced at the para- position of the phenyl group in urea 5, resulting in urea 6. The ^{t}BuP$_4$/urea 6 system resulted in high monomer conversion in decreased reaction time (91% after 3.5 h, **Table 3.1**, **Run 11**) compared to ^{t}BuP$_4$/urea 5 (**Table 3.1**, **Run 10**). These results demonstrate that a binary system comprised of ^{t}BuP$_4$ and urea can be used to prepare poly(D-CamL) with variable tacticity.

Proposed mechanism for modulation of tacticity

To help further explain the modulation of tacticity when the polymerization of D-CamL is catalyzed by La(N(SiMe$_3$)$_2$)$_3$, ^{t}BuP$_4$, and ^{t}BuP$_4$/urea, we proposed the mechanism shown in **Figure 3.3**. When the ^{t}BuP$_4$ was used to polymerize D-CamL without the addition of a urea, the weak interaction between the O^- and [^{t}BuP$_4$-H]$^+$ enables facile deprotonation (intra- and inter- chain

deprotonation shown in **Figure S3.2**) of the methylene near the carbonyl group forming a carbanion intermediate through which the trans- repeat unit can be formed. With the addition of a urea cocatalyst, H-bonding occurs between the urea, D-CamL, and the O^- on the propagating polymer chain-end. H-bonding between O^- and urea stabilizes the O^-, thereby further lowering the probability of carbanion intermediate formation. Therefore, addition of urea would alter the relative quantity of trans- repeat units. In contrast to ^{t}BuP$_4$, the La(N(SiMe$_3$)$_2$)$_3$ would not deprotonate the methylene near the carbonyl group. Therefore, isotactic poly(D-CamL) is obtained by using La(N(SiMe$_3$)$_2$)$_3$.

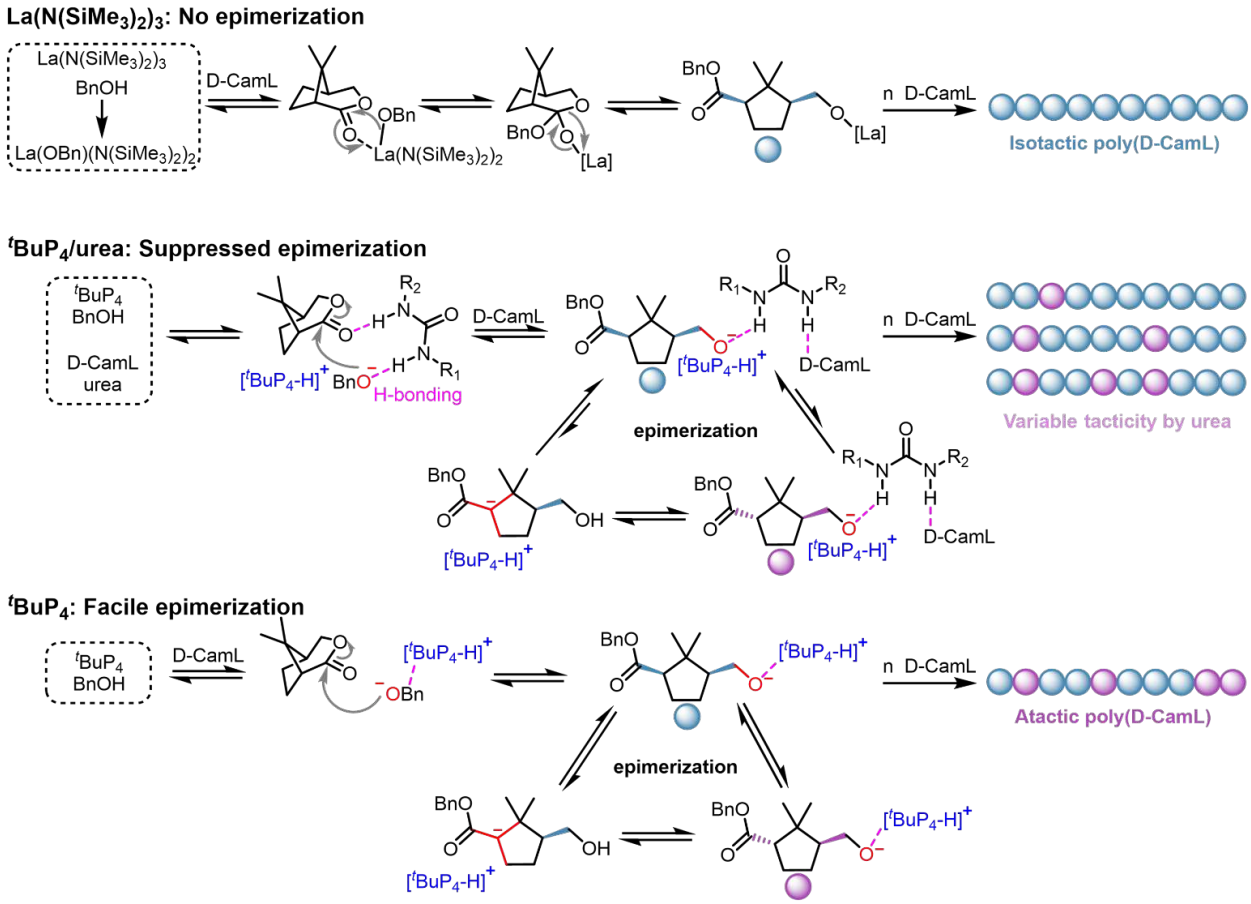

Figure 3.3: *Proposed mechanism of epimerization in the presence of ^{t}BuP$_4$, ^{t}BuP$_4$/urea, and La(N(SiMe$_3$)$_2$)$_3$.*

Materials Properties of poly(D-CamL)

$La(N(SiMe_3)_2)_3$, $^tBuP_4$/urea 1, and $^tBuP_4$/urea 6 were chosen as the catalyst systems to prepare larger quantities of poly(D-CamL) required for materials property analysis because these three systems allowed for production of polymers possessing a range of cis-/trans- ratios. Poly(D-CamL) catalyzed by $^tBuP_4$/urea 1, $^tBuP_4$/urea 6, and $La(NSiMe_3)_2)_3$ (**Table 3.2**, **Runs 2, 3,** and **1,** respectively) were obtained and the T_m increased from 169 ºC to 182 ºC and 186/225 ºC respectively (**Figure 3.3A**), in accordance with the cis-/trans- ratio change from 58/42 to 61/39 to 100/0. We also noticed that the ΔH_f of polymers reported in **Table 3.2** are lower than the ΔH_f the polymers reported in **Table 3.1**. This phenomenon could be attributed to slower rates for crystallization occurring in higher molecular weight polymers due to the reduced mobility of the chain segments; incomplete crystallization leads to reduced ΔH_f.

Table 3.2: *Polymerization results of D-CamL with tunable cis-trans- ratios.*[a]

Run	Monomer	Catalyst	Conv. (%) [b]	M_w (kDa) [c]	$Đ$ [c]	T_g (ºC) [d]	T_m (ºC) [d]	ΔH_f (J/g) [d]	cis-/trans- (%/%) [e]
1	D-CamL	$La(N(SiMe_3)_2)_3$	41	78.8	1.44	/	186/225	19.0	100/0
2	D-CamL	$^tBuP_4$/urea 1	56	48.1	1.45	58	169	24.0	58/42
3	D-CamL	$^tBuP_4$/urea 6	40	79.4	1.57	62	182	15.3	61/39
4	*rac*-CamL	$^tBuP_4$/urea 1	57	78.2	1.67	63	184	18.0	62/38

*[a]Conditions: Polymerizations were conducted in THF at 50 °C except **run 1**, which was performed in toluene at 100 °C, 12 hours duration, the monomer concentration is 1 g CamL in 1.5 mL solvent, and the feed ratio [M]:[I]:[Cat.] = 1000:1:3 except **run** 1 which [M]:[I]:[Cat.] = 1000:1:2. [b]Monomer conversions were measured by ^{1}H NMR of the crude solution after quenching in $CDCl_3$. [c]M_w, and Đ (Đ = M_w/M_n) determined by GPC coupled with light scattering at 40 °C in $CHCl_3$. [d]T_g, T_m, and ΔH_f measured by DSC in the second heating scan at a rate of 10 °C min^{-1}. [e]cis-/trans- ratio measured by ^{13}C NMR in the carbonyl region in $CDCl_3$. Note: All TGA and DSC results can be found in **Figures S3.22-S3.25**.*

The mechanical properties of poly(D-CamL) with varying tacticity were investigated by tensile testing of dog bone-shaped specimens prepared from films produced by compression molding and quenched with water cooling. Atactic poly(D-CamL) (M_w = 48.1 kDa, **Table 3.2**, **Run 2**) exhibited an ε_B, 218 ± 24%, Young's modulus of E = 1.64 ± 0.08 GPa, and a high yield stress of 28.0 ± 2.2 MPa (**Figure 3.4B**). These results revealed that atactic poly(D-CamL) catalyzed by ^{t}BuP$_4$/urea 1 was a hard and strong material with moderate ductility which has higher E and comparable yield stress to HDPE[8] (E = 1.10 GPa, yield stress of around 25 MPa).

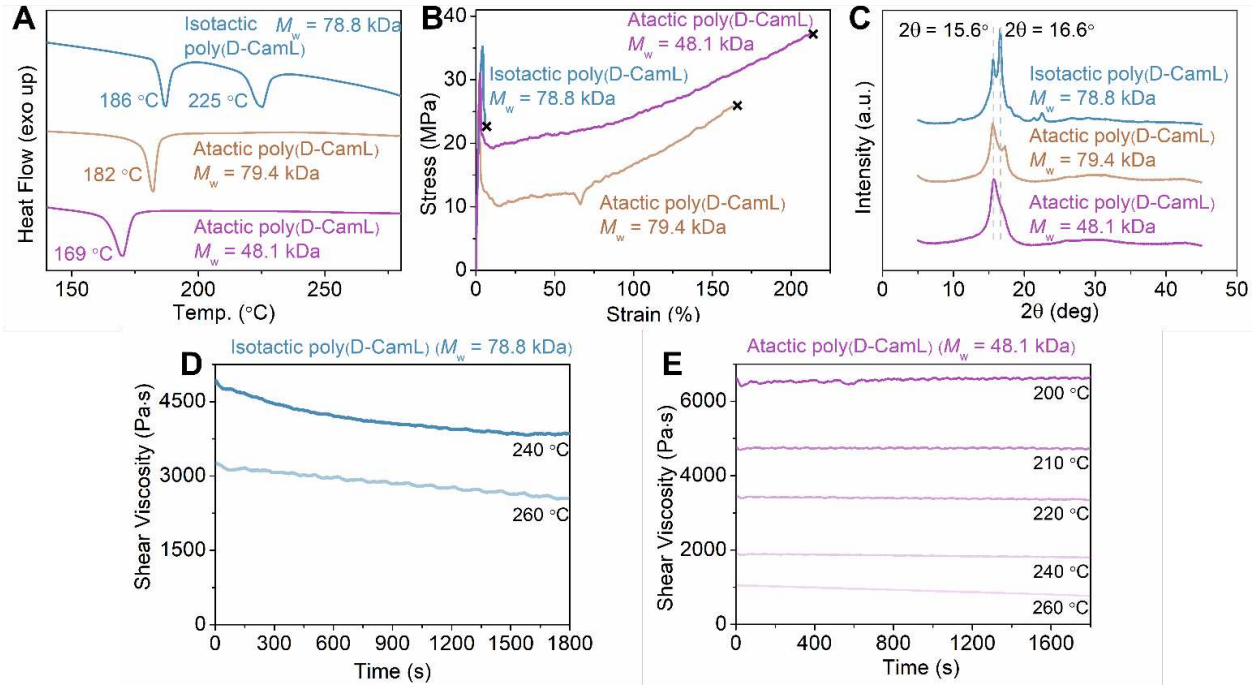

Figure 3.4: *Thermal, mechanical, Wide-angle X-ray diffraction (WAXD), and rheology characterization results of poly(D-CamL) from Table 3.2, Runs 1-3.*
(A) *DSC curves of the poly(D-CamL).* ***(B)*** *Representative stress-strain curves of the poly(D-CamL), extension rate = 5 mm/min, ambient condition.* ***(C)*** *WAXD plots of the poly(D-CamL).* ***(D)*** *&* ***(E)*** *Shear viscosity plots ($\dot{r}$ = 0.5 s^{-1}) in melt of isotactic poly(D-CamL) (M_w = 78.8 kDa) and atactic poly(D-CamL) (M_w = 48.1 kDa).*

The ^{t}BuP$_4$/urea 6 catalyzed poly(D-CamL) (M_w = 79.4 kDa, **Table 3.2**, **Run 3**) had a higher tacticity than ^{t}BuP$_4$/urea 1 catalyzed poly(D-CamL) (**Table 3.2**, **Run 2**) and exhibited a decreased ε_B, 163 ± 22% (**Figure 3.4B**). In contrast, the isotactic poly(D-CamL) (M_w = 78.8 kDa, **Table 3.2**, **Run 1**) catalyzed by La(N(SiMe$_3$)$_2$)$_3$ was brittle; the ε_B was only 6 ± 2%, but the yield stress was notably high at 33.8 ± 2.7 MPa (**Figure 3.4B**). Overall, the results of the tensile testing for poly(D-CamL) indicate that isotactic poly(D-CamL) has the highest yield stress but the lowest ε_B, while atactic poly(D-CamL) has a higher ε_B for greater ductility.

The WAXD (Wide-angle X-ray diffraction, **Figure 3.4C**) revealed one main peak at 2θ = 15.6º for atactic poly(D-CamL) (**Table 3.2**, **Run 2**), whereas WAXD of atactic poly(D-CamL) (**Table 3.2**, **Run 3**) exhibited a shoulder peak at 2θ = 16.6º because of the increased cis-/trans-ratio. Notably, the isotactic poly(D-CamL) (**Table 3.2**, **Run 1**) showed two main peaks at 2θ = 15.6º and 16.6º. The lack of the peak at 2θ = 16.6º of atactic poly(D-CamL) (**Table 3.2**, **Run 2**) could be explained by crystal defects in atactic poly(D-CamL) arising from chain disorder.[57] As a result, the isotactic poly(D-CamL) has increased crystallinity which could be further supported by the DSC experiments with the second heating scans performed at different heating rates (2.5, 10, and 20 °C/min) (**Figure S3.26**). The DSC results showed a decrease in the area (ΔH_f value) of the higher T_m peak with increasing the heating rate, suggesting the formation of more ordered and thicker crystallization zone after the lower T_m resulting in the appearance of a higher T_m in isotactic poly(D-CamL). Significantly, regardless of tacticity, based on WAXD and DSC results, we observed intrinsic crystallinity in all poly(D-CamL) samples. This unique property is not common in polyesters and may be imparted by the cyclopentylene and gem-dimethyl structures in the polymer chain.[28,29] Additionally, the circular dichroism (CD) spectra (**Figure S3.27**) of isotactic poly(D-CamL) (**Table 3.2**, **Run 1**) and atactic poly(D-CamL) (**Table 3.2**, **Run 2**) were obtained. Isotactic poly(D-CamL) showed a stronger positive Cotton effect than the atactic poly(D-CamL), which confirmed that the isotactic poly(D-CamL) showed higher optical activity than the atactic poly(D-CamL). The atactic sample also exhibited rather weak positive Cotton effect, supporting

our conclusion that the atactic poly(D-CamL) has a decreased cis-/trans- ratio of 58/42 compared to the isotactic poly(D-CamL) which has a cis-/trans- ratio of 100/0.

Thermomechanical properties of isotactic poly(D-CamL) (**Table 3.2**, **Run 1**) and atactic poly(D-CamL) (**Table 3.2**, **Run 2**) were evaluated using dynamic mechanical analysis (DMA) in a tension film mode (**Figure S23**). Isotactic poly(D-CamL) (**Table 3.2**, **Run 1**) exhibited a slightly higher storage modulus of E' = 3289 MPa than atactic poly(D-CamL) (**Table 3.2**, **Run 2**) of E' = 3135 MPa in the glassy state. After the glass-transition region with an alpha transition (T_α = 86 °C and T_α = 75 °C respectively, defined by the peak maxima of tanδ, E''/E'), E' of isotactic and atactic poly(D-CamL) decreased by about one order of magnitude after T_α, meaning these materials still maintain a relatively high storage moduli in the rubbery state.

To evaluate the stability of these polymers to thermal processing, rheological experiments were performed using a continuous flow study at a shear rate of 0.5 s^{-1}. The temporal changes in shear viscosity for both isotactic poly(D-CamL) (**Table 3.2**, **Run 1**) and atactic poly(D-CamL) (**Table 3.2**, **Run 2**) were monitored at temperatures surpassing T_m (**Figures 3.4D** and **3.4E**). The shear viscosity of atactic poly(D-CamL) (**Table 3.2**, **Run 2**) remained nearly constant without any noticeable decline for 30 minutes when exposed to temperatures ranging from 200 °C to 240 °C. Upon heating for 30 minutes at 260 °C, the shear viscosity decreased from 1063 to 769 Pa•s while the isotactic poly(D-CamL) (**Table 3.2**, **Run 1**) showed a decrease in shear viscosity, from 4908 to 3850 Pa•s, upon heating for 30 minutes at 240 ºC. These results demonstrated the thermal processability of atactic poly(D-CamL) (**Table 3,2**, **Run 2**) but not isotactic poly(D-CamL) (**Table**

3.2, **Run 1**). The shear thinning experiment (**Figure S24**) also showed a rapid decrease in viscosity of atactic poly(D-CamL) (**Table 3.2**, **Run 2**) upon its exposure to sheer strain, which is a characteristic that enhances polymer processability.

Syndiotactic-rich polymers from *rac*-CamL

D-CamL used in the experiments described thus far was synthesized from natural camphor. In contrast with natural camphor, synthetic camphor is typically available as a racemic mixture. Given the prevalence of racemic camphor, we sought to examine the properties of polymers derived from a racemic mixture. The racemic monomer, *rac*-CamL, was synthetized according to a similar procedure to the one used to synthesize D-CamL (**Figure S3.1**).

Atactic poly(*rac*-CamL) (M_w = 78.2 kDa, **Table 3.2**, **Run 4**) was synthesized using ^{t}BuP$_4$/urea 1 for mechanical testing. The cis-/trans- ratio of atactic poly(*rac*-CamL) was 62/38 and the T_m was 184 °C (**Figure 3A**, **Table 2**, **Run 4**,). Tensile testing (**Figure 3B**) revealed a notably higher yield stress of nearly 40 MPa and ε_B, 121 ± 9% than that of isotactic poly(D-CamL) (**Table 2**, **Run 1**). Upon WAXD analysis (**Figure 3C**), atactic poly(*rac*-CamL) exhibited two distinct sharp peaks at 2θ = 16.0º and 17.9º which showed a slight shift in comparison to isotactic poly(D-CamL), indicating atactic poly(*rac*-CamL) may crystallize differently than poly(D-CamL). ^{13}C NMR analysis revealed that atactic poly(*rac*-CamL) (M_w = 78.2 kDa) has a higher proportion of D-L linkages at 173.65 ppm than D-D/L-L linkages at 173.59 ppm (**Figure S25**), indicating that atactic poly(*rac*-CamL) tends to be syndiotactic-rich. The discrepancy between D-L linkage content in atactic and isotactic poly(*rac*-CamL) may be caused by the larger counterion ([^{t}BuP$_4$-

H]$^+$) at the polymer chain ends leading to alternating D-L insertion, whereas the La(N(SiMe$_3$)$_2$)$_3$ does not have this same effect.

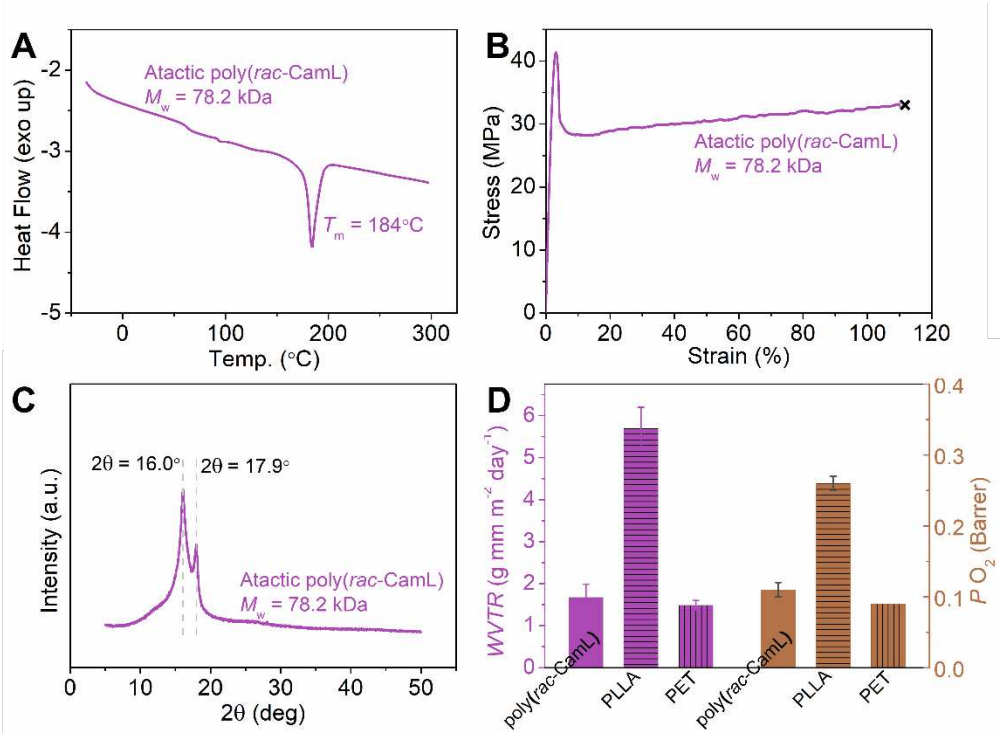

Figure 3.5: *Thermal, mechanical, WAXD, and permeability characterization results of atactic poly(rac-CamL) from Table 2, Run 4.*

(A) *DSC trace of poly(rac-CamL).* ***(B)*** *Representative stress-strain curve of the atactic poly(rac-CamL), extension rate = 5 mm/min, ambient condition.* ***(C)*** *WAXD of the poly(rac-CamL).* ***(D)*** *Water vapor transmission rate and oxygen permeability of poly(rac-CamL), PLLA (M_w = 162 kDa), and PET (intrinsic viscosity of 0.80 dL g^{-1} in m-cresol).*

To assess the potential of poly(CamL) for use as a packaging material, we conducted barrier property tests on syndiotactic-rich poly(*rac*-CamL) (**Table 3.2**, **Run 4**). Syndiotactic-rich poly(*rac*-CamL) demonstrates a relatively low water vapor transmission rate (*WVTR*) of 1.68 ± 0.31 (g mm m^{-2} day^{-1}), and an outstanding oxygen permeability (*P* O$_2$) character of 0.11 ± 0.01 Barrer. Desirable barrier properties are likely attributable to the polymer's T_g being above-room-temperature (63 °C) and semicrystalline nature. Both the *WVTR* and *P* O$_2$ are much lower than that

of commercial poly(L-lactic acid) (PLLA) and approach that of commercial polyethylene terephthalate (PET) which is widely used in packaging materials (**Figure 3.5D**);[19,58,59] these results demonstrate that syndiotactic-rich poly(*rac*-CamL) could be suitable for use as a packaging material.

Chemical recyclability and repolymerization

To investigate the thermodynamics of the D-CamL polymerization, the change in enthalpy (ΔH^{o}_{p}), change in entropy (ΔS^{o}_{p}), and $T_{ceiling}$ were measured. The equilibrium monomer concentration was determined at varied temperatures and plotted as a function of temperature to yield a van 't Hoff plot (**Figure S26**). This analysis provided the thermodynamic parameters (ΔH^{o}_{p} = -21.0 kJ mol^{-1}, ΔS^{o}_{p} = -55.5 J mol^{-1} K^{-1}) while the $T_{ceiling}$ at $[M]_0$ = 1.0 M was determined to be 381 K (105 ºC). The low $T_{ceiling}$ value suggested that poly(D-CamL) could be depolymerized to D-CamL at elevated temperature.

Due to the epimerization observed during polymerization, we hypothesized that a sufficiently strong base would be necessary to support the onset of epimerization during depolymerization and achieve recovery of D-CamL from atactic poly(D-CamL). Based on this hypothesis, ^{t}BuOK was selected to depolymerize atactic poly(D-CamL) (**Table 3.2**, **Run 2**). Atactic poly(D-CamL), which was homogeneously mixed with ^{t}BuOK, was successfully converted to D-CamL (shown in **Figure 4A**) in 88% isolated yield in a sublimator at 200 ºC and 200 millitorr. The recovered D-CamL was successfully polymerized again using ^{t}BuP$_4$/urea 1,

forming poly(D-CamL) (48.4 kDa) with mechanical properties comparable to virgin poly(D-CamL) (**Figure 4B**), demonstrating successful closed-loop recycling.

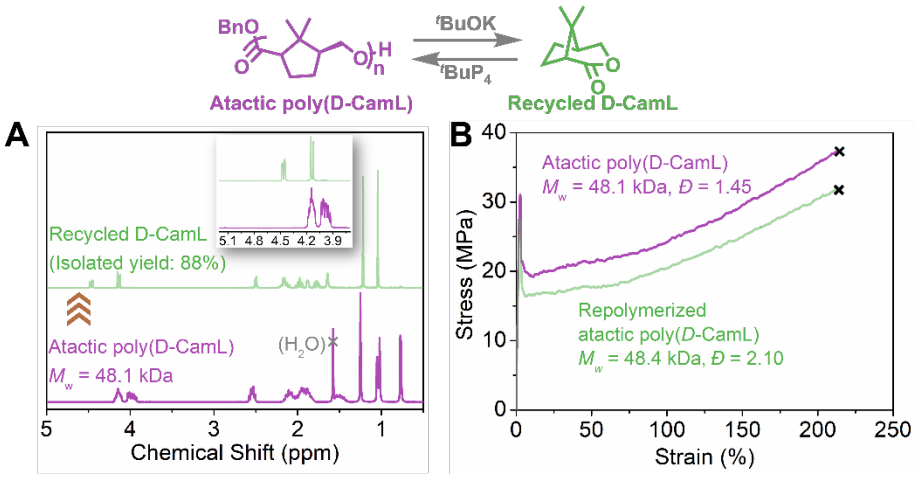

Figure 3.6: *1H NMR and mechanical characterization results of depolymerization of atactic poly(D-CamL) and repolymerization of recycled D-CamL.*

(A) *^{1}H NMR ($CDCl_3$, 23 °C) spectra of the poly(D-CamL) (M_w = 48.1 kDa) and recycled D-CamL. Inset: enlarged area from 5.2 ppm to 3.7 ppm.* ***(B)*** *Representative stress-strain curves of the poly(D-CamL) (M_w = 48.1 kDa) and the repolymerized poly(D-CamL) (M_w = 48.4 kDa).*

Conclusion

Through combining hybridization and gem-dialkyl substitution strategies, a camphor-derived, high-performance aliphatic polyester was efficiently synthesized and selectively depolymerized back to monomer in high isolated yield. The ROP of CamL was catalyzed by a La complex, superbase, or a superbase/urea binary catalyst system; these different catalyst systems allowed for the preparation of isotactic, atactic, and syndiotactic-rich poly(CamL) materials from the optically pure or racemic monomer. Variation in polymer tacticity modulates materials properties such as T_m, ductility, yield stress, and Young's modulus. Thermal and mechanical

characterization demonstrated that poly(CamL) exhibits comparable and/or enhanced properties compared to PLA, including similar T_m, T_g, and comparable yield stress while exhibiting better ductility and intrinsic crystallinity. Furthermore, low water vapor transmission rate and low oxygen permeability character confirmed that poly(CamL) has the potential to be used as packaging material. Above all, this combination strategy produced a polymer that not only showcases the potential of bio-based polymers in reducing reliance on fossil fuels but also emphasizes the importance of recyclability and performance in the development of next-generation plastics.

REFERENCES

1. Jambeck, J.R., Geyer, R., Wilcox, C., Siegler, T.R., Perryman, M., Andrady, A., Narayan, R., and Law, K.L. (2015). Plastic Waste Inputs from Land into the Ocean. Science *347*, 768-771.
2. MacLeod, M., Arp, H.P.H., Tekman, M.B., and Jahnke, A. (2021). The Global Threat from Plastic Pollution. Science *373*, 61-65.
3. Schyns, Z.O.G., and Shaver, M.P. (2021). Mechanical Recycling of Packaging Plastics: A Review. Macromol. Rapid Commun. *42*, 2000415.
4. Kumar, R., Sadeghi, K., Jang, J., and Seo, J. (2023). Mechanical, Chemical, and Bio-recycling of Biodegradable Plastics: A Review. Sci. Total Environ. *882*, 163446.
5. Jehanno, C., Alty, J.W., Roosen, M., De Meester, S., Dove, A.P., Chen, E.Y.X., Leibfarth, F.A., and Sardon, H. (2022). Critical Advances and Future Opportunities in Upcycling Commodity Polymers. Nature *603*, 803-814.
6. Coates, G.W., and Getzler, Y.D.Y.L. (2020). Chemical Recycling to Monomer for An Ideal, Circular Polymer Economy. Nat. Rev. Mater. *5*, 501-516.
7. Nicholson, S.R., Rorrer, J.E., Singh, A., Konev, M.O., Rorrer, N.A., Carpenter, A.C., Jacobsen, A.J., Roman-Leshkov, Y., and Beckham, G.T. (2022). The Critical Role of Process Analysis in Chemical Recycling and Upcycling of Waste Plastics. Annu. Rev. Chem. Biomol. Eng. *13*, 301-324.
8. Zhao, Y., Rettner, E.M., Harry, K.L., Hu, Z., Miscall, J., Rorrer, N.A., and Miyake, G.M. (2023). Chemically Recyclable Polyolefin-like Multiblock Polymers. Science *382*, 310-314.
9. Shi, C., Quinn, E.C., Diment, W.T., Chen, E.Y.X. (2024). Recyclable and (Bio)degradable Polyesters in a Circular Plastic Economy. Chem. Rev. *124*, 4393-4478.
10. Schwab, S. T., Baur, M., Nelson, T. F., Mecking, S. (2024). Synthesis and Deconstruction of Polyethylene-type Materials. Chem. Rev. *124*, 2327-2351.
11. Zhu, Y., Romain, C., and Williams, C.K. (2016). Sustainable Polymers from Renewable Resources. Nature *540*, 354-362.
12. Abdelshafy, A., Hermann, A., Herres-Pawlis, S., and Walther, G. (2023). Opportunities and Challenges of Establishing a Regional Bio-based Polylactic Acid Supply Chain. Glob. Chall. *7*, 2200218.
13. Jamshidian, M., Tehrany, E.A., Imran, M., Jacquot, M., and Desobry, S. (2010). Poly-Lactic Acid: Production, Applications, Nanocomposites, and Release Studies. Compr. Rev. Food Sci. Food Saf. *9*, 552-571.
14. Gallin, C.F., Lee, W.-W., and Byers, J.A. (2023). A Simple, Selective, and General Catalyst for Ring Closing Depolymerization of Polyesters and Polycarbonates for Chemical Recycling. Angew. Chem., Int. Ed. *62*, e202303762.

15. 15. McGuire, T.M., Buchard, A., and Williams, C. (2023). Chemical Recycling of Commercial Poly(L-lactic acid) to L-Lactide Using a High-Performance Sn(II)/Alcohol Catalyst System. J. Am. Chem. Soc. *145*, 19840-19848.
16. Garlotta, D. (2001). A Literature Review of Poly(Lactic Acid). J. Polym. Environ. *9*, 63-84.
17. Naser, A.Z., Deiab, I., and Darras, B.M. (2021). Poly(lactic acid) (PLA) and Polyhydroxyalkanoates (PHAs), Green Alternatives to Petroleum-based Plastics: A Review. RSC Adv. *11*, 17151-17196.
18. Chile, L.-E., Mehrkhodavandi, P., and Hatzikiriakos, S.G. (2016). A Comparison of the Rheological and Mechanical Properties of Isotactic, Syndiotactic, and Heterotactic Poly(lactide). Macromolecules *49*, 909-919.
19. Sangroniz, A., Zhu, J.-B., Tang, X., Etxeberria, A., Chen, E.Y.X., and Sardon, H. (2019). Packaging Materials with Desired Mechanical and Barrier Properties and Full Chemical Recyclability. Nat. Commun. *10*, 3559.
20. Mohan, S., and Panneerselvam, K. (2022). A Short Review on Mechanical and Barrier Properties of Polylactic Acid-based Films. Mater. Today: Proc. *56*, 3241-3246.
21. Abel, B.A., Snyder, R.L., and Coates, G.W. (2021). Chemically Recyclable Thermoplastics from Reversible-deactivation Polymerization of Cyclic Acetals. Science *373*, 783-789.
22. Hester, H.G., Abel, B.A., and Coates, G.W. (2023). Ultra-High-Molecular-Weight Poly(Dioxolane): Enhancing the Mechanical Performance of a Chemically Recyclable Polymer. J. Am. Chem. Soc. *145*, 8800-8804.
23. Shi, C., Reilly, L.T., Phani Kumar, V.S., Coile, M.W., Nicholson, S.R., Broadbelt, L.J., Beckham, G.T., and Chen, E.Y.X. (2021). Design Principles for Intrinsically Circular Polymers with Tunable Properties. Chem *7*, 2896-2912.
24. Li, X.L., Clarke, R.W., Jiang, J.Y., Xu, T.Q., and Chen, E.Y.X. (2023). A Circular Polyester Platform based on Simple gem-Disubstituted Valerolactones. Nat. Chem. *15*, 278-285.
25. Jung, M.E., and Piizzi, G. (2005). gem-Disubstituent Effect: Theoretical Basis and Synthetic Applications. Chem. Rev. *105*, 1735-1766.
26. Bachrach, S.M. (2008). The gem-Dimethyl Effect Revisited. J. Org. Chem. *73*, 2466-2468.
27. Zhou, Z., LaPointe, A.M., Shaffer, T.D., and Coates, G.W. (2023). Nature-inspired Methylated Polyhydroxybutyrates from C1 and C4 Feedstocks. Nat. Chem. *15*, 856-861.
28. Zhou, L., Zhang, Z., Shi, C., Scoti, M., Barange, D.K., Gowda, R.R., and Chen, E.Y.X. (2023). Chemically Circular, Mechanically Tough, and Melt-processable Polyhydroxyalkanoates. Science *380*, 64-69.
29. Shi, C., McGraw, M.L., Li, Z.-C., Cavallo, L., Falivene, L., and Chen, E.Y.X. High-performance pan-tactic Polythioesters with Intrinsic Crystallinity and Chemical Recyclability. Sci. Adv. *6*, eabc0495.
30. Shi, C., Li, Z.-C., Caporaso, L., Cavallo, L., Falivene, L., and Chen, E.Y.X. (2021). Hybrid Monomer Design for Unifying Conflicting Polymerizability, Recyclability, and Performance Properties. Chem *7*, 670-685.

31. Shi, C., Clarke, R.W., McGraw, M.L., and Chen, E.Y.X. (2022). Closing the "One Monomer-Two Polymers-One Monomer" Loop via Orthogonal (De)polymerization of a Lactone/Olefin Hybrid. J. Am. Chem. Soc. *144*, 2264-2275.
32. 32. Shi, C., Reilly, L.T., and Chen, E.Y.X. (2023). Hybrid Monomer Design Synergizing Property Trade-offs in Developing Polymers for Circularity and Performance. Angew. Chem., Int. Ed. *62*, e202301850.
33. Zielinska-Blajet, M., and Feder-Kubis, J. (2020). Monoterpenes and Their Derivatives-Recent Development in Biological and Medical Applications. Int. J. Mol. Sci. *21*.
34. Masyita, A., Mustika Sari, R., Dwi Astuti, A., Yasir, B., Rahma Rumata, N., Emran, T.B., Nainu, F., and Simal-Gandara, J. (2022). Terpenes and Terpenoids as Main Bioactive Compounds of Essential Oils, Their Roles in Human Health and Potential Application as Natural Food Preservatives. Food Chem.: X *13*, 100217.
35. Lu, J., Kamigaito, M., Sawamoto, M., Higashimura, T., and Deng, Y.-X. (1997). Living Cationic Isomerization Polymerization of β-Pinene. 1. Initiation with HCl–2-Chloroethyl Vinyl Ether Adduct/$TiCl_3(O^iPr)$ in Conjunction with $^nBu_4NCl$. Macromolecules *30*, 22-26.
36. Lowe, J.R., Martello, M.T., Tolman, W.B., and Hillmyer, M.A. (2011). Functional Biorenewable Polyesters from Carvone-derived Lactones. Polym. Chem. *2*, 702-708.
37. Satoh, K., Nakahara, A., Mukunoki, K., Sugiyama, H., Saito, H., and Kamigaito, M. (2014). Sustainable Cycloolefin Polymer from Pine Tree Oil for Optoelectronics Material: Living Cationic Polymerization of β-Pinene and Catalytic Hydrogenation of High-Molecular-Weight Hydrogenated Poly(β-Pinene). Polym. Chem. *5*, 3222-3230.
38. Hillmyer, M.A., and Tolman, W.B. (2014). Aliphatic Polyester Block Polymers: Renewable, Degradable, and Sustainable. Acc. Chem. Res. *47*, 2390-2396.
39. Winnacker, M., and Rieger, B. (2015). Recent Progress in Sustainable Polymers Obtained From Cyclic Terpenes: Synthesis, Properties, and Application Potential. ChemSusChem *8*, 2455-2471.
40. Roth, S., Funk, I., Hofer, M., and Sieber, V. (2017). Chemoenzymatic Synthesis of a Novel Borneol-Based Polyester. ChemSusChem *10*, 3574-3580.
41. Winnacker, M. (2018). Pinenes: Abundant and Renewable Building Blocks for a Variety of Sustainable Polymers. Angew. Chem., Int. Ed. *57*, 14362-14371.
42. Luo, Y.-C., Zhang, H.-H., Wang, Y., and Xu, P.-F. (2010). Synthesis of α-Amino Acids Based on Chiral Tricycloiminolactone Derived from Natural (+)-Camphor. Acc. Chem. Res. *43*, 1317-1330.
43. Chen, W., Vermaak, I., and Viljoen, A. (2013). Camphor--a fumigant during the Black Death and a coveted fragrant wood in ancient Egypt and Babylon--a Review. Molecules *18*, 5434-5454.
44. Roth, S. (2020). Biotransformation of Camphor-derivatives for the Synthesis of Bio-based Polymers. Technische Universität München.

45. Mossa, J.S., and Hassan, M.M.A. (1984). Camphor. In Analytical Profiles of Drug Substances, K. Florey, ed. (Academic Press), pp. 27-93.
46. Pang, C., Jiang, X., Yu, Y., Chen, L., Ma, J., and Gao, H. (2019). Copolymerization of Natural Camphor-Derived Rigid Diol with Various Dicarboxylic Acids: Access to Biobased Polyesters with Various Properties. ACS Macro Lett. *8*, 1442-1448.
47. Nsengiyumva, O., and Miller, S.A. (2019). Synthesis, Characterization, and Water-degradation of Biorenewable Polyesters Derived from Natural Camphoric Acid. Green Chem. *21*, 973-978.
48. Jiang, B., and Thomas, C.M. (2023). Efficient Synthesis of Camphor-based Polycarbonates: A Direct Route to Recyclable Polymers. Catal. Sci. Technol. *13*, 3910-3915.
49. Robert, C., de Montigny, F., and Thomas, C.M. (2011). Tandem synthesis of alternating polyesters from renewable resources. Nat. Commun. *2*, 586.
50. Xie, H., Feng, J., Yang, X., Zhao, Y., Song, P., Wang, H., and Xu, Z. (2022). One-pot Sequence-selective Synthesis of Polylactone-containing Block Terpolymers Based on Renewable Terpenoid-derived Monomer and A Simple Organocatalyst. J. Polym. Sci. *60*, 2889-2898.
51. Boileau, S., and Illy, N. (2011). Activation in Anionic Polymerization: Why Phosphazene Bases are very Exciting Promoters. Prog. Polym. Sci. *36*, 1132-1151.
52. Hong, M., and Chen, E.Y.X. (2016). Towards Truly Sustainable Polymers: A Metal-Free Recyclable Polyester from Biorenewable Non-Strained γ-Butyrolactone. Angew. Chem., Int. Ed. *55*, 4188-4193.
53. Liu, S., Ren, C., Zhao, N., Shen, Y., and Li, Z. (2018). Phosphazene Bases as Organocatalysts for Ring-Opening Polymerization of Cyclic Esters. Macromol. Rapid Commun. *39*, 1800485.
54. Lin, B., and Waymouth, R.M. (2017). Urea Anions: Simple, Fast, and Selective Catalysts for Ring-Opening Polymerizations. J. Am. Chem. Soc. *139*, 1645-1652.
55. Li, M., Tao, Y., Tang, J., Wang, Y., Zhang, X., Tao, Y., and Wang, X. (2019). Synergetic Organocatalysis for Eliminating Epimerization in Ring-Opening Polymerizations Enables Synthesis of Stereoregular Isotactic Polyester. J. Am. Chem. Soc. *141*, 281-289.
56. Wang, X., and Hadjichristidis, N. (2019). Poly(amine-co-ester)s by Binary Organocatalytic Ring-Opening Polymerization of N-Boc-1,4-oxazepan-7-one: Synthesis, Characterization, and Self-Assembly. Macromolecules *53*, 223-232.
57. Van der Meer, D.-W. (2003). Structure-property Relationships in Isotactic Polypropylene. University of Twente.
58. Marsh, K., and Bugusu, B. (2007). Food Packaging—Roles, Materials, and Environmental Issues. J. Food Sci. *72*, R39-R55.
59. Sangroniz, A., Chaos, A., Iriarte, M., del Río, J., Sarasua, J.-R., and Etxeberria, A. (2018). Influence of the Rigid Amorphous Fraction and Crystallinity on Polylactide Transport Properties. Macromolecules *51*, 3923-3931.

CHAPTER 4 – PHOTOINDUCED ORGANOCATALYZED CONTROLLED RADICAL VINYL ADDITION POLYMERIZATION OF α-METHYLENE-δ-VALEROLACTONE AND α-METHYLENE-γ-BUTYROLACTONE

Overview

α-Methylene-δ-valerolactone (MVL) is an intriguing monomer for use in synthesis of sustainable polyolefin-like material in that it can be derived from bio-mass and can be thermally depolymerized, giving rise to a circular polymer life cycle. There remains a need for a controlled method of MVL polymerization that results in polymer chains of uniform and predictable molecular weight if this system is to be used for applications in which low dispersities and targeted molecular weights are important. We herein report the use of photoinduced organocatalyzed atom transfer radical polymerization (O-ATRP) for controlled vinyl addition polymerization of MVL and its five-membered analog, α-methylene-γ-butyrolactone (MBL). Targeted molecular weights (I^* up to 95%) and low dispersities (> 1.6) were achieved. Use of visible-light-mediated photoredox catalysis enables selective polymerization at the vinyl position thereby preventing the appearance of undesired ring opening polymerization (ROP) products that can be produced by the same monomers. Copolymerization of MVL and MBL has not yet been reported and is successfully achieved in this work, thereby presenting an example of potential copolymerization of MVL with another monomer species by vinyl addition polymerization (VAP). Catalyst selection principles, monomer synthesis, and polymerization methods and results are discussed. Overall,

this work represents examples of controlled radical polymerization and copolymerization of two bio-based vinyl lactone monomers.

Introduction

Controlled radical polymerization (CRP) is an intriguing method of polymerization in that it can allow for precision synthesis of polymers with predetermined molecular weight and low dispersity ($Đ$).[1] Given that polymer molecular weight is of the utmost importance when it comes to polymer properties, synthesis of polymers with targeted molecular weights is highly important in the field of polymer chemistry.[2] In addition, there are many applications for which low dispersity polymers are desirable or necessary.[3-5] Thus, methods enabling precision polymer synthesis are often sought after. CRP is one of the primary methods used to achieve precision polymer synthesis.[6] Methods of controlled radical polymerization include radical addition chain transfer polymerization (RAFT) and atom transfer radical polymerization (ATRP).[7] In the realm of ATRP, the majority of polymerizations are driven by metals.[8] For polymer applications in which metal contamination may cause issues, such as biological and elecgtronic applications, the use of organic catalysis is more appropriate than metal catalysis; herein lies one of the primary motivations behind the study of organocatalyzed ATRP (O-ATRP).[9] Organic photoredox catalysis has gained popularity in recent years as organic photoredox catalysts (OPC) are able to drive CRP without the need for metals.

Within the scope of controlled radical polymerization, targeting of polymer systems that are sustainable is highly important. One of the foremost problems plaguing the environment today is the immense amount of plastic waste existing in the ocean, landfills, and as pollution. One of the reasons behind this is that polymeric materials have poor end-of-life options.[10] The majority of recyclable polymers are mechanically recycled, which is a poor solution to the plastic problem.[11] Most mechanical recycling includes melt processing and extrusion; the shear force needed for melting and extrusion frequently leads to a decrease in molecular weight of the polymer sample, thereby altering and/or decreasing materials properties.[11] Chemical recycling to monomer is one of several end-of-life options for polymers that is more sustainable than mechanical recycling.[12] The ability to convert polymers back into their constituent monomer units ultimately enables a circular polymer lifecycle, thereby addressing poor end-of-life options. Additionally, the implementation of materials with infinite recyclability eliminates the need for continuous harvesting of materials from the environment. In considering the design of such materials, monomer design is paramount. An appropriately designed monomer can enable high recovery of monomer upon subjection to depolymerization conditions.

Chemical recycling of a range of polymer types has been investigated in recent years, including that of vinyl addition polymers such as PMMA.[13-15] Many of these works involve thermal depolymerization, wherein the depolymerization temperature is dictated by the ceiling temperature of the polymer. As such, use of polymer systems with low ceiling temperatures remains desirable as this can allow for depolymerization under relatively low-energy

conditions.[16] One such polymer that has been reported to be chemically recyclable under neat conditions due to a low ceiling temperature is poly-α-methylene-δ-valerolactone (PMVL).[17] This polymer possesses a range of characteristics that make it an attractive candidate for sustainability in that not only is the polymer able to be chemically recycled in high yield under mild conditions, but also the monomer (α-methylene-δ-valerolactone, MVL) can be made from bio-derived sources thereby adding another layer of sustainability.[17] Reports of MVL polymerization are limited and do not include methods for controlled polymerization. As such, a need exists for a controlled method of MVL polymerization; we posited that controlled polymerization of this monomer could be achieved through O-ATRP.

The five-membered analog of MVL, α-methylene-γ-butyrolactone (MBL), is also bio-based. MBL has many more examples in the literature of its use as a monomer than α-methylene-δ-valerolactone (MVL).[18-20] Neither of these systems have been reported to be polymerized by O-ATRP. As such, we herein report methods of controlled O-ATRP for the vinyl addition polymerization of MVL and MBL. In addition, we report the copolymerization of these two monomers, which to our knowledge has not yet been reported.

Results and Discussion

Vinyl Addition Polymerization of MVL

a-Methylene-d-valerolactone (MVL) has been reported in previous literature to be polymerized at the vinyl position by free radical polymerization (FRP) initiated by azobisisobutylnitrile (AIBN).[21] However, to our knowledge, controlled radical polymerization (CRP) of MVL has not been reported. Given the reports of successful free radical polymerization of MVL, we hypothesized that controlled radical polymerization may be possible. Previous works from the Miyake group have demonstrated that CRP of acrylate and methacrylate monomers can be achieved though organocatalyzed atom transfer radical polymerization (O-ATRP) driven by visible light.[22, 23] Since MVL is structurally similar to acrylates and methacrylates, we hypothesized that visible-light-driven O-ATRP would also be able to polymerize MVL. Additionally, we hypothesized that the activity of the propagating radical for MVL would be similar to that of acrylates and methacrylates. To achieve control in O-ATRP, activation and deactivation must be balanced (**Figure 4.1A**); this balance is achieved in this system by an organic photocatlayst (PC). Given the proposed activity of the MVL propagating radical, we hypothesized that the acridine family of photocatalysts would perform well in this system because they have highly oxidizing radical cations and are therefore able to enable controlled polymerization of acrylates (**Figure 4.1B**).[22]

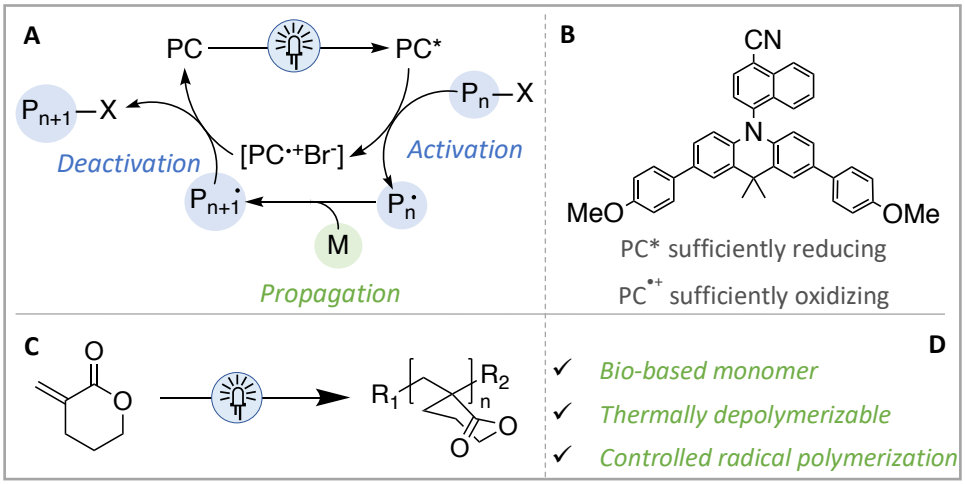

Figure 4.1: *A: general mechanism for O-ATRP; B: structure of acridine PC; C: general scheme for O-ATRP of MVL; D: primary takeaways for this work*

To test our initial hypotheses, an acridine photocatalyst was employed in O-ATRP of MVL. Initial investigations of the acridine PC were highly promising in that the PC enabled moderate to good control over the vinyl addition polymerization of MVL. Control in O-ATRP can be evaluated through three primary avenues: evaluation of polymer dispersity, comparison of experimental molecular weight and theoretical molecular weight, and evaluation of adherence to first-order kinetic analysis with respect to monomer. In the case of dispersity, a value of less than 1.2 is typically considered to coincide with "good" polymerization control, while dispersities of less than 1.5 correspond to "moderate" polymerization control.[15] The relationship between theoretical molecular weight ($M_{n,theo}$) and experimental molecular weight ($M_{n,exp}$) can be evaluated through calculation of initiator efficiency (I^*, where $I^* = M_{n,theo}/M_{n,exp}$); in a well-controlled polymerization, I^* should be close to 100%. Finally, in a controlled polymerization, pseudo-first-order kinetics with respect to monomer should be observed, indicating that the concentration of

propagating radical is both low and constant.[9] In the case of initial O-ATRP of MVL with an acridine PC, the aforementioned metrics for polymerization control were used to determine that observed polymerization control was moderate to good (**Figure 4.2**, **Table 4.1**).

In order to build on the promising initial O-ATRP of MVL, a range of catalysts, solvents, and initiators were employed methodically to optimize polymerization conditions. It was determined that acridine **PC 1** performed the best among the series (**Figure 4.3**). The performance of **PC 1** compared to that of **PC 2** and **PC 3** supports previously established work suggesting that both charge transfer and redox reversibility are important for success in O-ATRP.[9] **PC 2** does not exhibit good redox reversibility which could have led to high dispersities observed. **PC 3** is hypothesized to exhibit less charge transfer than **PC 1**, which

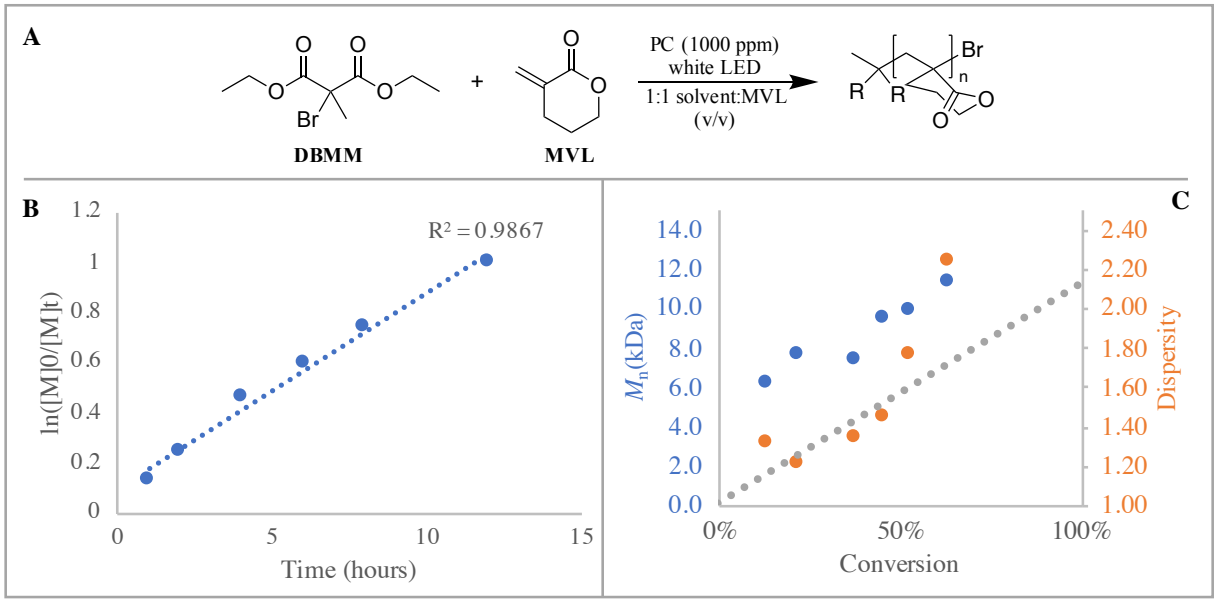

Figure 2: *A: polymerization scheme for MVL using O-ATRP (see SI: General Polymerization Procedure for more details); B: plot of M_n and dispersity as a function of conversion for initial O-ATRP attempt; C: first order kinetic plot for initial O-ATRP attempt*

PC	Solvent	Time (hours)	Conversion [a] (%)	M_w [b] (kDa)	M_n [b] (kDa)	$Đ$ (M_w/M_n)	I^* [c] (%)
1	DMAc	1	13	8.19	6.20	1.32	25
		2	21	9.37	7.71	1.22	34
		4	37	9.98	7.44	1.34	58
		6	45	13.9	9.43	1.45	55
		8	52	17.5	9.94	1.76	61
		12	63	25.4	11.3	2.24	64

Table 4.1: *polymerization results from initial polymerization attempt. [a] determined by ^{1}H NMR in chloroform-d [b] determined by GPC coupled with multi angle light scattering [c] $I^* = (M_{n,theo}/M_{n,exp})$ x 100*

explains why polymerization with **PC 1** was more controlled than **PC 3.** In the case of the phenazine PC (**PC 4**),we hypothesize that poor performance can be attributed to the fact that **PC 4** has a less oxidizing radical cation than **PC 1** leading to inefficient deactivation. Finally, the phenoxazine PC (**PC 5**) performed similarly to the series of acridines (**PC 1 – PC3**) which can be attributed to its radical cation oxidation potential.[22] Ultimately, **PC 1** was chosen over **PC 5** because of consistent initiator efficiencies and adherence to pseudo-first-order kinetics with respect to monomer (**Figure S4.12**).

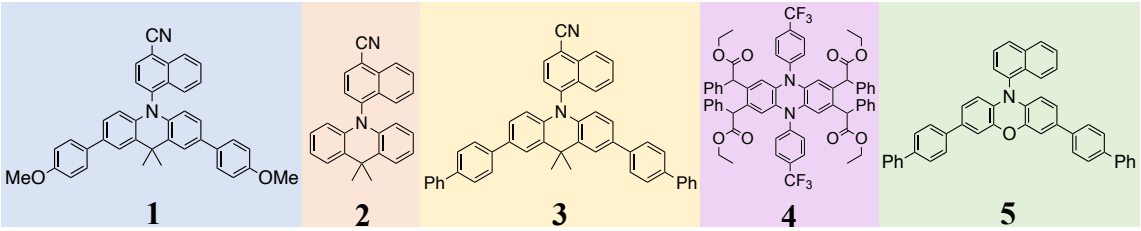

Figure 4.3: *structures of photocatalysts employed in catalyst optimization*

Previous reports of O-ATRP of acrylates and methacrylates show that solvent polarity has a significant effect on polymerization control.[24] Thus, following investigation of PCs, effects of

solvent on polymerization control were explored. Solvents included in the screen were limited by the solubility of PMVL; a range of solvents were investigated for PMVL solubility, but only the reported four solvents were able to dissolve the polymer and therefore were the only ones included in the reported solvent screen. Dimethyl sulfoxide (DMSO) was chosen as the optimal solvent for this system due to low dispersities observed throughout the polymerization (**Figure S4.13**). Delta-valerolactone (DVL) was included in the solvent screen because it is the starting material used to synthesize MVL. Industrially, separation of starting materials and target products consumes a significant amount of energy.[25] Thus, the ability to use the starting material as a solvent would decrease the overall energetic cost of the process of MVL synthesis and polymerization. Excitingly, DVL was able to dissolve PMVL, and MVL could be successfully polymerized using DVL as a solvent (**Figure S4.15**). However, DVL did not improve polymerization control relative to the starting conditions, and therefore was not investigated further in this work.

Similar to reports on solvent effects, initiator structure has also been shown to impact polymerization control in O-ATRP.[26] Therefore, a range of initiators were investigated to determine their effects on initiator efficiency and polymerization control. Methyl a-bromoisobutyrate (MB^{i}B) and methyl-2-bromopropionate (M2BP) both lead to improved dispersities but lower initiator efficiencies than the initial experiments in which diethyl-2-bromo-2-methylmalonate (DBMM) was used as the initiator. Ethyl a-bromophenylacetate (EBP) exhibited lower dispersities than DBMM, but initiator efficiencies were lower when EBP was

employed. Ultimately, DBMM was chosen as the optimal initiator for this system along with **PC 1** as a catalyst and DMSO as a solvent (**Figure 4.4, Table 4.2**).

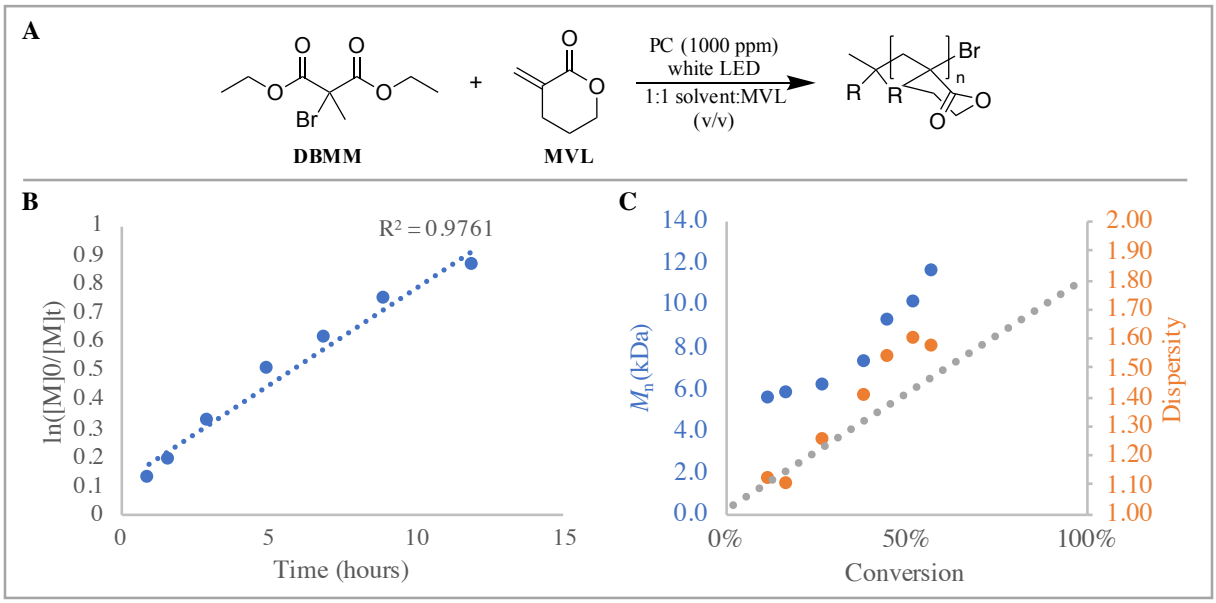

Figure 4.4: *A: polymerization scheme for MVL using O-ATRP (see SI: General Polymerization Procedure for more details); B: first order kinetic plot for optimized O-ATRP of MVL; C: plot of M_n and dispersity as a function of conversion for optimized O-ATRP of MVL*

PC	Solvent	Time (hrs)	Conversion[(a)] (%)	M_w[(b)] (kDa)	M_n[(b)] (kDa)	$Đ$ (M_w/M_n)	I^*[(c)] (%)
		1	12	6.01	5.40	1.11	28
		1.67	18	6.26	5.73	1.09	37
		3	28	7.54	6.05	1.24	54
1	DMSO	5	39	10.1	7.20	1.40	64
		7	46	14.1	9.18	1.53	58
		9	53	16.0	10.0	1.59	61
		12	58	18.0	11.5	1.57	58

Table 4.2: *polymerization results from optimized O-ATRP of MVL [a)] determined by ^{1}H NMR in chloroform-d [b)] determined by GPC coupled with multi angle light scattering [c)] $I^* = (M_{n,theo}/M_{n,exp}) \times 100$*

Reversible addition fragmentation chain transfer polymerization (RAFT) and free radical polymerization (FRP) of MVL were also investigated. Free radical polymerization (FRP) of MVL

has been previously published.[27] However, these reports were somewhat old and did not include information about polymer dispersities. Interestingly, when we polymerized MVL via FRP with AIBN as an initiator, as has been previously reported, dispersities were incredibly low (1.01-1.02, **Table S4.6**). This was intriguing, as free radical polymerizations have a theoretical minimum dispersity of 1.5.[28] FRP resulted in poor initiator efficiency (13%). RAFT polymerization of MVL, however, has not yet been published. RAFT of MVL resulted in a polymer with low dispersity (1.08) and a moderate initiator efficiency (73%, **Table S4.7**).

2.2. Vinyl Addition Polymerization of MBL

As discussed previously, MBL is a five-membered analog of MVL. However, MBL is commercially available whereas MVL is not. As such, we sought to investigate O-ATRP of MBL given its availability relative to MVL. The same conditions were used for initial polymerization of MBL as for initial polymerization of MVL. Notably, MBL polymerized much more rapidly than MVL, reaching full conversion in three hours or less. We hypothesize that this discrepancy in rate is due to increased planarity of the propagating radical of PMBL relative to that of PMVL.[29] Considering structural similarities between MVL and MBL, we hypothesized that results of optimization studies would match those observed in the case of MVL. The same series of conditions were screened for both MVL and MBL. Our hypothesis was partially supported in that the same catalyst (**PC 1**) worked best for both O-ATRP of MBL and O-ATRP of MVL (**Figure 4.5**, **Table 4.3**). However, differences between MVL and MBL optimization results arose during

solvent and initiator optimization. In terms of solvent, DMAc lead to improved control relative to both DMSO and DMF, a different result than was observed in the case of PMVL (**Figure S4.27**, **Figure S4.28**). Given slight differences in the activity of PMVL and PMBL propagating radicals, it is apparent that in the case of PMBL a more polar solvent does not lead to improved control. Finally, in terms of initiator structure, DBMM showed superior function among the employed series of initiators (**Table S4.10**, **Figure 4.5**, **Table 4.3**). Both FRP and RAFT of MBL are well reported and therefore were not investigated in this work.[30, 31]

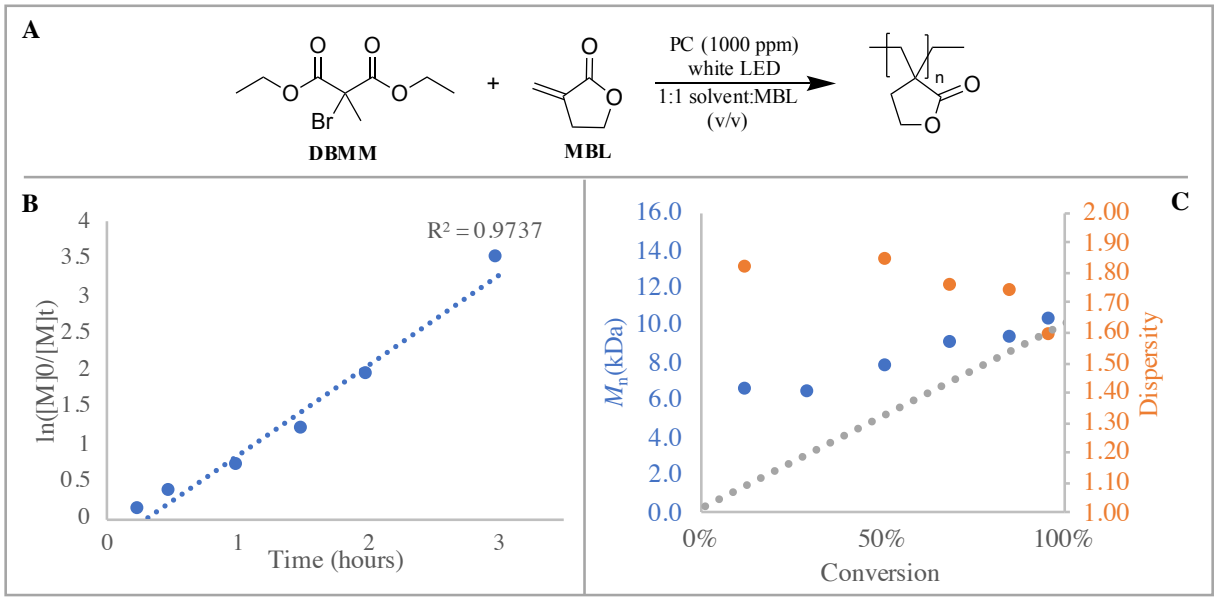

Figure 5: *A: polymerization scheme for MBL using O-ATRP (see SI: General Polymerization Procedure for more details); B: first order kinetic plot for optimized O-ATRP of MBL; C: plot of M_n and dispersity as a function of conversion for optimized O-ATRP o MBL.*

PC	Solvent	Time (hours)	Conversion[(a)] (%)	M_w[(b)] (kDa)	M_n[(b)] (kDa)	$Đ$ (M_w/M_n)	I^*[(c)] (%)
1	DMAc	0.25	13	11.8	6.50	1.81	23
		0.5	30	13.2	6.35	2.07	50
		1	52	14.4	7.85	1.84	68
		1.5	70	15.8	9.00	1.75	79
		2	86	16.1	9.28	1.74	94
		3	97	16.3	10.3	1.59	95

Table 3: *polymerization results from optimized O-ATRP of MBL [a] determined by ^{1}H NMR in chloroform-d [b] determined by GPC coupled with multi angle light scattering [c] I* = ($M_{n,theo}/M_{n,exp}$) x 100*

2.3. Copolymerization of MVL and MBL via O-ATRP

As mentioned previously, MBL and MVL have both been reported separately as monomers polymerizable by radical vinyl addition polymerization. However, to our knowledge, a copolymer of the two has not yet been investigated. As such, we posited that a method for copolymerization of the two could be quite useful as this may enable use of MBL and MVL in the synthesis of a wider range of materials. Given the success of O-ATRP for synthesis of the two homopolymers, we hypothesized that O-ATRP could also be used to copolymerize the two monomers. The optimized conditions for MVL polymerization were used to achieve copolymerization (**Figure 4.6**). Three different addition sequences were investigated (**Table S4.13**). First, both MVL and MBL were added to the polymerization mixture at the beginning of the reaction. Interestingly, we observed that while both monomers did polymerize, MVL was consumed faster than MBL; this was contrary to our prior observations that MBL polymerizes faster than MVL. We hypothesize that MBL has a lower reactivity ratio when adding to PMVL than when adding to PMBL.

MVL and MBL were also copolymerized in sequential addition in which MVL was added first, allowed to polymerize for 24 hours, followed by the addition of MBL. The sequence of addition was also reversed, wherein MBL was added first, allowed to polymerize for 24 hours, followed by the addition of MVL. In the ladder case, MBL reached full conversion and MVL polymerized but not completely. In the former case, similar to the simultaneous addition

polymerization, MBL did not fully polymerize when added to PMVL. This supports the aforementioned hypothesis that the reactivity between MBL and PMVL is lower than between MBL and PMBL. Ultimately, the copolymerization in which MVL and MBL were added simultaneously was the most effective, resulting in polymer with low dispersity. This method is a promising route towards copolymerization of MVL with other vinyl monomers.

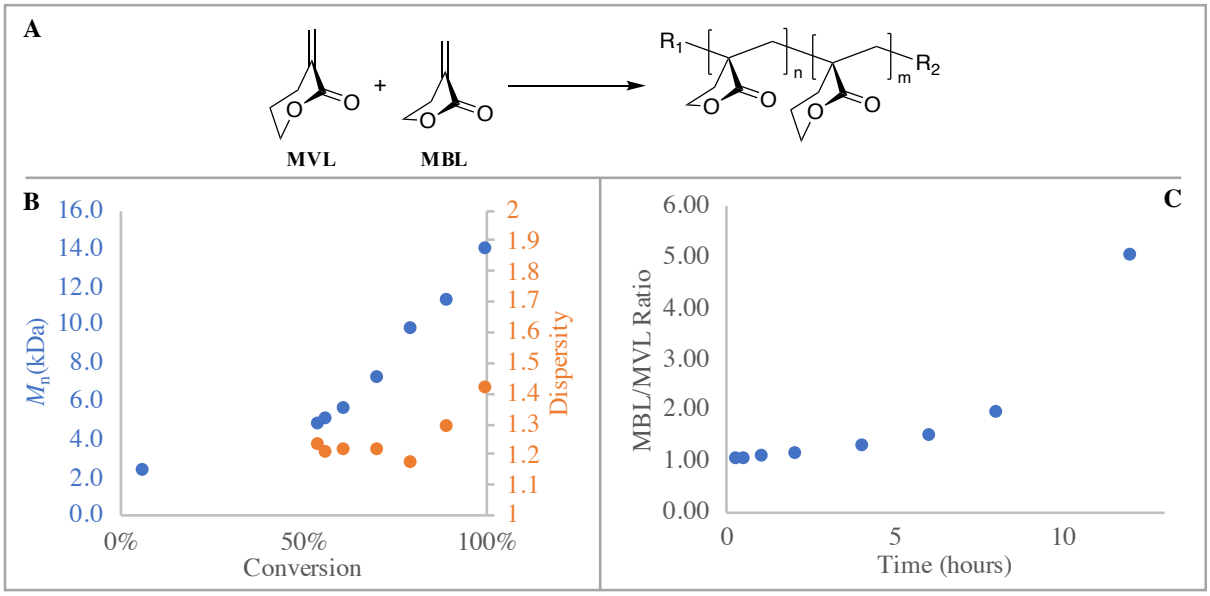

Figure 4.6: *A: polymerization scheme for copolymerization of MBL and MVL (see SI: Copolymerization Procedures for more details); B: plot of M_n (blue) and dispersity (blue) as a function of average MBL/MVL conversion; C: plot of MBL/MVL ratio as a function of time.*

PC	Addition Order[a]	Time (hours)	Conversion[b] (average, %)	MBL/MVL ratio[b]	M_w[c] (kDa)	M_n[c] (kDa)	$Đ$ (M_w/M_n)
		0.25	6	1.00	4.59	2.27	2.02
		0.5	54	1.01	5.74	4.68	1.23
		1	56	1.03	6.05	5.01	1.21
		2	61	1.09	6.79	5.60	1.21
1	Simultaneous	4	70	1.23	8.77	7.24	1.21
		6	79	1.47	11.3	9.68	1.17
		8	89	1.93	14.5	11.3	1.29
		12	97	4.99	17.2	10.7	1.61
		24	100	100% MBL	19.6	13.9	1.41

Table 4.4: *polymerization results from copolymerizations of MBL and MVL. [a] for simultaneous addition, both monomers were added at the start of the polymerization. For sequential additions, the first monomer was added, allowed to polymerize for 24 hours, and then the second monomer*

was added. [b] *determined by* ^{1}H *NMR in deuterated DMSO* [c] *determined by GPC coupled with multi angle light scattering*

Conclusion

We herein report a method of photoinduced, organocatalyzed, controlled radical polymerization of both α-methylene-δ-valerolactone (MVL) and α-methylene-γ-butyrolactone (MBL) as well as a copolymerization of the two monomers. An acridine photocatalyst was employed to achieve controlled synthesis of the two homopolymers, achieving dispersities between 1.20 and 1.50. In addition, FRP and RAFT of MVL were investigated, both of which resulted in dispersities of less than 1.10. Overall, this work represents a method of controlled polymerization of two sustainable monomers, thereby contributing to advancements in the fields of both sustainable polymer chemistry and controlled polymerization.

REFERENCES

1. K. Matyjaszewski, J. Xia, *Chem. Rev.*, **2001**, *101*, 2921-2990.
2. F. Rodriguez, C. Cohen, C. K. Ober, L. A. Archer, *Principles of Polymer Systems*, 6th ed.: CRC press, 2014.
3. R. Whitfield, N. P. Truong, D. Messmer, K. Parkatzidis, M. Rolland, A. Anastasaki, *Chem. Sci.* **2019**, *10*, 8724–8734.
4. T. Gentekos, R. J. Sifri, B. P. Fors, *Nat. Rev. Mater.* **2019**, *4*, 761–774.
5. M. Nadgorny, D. T. Gentekos, Z. Xiao, S. P. Singleton, B. P. Fors, L. A. Connal, *Macromol. Rapid Commun.* **2017**, *38*, 1700352.
6. Y.-N. Zhou, J.-J. Li, T.-T. Wang, Y.-Y. Wu, Z.-H. Luo, *Prog. Polym. Sci.* **2022**, *130*, 101555.
7. N. P. Truong, G. R. Jones, K. G. E. Bradford, D. Konkolewicz, A. Anastasaki, *Nat. Rev. Chem.* **2021**, *5*, 859–869.
8. K. Matyjaszewski, *Macromol.* **2012**, *45*, 4015–4039.
9. D. A. Corbin, G. M. Miyake, *Chem. Rev.* **2022**, *122*, 1830–1874.
10. J.P. Greene, End-of-Life Options for Plastics. In *Sustainable Plastics*, 1st ed.; John Wiley & Sons, 2014; pp 129 – 144.
11. Z. O. G. Schyns, M. P. Shaver, *Macromol. Rapid Commun.* **2021**, *42*, 2000415.
12. G.W. Coates, Y.D.Y.L. Getzler, *Nat. Rev. Mater.* **2020**, *18*, 501–516.
13. J. B. Young, R. W. Hughes, A. M. Tamura, L. S. Bailey, K. A. Stewart, B. S. Sumerlin, *Chem*, **2023**, *9*, 2669-2682.
14. H. S. Wang, N. P. Truong, Z. Pei, M. L. Coote, A. Anastasaki, *J. Am. Chem. Soc.* **2022**, *144*, 4678–4684.
15. C. B. Godiya, S. Gabrielli, S. Materazzi, M. S. Pianesi, N. Stefanini, E. Marcantoni, *Environ. Manage.* **2019**, *231*, 1012-1020.
16. V. Lohmann, G. R. Jones, N. P. Truong, A. Anastasaki, *Chem. Sci.* **2024**, *15*, 832-853.
17. R. A. Gilsdorf, E. R. Chokkapu, A. Athaley, T. Uekert, R. R. Gowda, A. Singh, J. S. DesVeaux, G. T. Beckham, E. Y.-X. Chen, *Cell Rep. Phys. Sci.* **2024**, *5*, 101938.
18. F. G. Versteeg, N. C. Hegeman, K. O. Sebakhy, F. Picchioni, *Macromol. Rapid Commun.* **2022**, *43*, 2200045.
19. L. Hu, J. He, Y. Zhang, E. Y.-X. Chen, *Macromol.* **2018**, *51*, 1296–1307.
20. A. Elshewy, M. El Hariri El Nokab, J. Es Sayed, Y. Alassmy, M. Abduljawad, D. D'hooge, P. Van Steenberge, M. Habib, K. Sebakhy, A. Elshewy, *ACS Appl. Polym. Mater.* **2023**, *6,* 115-125.
21. M. Ueda, T. Suzuki, M. Takahashi, Z. B. Li, K. Koyama, C. U. Pittman, *Macromol.* **1986**, *19*, 558-565.

22. B. L. Buss, C.-H. Lim, G. M. Miyake, *Angew. Chem. Int. Ed.* **2020**, *59*, 3209.
23. K. O. Puffer, D. A. Corbin, G. M. Miyake, *ACS Catal.* **2023**, *13*, 14042–14051.
24. B. McCarthy, S. Sartor, J. Cole, N. Damrauer, G. M. Miyake, *Macromol*. **2020**, *53*, 9208–9219.
25. A. Lucia, A. Amale, R. Taylor, *Ind. Eng. Chem. Res.* **2006**, *45*, 8319–8328.
26. N. A. Swisher, D. A. Corbin, G. M. Miyake, *ACS Macro Lett*. **2021**, *10*, 453–459.
27. M. Ueda, M. Takahashi, Y. Imai, C. U. Pittman, *Macromol.* **1983**, *16*, 1300-1305.
28. K. Endo, K. Murata, T. Otsu, *Macromol.* **1992**, *25*, 5554.
29. J. W. Stansbury, J. M. Antonucci, *Dent. Mater.* **1992**, *8*, 270–273.
30. F. G. Versteeg, N. C. Hegeman, K. O. Sebakhy, F. Picchioni, *Macromol. Rapid Commun.* **2022**, *43*, 2200045.
31. M. Ueda, M. Takahashi, Y. Imai, C. U. Pittman, *J. Polym. Sci., Polym. Chem. Ed*. **1982**, *20*, 2819–2828.

CHAPTER 5 – SUMMARY

In summary, this thesis describes several works in which sustainable polymer synthesis is targeted. In Chapter 2, photoinduced organocatalyzed radical ring opening polymerization of a series of functionalized vinyl cyclopropanes is reported. This work provides an example of sustainably-driven polymerization. In Chapter 3, ring opening polymerization of a chemically recyclable, bio-based lactone is described. This work is represents potential alleviation of environmental issues brought about by both unsustainable sourcing of monomers and poor end-of-life options for polymeric materials. Finally, in Chapter 4, the polymerization of two bio-based monomers via sustainable polymerization methods is described; the polymers synthesized in this chapter are also chemically recyclable. Ultimately, these works examine potential solutions to all unsustainable aspects of a polymer's life cycle from monomer source, to polymerization method, to end-of-life.

APPENDIX A – SUPPLEMENTARY INFORMATION FOR CHAPTER 2

Materials and Methods

Materials:

Phenoxazine was purchased from Beantown Chemical. *Trans*-1,4-dibromo-2-butene, diethyl malonate and 6-bromohexanoic acid were purchased from TCI America. Dehydroabietic acid was purchased from Astatech. Deuterated chloroform was purchased from Cambridge Isotope Laboratories. All other chemicals and anhydrous solvents were purchased from Sigma-Aldrich.

Ethyl α-bromophenylacetate (EBP), methyl 2-bromopropionate (M2BP) and diethyl 2-bromo-2-methylmalonate (DBMM) were purified by vacuum distillation, degassed by three freeze-pump-thaw cycles and stored at −34 °C in the freezer of a nitrogen-filled glovebox. All alkyl halides were allowed to warm to room temperature before use.

Photocatalysts (PCs) *N,N*-diaryl dihydrophenazines **1**–**2**,[1] 3,7-di(4-biphenyl)-N-naphthylphenoxazine **3**,[2] and EtVCP-C2[3] were synthesized according to our previous reports.

Methods:

Thin layer chromatography was performed on EMD Milipore silica gel 60 F254 glass plates. Column chromatography was performed on *SiliCycle*®*SilicaFlash*® P60, 40-63 μm, 60A. Visualization was accomplished with silica-I_2.

White-light LED beaker: a 45 cm of double density white LEDs (Creative Lighting Solutions, item no. CL-FRS1210-5M-12V-WH, 18 W/5 meters) was wrapped around the inside of a 400 mL beaker, and powered by a 12VDC power Supply (2.1A Commercial, 25W Power Supply by Creative Lighting Solutions LLC). The wattage of this setup is ~1.6 W.

The 34 W blue LED (HP150, 1.5 A, 34W) was purchased from *Kessil*.

^{1}H and ^{13}C spectra were recorded on a Bruker 400 Hz (100 Hz for ^{13}C) spectrometer at ambient temperature. All NMR spectra are referenced to the residual solvent ($CHCl_3$) signal.

Analysis of polymer molecular weight and dispersity was performed using gel permeation chromatography (GPC) coupled with multi-angle light scattering (MALS), using an Agilent HPLC fitted with one guard column and three PLgel 5 μm MIXED-C gel permeation columns in series.

The detectors were a Wyatt Technology TrEX differential refractometer and a Wyatt Technology mini DAWN TREOS light scatter detector. The solvent used was THF with a flow rate of 1.0 mL/minute.

Glass transition temperatures (T_g) and melting point (T_m) of the polymers were measured by differential scanning calorimetry (DSC) on a DSC 2500 (TA Instrument) at a rate of 10 °C/min. T_g values reported were from the second heating scan (from −80 to 200 °C, isothermed for 1 min) after the thermal history (the first scan) being removed. Decomposition temperatures (T_d) at 10% of weight loss and maximum rate decomposition temperatures (T_{max}) of the polymers were measured by thermal gravimetric analysis (TGA) on a Q50 TGA Analyzer (TA Instrument), by heating the polymer samples from 25 to 700 °C at the rate of 10 °C/min.

Synthesis of Functionalized Vinylcyclopropanes

Ethyl 1-cyano-2-vinylcyclopropane-1-carboxylate (EtVCP-CN)

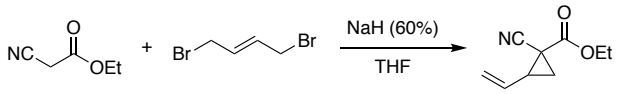

To a mixture of NaH (60% pure, 4.8 g, 120.0 mmol, 2.4 equiv.) in anhydrous THF (150 mL) at 0 °C, under N_2 atmosphere, *trans*-1,4-dibromo-2-butene (11.0 g, 50.0 mmol, 1.0 equiv.) was added in one portion, followed by dropwise of the malonate (5.32 mL, 50.0 mmol, 1.0 equiv.). The mixture was then vigorously stirred at room temperature for 30 min. The reaction was carefully quenched by slow addition of sat. NH_4Cl, extracted with diethyl ether three times. The combined organic layer was washed with H_2O and brine, dried over anhydrous Na_2SO_4 and concentrated under vacuum. The residue was purified by vacuum distillation. Colorless oil, inseparable 7:3 mixture of diasteromers. 6.7 g, 81% yield. R_f = 0.35 (30% EtOAc in hexane). **^{1}H NMR** (400 MHz, $CDCl_3$) δ 5.72 – 5.57 (m, 1H), 5.47 – 5.40 (m, 1H), 5.37 (d, *J* = 10.3 Hz, 0.70 H), 5.27 (d, *J* = 10.4 Hz, 0.30 H), 4.32 – 4.12 (m, 2H), 2.69 – 2.44 (m, 1H), 2.01 – 1.83 (m, 1.30 H), 1.64 (dd, *J* = 7.9, 5.1 Hz, 0.70 H), 1.38 – 1.31 (m, 3H). **^{13}C NMR** (100 MHz, $CDCl_3$) δ 167.1, 165.2, 132.1, 130.5, 121.3, 120.8, 118.7, 116.7, 63.0, 62.8, 35.7, 33.7, 23.9, 22.5, 21.1, 20.3, 14.1, 14.1.

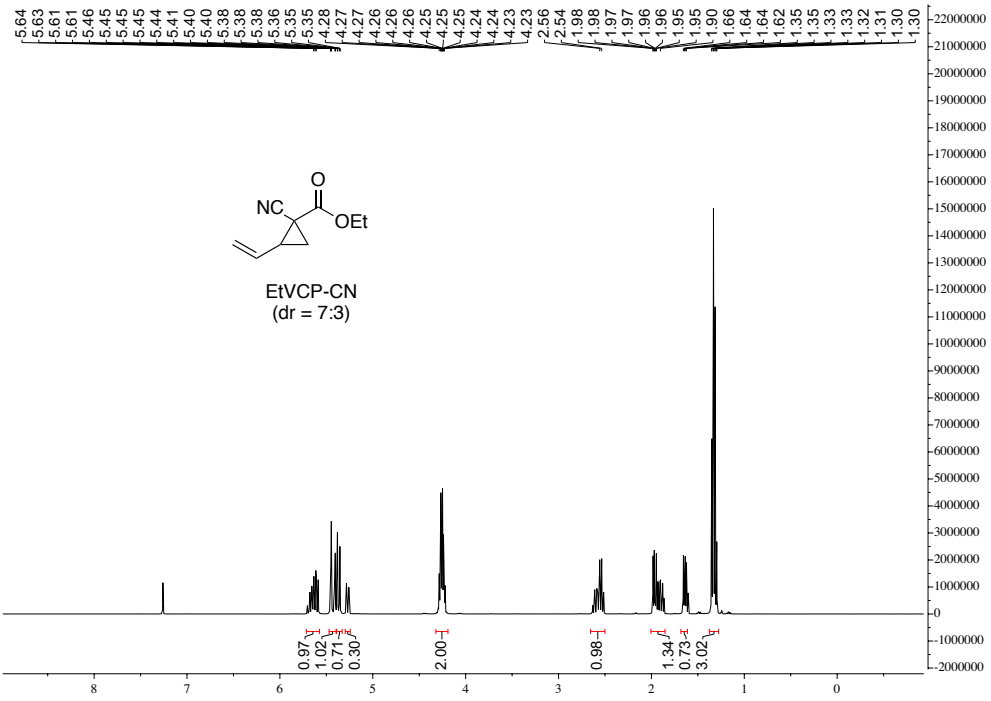

Figure S2.1. ^{1}H-NMR spectrum of EtVCP-CN in $CDCl_3$.

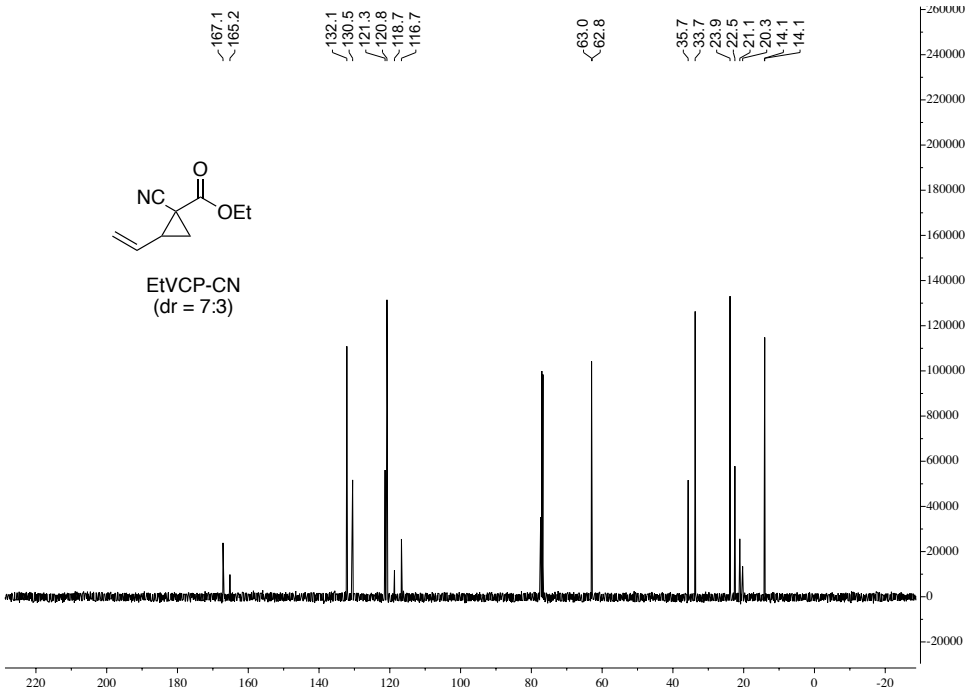

Figure S2.2. ^{13}C-NMR spectrum of EtVCP-CN in $CDCl_3$.

Ethyl 1-(phenylcarbamoyl)-2-vinylcyclopropane-1-carboxylate (EtVCP-NHPh)

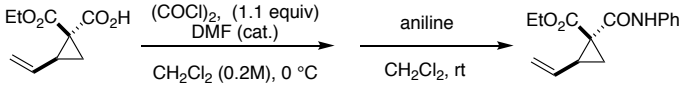

To a solution of 1-(ethoxycarbonyl)-2-vinylcyclopropane-1-carboxylic acid[4] (3.68 g, 20.0 mmol, 1.1 equiv) and 3 drops of DMF in anhydrous DCM (100 mL) at 0 °C, oxalyl chloride (1.86 mL, 22.0 mmol, 1.1 equiv) was added dropwise. The reaction was then vigorously stirred at room temperature for 3 h. Then the mixture was cooled to 0 °C, and aniline (1.82 mL, 20.0 mmol, 1.0 equiv) was added dropwise. The mixture was gradually warmed up to room temperature and stirred overnight. The white precipitate was filtered off and the filtrate was concentrated *in vacuo*. The residue was purified by silica gel flash chromatography using hexane/EtOAc (10:1) as the eluent to give the EtVCP-NHPh as an inseparable 10:1 mixture of diasteromers. White solid (2.78 g, 54% yield for two steps). R_f = 0.35 (25% EtOAc in hexane). **^{1}H NMR** (400 MHz, $CDCl_3$) δ 10.59 (s, 1H), 7.66 – 7.49 (m, 2H), 7.36 – 7.28 (m, 2H), 7.14 – 7.04 (m, 1H), 5.71 (ddd, *J* = 17.1, 10.2, 8.7 Hz, 1H), 5.37 (dd, *J* = 17.1, 1.1 Hz, 1H), 5.21 (dd, *J* = 10.1, 1.2 Hz, 1H), 4.33 – 4.17 (m, 2H), 2.64 (dd, *J* = 8.7, 8.1 Hz, 1H), 2.20 (dd, *J* = 9.2, 4.4 Hz, 1H), 1.98 (dd, *J* = 8.1, 4.4 Hz, 1H), 1.33 (t, *J*

= 7.1 Hz, 3H). **^{13}C NMR** (100 MHz, $CDCl_3$) δ 171.7, 166.1, 138.1, 133.0, 128.9, 124.1, 120.0, 61.8, 38.1, 34.7, 21.7, 14.2.

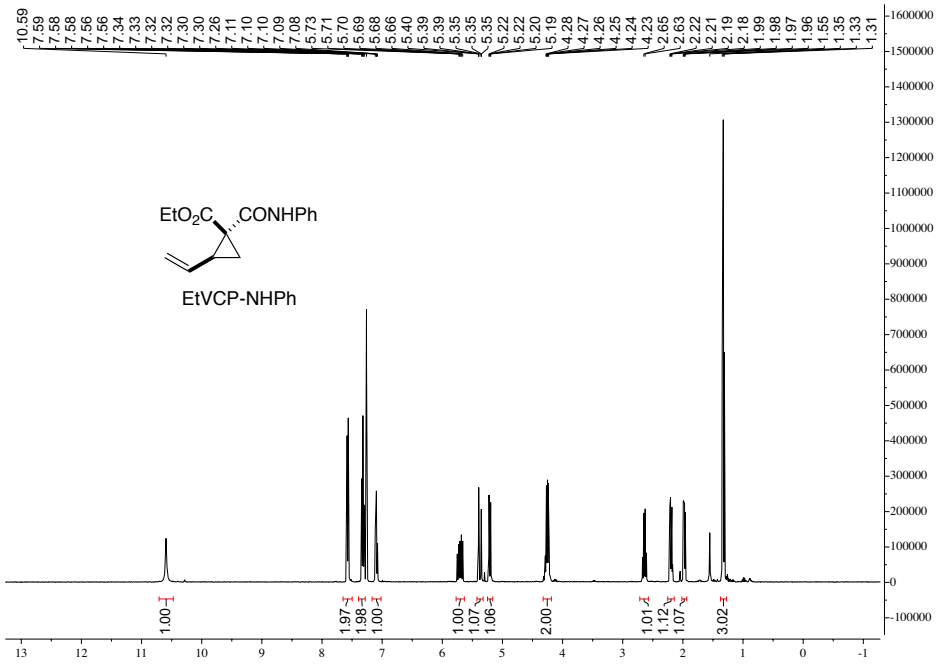

Figure S2.3. ^{1}H-NMR spectrum of EtVCP-NHPh in $CDCl_3$

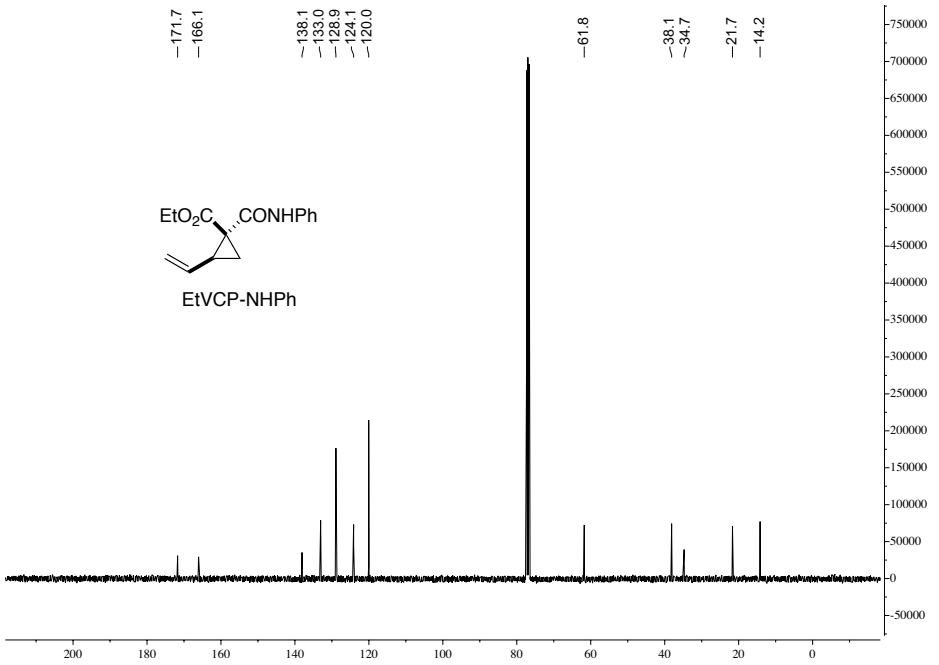

Figure S2.4. ^{13}C-NMR spectrum of EtVCP-NHPh in $CDCl_3$.

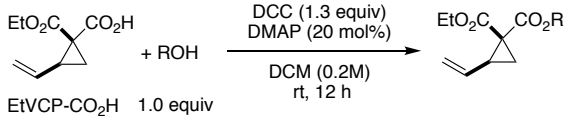

General Procedure A: To a solution of 1-(ethoxycarbonyl)-2-vinylcyclopropane-1-carboxylic acid (1.1 equiv.) in anhydrous DCM (0.2 M) at 0 °C, appropriate alcohol (1.0 equiv), DMAP (0.20 equiv.), and DCC (1.3 equiv.) was sequentially added. The mixture was then vigorously stirred at room temperature for 12h. The white precipitate was filtered off and the filtrate was concentrated *in vacuo*. The residue was purified by silica gel chromatography using hexane/EtOAc as the eluent.

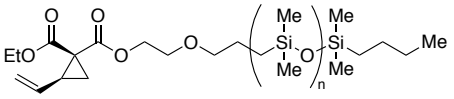

EtVCP-PDMS (1.4 kDa)

Synthesized from 1-(ethoxycarbonyl)-2-vinylcyclopropane-1-carboxylic acid and *1.0 kDa monocarbinol terminated polydimethylsiloxane* (5.0 mmol scale). Colorless oil, inseparable 10:1 mixture of diasteromers. 5.23g, 88% yield. R_f = 0.30 (5% EtOAc in hexane). **^{1}H NMR** (400 MHz, $CDCl_3$) δ 5.44 (ddd, *J* = 17.0, 10.2, 8.3 Hz, 1H), 5.29 (dd, *J* = 17.2, 1.6 Hz, 1H), 5.13 (dd, *J* = 10.1, 1.7 Hz, 1H), 4.35 – 4.07 (m, 4H), 3.62 (t, *J* = 5.0 Hz, 2H), 3.41 (t, *J* = 7.0 Hz, 2H), 2.60 (q, *J* = 8.3 Hz, 1H), 1.71 (dd, *J* = 7.6, 4.9 Hz, 1H), 1.64 – 1.50 (m, 3H), 1.36 – 1.16 (m, 7H), 0.92 – 0.78 (m, 3H), 0.59 – 0.46 (m, 4H), 0.09 – 0.03 (m, 89H). **^{13}C NMR** (101 MHz, $CDCl_3$) δ 168.6, 166.2, 132.0, 117.5, 73.1, 67.2, 63.7, 60.4, 34.8, 30.3, 25.3, 24.4, 22.4, 19.5, 16.9, 13.1, 13.0, 12.8, 0.4, 0.1, 0.0, -0.4, -0.9, -1.0. M_n (^{1}H-NMR) = 1.4 kDa.

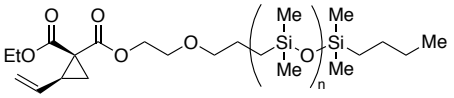

EtVCP-PDMS (5.0 kDa)

Synthesized from 1-(ethoxycarbonyl)-2-vinylcyclopropane-1-carboxylic acid and *5.0 kDa monocarbinol terminated polydimethylsiloxane* (1.0 mmol scale). Colorless oil, inseparable 10:1 mixture of diasteromers. 4.75g, 91% yield. R_f = 0.35 (5% EtOAc in hexane). **^{1}H NMR** (400 MHz, $CDCl_3$) δ 5.44 (ddd, *J* = 17.1, 10.2, 8.2 Hz, 1H), 5.29 (dd, *J* = 17.1, 1.6 Hz, 1H), 5.13 (dd, *J* = 10.1, 1.6 Hz, 1H), 4.38 – 4.06 (m, 4H), 3.62 (t, *J* = 5.0 Hz, 2H), 3.40 (t, *J* = 7.0 Hz, 2H), 2.60 (q, *J* = 8.3 Hz, 1H), 1.70 (dd, *J* = 7.6, 4.9 Hz, 1H), 1.65 – 1.50 (m, 3H), 1.35 – 1.15 (m, 7H), 0.94 – 0.78 (m, 3H), 0.60 – 0.45 (m, 4H), 0.09 – 0.03 (m, 410H). **^{13}C NMR** (101 MHz, $CDCl_3$) δ 168.6, 166.2, 132.0, 117.5, 73.1, 67.2, 63.7, 60.4, 34.8, 30.3, 25.3, 24.4, 22.4, 19.5, 16.9, 13.1, 13.0, 12.8, 0.4, 0.1, 0.0, -0.4, -0.9, -1.0. M_n (^{1}H-NMR) = 5.0 kDa.

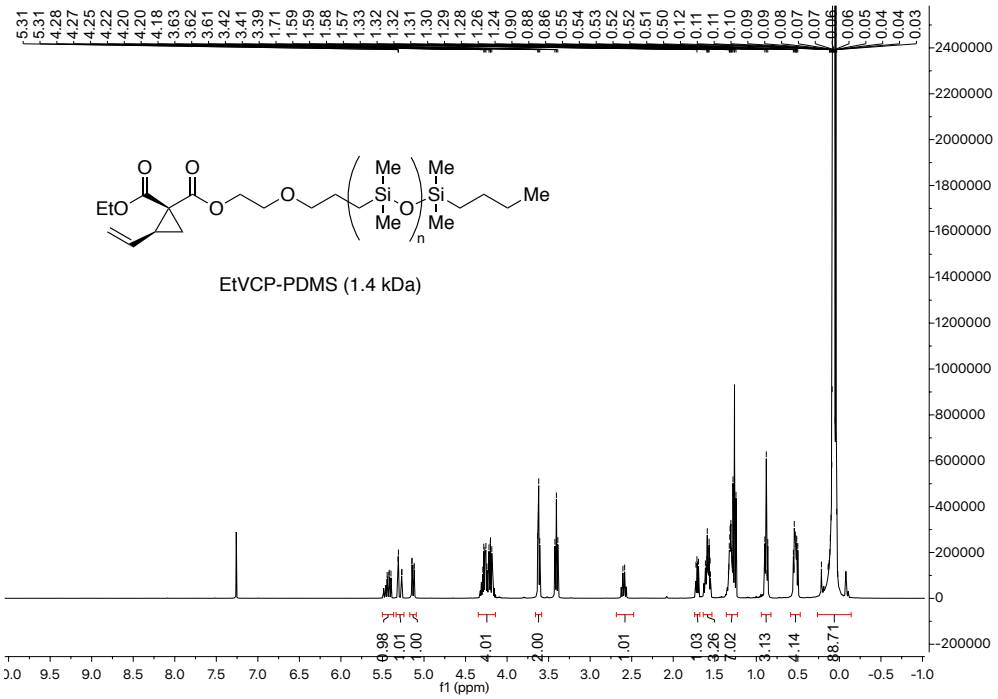

Figure S2.5. ^{1}H-NMR spectrum of EtVCP-PDMS (1.4 kDa) in $CDCl_3$.

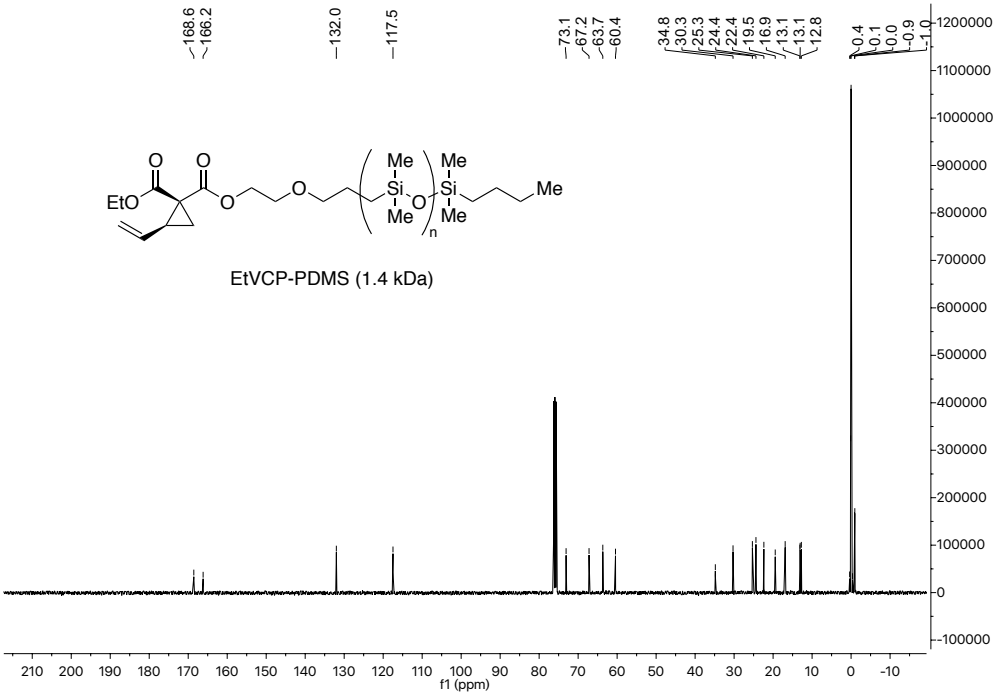

Figure S2.6. ^{13}C-NMR spectrum of EtVCP-PDMS (1.4 kDa) in $CDCl_3$

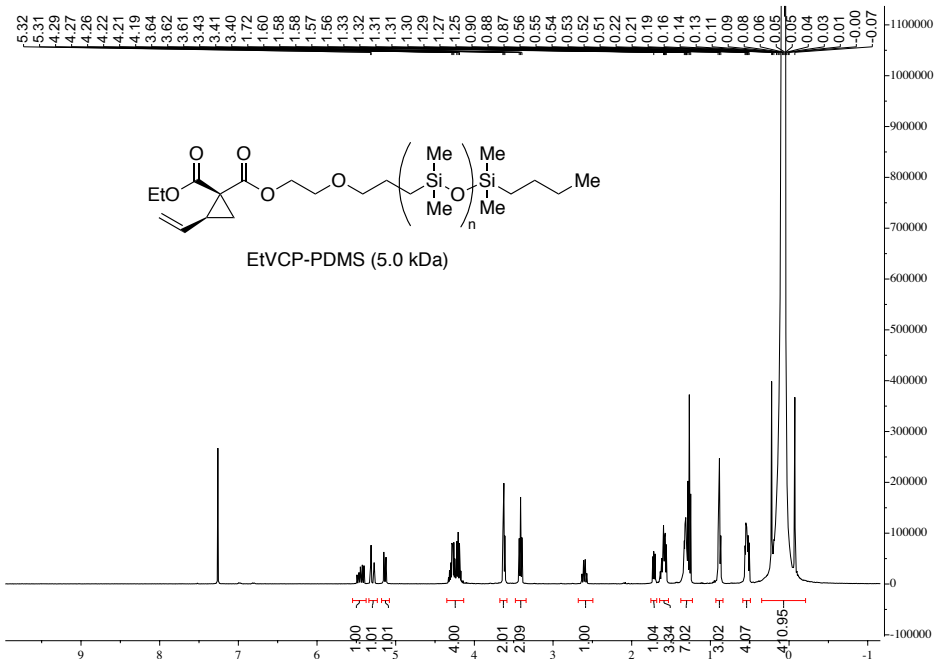

Figure S2.7. ^{1}H-NMR spectrum of EtVCP-PDMS (5.0 kDa) in $CDCl_3$.

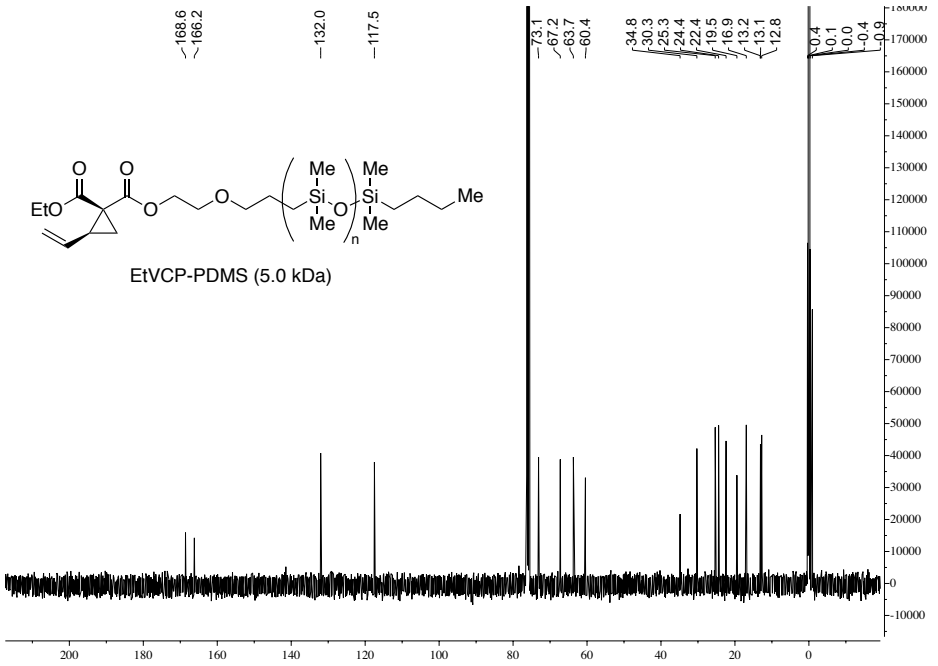

Figure S2.8. ^{13}C-NMR spectrum of EtVCP-PDMS (5.0 kDa) in $CDCl_3$.

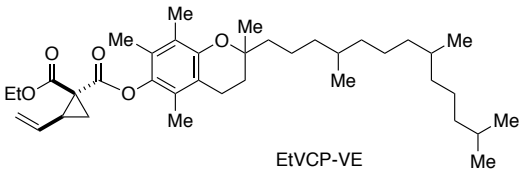

Synthesized from 1-(ethoxycarbonyl)-2-vinylcyclopropane-1-carboxylic acid and *vitamin E* (20.0 mmol scale). Colorless oil, inseparable 10:1 mixture of diasteromers. 11.02 g, 92% yield. R_f = 0.40 (15% EtOAc in hexane). **^{1}H NMR** (400 MHz, $CDCl_3$) δ 5.54 (ddd, *J* = 17.0, 10.2, 8.3 Hz, 1H), 5.37 (dd, *J* = 17.0, 1.5 Hz, 1H), 5.20 (dd, *J* = 10.1, 1.6 Hz, 1H), 4.32 – 4.19 (m, 2H), 2.74 (q, *J* = 8.3 Hz, 1H), 2.59 (t, *J* = 6.8 Hz, 2H), 2.20 – 1.90 (m, 9H), 1.89 – 1.71 (m, 3H), 1.67 (dd, *J* = 9.0, 4.8 Hz, 1H), 1.63 – 1.01 (m, 27H), 0.92 – 0.80 (m, 12H). **^{13}C NMR** (101 MHz, $CDCl_3$) δ 168.50, 167.3, 149.5, 140.4, 132.8, 126.8, 125.0, 123.1, 118.8, 117.5, 75.1, 61.7, 39.4, 37.56, 37.53, 37.46, 37.42, 37.39, 37.38, 37.34, 37.29, 35.9, 32.8, 32.8, 32.7, 32.6, 31.0, 28.0, 24.8, 24.8, 24.5, 22.7, 22.6, 21.0, 21.0, 20.8, 20.6, 19.8, 19.7, 19.7, 19.6, 19.60, 14.2, 12.8, 12.0, 11.8.

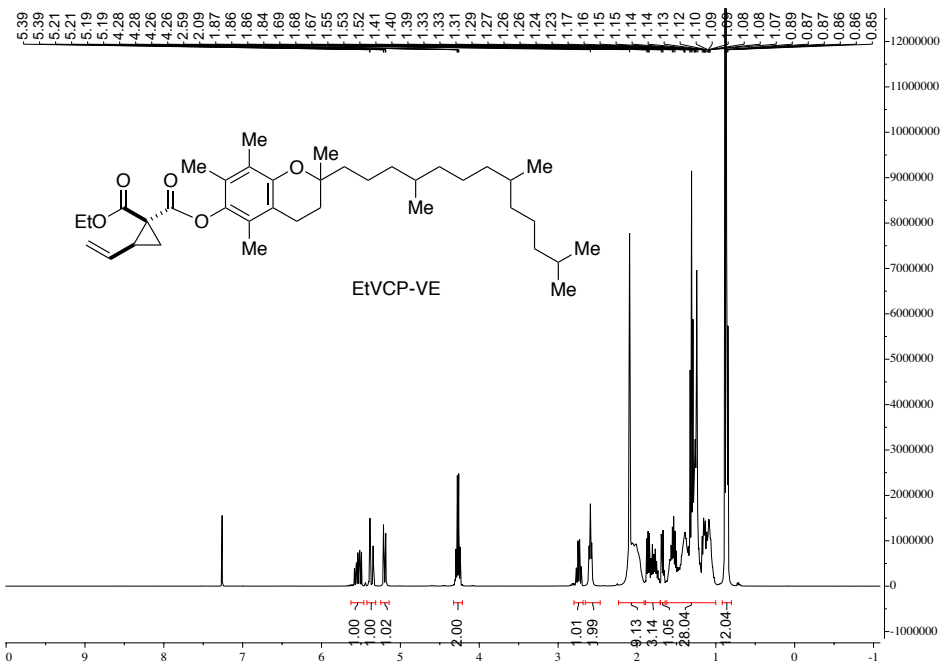

Figure S2.9. ^{1}H-NMR spectrum of EtVCP-VE in $CDCl_3$.

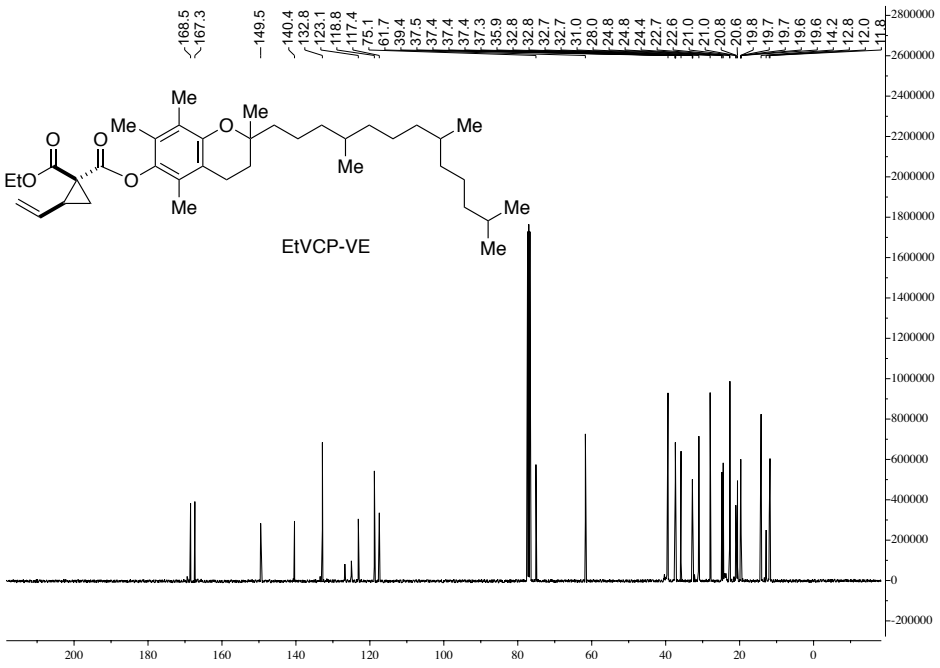

Figure S2.10. ^{13}C-NMR spectrum of EtVCP-VE in $CDCl_3$.

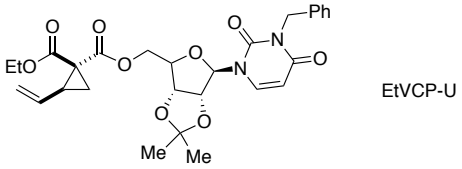

Synthesized from 1-(ethoxycarbonyl)-2-vinylcyclopropane-1-carboxylic acid and *3-N-benzyl-2',3'-O-isopropylideneuridine*[5] (20.0 mmol scale). White solid, inseparable 10:1 mixture of diasteromers. 8.5 g, 79% yield. R_f = 0.30 (70% EtOAc in hexane). **^{1}H NMR** (400 MHz, $CDCl_3$) δ 7.49 – 7.42 (m, 2H), 7.36 – 7.21 (m, 4H), 5.86 – 5.70 (m, 2H), 5.51 – 5.37 (m, 1H), 5.31 (d, *J* = 17.1 Hz, 1H), 5.20 – 5.10 (m, 2H), 5.05 (d, *J* = 13.8 Hz, 1H), 4.89 (ddd, *J* = 16.6, 6.5, 2.4 Hz, 1H), 4.84 – 4.80 (m, 1H), 4.53 (dd, *J* = 11.9, 3.6 Hz, 0.5H), 4.42 – 4.29 (m, 2H), 4.27 – 4.09 (m, 2.5H), 2.67 – 2.51 (m, 1H), 1.76 (ddd, *J* = 7.8, 5.0, 3.0 Hz, 1H), 1.63 – 1.58 (m, 1H), 1.58 – 1.54 (m, 3H), 1.38 – 1.31 (m, 3H), 1.28 – 1.19 (m, 3H). **^{13}C NMR** (100 MHz, $CDCl_3$) δ 169.32, 169.28, 166.9, 162.5, 150.8, 139.5, 138.8, 136.50, 136.48, 132.6, 132.4, 129.13, 129.10, 128.4, 127.7, 119.2, 119.2, 114.7, 114.5, 102.4, 102.2, 94.3, 94.1, 84.9, 84.5, 84.39, 84.35, 80.8, 80.7, 65.0, 64.6, 61.62, 61.56, 44.2, 35.51, 35.47, 32.3, 32.1, 27.2, 27.1, 25.4, 25.3, 21.1, 21.0, 14.2.

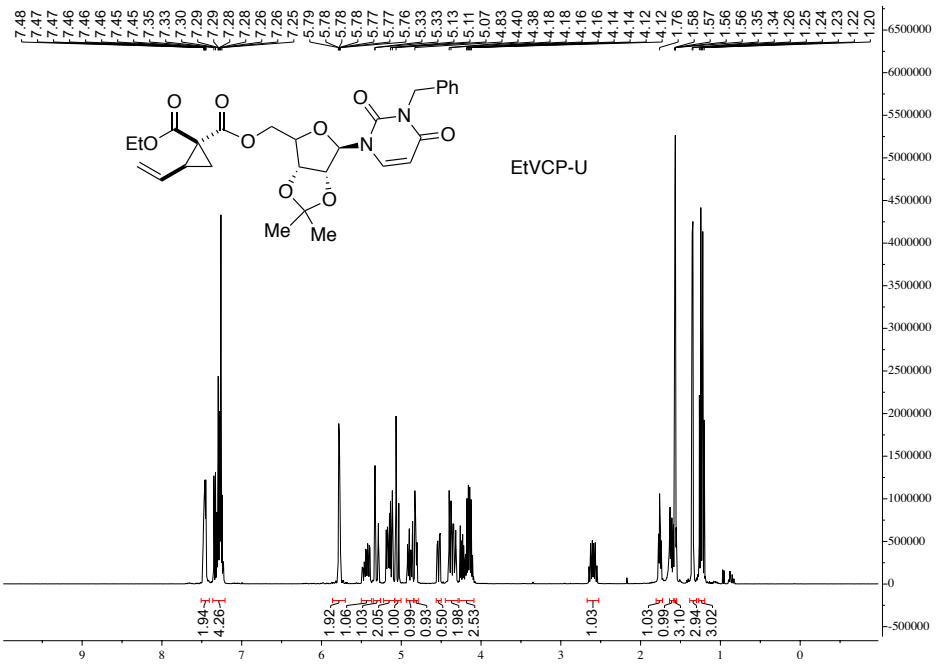

Figure S2.11. ^{1}H-NMR spectrum of EVCP-U in $CDCl_3$.

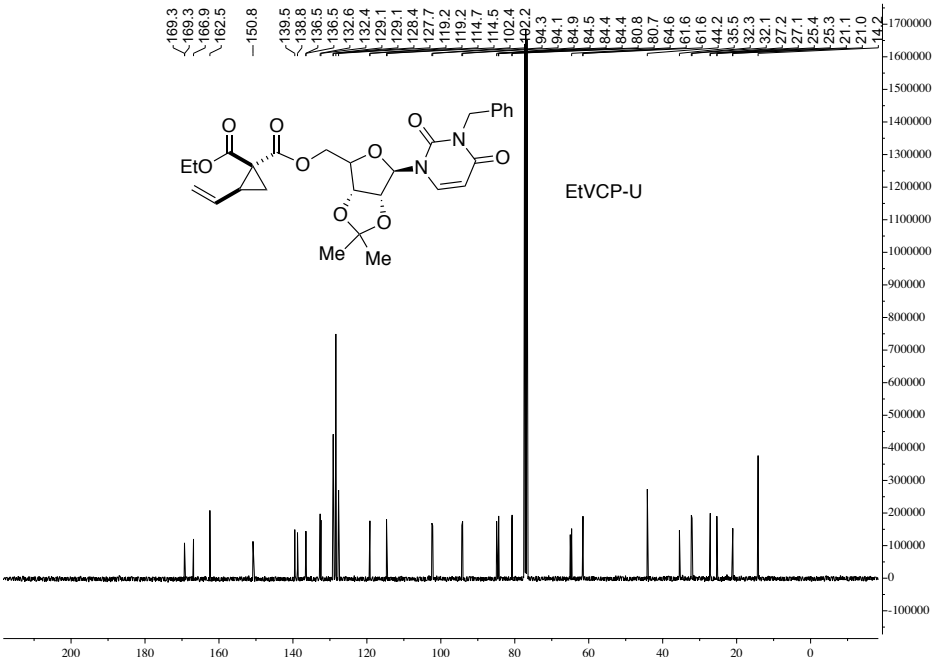

Figure S2.12. ^{13}C-NMR spectrum of EtVCP-U in $CDCl_3$.

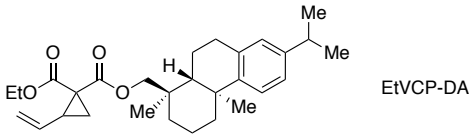

Synthesized from 1-(ethoxycarbonyl)-2-vinylcyclopropane-1-carboxylic acid and dehydroabietic methanol[6] (20.0 mmol scale). White solid, inseparable 10:1 mixture of diasteromers. 6.2 g, 68% yield. R_f = 0.35 (20% EtOAc in hexane). **^{1}H NMR** (400 MHz, $CDCl_3$) δ 7.17 (dd, *J* = 8.1, 1.4 Hz, 1H), 6.99 (dt, *J* = 8.1, 2.3 Hz, 1H), 6.88 (d, *J* = 2.0 Hz, 1H), 5.50 – 5.35 (m, 1H), 5.32 – 5.22 (m, 1H), 5.16 – 5.08 (m, 1H), 4.36 – 3.60 (m, 4H), 2.98 – 2.72 (m, 3H), 2.61 – 2.51 (m, 1H), 2.36 – 2.24 (m, 1H), 1.86 – 1.32 (m, 10H), 1.27 – 1.19 (m, 9H), 1.13 (t, *J* = 7.1 Hz, 1.7H), 1.04 (t, *J* = 7.1 Hz, 1.3H), 0.96 (d, *J* = 2.0 Hz, 3H). **^{13}C NMR** (100 MHz, $CDCl_3$) δ 169.8, 167.30, 167.27, 147.04, 146.98, 145.6, 134.7, 134.6, 133.1, 133.0, 126.8, 126.7, 124.3, 124.2, 123.9, 123.8, 118.4, 73.9, 73.8, 61.51, 61.48, 44.7, 44.3, 38.5, 38.4, 37.40, 37.36, 37.0, 36.9, 35.99, 35.97, 35.62, 35.60, 33.5, 31.19, 31.17, 30.2, 30.0, 25.3, 25.2, 24.04, 24.01, 23.98, 20.5, 19.1, 19.0, 18.51, 18.47, 17.4, 17.3, 14.1, 14.0.

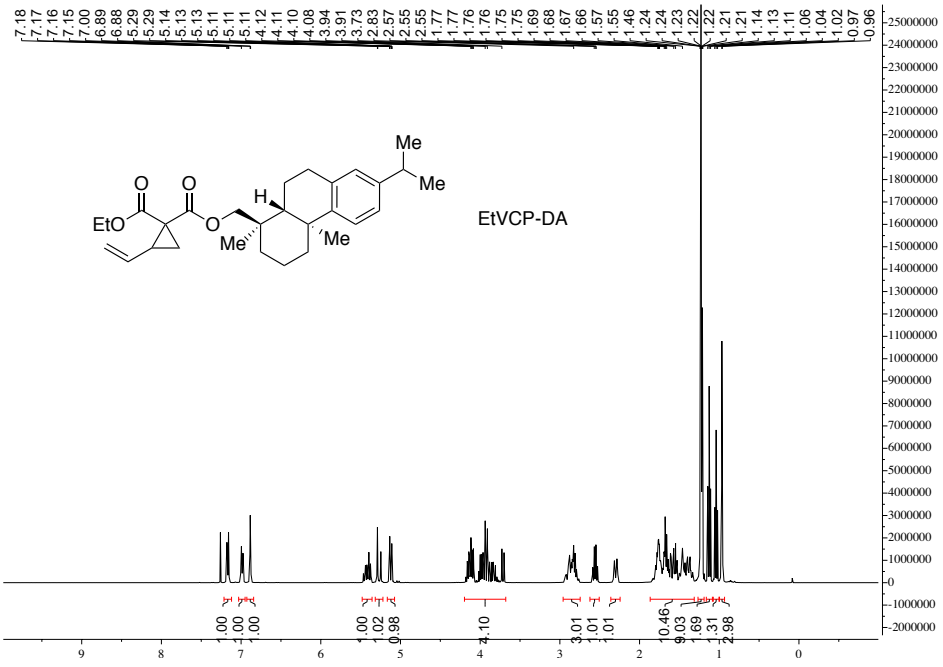

Figure S2.13. ^{1}H-NMR spectrum of EtVCP-DA in $CDCl_3$.

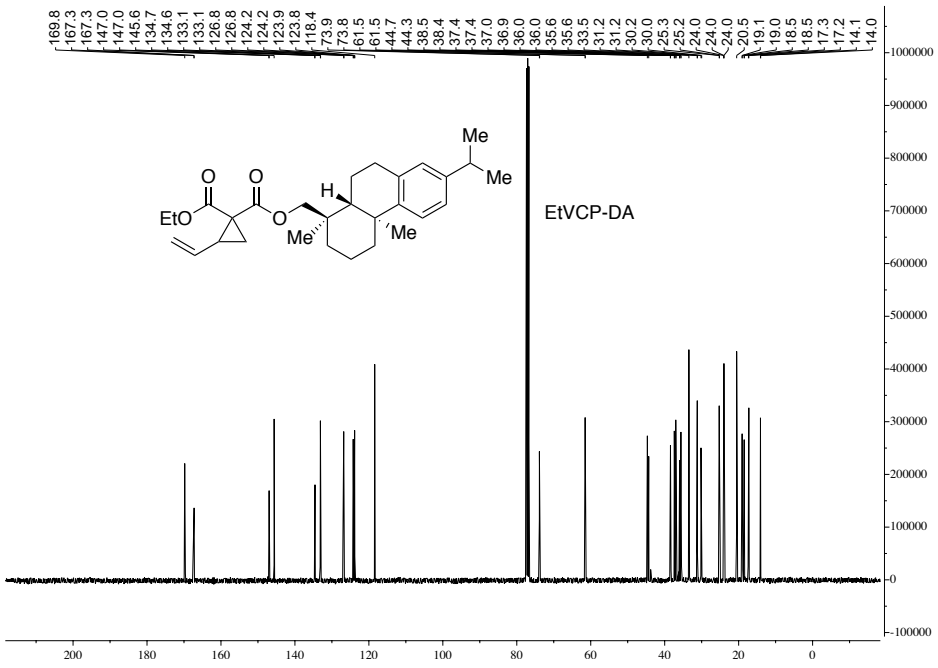

Figure S2.14. ^{13}C-NMR spectrum of EtVCP-DA in $CDCl_3$.

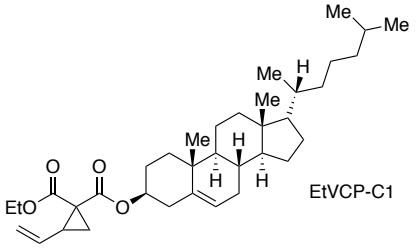

Synthesized from 1-(ethoxycarbonyl)-2-vinylcyclopropane-1-carboxylic acid and *cholesterol* (6.0 mmol scale). White solid, inseparable 10:1 mixture of diasteromers. 2.73 g, 82% yield. R_f= 0.40 (5% EtOAc in hexane). **^{1}H NMR** (400 MHz, $CDCl_3$) δ 5.52 – 5.23 (m, 3H), 5.12 (dd, *J* = 10.1, 1.7 Hz, 1H), 4.75 – 4.55 (m, 1H), 4.34 – 4.09 (m, 2H), 2.63 – 2.47 (m, 1H), 2.40 – 2.22 (m, 2H), 2.12 – 1.76 (m, 5H), 1.71 – 0.74 (m, 38H), 0.67 (s, 3H).. **^{13}C NMR** (100 MHz, $CDCl_3$) δ 169.0, 167.5, 139.4, 133.2, 122.8, 118.3, 75.3, 61.4, 56.7, 56.1, 50.0, 42.3, 39.7, 39.5, 37.9, 36.9, 36.6, 36.2, 36.1, 35.8, 31.9, 31.8, 30.9, 28.2, 28.0, 27.6, 24.3, 23.8, 22.8, 22.6, 21.0, 20.3, 19.3, 18.7, 14.2, 11.8.

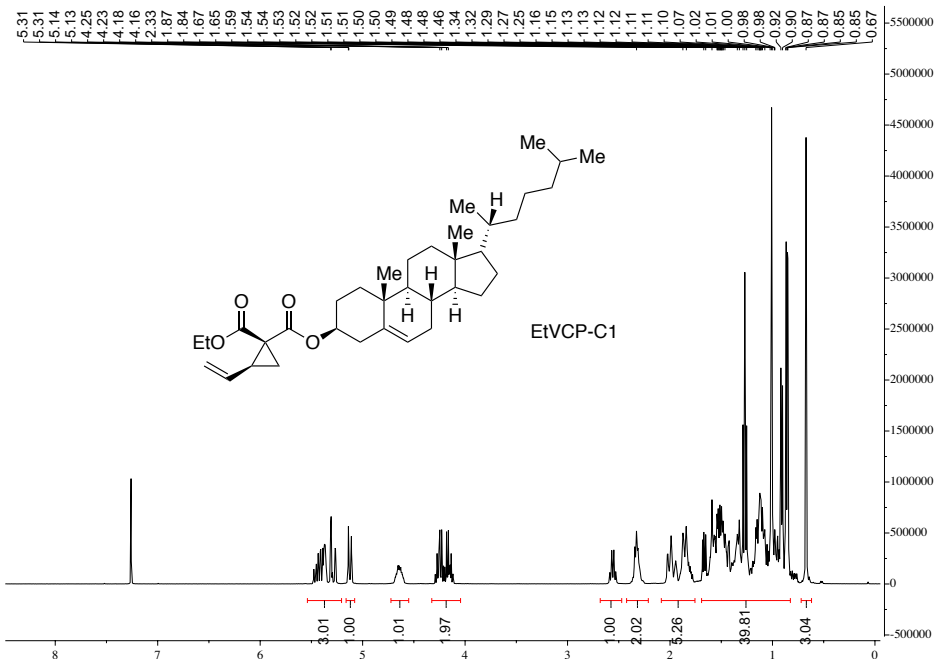

Figure S2.15. ^{1}H-NMR spectrum of EtVCP-C1 in $CDCl_3$.

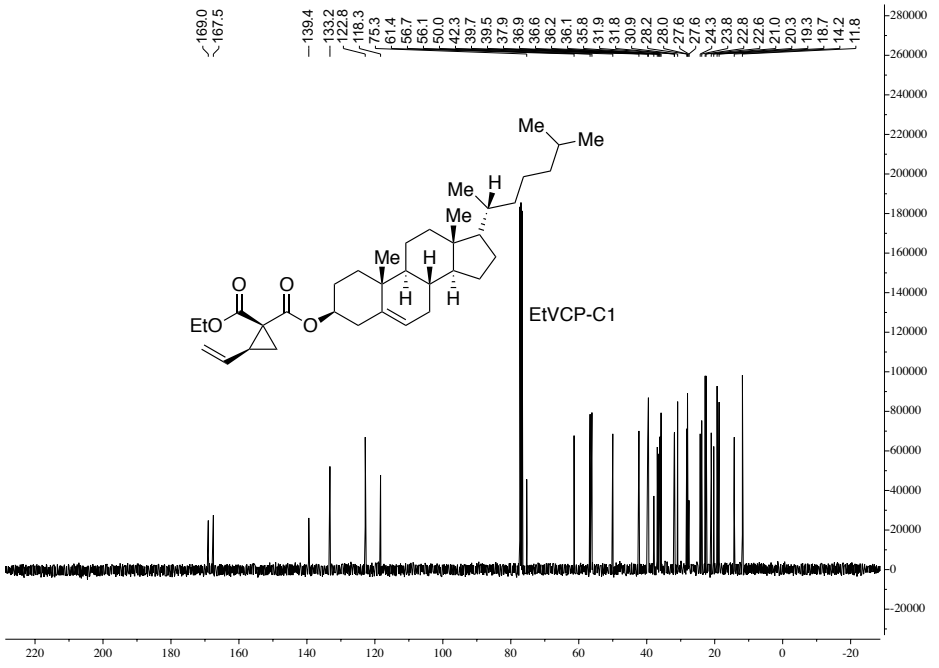

Figure S2.16. ^{13}C-NMR spectrum of EtVCP-C1 in $CDCl_3$.

Impact of Additives On Organocatalyzed Photoreodx Radical Ring-Opening Polymerization of EtVCP

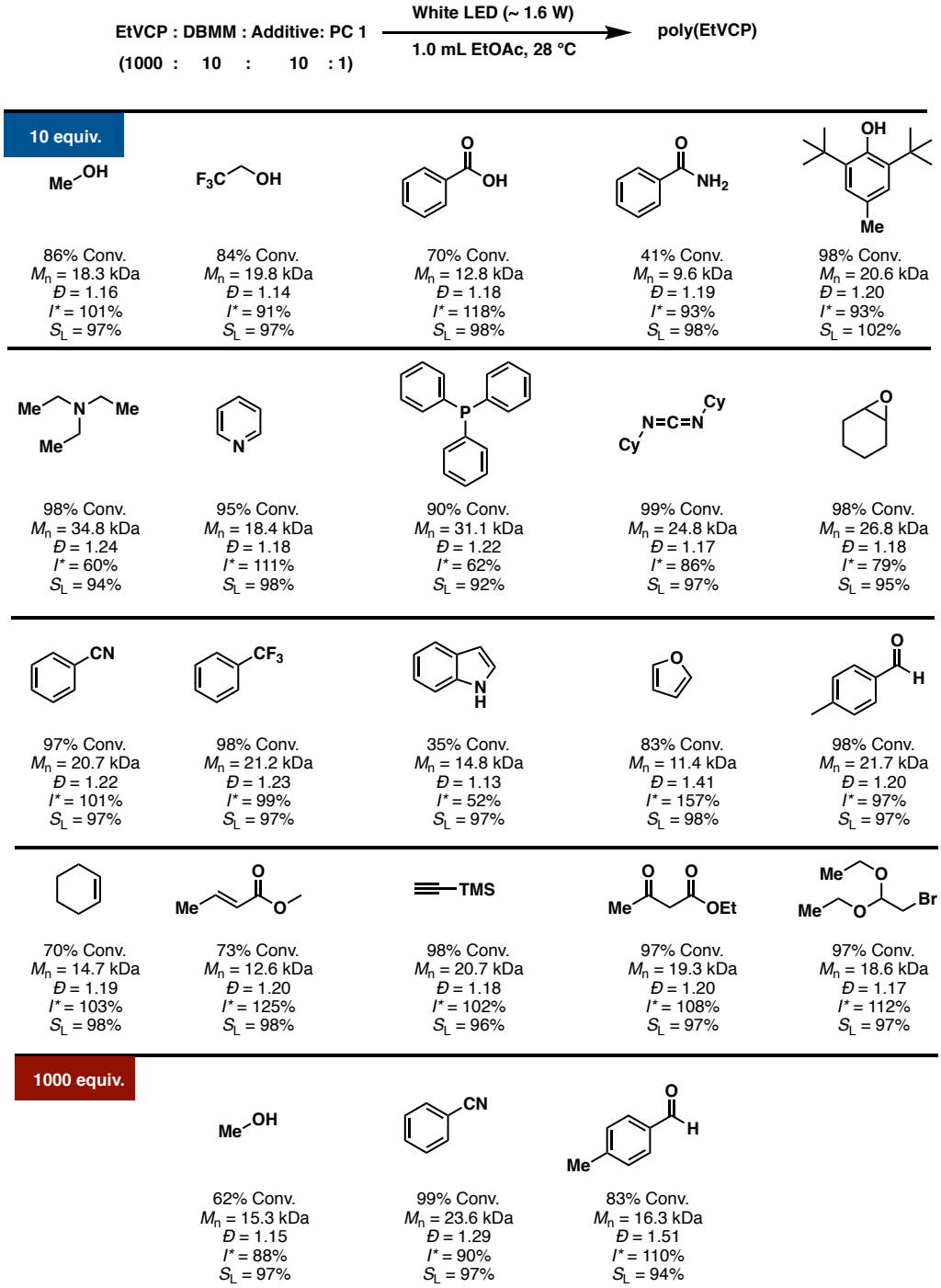

Figure S2.17. Impact of additives on organocatalyzed radical ring-opening polymerization of EtVCP.

Polymerization of CNVCP, EtVCP-CN and EtVCP-NHPh

General Procedures

General Procedure B: 1.0 mL of freshly made solution (1.0 mM) of photoredox catalyst (PC) in anhydrous dichloromethane was added to a 20 mL scintillation vial equipped with a small magnetic stir bar. The solvent was removed and the vial was dried under vacuum for 12 h, then transferred into a N_2-filled glove box. To this vial, solvent, monomer (1.0 mmol) and 0.10 M of the initiator stock solution were sequentially added. The vial was then tightly capped and placed into a white-light LED beaker while stirring in the glove box. The temperature was about 28 °C with a cooling fan. For the analysis of the polymerization at a given time point, a 0.10 mL aliquot of the reaction mixture was taken via syringe and immediately quenched by injecting into a 1.5 mL vial containing ~0.70 mL $CDCl_3$ with 250 ppm butylated hydroxytoluene (BHT). This aliquot was then analyzed via ^1H NMR for monomer conversion. The aliquot was then dried under vacuum to remove all volatiles, re-dissolved in THF and passed through a syringe filter for direct analysis by GPC. For purification, the polymerization mixture was slowly added into 50.0 mL of methanol while stirring at 0 °C. The precipitated polymer was collected by vacuum filtration, washed with cold methanol (5.0 mL × 3) and dried overnight under vacuum at 50 °C to a constant weight.

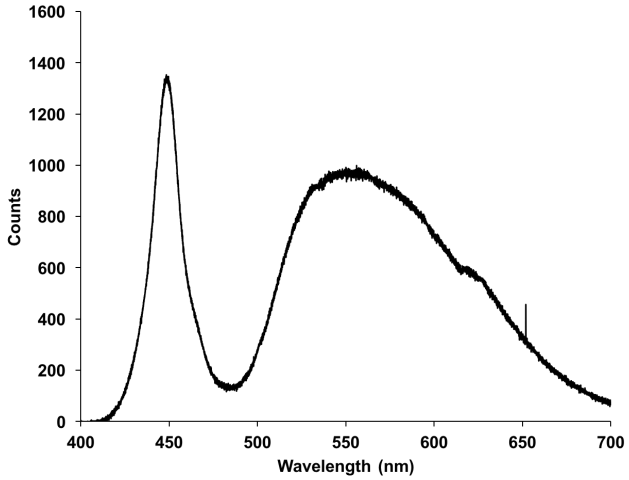

Figure S2.18. Emission spectra of the white LED.

General Procedure C: 1.0 mL of freshly made solution (1.0 mM) of photoredox catalyst (PC) in anhydrous dichloromethane (DCM) was added to a 25 mL Schlenk storage tube equipped with a

small magnetic stir bar. DCM was removed under vacuum, then transferred into a N_2-filled glove box. To this tube, anhydrous EtOAc, monomer (1.0 mmol), and 0.10 M DBMM stock solution in anhydrous EtOAc were sequentially added. The Schlenk tube was then tightly capped, taken out of the glove box, then placed into pre-heat oil bath (60 °C) while stirring. A 34 W Kessil blue LED was then immediately turned on. The distance between the Schlenk tube and the blue LED was about 5 cm. The monomer conversion and S_L were determined by crude ^{1}H-NMR while M_n and $Đ$ of the obtained polymer was determined by the GPC. Purification of the polymer followed the procedure described in **General Procedure B.**

Optimization

Table S2.1. Initiator screening for polymerization of EtVCP-CN[a]

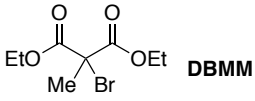

DBMM

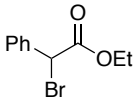

EBP

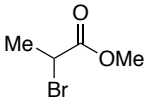

Me2BP

Entry	Initiator	Conv. (%)	M_n (kDa)	$Đ$ (M_w/M_n)	I^* (%)	S_L (%)
1	DBMM	90	17.6	1.22	86	99
2	EBP	71	21.8	1.40	55	97
3	M2BP	64	17.2	1.44	62	99

[a]Polymerizations of [EtVCP-CN]/[initiator]/[**1**] (1000/10/1) were performed in 1.0 mL of anhydrous EtOAc for 12 h, with white LEDs irradiation at 28 °C.

Table S2.2. Solvent screening for polymerization of EtVCP-CN[a]

Entry	Solvent	Conv. (%)	M_n (kDa)	$Đ$ (M_w/M_n)	I^* (%)	S_L (%)
1	DMAc	76	19.3	1.31	66	99
2	EtOAc	90	17.6	1.22	86	99
3	PhCl	85	17.2	1.47	83	98
4	DCE	51	14.9	1.64	58	99

[a]Polymerizations of [EtVCP-CN]/[DBMM]/[**1**] (1000/10/1) were performed in 1.0 mL of anhydrous solvent for 12 h, with white LEDs irradiation at 28 °C. DCE = 1,2-dichloroethane

Table S2.3. PC screening for polymerization of EtVCP-CN[a]

Entry	PC	Conv. (%)	M_n (kDa)	$Đ$ (M_w/M_n)	I^* (%)	S_L (%)
1	**1**	90	17.6	1.22	86	99
2	**2**	53	10.3	1.18	87	99
3	**3**	66	19.9	1.33	56	97

[a]Polymerizations of [EtVCP-CN]/[DBMM]/[**PC**] (1000/10/1) were performed in 1.0 mL of anhydrous EtOAc for 12 h, with white LEDs irradiation at 28 °C.

Table S2.4. Control experiments[a]

Entry	Light	**PC 1**	DBMM	Conv. (%)	$M_{n(GPC)}$ (kDa)	$Đ$ (M_w/M_n)	I^* (%)	S_L (%)
1	–	–	–	0	–	–	–	–
2	–	√	–	0	–	–	–	–
3	–	–	√	0	–	–	–	–
4	–	√	√	0	–	–	–	–
5	√	–	–	0	–	–	–	–
6	√	√	–	0	–	–	–	–
7	√	–	√	0	–	–	–	–

[a]Polymerizations of [EtVCP-CN]/[DBMM]/[**1**] (1000/10/1) were performed in 1.0 mL of anhydrous EtOAc for 12h, with white LEDs irradiation at 28 °C.

[1]H-NMR Spectrum of Poly(EtVCP-CN) and Poly(EtVCP-NHPh)

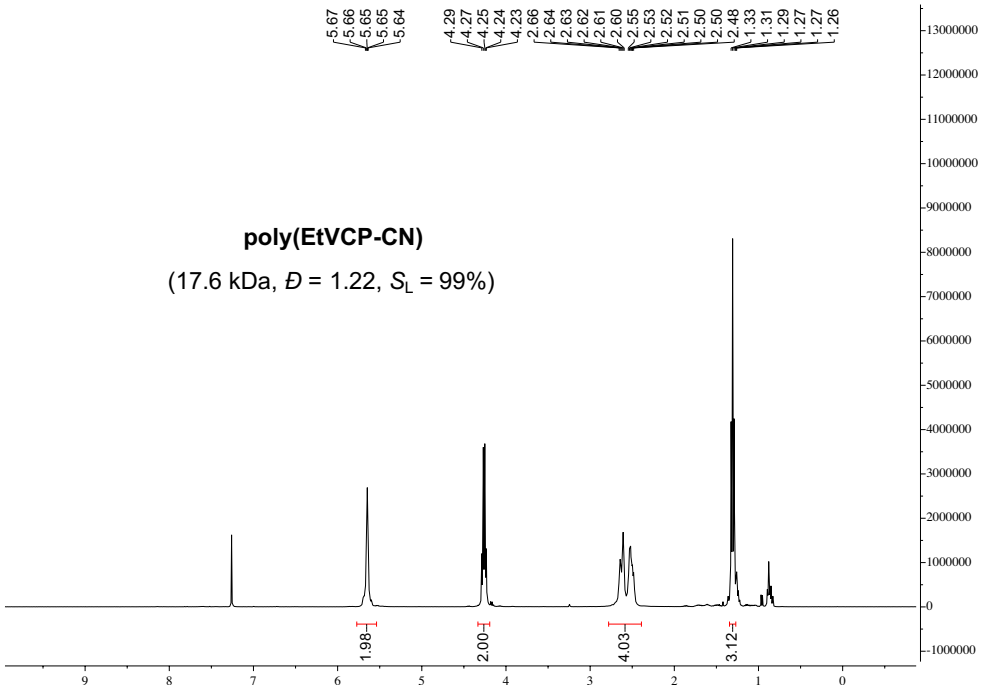

Figure S2.19. [1]H-NMR spectra of poly(EtVCP-CN).

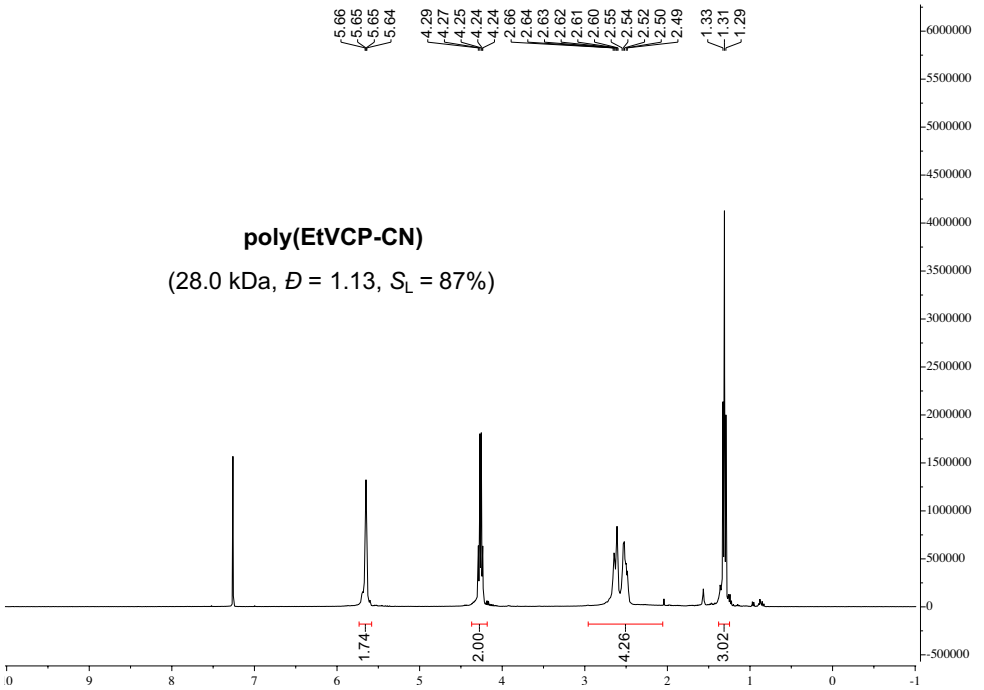

Figure S2.20. [1]H-NMR spectra of poly(EtVCP-CN).

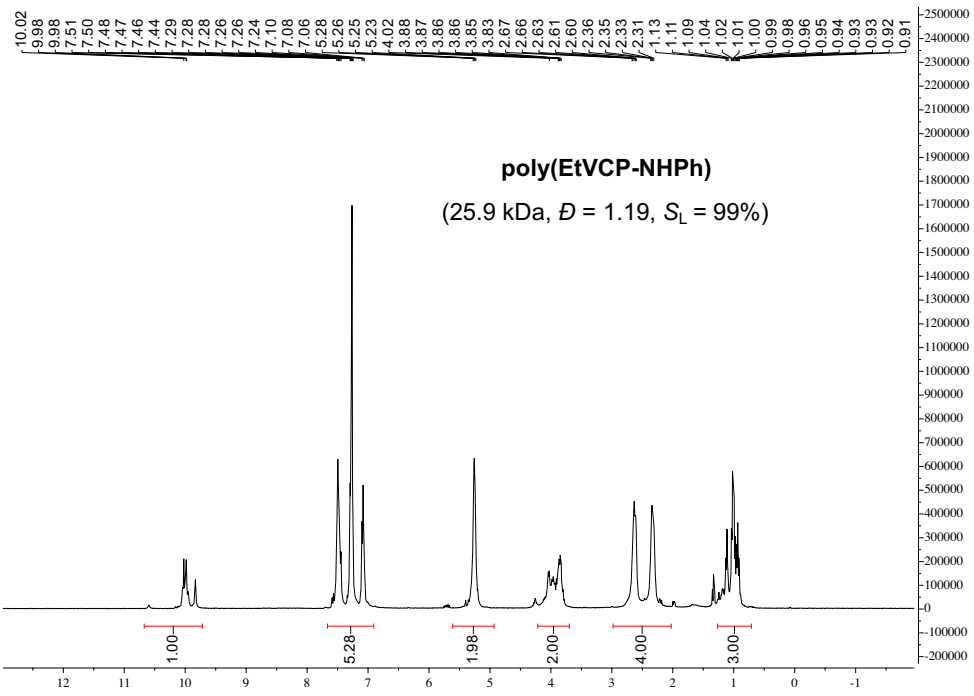

Figure S2.21. [1]H-NMR spectra of poly(EtVCP-NHPh).

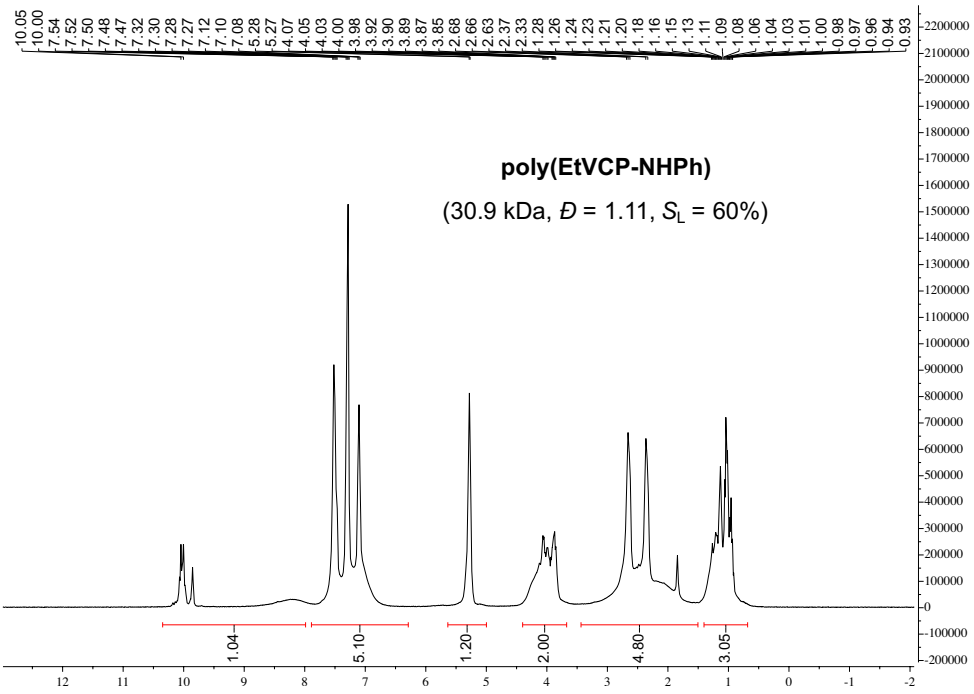

Figure S2.22. [1]H-NMR spectra of poly(EtVCP-NHPh).

GPC Traces of Poly(EtVCP-CN) and Poly(EtVCP-NHPh)

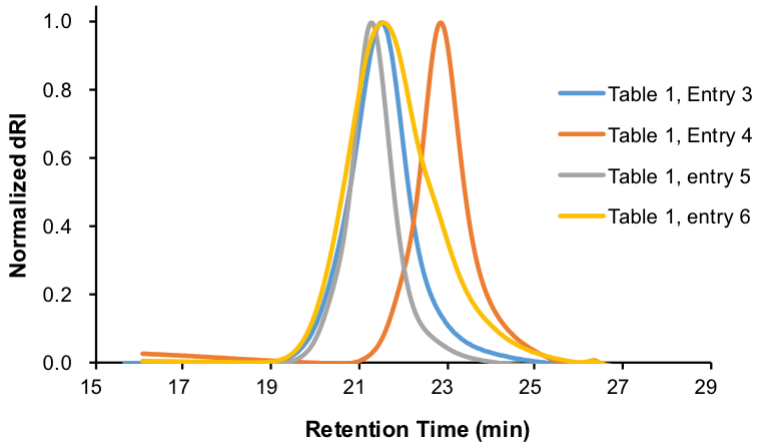

Figure S2.23. Overlay of GPC traces for poly(EtVCP-CN) in Table 2.1.

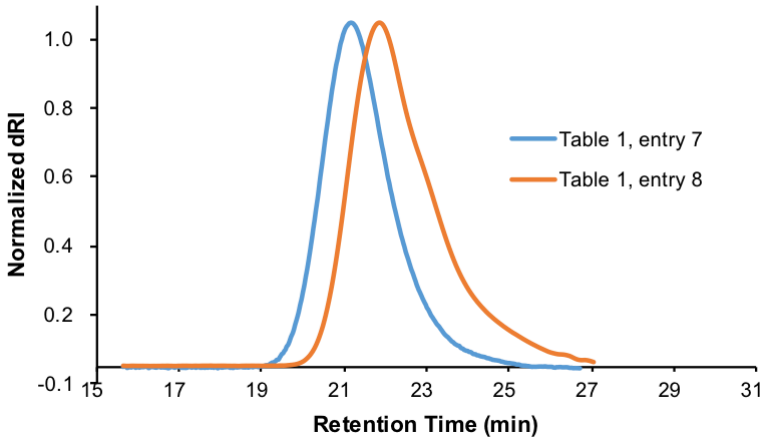

Figure S2.24. Overlay of GPC traces for poly(EtVCP-NHPh) in Table 2.1.

DCS and TGA Analysis of Poly(EtVCP-CN) and Poly(EtVCP-NHPh)

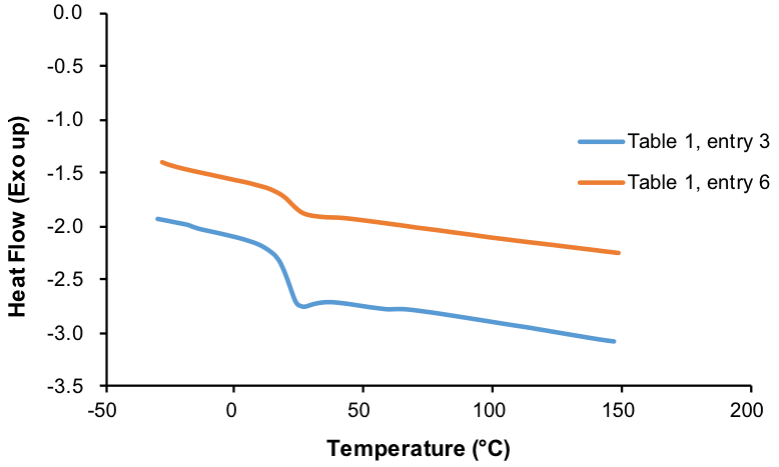

Figure S2.25. Overlay of DSC curves for poly(EtVCP-CN) in Table 2.1, entry 3 (23 °C) and entry 6 (21 °C).

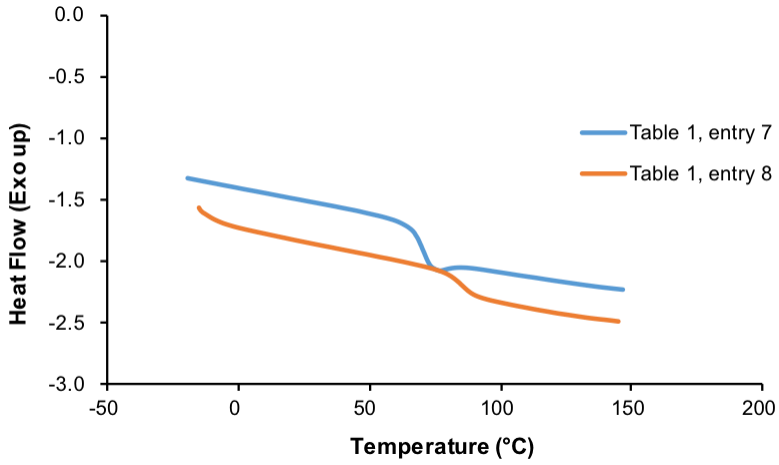

Figure S2.26. Overlay of DSC curves for poly(EtVCP-NHPh) in Table 2.1, entry 7 (71 °C) and entry 8 (77 °C)

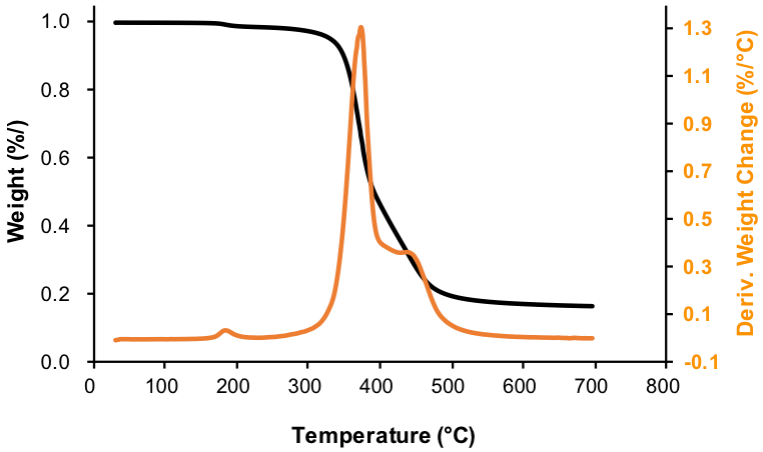

Figure S2.27. TGA and DTG curves for poly(EtVCP-CN) in Table 2.1, entry 3. T_d (10% weight loss) = 349 °C; T_{max} = 375 °C.

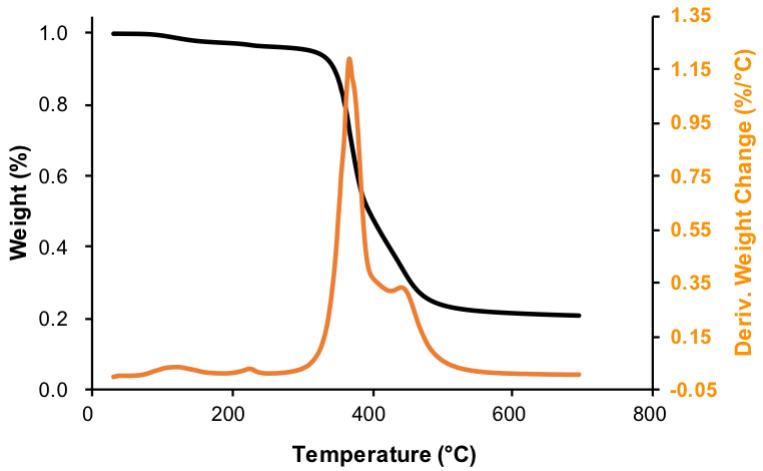

Figure S2.28. TGA and DTG curves for poly(EtVCP-CN) in Table 2.1, entry 6. T_d (10% weight loss) = 346 °C; T_{max} = 367 °C.

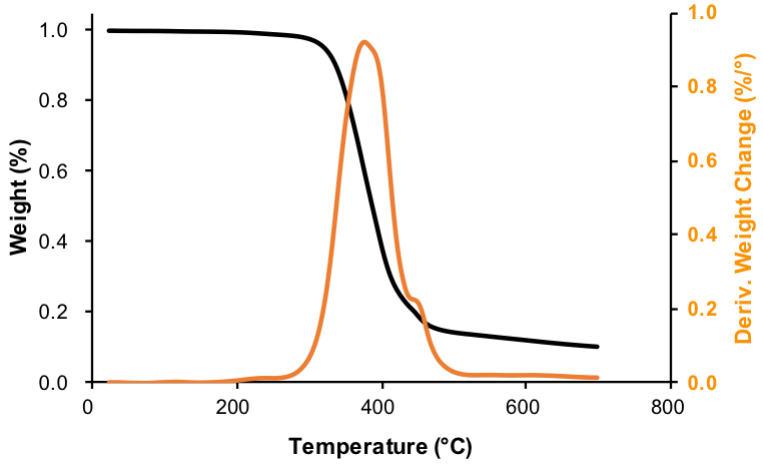

Figure S2.29. TGA and DTG curves for poly(EtVCP-NHPh) in Table 2.1, entry 7. T_d (10% weight loss) = 337 °C; T_{max} = 377 °C.

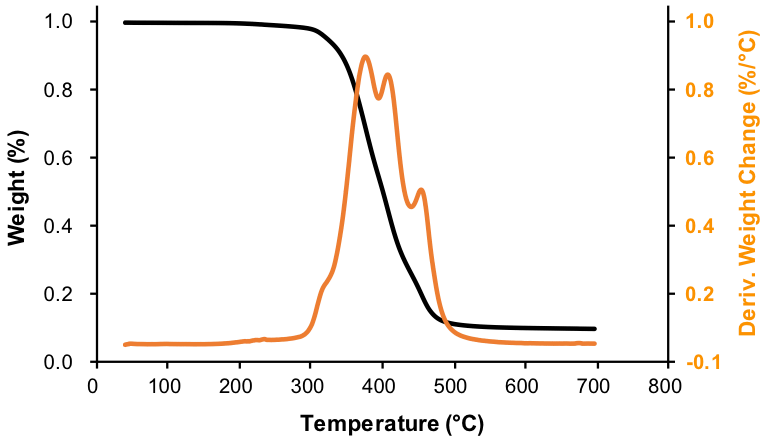

Figure S2.30. TGA and DTG curves for poly(EtVCP-NHPh) in Table 2.1, entry 8. T_d (10% weight loss) = 343 °C; T_{max1} = 376 °C, T_{max2} = 406 °C, T_{max3} = 456 °C.

Polymerization of Natural Product-Derived Vinycylopropanes

General Experimental Procedures

General Procedure D: 1.0 mL of freshly made solution (1.0 mM) of photoredox catalyst (PC) in anhydrous dichloromethane (DCM) was added to a 20 mL scintillation vial equipped with a small magnetic stir bar. DCM was removed and the vial was transferred into a N_2-filled glove box. To this vial, solvent, monomer (0.5 mmol) and 0.10 M of the initiator stock solution were sequentially added. The vial was then tightly capped and placed into a white-light LED beaker while stirring in the glove box. The temperature was about 28 °C with a cooling fan. At a given time point, a 0.10 mL aliquot of the reaction mixture was taken via syringe and immediately quenched by injecting into a 1.5 mL vial containing ~0.70 mL $CDCl_3$ with 250 ppm butylated hydroxytoluene (BHT). This aliquot was then analyzed via ^{1}H NMR for monomer conversion. The aliquot was then dried under vacuum to remove all volatiles, re-dissolved in THF and passed through a syringe filter for direct analysis by GPC. For purification, the polymerization mixture was slowly added into 30.0 mL of methanol (for polymerizations of EtVCP-VE, EtVCP-DA and EtVCP-C) or hexane (for polymerization of EtVCP-U) while stirring at 0 °C. The precipitated polymer was collected by vacuum filtration, washed with cold methanol or hexane (5.0 mL × 3) and dried overnight under vacuum at 50 °C to a constant weight.

General Procedure E: 1.0 mL of freshly made solution (1.0 mM) of photoredox catalyst (PC) in anhydrous dichloromethane (DCM) was added to a 25 mL Schlenk storage tube equipped with a small magnetic stir bar. DCM was removed and the tube was transferred into a N_2-filled glove box. Then solvent, monomer (0.5 mmol), and 0.10 M DBMM stock solution were sequentially added. The Schlenk tube was then tightly capped, taken out of the glove box, then placed into pre-heat oil bath (60 °C) while stirring. A 34 W Kessil blue LED was then immediately turned on. The distance between the Schlenk tube and the blue LED was about 5 cm. The monomer conversion and S_L were determined by crude ^{1}H-NMR while M_n and $Đ$ of the obtained polymer was determined by the GPC. Purification of the polymer followed the procedure described in **General Procedure D.**

Optimization for Polymerization of EtVCP-VE

Table S2.5. Initiator screening for polymerization of EtVCP-VE[a]

Entry	Initiator	Conv. (%)	M_n (kDa)	$Đ$ (M_w/M_n)	I^* (%)	S_L (%)
1	DBMM	96	31.6	1.29	91	96
2	EBP	80	31.8	1.48	76	96
3	M2BP	66	27.9	1.41	72	96

[a]Polymerizations of [EtVCP-VE]/[initiator]/[**1**] (500/10/1) were performed in 1.0 mL of anhydrous EtOAc for 6 h, with white LEDs irradiation at 28 °C.

Table S2.6. Solvent screening for polymerization of EtVCP-VE[a]

Entry	Solvent	Conv. (%)	M_n (kDa)	$Đ$ (M_w/M_n)	I^* (%)	S_L (%)
1	DMAc	79	27.2	1.44	88	96
2	EtOAc	96	31.6	1.29	91	96
4	PhCl	94	27.6	1.23	103	96

[a]Polymerizations of [EtVCP-VE]/[DBMM]/[**1**] (500/10/1) were performed in 1.0 mL of anhydrous solvent for 6 h, with white LEDs irradiation at 28 °C. DCE = 1,2-dichloroethane.

Table S2.7. Control experiments[a]

Entry	Light	**PC 1**	DBMM	Conv. (%)	$M_{n(GPC)}$ (kDa)	$Đ$ (M_w/M_n)	I^* (%)	S_L (%)
1	–	–	–	0	–	–	–	–
2	–	√	–	0	–	–	–	–
3	–	–	√	0	–	–	–	–
4	–	√	√	0	–	–	–	–
5	√	–	–	0	–	–	–	–
6	√	√	–	0	–	–	–	–
7	√	–	√	0	–	–	–	–

[a]Polymerizations of [EtVCP-VE]/[DBMM]/[**1**] (500/10/1) were performed in 1.0 mL of anhydrous EtOAc for 12h, with white LEDs irradiation at 28 °C.

Kinetic Study and Pulsed-Irradiation Experiment

Table S2.8. Progress analysis for polymerization of EtVCP-VE at 28 °C with white LED[a]

Entry	Time (h)	Conv. (%) *Trans*	Conv. (%) *Cis*	M_n (kDa)	$Đ$ (M_w/M_n)	I^* (%)	S_L (%)
1	0.5	25	0	10.2	1.21	75	92
2	1	51	1	17.0	1.28	93	97
3	2	77	2	24.3	1.34	98	96
4	4	86	4	27.3	1.33	99	96
5	5	88	6	29.9	1.27	96	95

[a]The polymerization of [EtVCP-VE]/[DBMM]/[**1**] (500/10/1) was performed in 1.0 mL of anhydrous EtOAc, with white LED irradiation at 28 °C.

Note: The *trans*-EtVCP-VE was polymerized faster than *cis*-EtVCP-VE due to steric hindrance. However, this does not affect the intramolecular radical cyclization preference due to faster radical racemization after the ring-opening event.

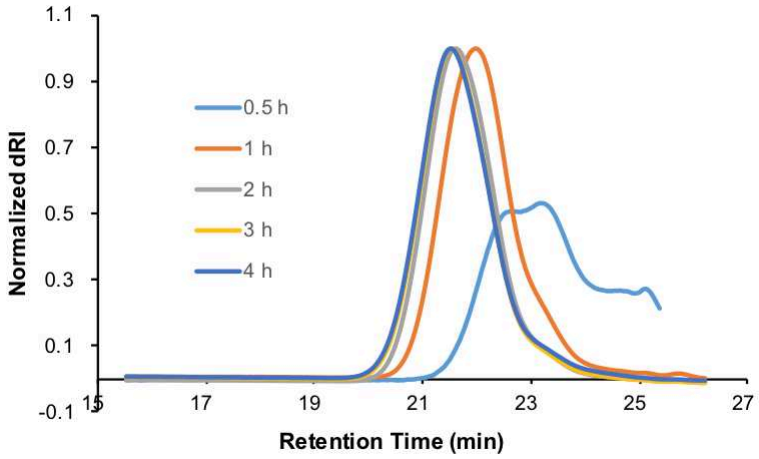

Figure S2.31. Overlay of GPC traces for poly(EtVCP-VE) in Table S2.8.

Table S2.9. Pulsed-irradiation experiment for polymerization of EtVCP-VE at 28 °C with white LED[a]

Entry	Time (h)	Conv. (%)	M_n (kDa)	$Đ$ (M_w/M_n)	I^* (%)	S_L (%)
1	0.5	26	14.1	1.44	57	91
2	1.5	26	14.0	1.51	57	91
3	3	72	24.5	1.31	89	96
4	15	72	24.3	1.32	90	96
5	16	86	26.9	1.32	97	96
6	20	86	26.8	1.32	97	96

[a]The polymerization of [EtVCP-VE]/[DBMM]/[**1**] (500/10/1) was performed in 1.0 mL of anhydrous EtOAc, with white LED irradiation at 28 °C.

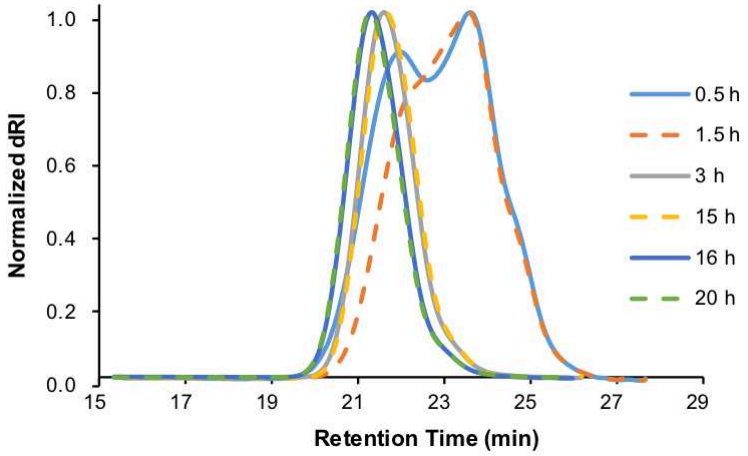

Figure S2.32. Overlay of GPC traces for poly(EtVCP-VE) in Table S2.9.

Chain-Extension Experiment

Poly(EtVCP-VE) macroinitiator (13.0 kDa, $Đ$ = 1.15, S_L = 92%) was synthesized and purified according to **General Procedure C** (1.0 mmol scale, [M]:[DBMM]:[1] = 250:10:1).

An oven-dried 20 mL scintillation vial was charged with a magnetic stir bar, the isolated poly(EtVCP) macroinitiator (130.0 mg, 0.010 mmol) and PC **1** (0.44 mg, 0.0010 mmol). The scintillation vial was transferred into a N_2-filled glovebox where 1.0 mL of anhydrous PhCl and EtVCP-C2 (166.7 mg, 0.25 mmol) were quickly added. The vial was then tightly capped and irradiated white LED while stirring in the glove box. After 12 h, a 0.10 mL aliquot was taken and quenched by injecting into a vial containing ~0.70 mL $CDCl_3$ with 250 ppm butylated hydroxytoluene (BHT). This aliquot was then analyzed via ^{1}H NMR for conversion of monomer to polymer (88% conv. was achieved in this reaction). The aliquot was then dried under vacuum for direct analysis by GPC equipped with multi-angle light scattering (M_n =31.6 kDa, $Đ$ = 1.39, I^* = 91%, S_L = 84%).

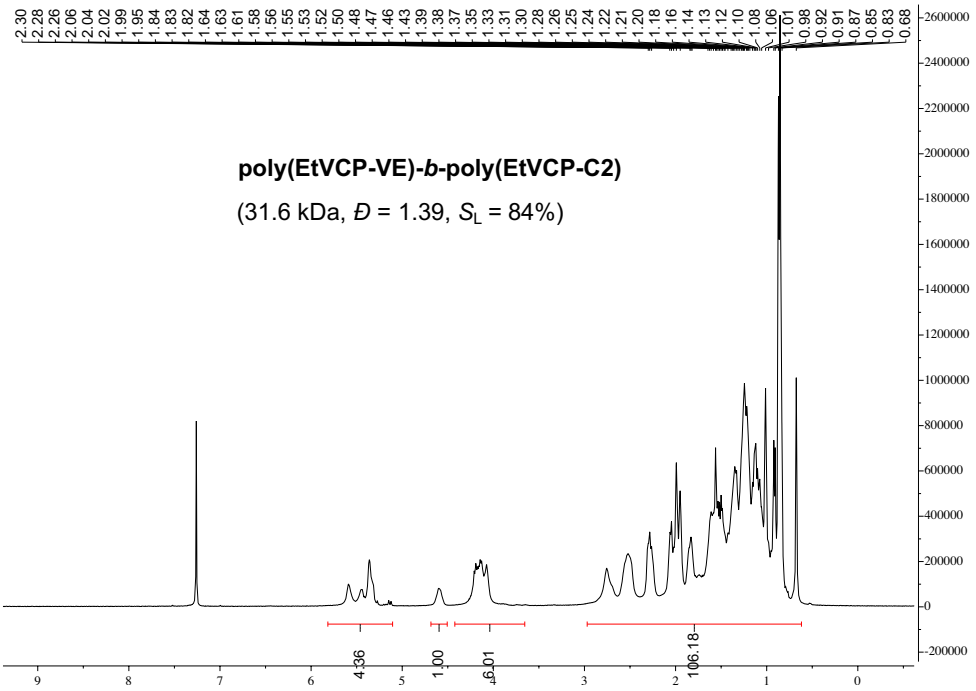

Figure S2.33. ^{1}H-NMR spectra of poly(EtVCP-VE)-*b*-poly(EtVCP-C2).

^{1}H-NMR Spectrum of Natural Product-Derived Poly(vinylcyclopropanes)

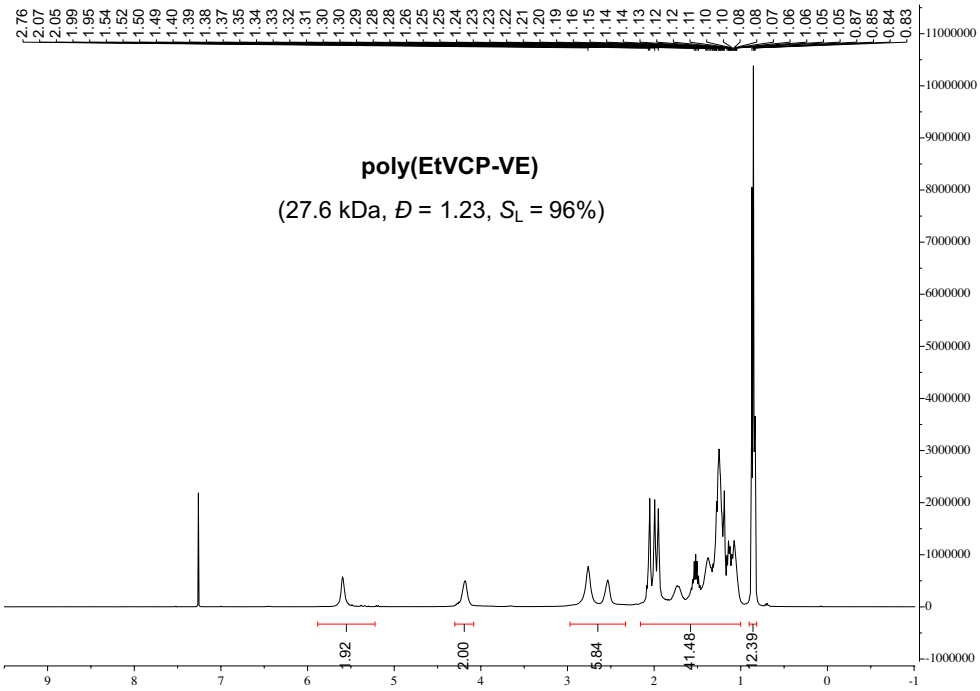

Figure S2.34. ^{1}H-NMR spectra of poly(EtVCP-VE) in Table 2.2, entry 4.

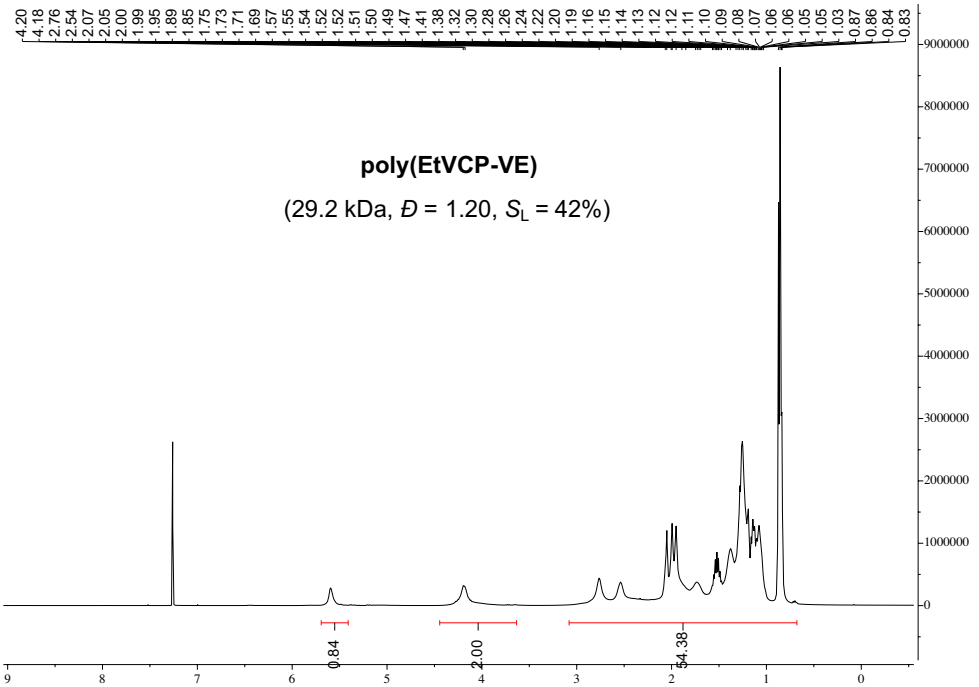

Figure S2.35. ^{1}H-NMR spectra of poly(EtVCP-VE) in Table 2.3, entry 3.

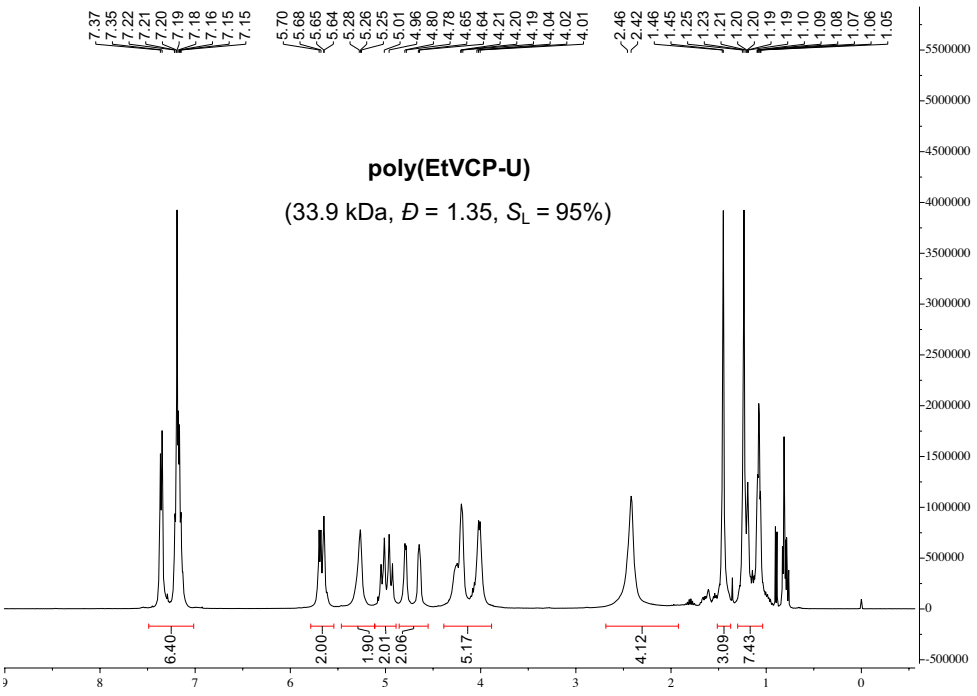

Figure S2.36. ^{1}H-NMR spectra of poly(EtVCP-U) in Table 2.2, entry 13.

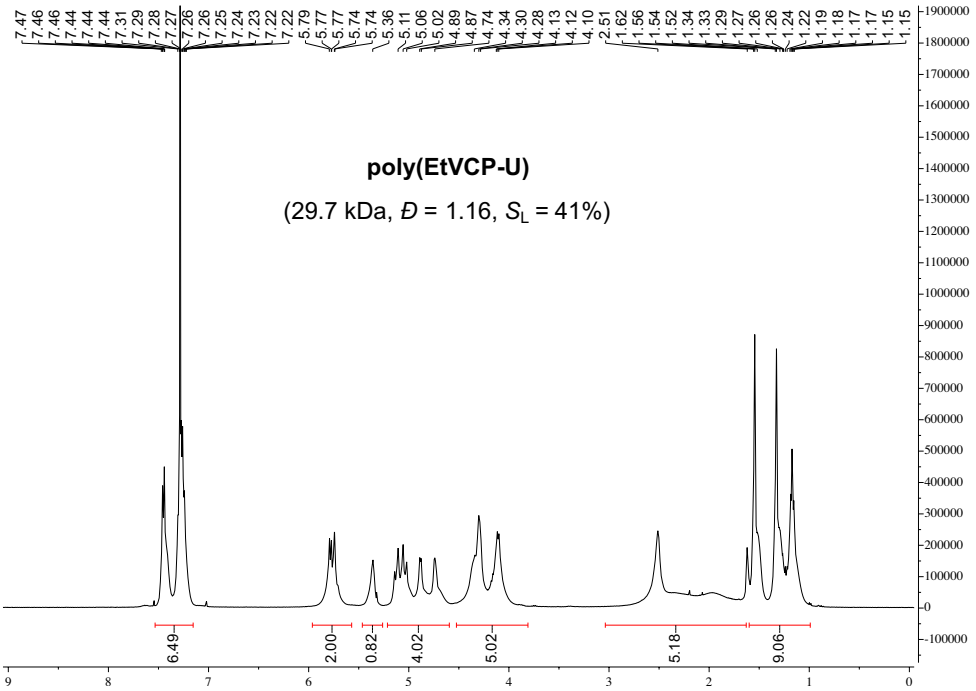

Figure S2.37. ^{1}H-NMR spectra of poly(EtVCP-U) in Table 2.3, entry 4.

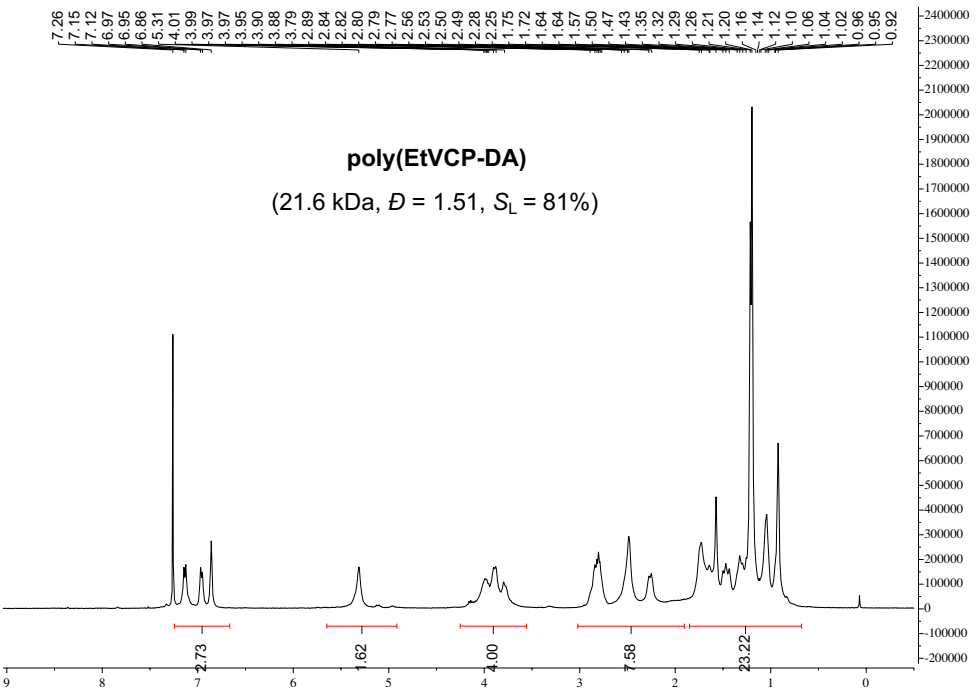

Figure S2.38. ^{1}H-NMR spectra of poly(EtVCP-DA) in Table 2.2, entry 14.

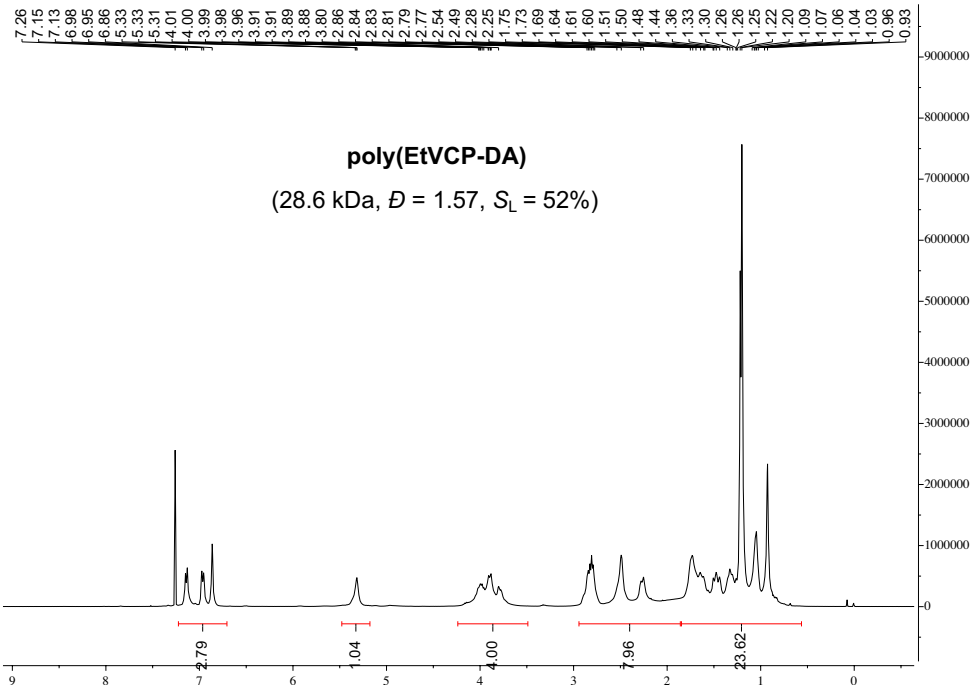

Figure S2.39. ^{1}H-NMR spectra of poly(EtVCP-DA) in Table 2.3, entry 6.

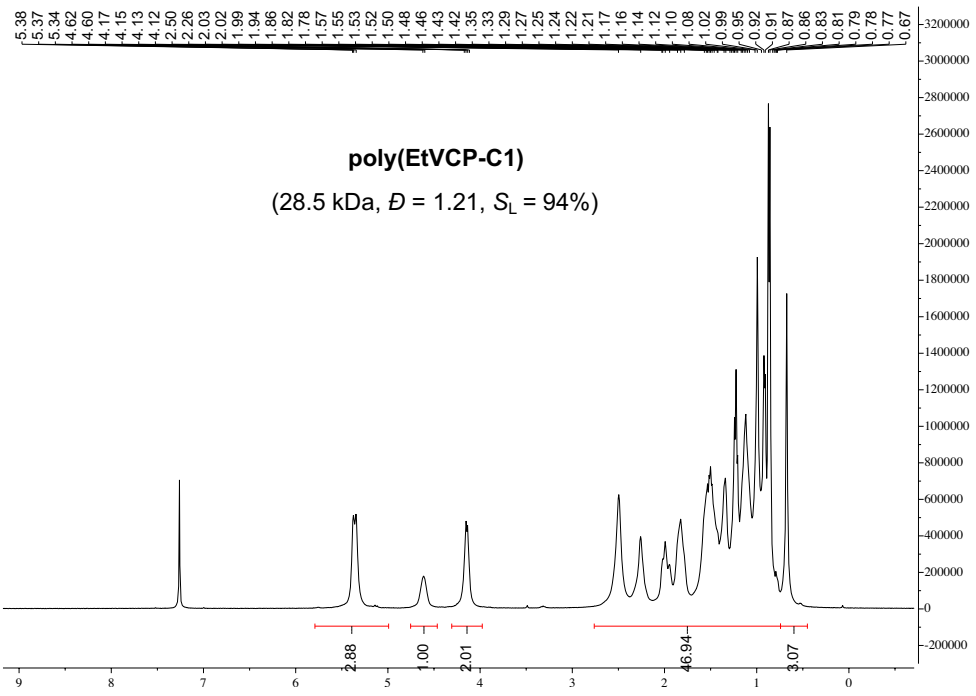

Figure S2.40. ^{1}H-NMR spectra of poly(EtVCP-C1) in Table 2.2, entry 17.

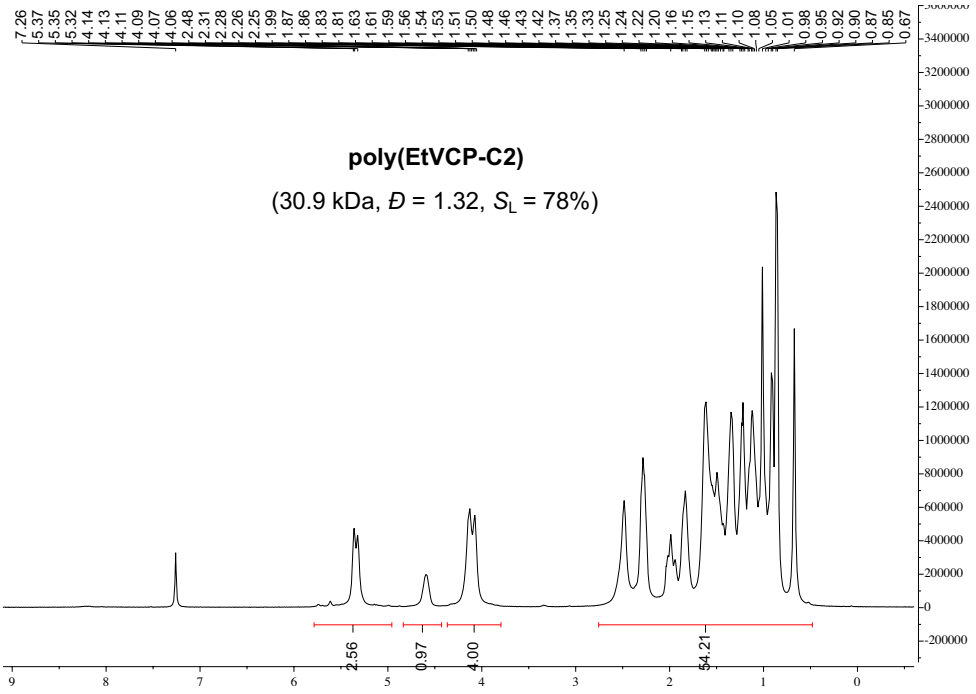

Figure S2.41. ^{1}H-NMR spectra of poly(EtVCP-C2) in Table 2.2, entry 18.

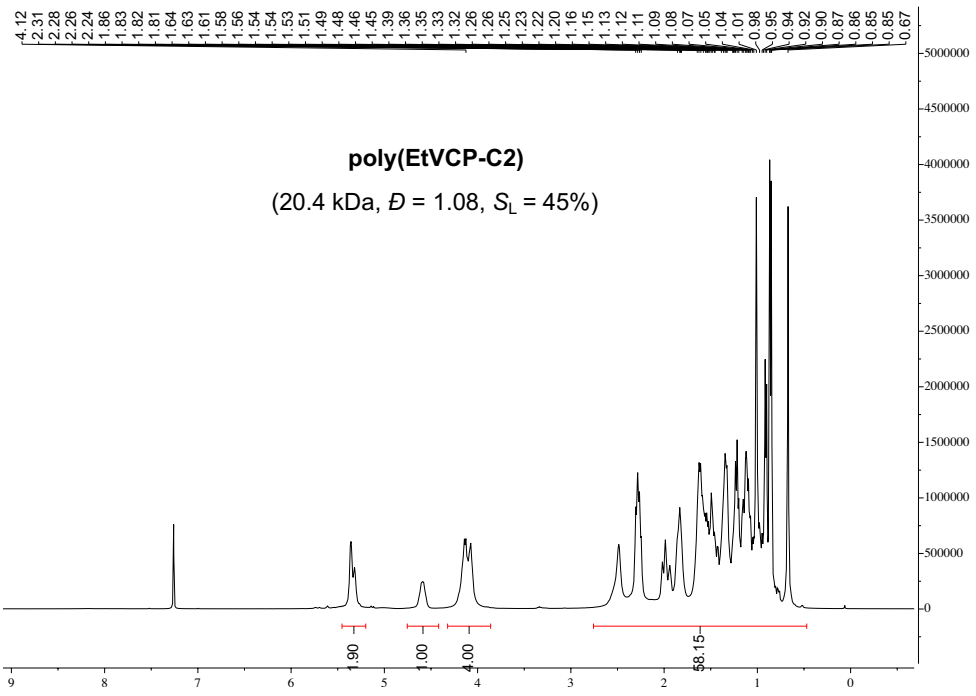

Figure S2.42. ^{1}H-NMR spectra of poly(EtVCP-C2) in Table 2.3, entry 11.

GPC Traces of Natural Product-Derived Poly(vinylcyclopropanes)

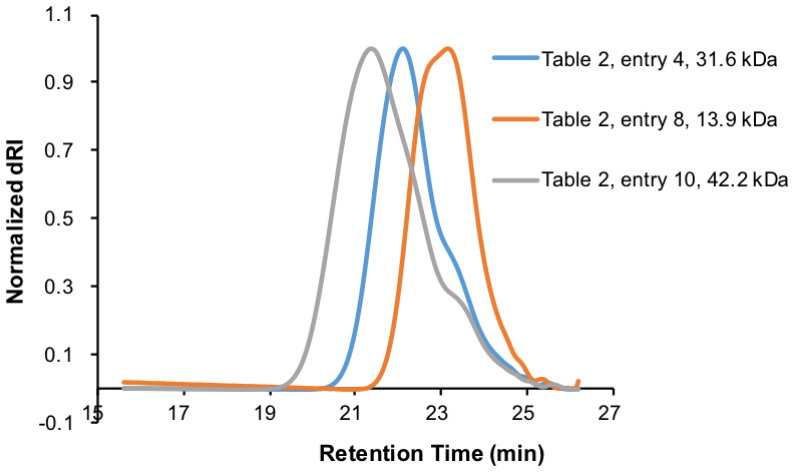

Figure S2.43. GPC traces of poly(EtVCP-VE) in Table 2.2.

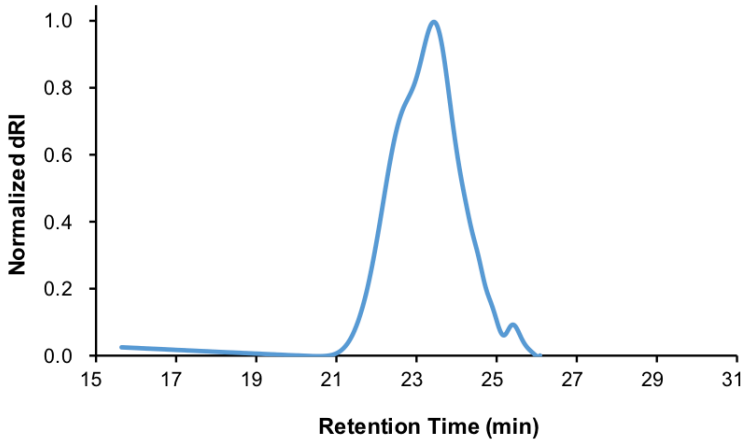

Figure S2.44. GPC traces of poly(EtVCP-VE) in Table 2.3, entry 3 (29.2 kDa, $Đ$ = 1.20, S_L = 42%).

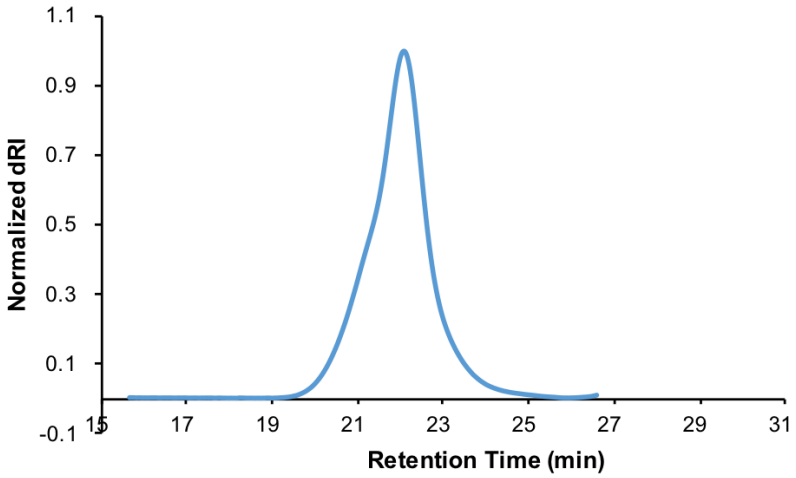

Figure S2.45. GPC traces of poly(EtVCP-U) in Table 2.2, entry 13 (33.9 kDa, $Đ$ = 1.35, S_L = 95%).

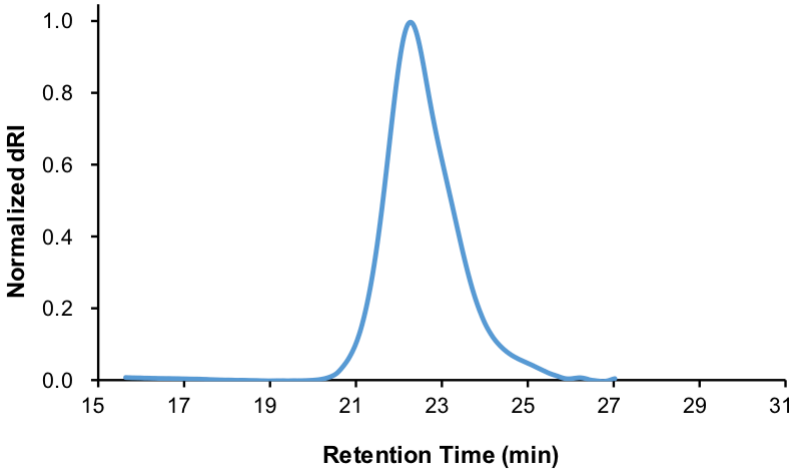

Figure S2.46. GPC traces of poly(EtVCP-U) in Table 2.3, entry 4 (29.7 kDa, $Đ$ = 1.16, S_L = 41%).

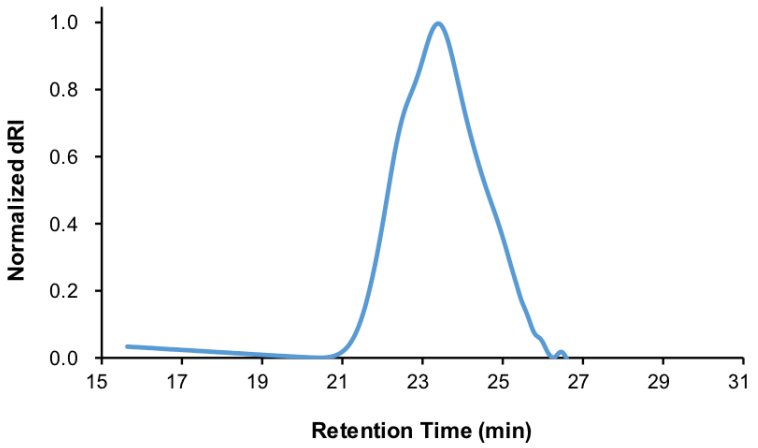

Figure S2.47. GPC traces of poly(EtVCP-DA) in Table 2.2, entry 14 (21.6 kDa, $Đ$ = 1.51, S_L = 81%).

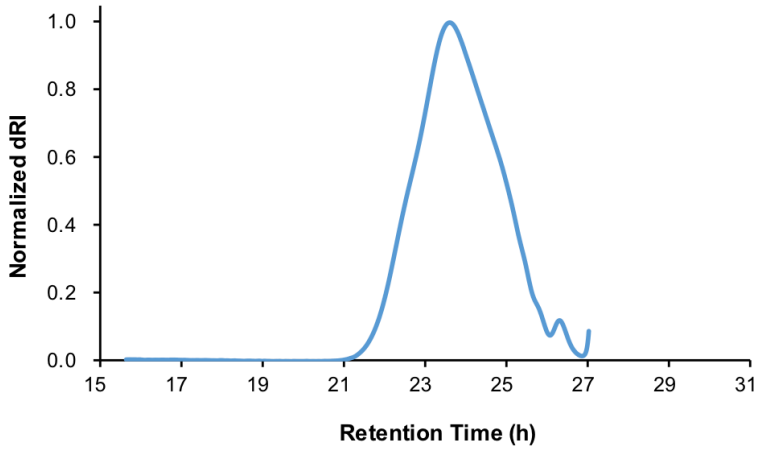

Figure S2.48. GPC traces of poly(EtVCP-DA) in Table 2.3, entry 6 (28.6 kDa, $Đ$ = 1.57, S_L = 52%).

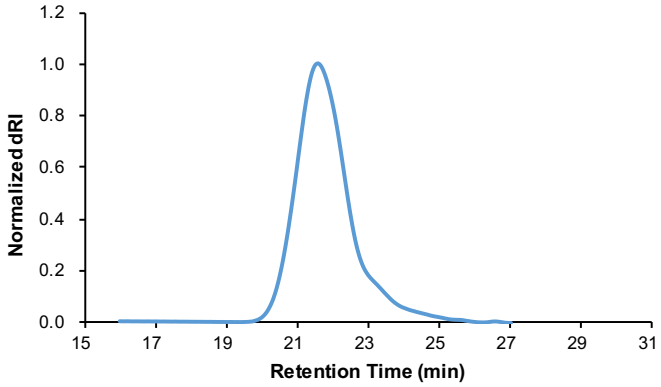

Figure S2.49. GPC traces of poly(EtVCP-C1) in Table 2.2, entry 17 (28.5 kDa, $Đ$ = 1.21, S_L = 94%).

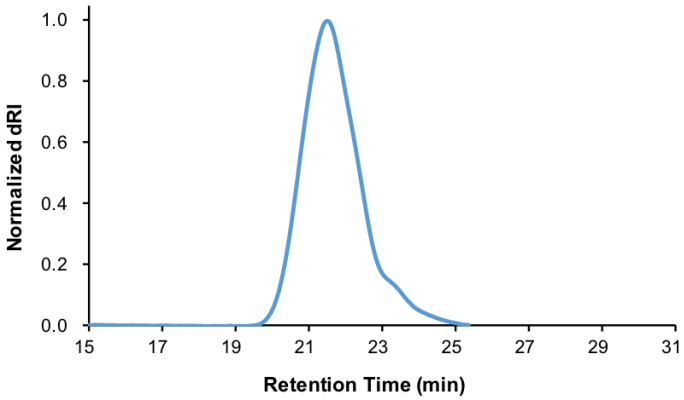

Figure S2.50. GPC traces of poly(EtVCP-C) in Table 2.2, entry 18 (30.9 kDa, $Đ$ = 1.32, S_L = 78%).

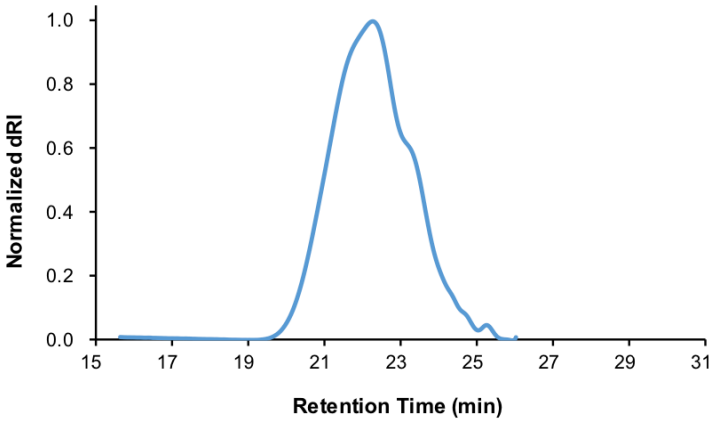

Figure S2.51. GPC traces of poly(EtVCP-C) in Table 2.3, entry 11 (20.4 kDa, $Đ$ = 1.08, S_L = 45%).

DSC and TGA Curves of Natural Product-Derived Poly(vinylcyclopropanes)

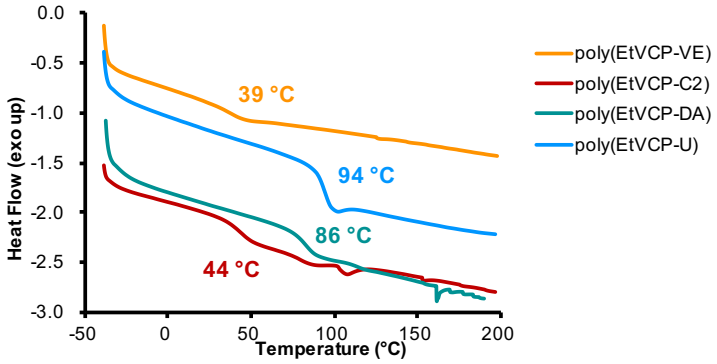

Figure S2.52. Overlay of DSC curves of poly(EtVCP-VE), poly(EtVCP-U), poly(EtVCP-DA), and poly(EtVCP-C2) in Table 2.2, entries 4, 13, 14, and 18.

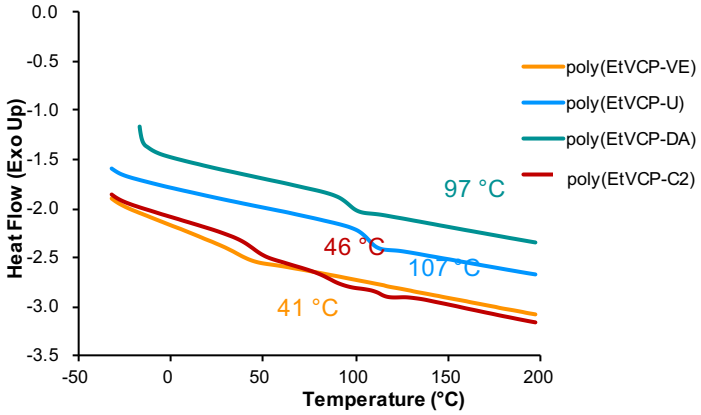

Figure S2.53. Overlay of DSC curves of poly(EtVCP-VE), poly(EtVCP-U), poly(EtVCP-DA), and poly(EtVCP-C2) in Table 2.3, entries 3, 4, 6, and 11.

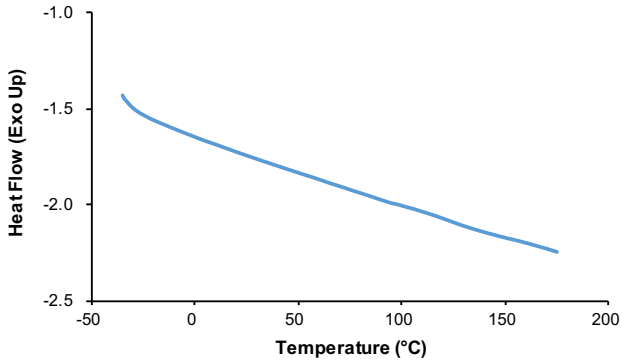

Figure S2.54. DSC curve of poly(EtVCP-C1) in Table 2.2, entries 17. No obvious T_g was observed.

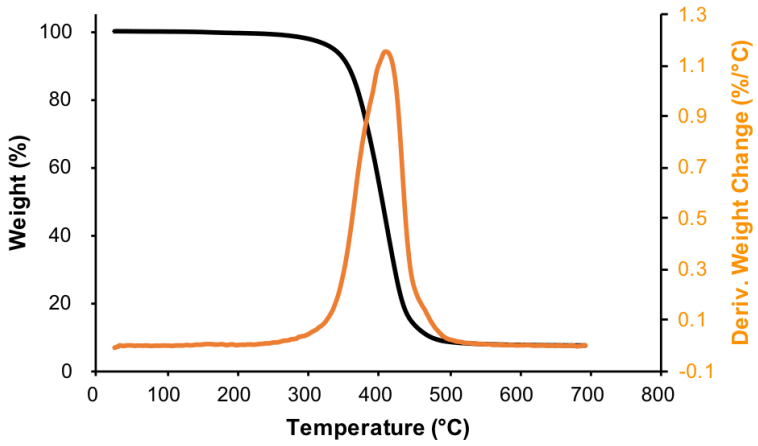

Figure S2.55. TGA and DTG curves of poly(EtVCP-VE) in Table 2.2, entry 4. T_d (10% weight loss) = 354 °C; T_{max} = 411 °C.

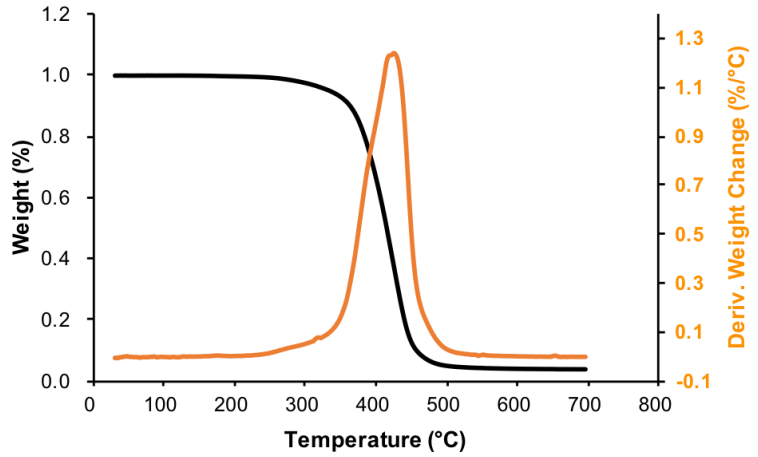

Figure S2.56. TGA and DTG curves of poly(EtVCP-VE) in Table 2.3, entry 3. T_d (10% weight loss) = 363 °C; T_{max} = 425 °C.

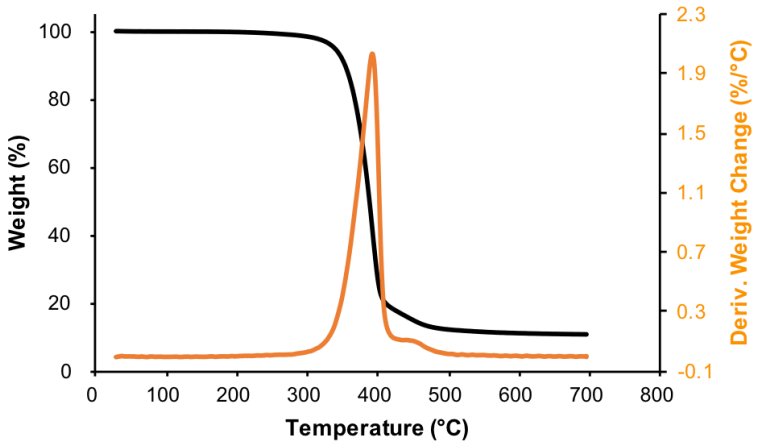

Figure S2.57. TGA and DTG curves of poly(EtVCP-U) in Table 2.2, entry 13. T_d (10% weight loss) = 354 °C; T_{max} = 393 °C.

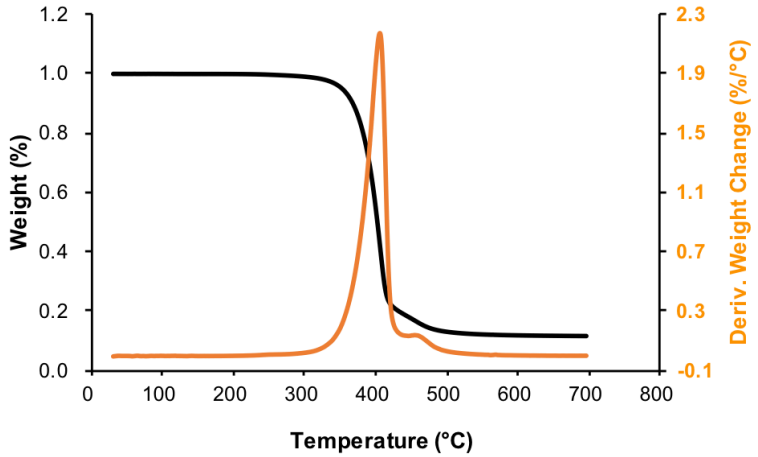

Figure S2.58. TGA and DTG curves of poly(EtVCP-U) in Table 2.3, entry 4. T_d (10% weight loss) = 367 °C; T_{max} = 405 °C.

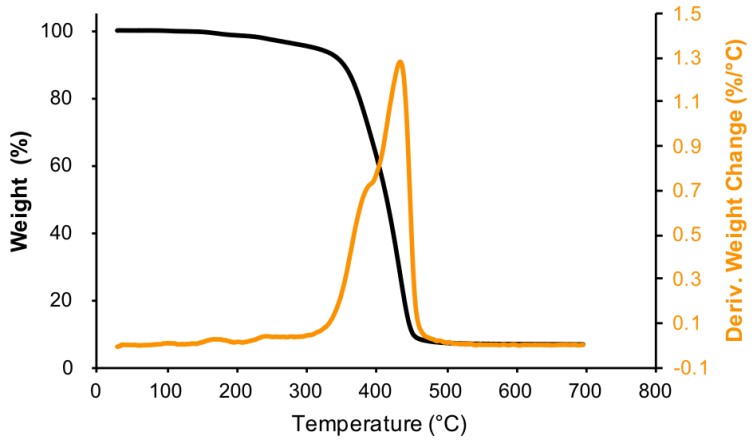

Figure S2.59. TGA and DTG curves of poly(EtVCP-DA) in Table 2.2, entry 14. T_d (10% weight loss) = 353 °C; T_{max} = 434 °C.

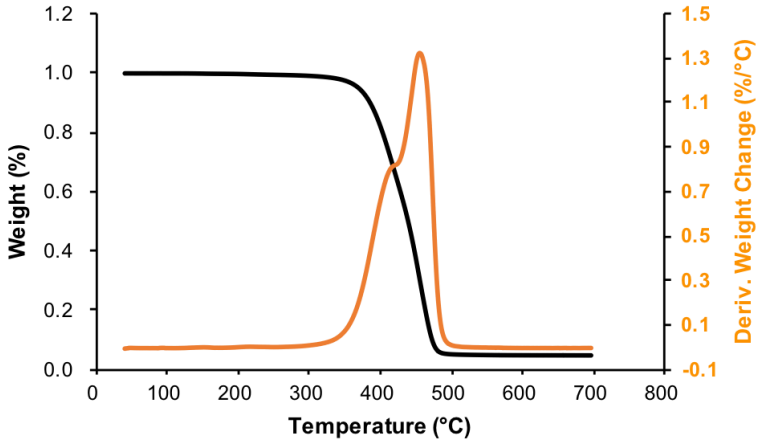

Figure S2.60. TGA and DTG curves of poly(EtVCP-DA) in Table 2.3, entry 6. T_d (10% weight loss) = 385 °C; T_{max} = 455 °C.

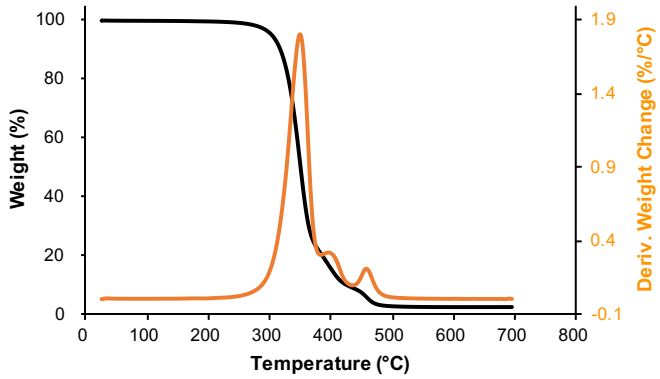

Figure S2.61. TGA and DTG curves of poly(EtVCP-C1) in Table 2.2, entry 17. T_d (10% weight loss) = 314 °C; T_{max} = 352 °C.

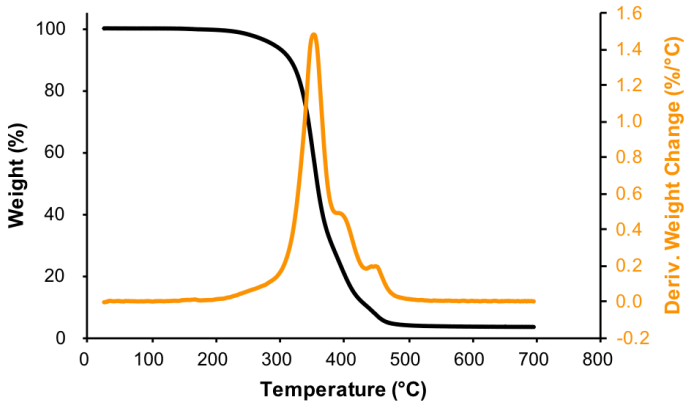

Figure S2.62. TGA and DTG curves of poly(EtVCP-C) in Table 2.2, entry 18. T_d (10% weight loss) = 314 °C; T_{max} = 352 °C.

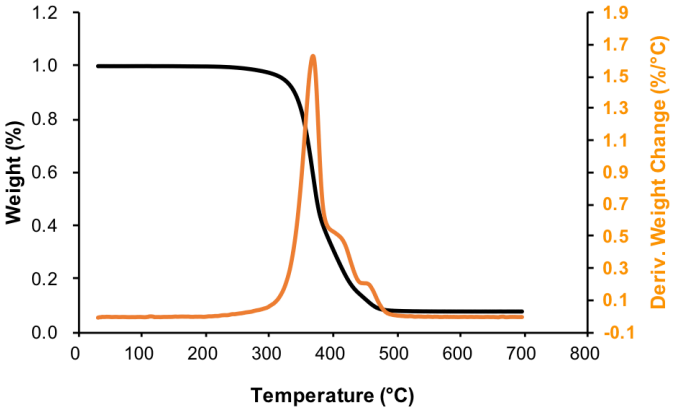

Figure S2.63. TGA and DTG curves of poly(EtVCP-C2) in Table 2.3, entry 11. T_d (10% weight loss) = 339 °C; T_{max} = 368 °C.

Polymerization of EtVCP-PDMS

General Experimental Procedure

General Procedure F: In a N_2-filled glove box, **M-1** or **M-2** (0.20 mmol), 0.10 M DBMM stock solution in EtOAc, and EtOAc were added to a 20 mL scintillation vial pre-charged with a small magnetic stir bar and PC **1**. The vial was then tightly capped and placed into a white-light LED beaker while stirring in the glove box. The temperature was about 28 °C with a cooling fan. For the analysis of the polymerization at a given time point, a 0.10 mL aliquot of the reaction mixture was taken via syringe and immediately quenched by injecting into a 1.5 mL vial containing ~0.70 mL $CDCl_3$ with 250 ppm butylated hydroxytoluene (BHT). This aliquot was then analyzed via ^{1}H NMR for monomer conversion. The aliquot was then dried under vacuum to remove all volatiles, re-dissolved in THF and passed through a syringe filter for direct analysis by GPC.

General Procedure G: In a N_2-filled glove box, **M-1** or **M-2** (0.20 mmol), 0.10 M DBMM stock solution in EtOAc, and EtOAc were added to a 25 mL Schlenk storage tube pre-charged with a small magnetic stir bar and PC **1**. The Schlenk tube was then tightly capped, taken out of the glove box, then placed into pre-heat oil bath (60 °C) while stirring. A 34 W Kessil blue LED was then immediately turned on. The distance between the Schlenk tube and the blue LED was about 5 cm. The monomer conversion and S_L were determined by crude ^{1}H-NMR while M_n and $Đ$ of the obtained polymer was determined by the GPC.

1H-NMR Spectrum of Brush Poly(EtVCP-PDMS)

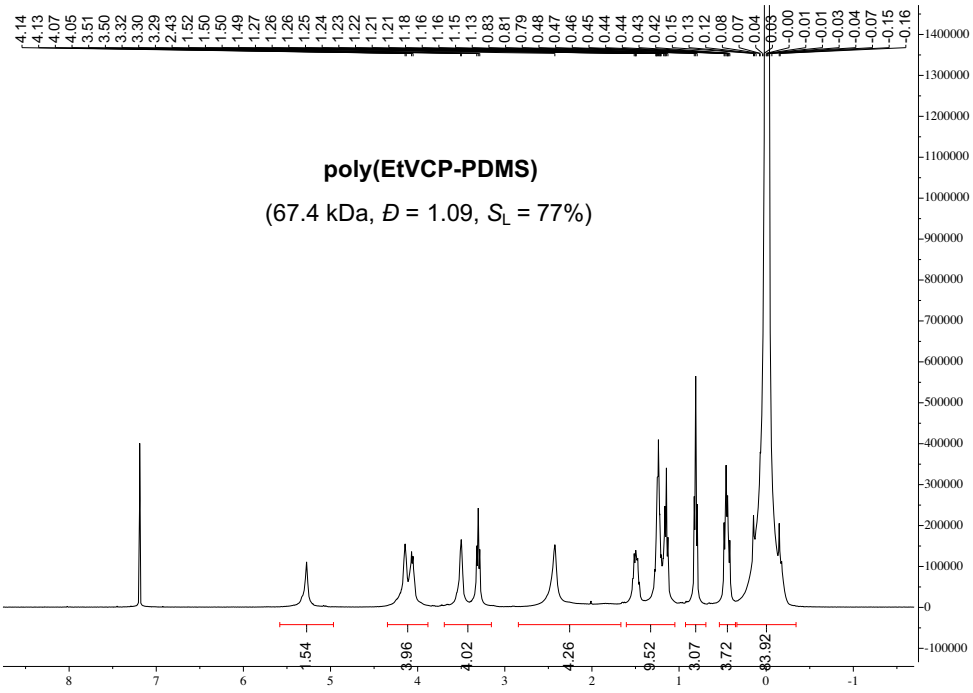

Figure S2.64. ^{1}H-NMR Spectrum of poly(EtVCP-PDMS) in Table 2.4, entry 1.

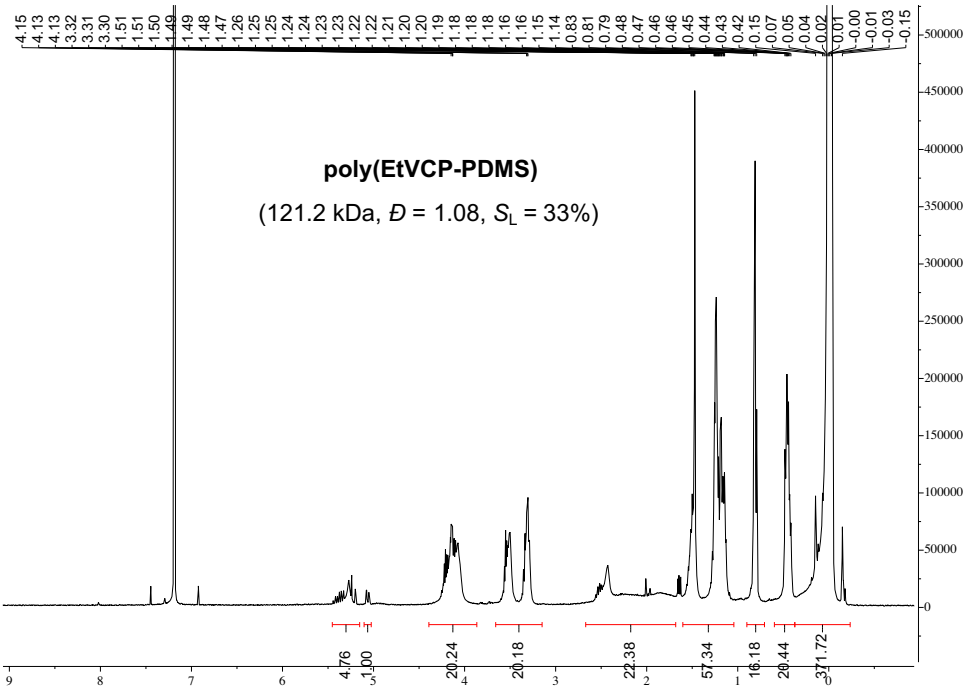

Figure S2.65. ^{1}H-NMR Spectrum of poly(EtVCP-PDMS) in Table 2.4, entry 8.

GPC Traces of Brush Poly(EtVCP-PDMS)

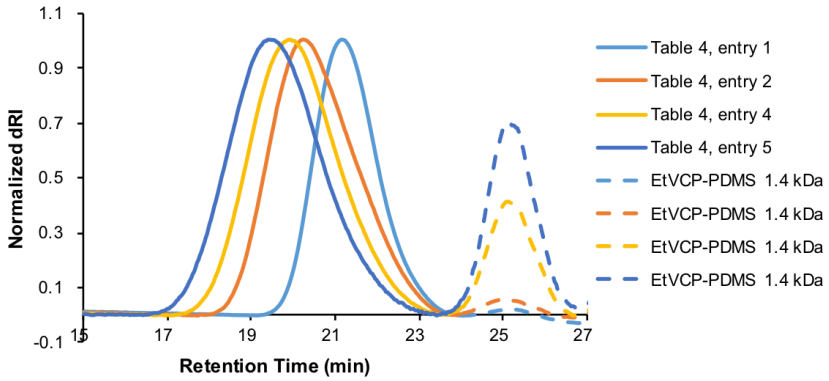

Figure S2.66. Overlay of GPC traces for brush poly(EtVCP-PDMS) in Table 2.4, entries 1-2 and 4-5.

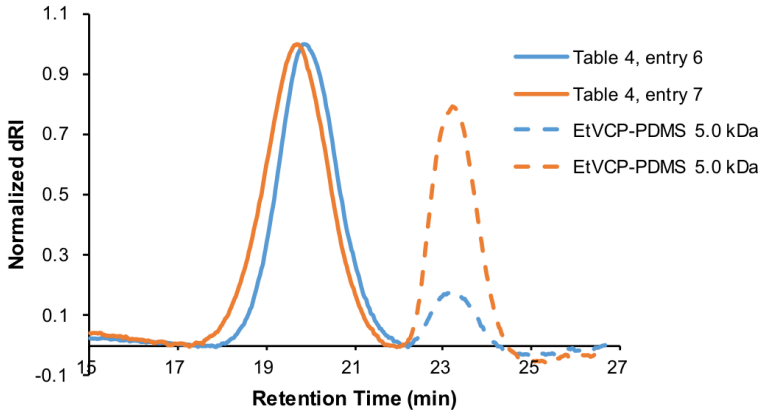

Figure S2.67. Overlay of GPC traces for brush poly(EtVCP-PDMS) in Table 2.4, entries 1-2 and 4-5.

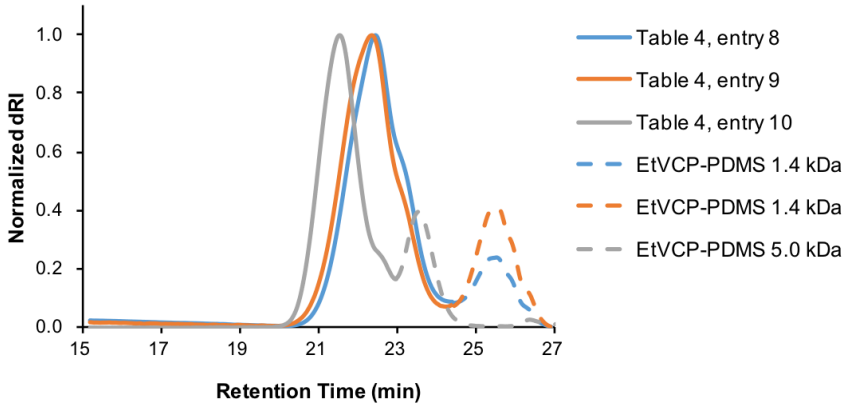

Figure S2.68. Overlay of GPC traces for brush poly(EtVCP-PDMS) in Table 2.4, entries 8-10.

DSC and TGA Curves of Brush Poly(EtVCP-PDMS)

Note: in DSC analysis, no T_gs were observed for poly(EtVCP-PDMS) across the range of −80 °C to 200 °C.

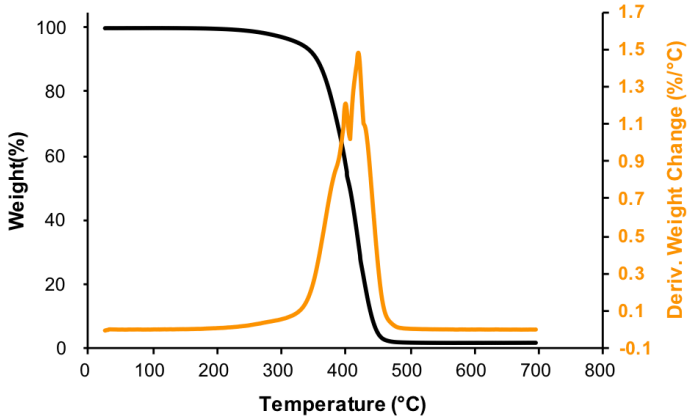

Figure S2.69. TGA and DTG curves of poly(EtVCP-PDMS) in Table 2.4, entry 1. T_d (10% weight loss) = 357 °C; T_{max} = 422 °C.

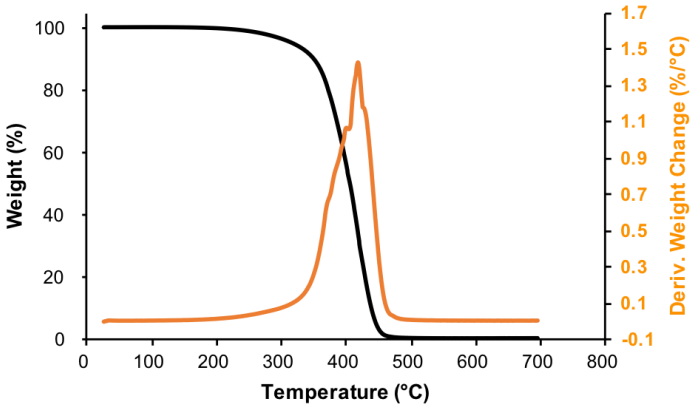

Figure S2.70. TGA and DTG curves of poly(EtVCP-PDMS) in Table 2.4, entry 8. T_d (10% weight loss) = 350 °C; T_{max} = 419 °C.

REFERENCES

1. Theriot, J. C.; Lim, C.-H.; Yang, H.; Ryan, M. D.; Musgrave, C. B.; Miyake, G. M. Organocatalyzed atom transfer radical polymerization driven by visible light. *Science* **2016,** *352,* 1082–1086.
2. Pearson, R. M.; Lim, C.-H.; McCarthy, B. G.; Musgrave, C. B.; Miyake, G. M. Organocatalyzed atom transfer radical polymerization using N-aryl phenoxazines as photoredox catalysts. *J. Am. Chem. Soc.* **2016,** *138,* 11399–11407.
3. Casper, P.; Ritter, H. A Novel Liquid-Crystalline Vinylcyclopropane-Derivative Bearing Cholesterol: Synthesis and Polymerization. *J. Macromol. Sci., Part A: Pure Appl.Chem.* **2003**, *40*, 107 – 113.
4. Emmett, M. R.; Kerr, M. A. Nucleophilic ring opening of cyclopropane hemimalonates using internal Brønsted acid activation. *Org. Lett.* **2011**, *13*, 4180-4183.
5. Sekine, M. General method for the preparation of N3- and O4-substituted uridine derivatives by phase-transfer reactions. *J. Org. Chem.* **1989**, *54*, 2321–2326.
6. Thommen, C.; Jana, C. K.; Neuburger, M.; Gademann, K. Syntheses of Taiwaniaquinone F and Taiwaniaquinol A via an Unusual Remote C–H Functionalization. *Org. Lett.* **2013**, *15*, 1390–1393.

APPENDIX B – SUPPLEMENTARY INFORMATION FOR CHAPTER 3

Materials

Monomer and catalyst synthesis.

Rac-10-camphorsulfonic acid, D-10-camphorsulfonic acid, 2,4,6-trimethylpyridine, ammonium persulfate ($(NH_4)_2S_2O_8$), 3-(trifluoromethyl)phenyl isocyanate, 4-*tert*-butylphenyl isocyanate, 4-(trifluoromethyl)phenyl isocyanate and phenyl isocyanate were purchased from Oakwood Chemical. Thionyl chloride ($SOCl_2$), sodium sulfite (Na_2SO_3), potassium permanganate ($KMnO_4$), sodium carbonate (Na_2CO_3), and aniline were purchased from Sigma-Aldrich. 3-Chloroperoxybenzoic acid (*m*-CPBA, 70-75%), cyclohexylamine, carbonyl diamide (urea), acetonitrile (ACN), ethyl ether (Et_2O), and dichloromethane (DCM) were purchased from Fisher Scientific Co. All purchased chemicals were used as received unless otherwise stated.

Polymerization

Acetonitrile (ACN), dimethylformamide (DMF), tetrahydrofuran (THF), and toluene were purchased from Fisher Scientific Co. All organic solvents were dried with calcium hydride (CaH_2), distilled under N_2, and stored over activated 4 Å molecular sieves in a nitrogen filled glovebox prior to use. Benzyl alcohol (BnOH) was purchased from Alfa Aesar Chemical Co. and was dried with CaH_2, distilled under N_2, and stored over activated 4 Å molecular sieves in a nitrogen filled glovebox prior to use. 1,8-diazabicyclo(5.4.0)undec-7-ene (DBU), 1,5,7-

triazabicyclo 4.4.0 dec-5-ene (TBD), 1-tert-butyl-2,2,4,4,4-pentakis(dimethylamino)-2λ^5,4λ^5-catenadi(phosphazene) (^{t}BuP$_2$, ~2.0 M in THF), 1-*tert*-Butyl-4,4,4-tris(dimethylamino)-2,2-bis[tris(dimethylamino)-phosphoranylidenamino]-2λ^5,4λ^5-catenadi(phosphazene) (^{t}BuP$_4$, ~0.8 M in hexane), thiourea, N, N′-dicyclohexylurea (urea 1), N, N′-diphenylurea (urea 2), and 1,1,1,3,3,3-Hexafluoroisopropanol (HFIP) were bought from Sigma-Aldrich. Sodium methoxide was obtained from Beantown Chemical Corporation. Tris[N,N-bis(trimethylsilyl)amide]lanthanum (La(N(SiMe$_3$)$_2$)$_3$) and tin octoate [Sn(Oct)$_2$] were purchased from Alfa Aesar Chemical Co. All purchased chemicals were used as supplied unless otherwise stated. Poly(L-lactic acid) (PLLA, M_w = 162 kDa, from Nature-works), and polyethylene terephthalate (PET, intrinsic viscosity of 0.80 dL g^{-1} in *m*-cresol) were provided by POLYMAT.

General Synthetic Methods

Synthesis of camphor-based monomer

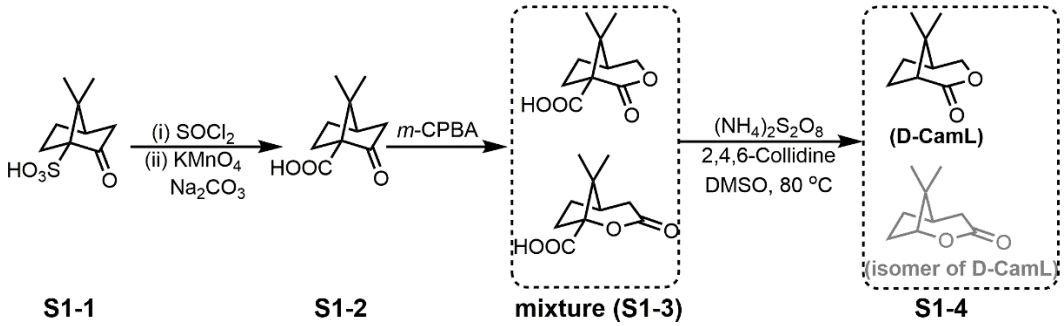

Figure S3.1. Preparation of D-CamL (or *rac*-CamL).

S1-2 was synthesized according to a modified literature procedure.[1]

D-10-camphorsulfonic acid (or *rac*-10-camphorsulfonic acid) (**S1-1**, 90.0 g, 0.387 mol) was dissolved in excess $SOCl_2$ (100 mL, 1.38 mol) at 70 °C and the resulting solution was refluxed for 4.0 hours. The $SOCl_2$ was then removed by distillation at 100 °C and could be recovered for use in subsequent syntheses. The concentrated reaction mixture was stirred in the $KMnO_4$ (124 g, 0.785 mmol) and Na_2CO_3 (114 g, 1.08 mol) solution in H_2O (1.00 L) and CH_3CN (700 mL) for 12 hours to afford (1R,4R)-7,7-dimethyl-2-oxobicyclo[2.2.1]heptane-1-carboxylic acid (**S1-2**). After 12 hours, the mixture was cooled in an ice water bath and aqueous sulfuric acid (3.00 M, 800 mL) was added dropwise. 160 g Na_2SO_3 was added until the reaction mixture became transparent. The product (**S1-2**) was extracted with Et_2O and the resulting solution was dried under reduced pressure.

S1-2 was used for the next step without further purification. Crude **S1-2** (70.0 g), urea (20.0 g, 0.333 mmol), and *m*-CPBA (140 g) were dissolved in 500 mL DCM and stirred for 12 hours at 60 °C. When the reaction was finished, the reaction mixture was extracted twice with saturated $NaHCO_3$ (aq) (200 mL + 100 mL). The pH of the combined aqueous solution was reduced to 5 using aqueous sulfuric acid (1.0 M) and then the solution was washed twice with DCM (100 mL + 100 mL). The pH of the aqueous solution was then reduced to 1 using aqueous sulfuric acid (1.0 M) and it was extracted three times with DCM (200 mL + 200 mL + 200 mL). The organic layers were combined, washed with brine, dried over anhydrous sodium sulfate, and concentrated under reduced pressure to yield crude product **S1-3**.

The crude **S1-3** was used directly in the subsequent decarboxylation reaction[2]. Crude **S1-3** (40.0 g) was dissolved in DMSO (500 mL) and the resulting solution was sparged with N_2 for 15 minutes in a 4 L round-bottom flask. Then, $(NH_4)_2S_2O_8$ (180 g, 789 mmol) and 2,4,6-trimethylpyridine (100 g, 825 mmol) were added directly to the 4 L round-bottom flask and the reaction mixture was sparged with N_2 for 10 minutes. A reflux condenser was then attached, and the mixture was stirred at room temperature for 1.0 hour. Then, the temperature of the reaction mixture was slowly raised to 60 °C. Once the solution changed color from orange-yellow to black and a large amount of gas was generated (the total volume of the reaction mixture in the flask should not exceed one-sixth of the flask's volume to account for gas production), the temperature was increased to 80 °C and the reaction was continued for an additional 5.0 hours. After the reaction was completed, 500 mL of water was added to the reaction mixture, followed by extraction with Et_2O (150 mL × 5). The combined organic phase was washed with aqueous Na_2HCO_3 (1 M, 100 mL × 2), and concentrated under reduced pressure. The crude product could be purified by column (EtOAc:Hexane = 1:2) and obtain **S1-4**. **D-CamL** was isolated from the mixture of isomers by recrystallization in mixed solvents (EtOAc:Hexane = 1:10). Yield of **D-CamL** ~ 15.0%.

D-CamL: ^{1}H NMR (400 MHz, $CDCl_3$) δ = 4.43 (ddq, *J* = 10.9, 3.3, 1.7 Hz, 1H), 4.10 (dq, *J* = 10.9, 1.3 Hz, 1H), 2.47 (ddt, *J* = 4.7, 3.3, 1.5 Hz, 1H), 2.23–2.04 (m, 2H), 2.02–1.88 (m, 1H), 1.85 (ddq, *J* = 6.3, 3.1, 1.4 Hz, 1H), 1.81–1.69 (m, 1H), 1.25–1.14 (m, 3H), 1.06–0.96 (m, 3H)

ppm. ^{13}C NMR (100 MHz, $CDCl_3$) δ = 175.0, 74.7, 52.9, 42.3, 40.6, 28.0, 27.8, 24.4, 21.3 ppm. HRMS (positive ESI) m/z calcd for $C_9H_{14}O_2$ $[M + H]^+$: 155.1072; found: 155.1064.

***rac*-CamL**: ^1H NMR (400 MHz, $CDCl_3$) δ = 4.44 (ddd, *J* = 10.9, 3.2, 1.7 Hz, 1H), 4.11 (dd, *J* = 10.9, 1.1 Hz, 1H), 2.48 (dt, *J* = 6.3, 1.3 Hz, 1H), 2.26–2.05 (m, 2H), 2.03–1.89 (m, 1H), 1.86 (dt, *J* = 6.1, 2.2 Hz, 1H), 1.82–1.69 (m, 1H), 1.19 (s, 3H), 1.02 (s, 3H) ppm. ^{13}C NMR (100 MHz, $CDCl_3$) δ = 175.0, 77.4, 77.0, 76.7, 74.7, 52.9, 42.3, 40.7, 27.9, 27.8, 24.4, 21.3 ppm.

Optical rotation characterization

The optical rotation experiments were carried out on a RUDOLPH research analytical automatic polarimeter.

D-CamL: $[\alpha]_D^{26.2}$ = +20.9, (*c* = 1.0, $CHCl_3$).

rac-CamL: $[\alpha]_D^{26.2}$ = -0.21, (*c* = 1.0, $CHCl_3$).

Synthesis of urea derivatives.

The substitute ureas were synthesized according to a modified literature procedure.[3]

0.50 g isocyanate was dissolved in dry THF (10 mL), and then 1.2 equiv of corresponding amine was added gradually. After 1.0 hour, the THF was removed under vacuum and the crude product was purified by recrystallization. After drying overnight in a vacuum oven (100 °C), the prepared substituted ureas were transferred to a N_2-filled glovebox for storage.

Urea 3: ^{1}H NMR (400 MHz, MeOD) δ = 7.66–7.54 (m, 4H), 7.47–7.38 (m, 2H), 7.35–7.23 (m, 2H), 7.04 (tt, *J* = 7.3, 1.2 Hz, 1H) ppm.

Urea 4: ^{1}H NMR (400 MHz, MeOD) δ = 7.89 (t, *J* = 2.0 Hz, 1H), 7.63–7.54 (m, 1H), 7.51–7.39 (m, 3H), 7.33–7.25 (m, 3H), 7.07–6.99 (m, 1H) ppm.

Urea 5: ^{1}H NMR (400 MHz, MeOD) δ = 7.37–7.29 (m, 2H), 7.29–7.18 (m, 2H), 6.95 (tt, *J* = 7.3, 1.2 Hz, 1H), 3.56 (tt, *J* = 10.4, 3.9 Hz, 1H), 1.91 (dt, *J* = 12.3, 4.1 Hz, 2H), 1.74 (dp, *J* = 12.0, 4.0 Hz, 2H), 1.62 (dp, *J* = 12.3, 4.0 Hz, 1H), 1.48–1.31 (m, 2H), 1.31–1.10 (m, 3H) ppm.

Urea 6: ^{1}H NMR (400 MHz, MeOD) δ = 7.37–7.08 (m, 4H), 3.55 (tt, *J* = 10.4, 3.9 Hz, 1H), 1.91 (dt, *J* = 12.3, 4.1 Hz, 2H), 1.74 (dq, *J* = 11.9, 3.9 Hz, 2H), 1.62 (dt, *J* = 12.7, 3.9 Hz, 1H), 1.47–1.33 (m, 2H), 1.29 (s, 9H), 1.27–1.11 (m, 3H) ppm.

General polymerization procedure

Polymerizations were performed inside a N_2-filled glovebox or outside in a sealed 10 mL glass reactor at a predetermined temperature. In either case, in the glovebox, a 2.5 dram vial was charged with monomer (100 mg, 0.649 mmol, 100 eq), urea/thiourea derivative (0.00649 mmol, 1 eq), and 100 μL solvent. In a separate vial, a mixture of catalyst (0.00649 mmol, 1 eq), initiator (0.00649 mmol, 1 eq), and solvent (100 μL) was stirred at ambient temperature (~25 °C) for 10 min. The polymerization was initiated by addition of the catalyst solution to the monomer solution. After polymerization the mixture was immediately quenched by addition of 0.5 mL of benzoic acid solution in $CDCl_3$ (10 mg/mL) and a 0.02 mL of aliquot was taken from the

reaction mixture for ^{1}H NMR analysis. The quenched mixture was then precipitated into 30 mL of methanol while stirring and the resulting solid was filtered, washed with cold methanol to remove any unreacted monomer, and dried in a vacuum oven at 100 °C for 24 hours.

Isotactic poly(D-CamL) from **Table 1**, **Run 1**. ^{1}H NMR (400 MHz, $CDCl_3$) δ = 4.13 (dd, *J* = 11.0, 5.4 Hz, 1H), 3.98 (dd, *J* = 10.9, 7.7 Hz, 1H), 2.52 (t, *J* = 9.4 Hz, 1H), 2.09 (tdd, *J* = 13.0, 9.9, 5.7 Hz, 1H), 1.99–1.75 (m, 3H), 1.51 (ddd, *J* = 14.7, 9.2, 3.6 Hz, 1H), 1.22 (s, 3H), 0.74 (s, 3H) ppm. ^{13}C NMR (100 MHz, $CDCl_3$) δ = 173.6, 65.2, 55.9, 49.3, 43.9, 27.6, 26.4, 24.4, 17.2 ppm.

Atactic poly(D-CamL) from **Table 1**, **Run 3**: ^{1}H NMR (400 MHz, $CDCl_3$) δ = 4.11 (ddt, *J* = 10.4, 8.0, 3.8 Hz, 1H), 3.95 (ddd, *J* = 22.6, 11.0, 7.7 Hz, 1H), 2.62–2.43 (m, 1H), 2.19–1.73 (m, 4H), 1.57–1.36 (m, 1H), 1.30–0.65 (m, 6H) ppm. ^{13}C NMR (100 MHz, $CDCl_3$) δ = 175.01, 173.6, 65.2, 55.9, 49.34, 47.6, 43.89, 28.1, 27.9, 27.6, 26.6, 26.4, 26.0, 25.4, 24.4, 17.12 ppm.

Polymerization procedure for kinetic analysis

Polymerizations were prepared inside a N_2-filled glovebox. A 2.5 dram vial was charged with monomer (500 mg, 3.25 mmol, 100 eq) and 1000 μL solvent. In a separate vial, a mixture of ^{t}BuP$_4$ (~0.8M in hexanes, 40 μL, 0.0325 mmol, 1 eq), initiator (0.0325 mmol, 1 eq), and THF (1000 μL) was stirred at ambient temperature (~25 °C) for 10 min. The polymerization was initiated by addition of the catalyst solution (^{t}BuP$_4$ solution) to the monomer solution and the start time was recorded as t = 0. At predetermined times throughout the polymerization (1 min, 5

min, 10 min, 15 min, 30 min, 45 min, and 90 min), 100 μL aliquots were taken and immediately added to 400 μL of benzoic acid solution in $CDCl_3$ (4.5 mg/mL). Quenched aliquots were analyzed directly by ^{1}H NMR to determine conversion as a function of time which was then used to calculate monomer concentration at each time. Following NMR analysis, aliquots were dried to afford crude polymer which was then analyzed by gel-permeation chromatography (GPC) without further purification.

Polymerization procedure for determination of thermodynamic parameters.

In a N_2-filled glovebox, a 4 mL vial was charged with D-CamL (100 mg, 0.649 mmol, 50 eq), BnOH (1.35 μL, 0.0125 mmol, 1 eq), THF (549 μL) and ^{t}BuP$_4$ (16 μL, 0.0128 mmol, 1 eq). The resulting solution was thoroughly mixed and divided into three small reaction vials which were then sealed with gas-tight caps and wrapped in insulating tape. The three sealed vials were placed in a pre-equilibrated oil bath and allowed to stir for 24, 48, and 60 hours, respectively. This procedure was repeated at a range of different temperatures (26.8 °C, 34.9 °C, 42 °C, 50.5 °C, and 62 °C). The Van't Hoff plot of $\ln[M]_{eq}$ versus $1/T$ shown in **Figure S25** was used to calculate thermodynamic parameters associated with polymerization. $\Delta H°_p = -21.0$ kJ mol^{-1} and $\Delta S°_p = -55.5$ J mol^{-1} K^{-1} based on Equation ***(1)***. The calculated $T_c = 105$ °C when $[M]_0 = 1.0$ M based on Equation ***(2)***.

(1) $$\ln[M]_{eq} = \Delta H_p/RT - \Delta S°_p/R$$

(2) $$T_c = \Delta H°_p/(\Delta S°_p + R\ln[M]_0).$$

Isomerization of poly(D-CamL) by ^{t}BuP$_4$.

Isotactic poly(D-CamL) (20 mg, 70 eq) was combined with ^{t}BuP$_4$ (2.3 μL, ~0.8M in hexanes, 1 eq relative to monomer repeat unit) in 240 μL THF. After stirring for 4 hours, the reaction was quenched by addition of 0.10 mL of benzoic acid solution in $CDCl_3$ (10 mg/mL) and the quenched mixture was then precipitated into 10 mL of vigorously stirring methanol. The resulting solid was filtered, washed with cold methanol, and dried in a vacuum oven at 100 °C for 24 hours. The purified poly(D-CamL) was characterized by ^{13}C NMR (**Figure S16**).

Chemical recycling of poly(D-CamL).

Chemical recycling was performed in the presence of ^{t}BuOK (5 mol % relative to the repeat unit of poly(D-CamL)) with a small amount of THF to help disperse ^{t}BuOK on the poly(D-CamL) surface. Poly(D-CamL), ^{t}BuOK, and THF were placed into a sublimator, and the solvent was allowed to evaporate in air. The vessel was then heated at 200 °C for 2.0 hours under reduced pressure (200 millitorr) to yield recycled D-CamL.

Repolymerization of recycled D-CamL.

The recovered D-CamL was purified by recrystallization and sublimation before repolymerization according to the General polymerization procedure. The repolymerized poly(D-

CamL) was processed again and subjected to tensile testing for comparison to virgin poly(D-CamL).

Spectroscopic Characterization

Nuclear magnetic resonance measurement

Nuclear magnetic resonance (NMR) spectra were obtained using a Bruker 400 MHz NMR Spectrometer at 298 K. All ^{1}H NMR and ^{13}C NMR experiments are reported in parts per million (ppm), where chemical shifts were measured relative to the signals for residual chloroform in deuterated chloroform.

Determination of *dn*/*dc* value.

The refractive index increment (*dn*/*dc*) of poly(D-CamL) was determined to be 0.0756 ± 0.0005 mL/g, obtained by batch experiments using the Wyatt Optilab T-rEX dRI detector and calculated using the ASTRA software. A series of polymer solutions with known concentrations (0.25 mg/mL, 0.50 mg/mL, 1.0 mg/mL, 2.0 mg/mL, 5.0 mg/mL, and 10 mg/mL) were prepared in chloroform. Starting with the least concentrated, the solutions were sequentially injected into the dRI detector using Harvard Apparatus syringe pump 11 at a flow rate of 0.1 ml/min. The change in refractive index was measured and plotted as a function of concentration. The slope of the resulting linear fit is equal to the *dn*/*dc* of the polymer.

Absolute molecular weight measurements

Measurements of polymer weight-average molecular weight (M_w), number-average molecular weight (M_n), and polydispersity index ($Đ = M_w/M_n$) were performed via GPC. The GPC instrument consisted of an Agilent HPLC system equipped with one guard column and two PLgel 5-μm mixed-C gel permeation columns and coupled with a Wyatt DAWN HELEOS II multi (18)-angle light scattering detector and a Wyatt Optilab T-rEX dRI detector; the analysis was performed at 40 °C using chloroform as the eluent at a flow rate of 1.0 mL/min, using Wyatt ASTRA 7.1.2 MW characterization software.

Thermal analysis

Melting transition (T_m) and glass transition (T_g) temperatures were measured by differential scanning calorimetry (DSC) on an Auto Q20, TA Instrument. All T_m and T_g values were obtained from the second scan. Both the heating rate and cooling rate were 10 °C/min unless otherwise stated.

The decomposition temperatures ($T_{d,5}$), which are defined by the temperatures at 5% weight loss, and the maximum rate decomposition temperatures ($T_{d,max}$) of the polymers were determined through thermal gravimetric analysis (TGA) using a Q50 TGA Analyzer from TA Instruments. Polymer samples were subjected to a temperature ramp from room temperature to 700 °C at a

heating rate of 10 °C/min. T_{max} values were derived from plots of derivative (wt%/°C) versus temperature (°C).

Circular dichroism measurement

Circular dichroism (CD) spectra were recorded on an Aviv Model 202 Circular Dichroism CD Spectrometer equipped with a nitrogen purging set-up and an argon lamp. Measurements were carried out at 25 °C in a 1 mm optical path length quartz cuvette (Hellma Analytics, Germany). The spectra were recorded at a sample concentration of 1.0 mg/mL. HFIP was used as solvent.

Mechanical analysis

Tensile stress/strain testing was conducted using an Instron 5966 universal testing system with a 10 kN load cell. Dog-bone-shaped test specimens, prepared according to ASTM D638 standard (Type V), were fabricated via compression molding. A Carver Bench Top Laboratory Press (Model 4386) equipped with a two-column hydraulic unit (Carver, Model 3912, maximum force 24000 psi) was employed for this purpose, unless otherwise stated. Isolated polymer materials were sandwiched between non-stick Teflon sheets within a stainless-steel mold measuring 30 × 73.5 × 0.38 mm. Compression was carried out between two 6" × 6" steel electrically heated platens (EHP) with a clamp force of 5000 psi at a temperature 10 °C above the respective T_m of each material. Specimens generated through compression molding (high-temperature samples were cooled with a water flow) were cut to standard dimensions using an ASTM D638-5-IMP

cutting die (Qualitest). Mechanical behavior data were averaged across all specimens measured for each specific polymer species. The thickness, width, and grip length of the dog-bone specimens were measured for data normalization using Bluehill measurement software (Instron). Test specimens were secured in the screw-tight grip frame, and tensile stress and strain were monitored until the materials' break occurred at a grip extension speed of 5.0 mm/min under ambient conditions.

Storage modulus (E'), loss modulus (E''), and tan δ (E''/E') were determined via dynamic mechanical analysis (DMA) using a Q800 DMA analyzer (TA Instruments) operating in tension film mode. The testing was carried out at a maximum strain of 0.3 or 0.05% and a frequency of 1 Hz. The α-transition temperature was determined as the peak maximum of the δ curve. Samples were tested until yielding occurred (displacement amplitude exceeding 20 mm).

WAXD (Wide-angle X-ray diffraction)

Wide-angle X-ray diffraction of the polymers were collected with Ni filtered Cu Kα radiation (λ = 1.5418 Å) by using a Bruker D8 Discover DaVinci automatic diffractometer for measurements at room temperature. Before analysis, the polymer sample was prepared as thin film by the hot-compression method described in "mechanical analysis"; compression was carried out between two 6" × 6" steel electrically heated platens (EHP) with a clamp force of 5000 psi, at a temperature 10 °C above the respective T_m of each material, for 10 mins.

Barrier property measurements

The water vapor transmission rate was determined using the gravimetric method outlined in ASTM E96-95 at a temperature of 25 °C. The permeation cell used was made of polytetrafluoroethylene and partially filled with water. The membrane was placed on top and fixed with the other part of the cell. The weight change was measured using a Sartorius BP 210 D balance with a readability of 10^{-5} g, and the data was recorded for further analysis. The values presented are the average of at least three films.

Oxygen permeability was measured using a Mocon OX-TRAN 2/21 MH instrument at 1 atm, 23 °C, and 0% relative humidity (RH). The surface area exposed to oxygen was 5 cm^2. At least two films were measured for each reported value.

Supporting Tables and Figures

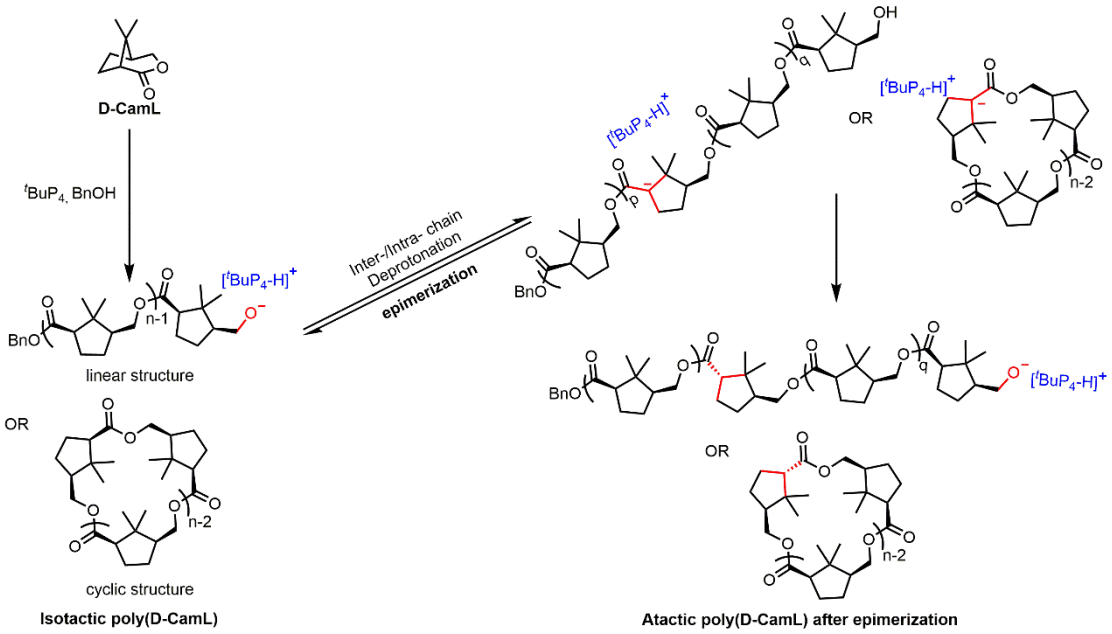

Figure S3.2. Proposed mechanism of epimerization at the stereocenter adjacent to the carbonyl.

.

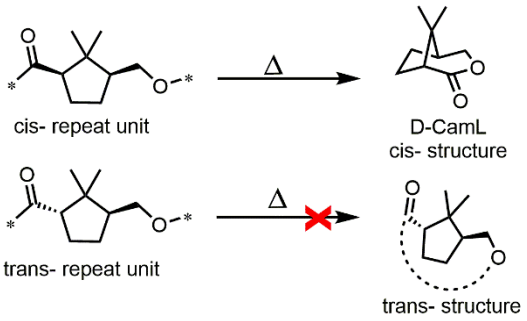

Figure S3.3. Thermally stable cis- structure vs. thermally unstable trans- structure

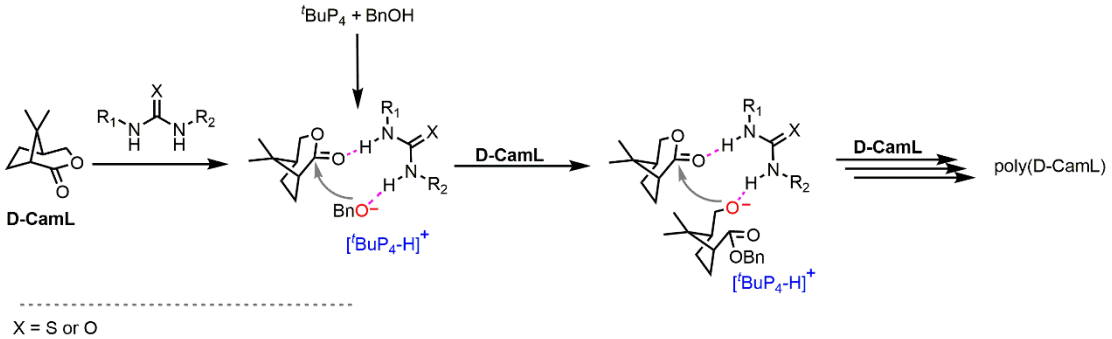

Figure S3.4. Proposed mechanism route of ^{t}BuP$_4$ catalyzed polymerization of D-CamL with cocatalyst (urea or TU).

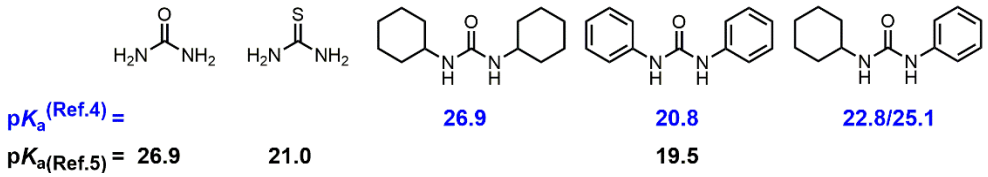

Figure S3.5. pK_a value of urea, thiourea, and urea derivatives.[4, 5]

Table S3.1. Polymerization results of D-camphor derived lactone with different catalysts. [a]

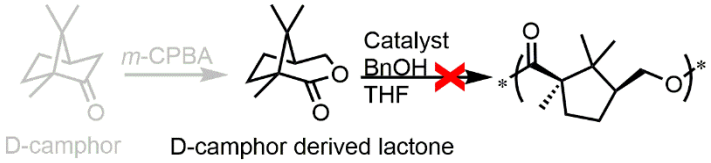

Run	Catalyst	Conv. (%) [b]	M_w (kDa) [c]	$Đ$ [c]
1	La[N(SiMe$_3$)$_2$]$_3$	/	/	/
2	DBU/TBD	/	/	/
3	^{t}BuP$_2$/^{t}BuP$_4$	/	/	/

[a] Conditions: the concentration of monomer is 100 mg monomer in 100 μL THF, the feed ratio was [M]:[BnOH]:[^{t}BuP$_4$] = 100:1:1 and all polymerizations run at room temperature for 12 hours. [b] Monomer conversions determined by ^{1}H NMR of the crude solution after the quench in CDCl$_3$. [c] number-average molecular weights (M_n), and dispersity indices ($Đ = M_w/M_n$) determined by gel-permeation chromatography (GPC) coupled with light scattering at 40 °C in CHCl$_3$.

Table S3.2. Polymerization results of D-CamL catalyzed by $Sn(Oct)_2$.

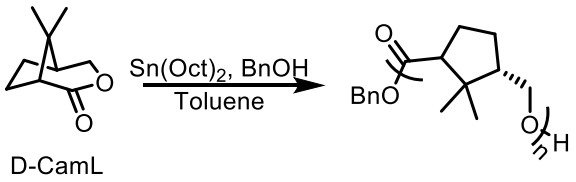

D-CamL

Run	Solvent	Conv. (%) [b]	M_w (kDa)	$Đ$
1	Toluene	0	/	/

[a] Conditions: the concentration of monomer is 100 mg D-CamL in 200 μL solvent, the feed ratio was [D-CamL]:[BnOH]:[$Sn(Oct)_2$] = 100:1:1 and all polymerizations run at room temperature for 8.0 hours. [b] Monomer conversions determined by ^{1}H NMR of the crude solution after the quench in $CDCl_3$.

Table S3.3. Polymerization results of D-CamL catalyzed by $^{t}BuP_4$ in different solvents.[a]

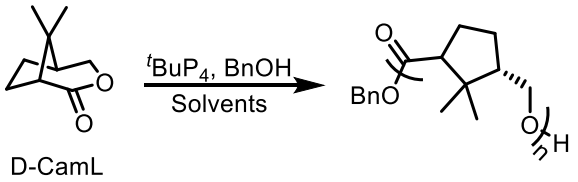

D-CamL

Run	Solvent	Conv. (%) [b]	M_w (kDa) [c]	$Đ$ [c]
1	ACN	0	/	/
2	DMF	80	25.5	1.96
3	Toluene	51	19.5	1.30

[a] Conditions: the concentration of monomer is 100 mg D-CamL in 200 μL solvent, the feed ratio was [D-CamL]:[BnOH]:[$^{t}BuP_4$] = 100:1:1 and all polymerizations run at room temperature for 1.0 hour. [b] Monomer conversions determined by ^{1}H NMR of the crude solution after the quench in $CDCl_3$. [c] weight-average molecular weights (M_w), and polydispersity index ($Đ = M_w/M_n$) determined by gel-permeation chromatography (GPC) coupled with light scattering at 40 °C in $CHCl_3$.

Table S3.4. Water vapor transmission rate (*WVTR*) and oxygen permeability ($P\ O_2$) of different polymers.

Samples	*WVTR* (g mm m^{-2} day^{-1})	$P\ O_2$ (Barrer)
poly(*rac*-CamL)	1.68 ± 0.31	0.11 ± 0.01
PLLA	5.7 ± 0.50	0.26 ± 0.01
PET	1.49 ± 0.11	0.09 ± 0.0

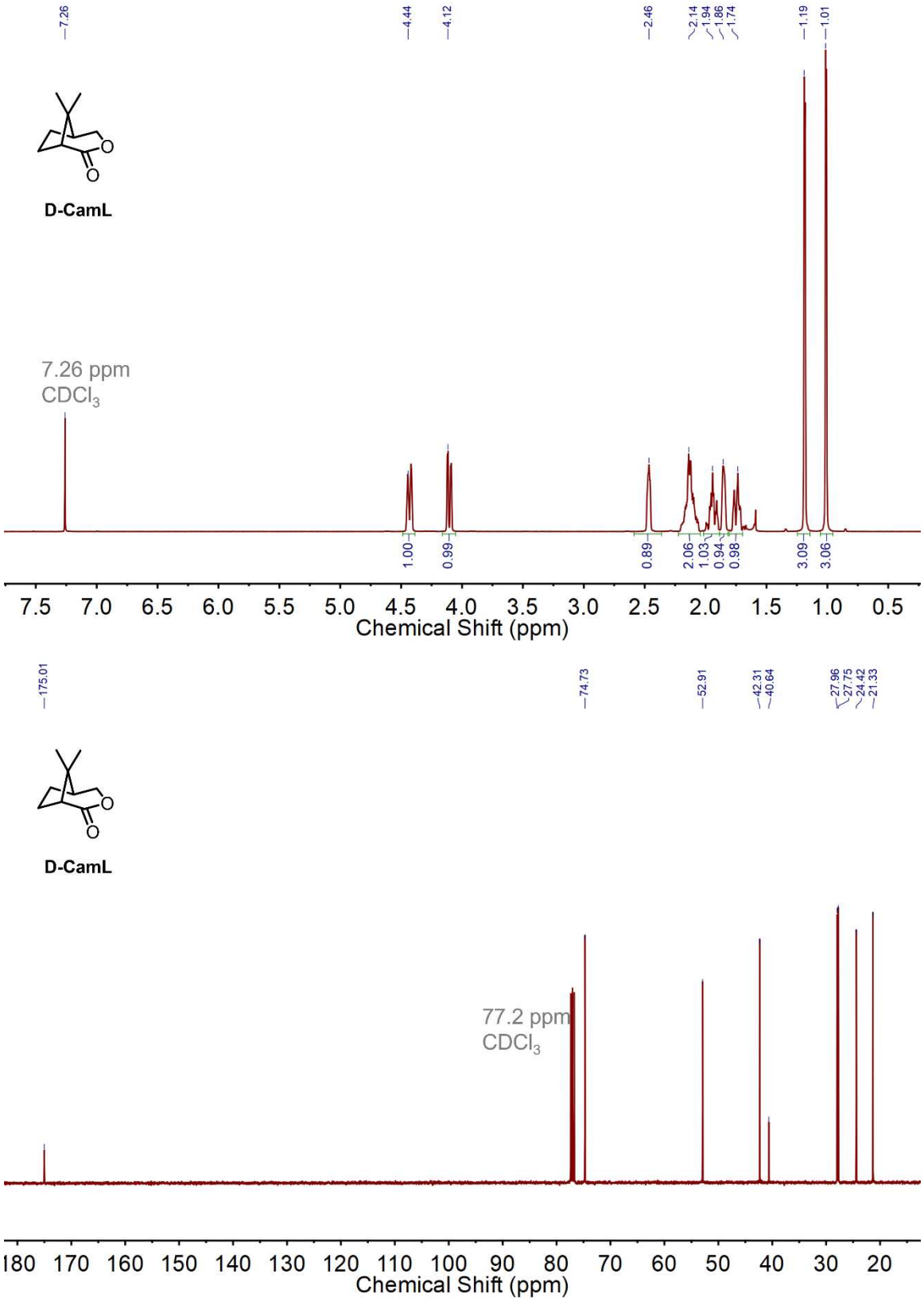

Figure S3.6. ^{1}H NMR (top) and ^{13}C NMR (bottom) ($CDCl_3$, 23 °C) spectra of D-CamL.

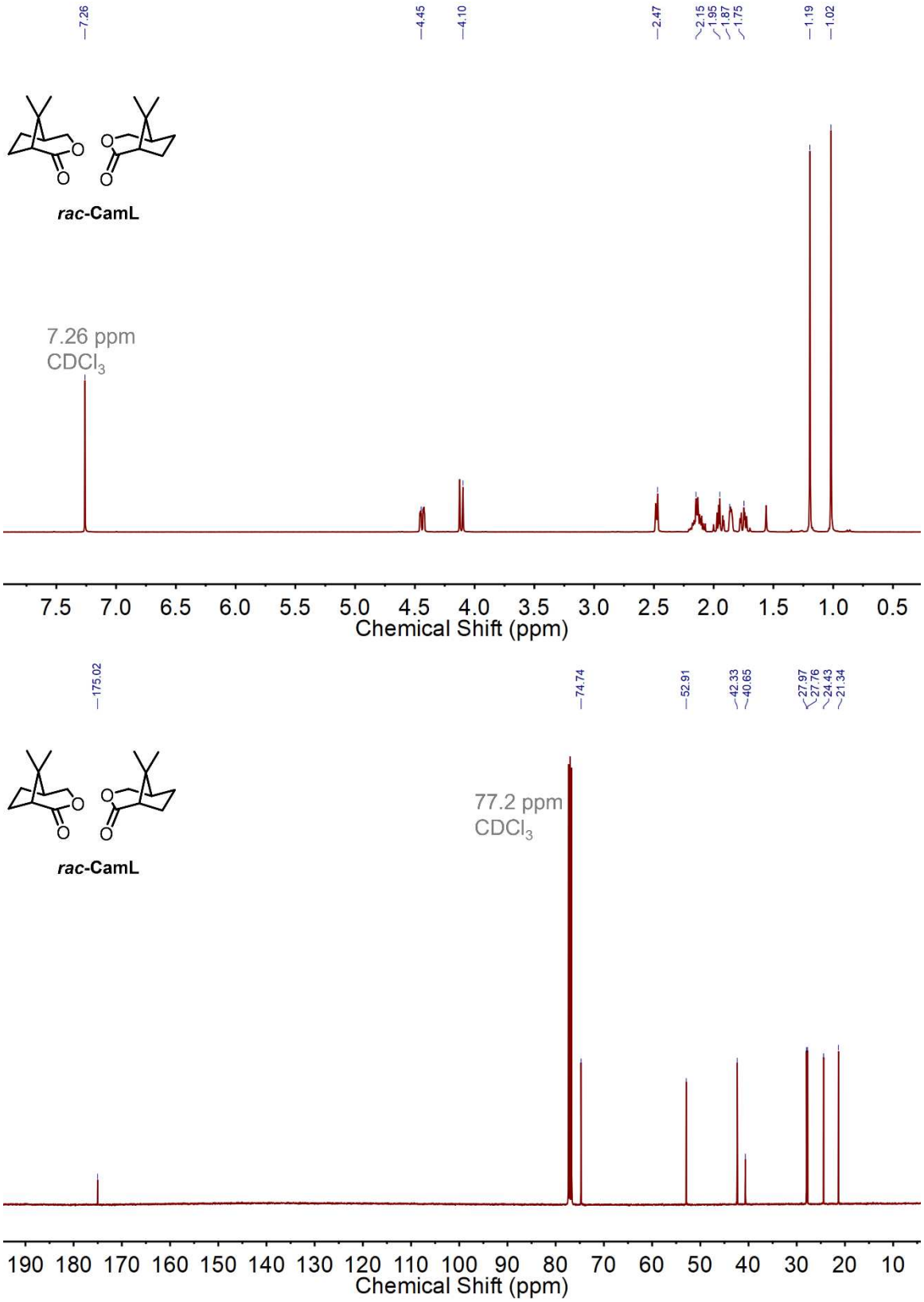

Figure S3.7. ^{1}H NMR (top) and ^{13}C NMR (bottom) ($CDCl_3$, 23 °C) spectra of *rac*-CamL.

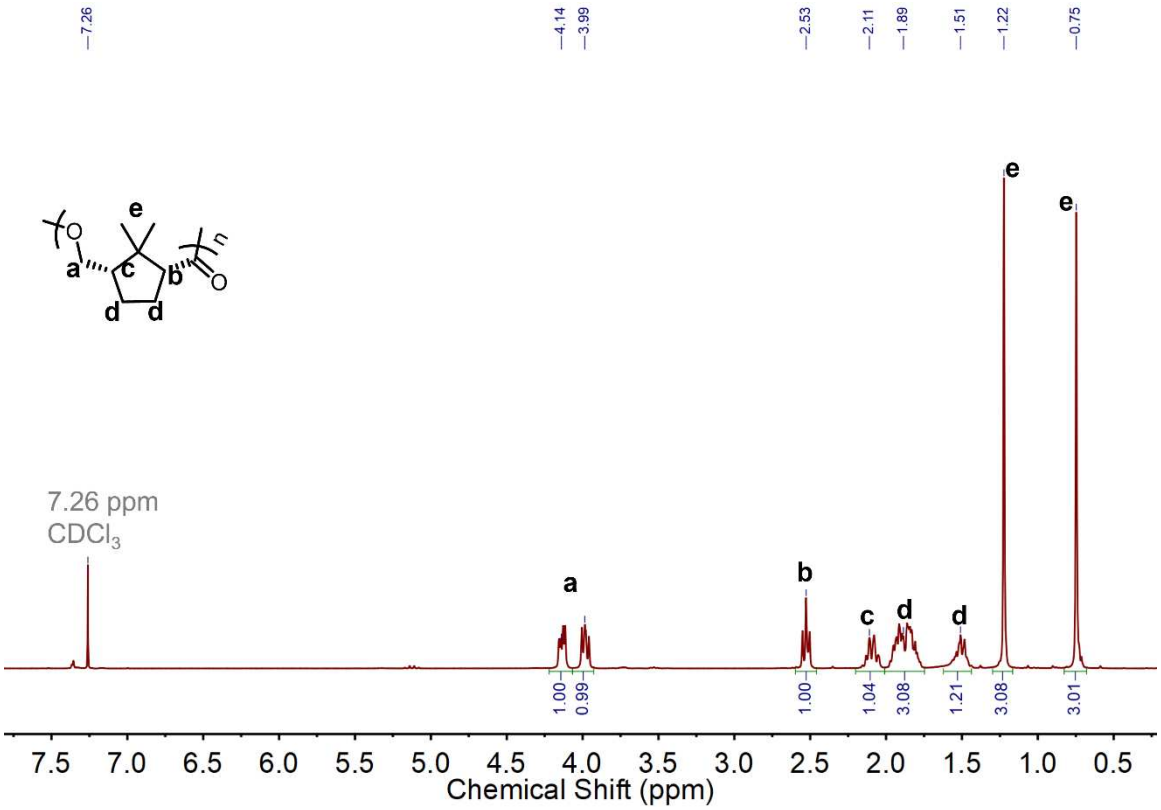
7.26
4.14
3.99
2.53
2.11
1.89
1.51
1.22
0.75
e
a
c
b
d
d
7.26 ppm
CDCl3
a
b
c
d
d
e
e
1.00
0.99
1.00
1.04
3.08
1.21
3.08
3.01
7.5 7.0 6.5 6.0 5.5 5.0 4.5 4.0 3.5 3.0 2.5 2.0 1.5 1.0 0.5
Chemical Shift (ppm)

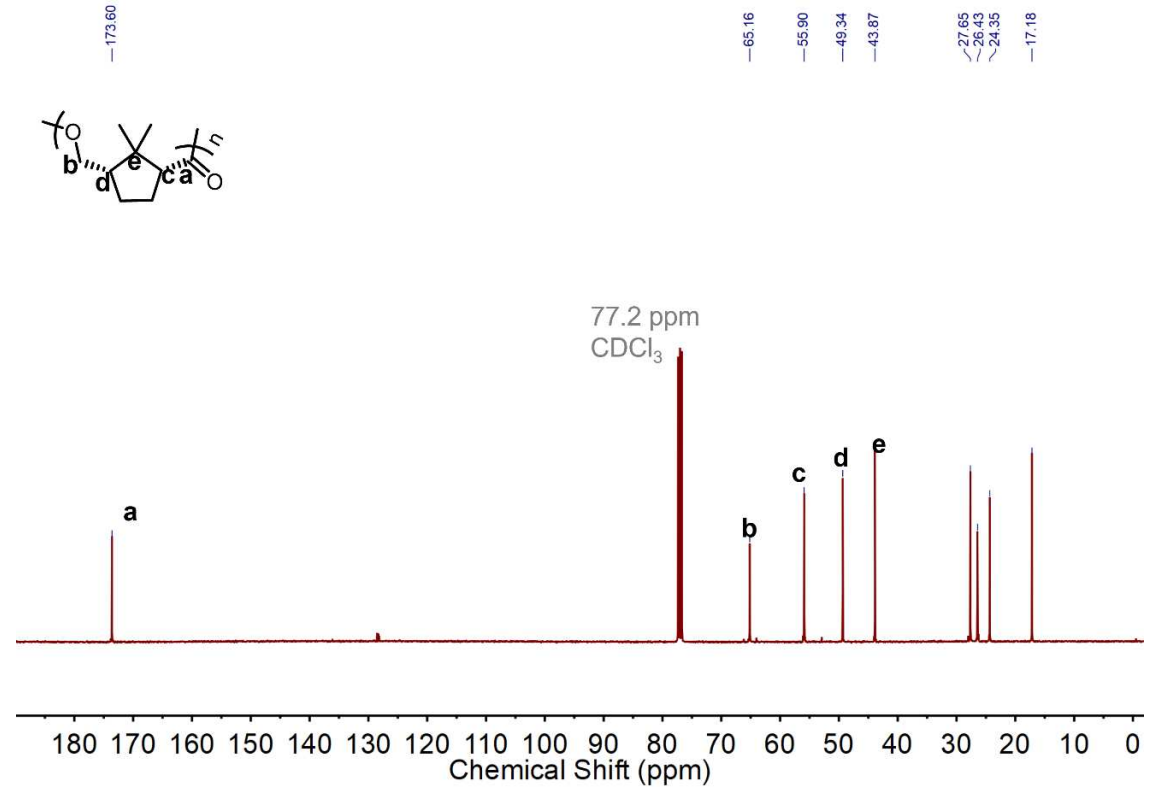
173.60
65.16
55.90
49.34
43.87
27.65
26.43
24.35
17.18
b
d
e
c
a
77.2 ppm
CDCl3
a
b
c
d
e
180 170 160 150 140 130 120 110 100 90 80 70 60 50 40 30 20 10 0
Chemical Shift (ppm)

Figure S3.8. ^{1}H NMR (top) and ^{13}C NMR (bottom) ($CDCl_3$, 23 °C) spectra of isotactic poly(D-CamL) (M_w = 9.80 kDa) from **Table 3.1**, **Run 1**.

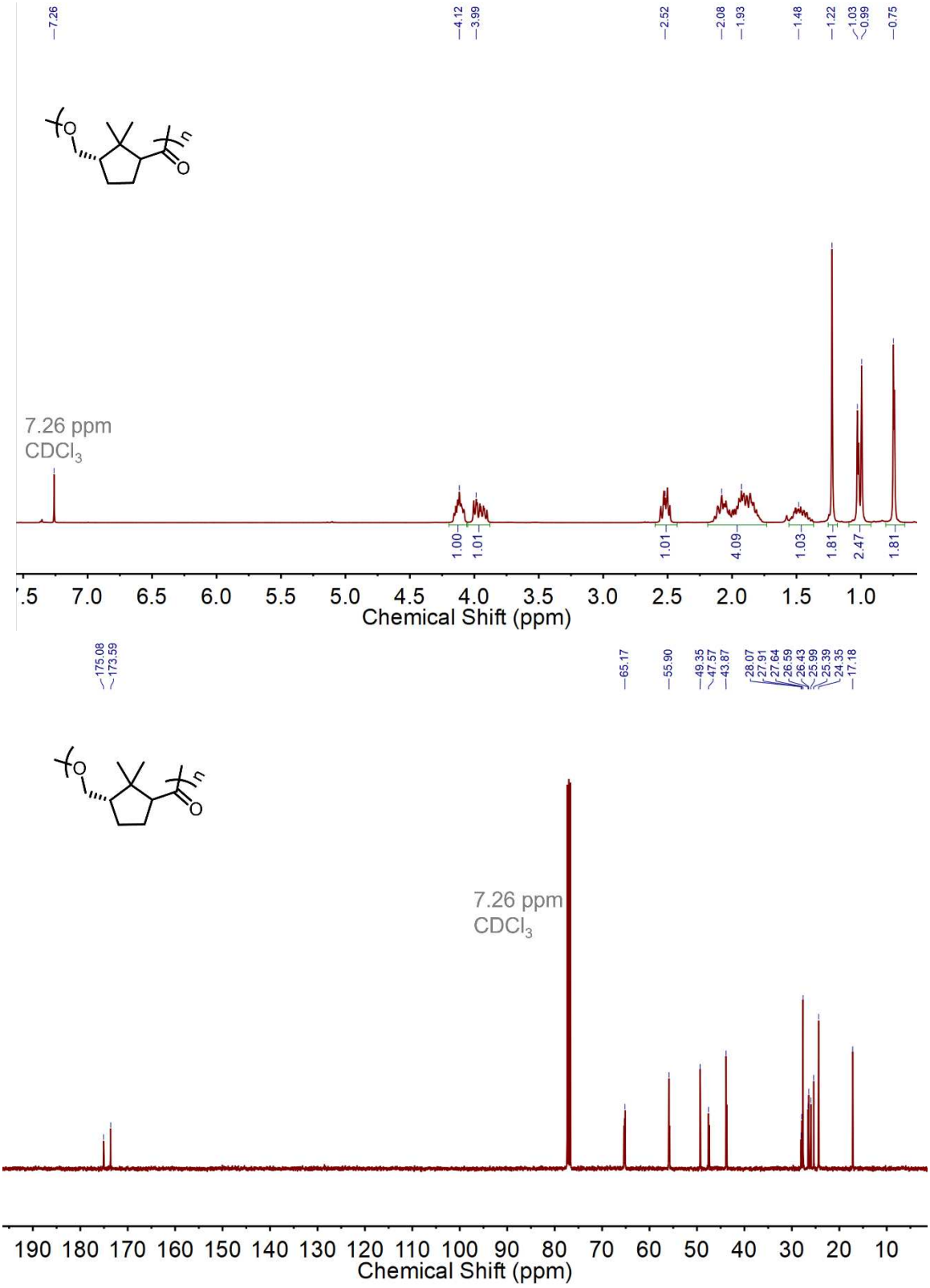

Figure S3.9. ^{1}H NMR (top) and ^{13}C NMR (bottom) ($CDCl_3$, 23 °C) spectra of atactic poly(D-CamL) (M_w = 34.5 kDa) from **Table 3.1**, **Run 3**.

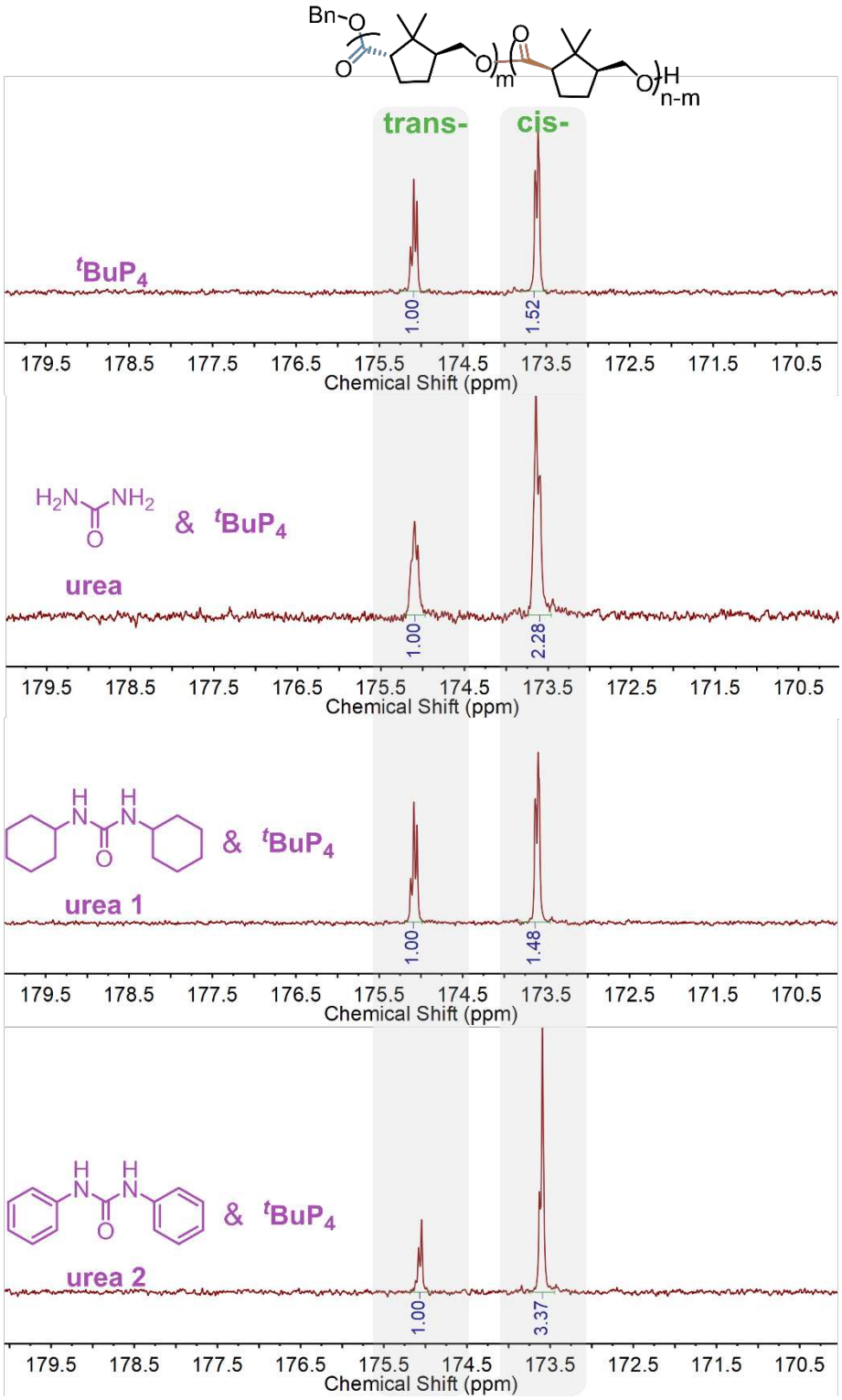

Figure S3.10. ^{13}C NMR ($CDCl_3$, 23 °C) spectra in the carbonyl region of poly(D-CamL) catalyzed by $^{t}BuP_4$ or $^{t}BuP_4$ and substituted urea (urea 1, urea 2, and urea 3) in **Table 3.1**.

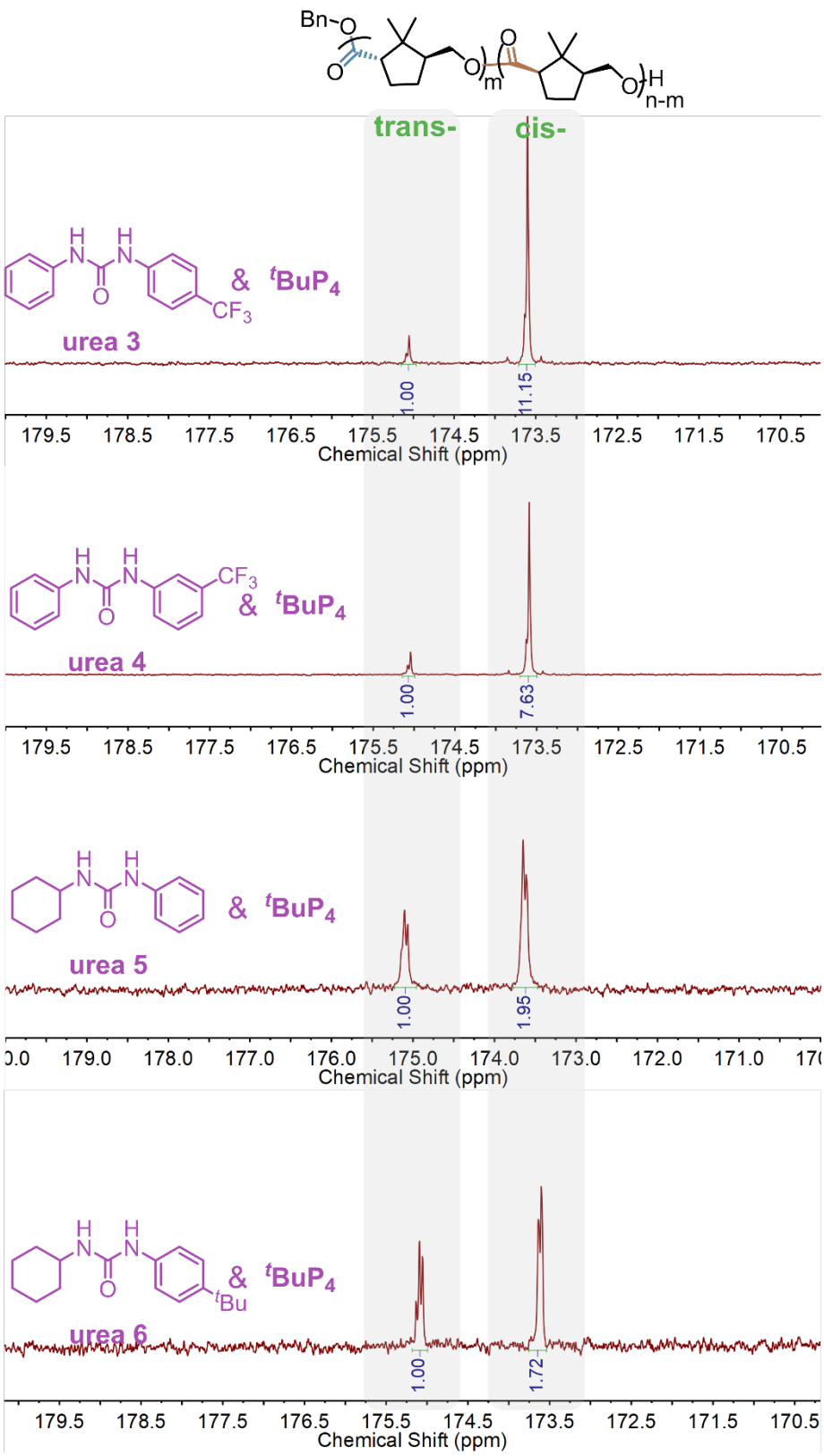
Bn-O
O
O
m
O
O
H
n-m
trans-
cis-
urea 3
& tBuP4
1.00
11.15
179.5 178.5 177.5 176.5 175.5 174.5 173.5 172.5 171.5 170.5
Chemical Shift (ppm)
urea 4
& tBuP4
1.00
7.63
179.5 178.5 177.5 176.5 175.5 174.5 173.5 172.5 171.5 170.5
Chemical Shift (ppm)
urea 5
& tBuP4
1.00
1.95
179.0 178.0 177.0 176.0 175.0 174.0 173.0 172.0 171.0
Chemical Shift (ppm)
urea 6
& tBu
& tBuP4
1.00
1.72
179.5 178.5 177.5 176.5 175.5 174.5 173.5 172.5 171.5 170.5
Chemical Shift (ppm)

Figure S3.11. ^{13}C NMR ($CDCl_3$, 23 °C) spectra in the carbonyl region of poly(D-CamL) catalyzed by $^{t}BuP_4$ and substituted urea (urea 4, urea 5, and urea 6) in **Table 3.1**.

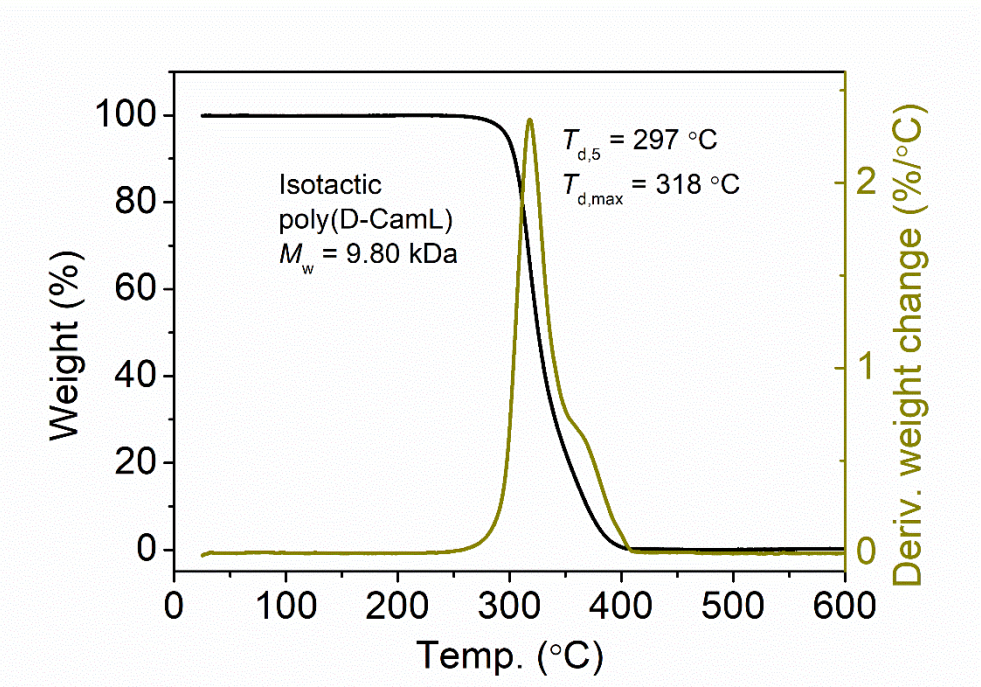

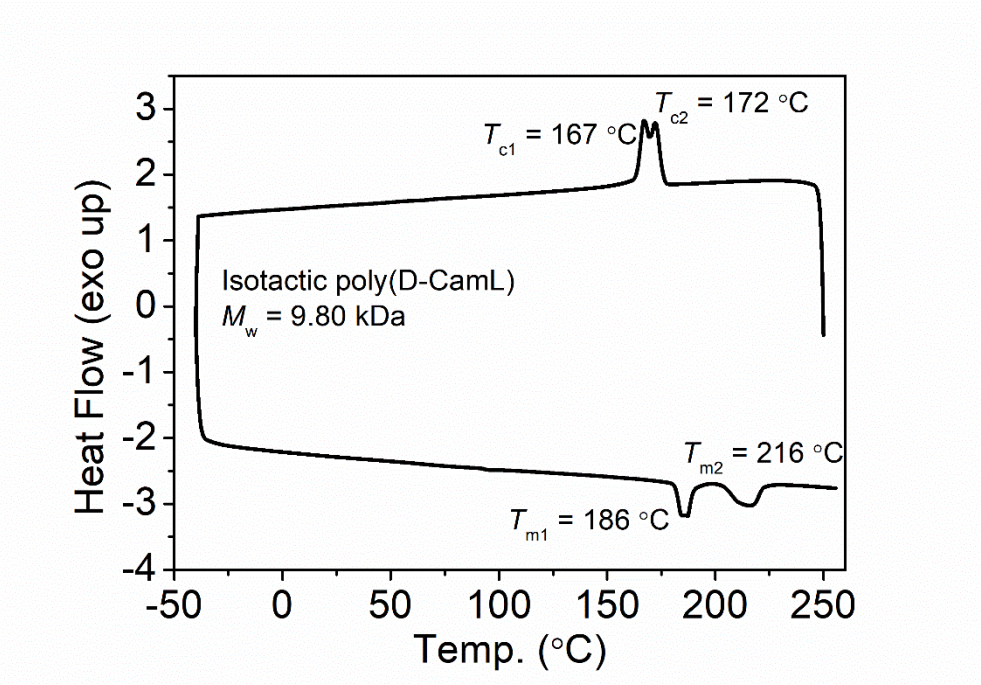

Figure S3.12. TGA curve (top) and DSC curve (bottom) of obtained isotactic poly(D-CamL) (M_w = 9.80 kDa) from **Table 3.1**, **Run 1**. (1st cooling scan and 2nd heating scan, rates of heating: 10 °C/min).

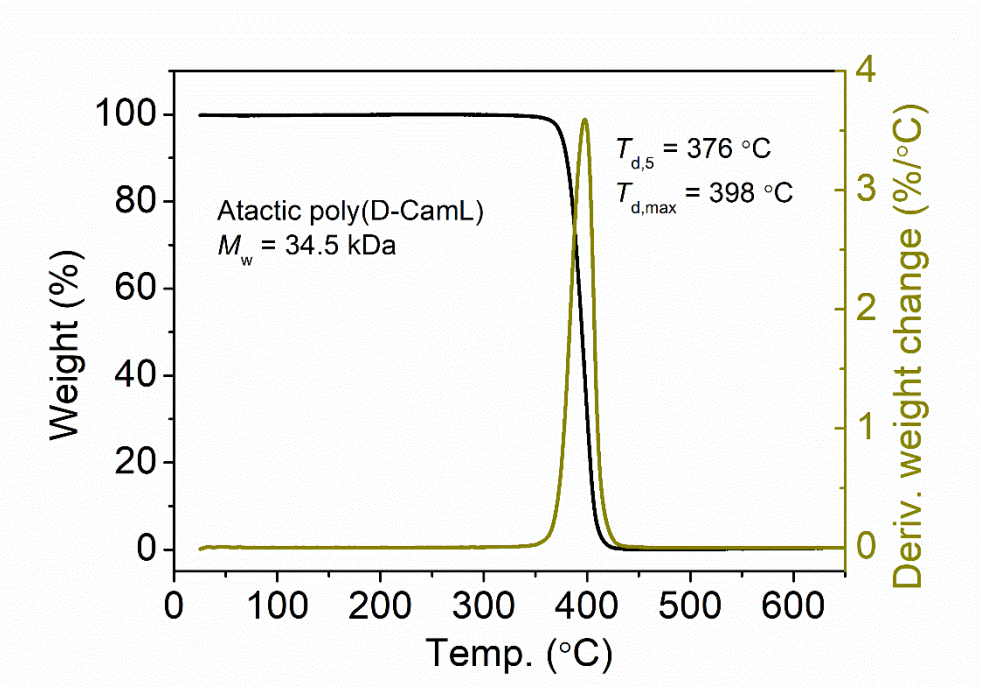

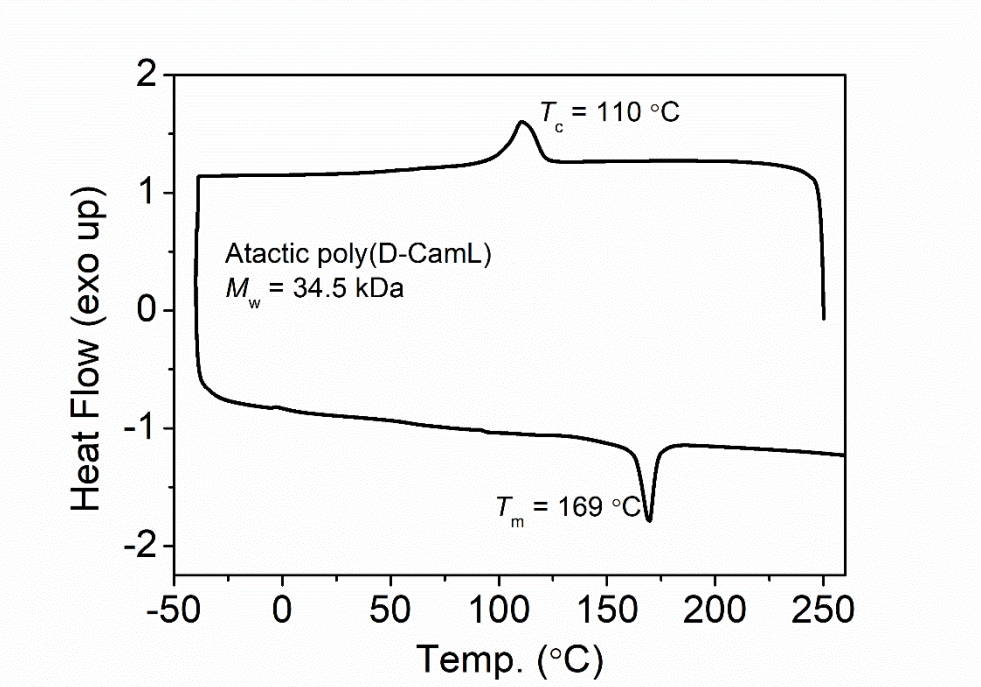

Figure S3.13. TGA curve (top) and DSC curve (bottom) of obtained atactic poly(D-CamL) (M_w = 34.5 kDa) from **Table 3.1**, **Run 3**. (1st cooling scan and 2nd heating scan, rates of heating: 10 °C/min).

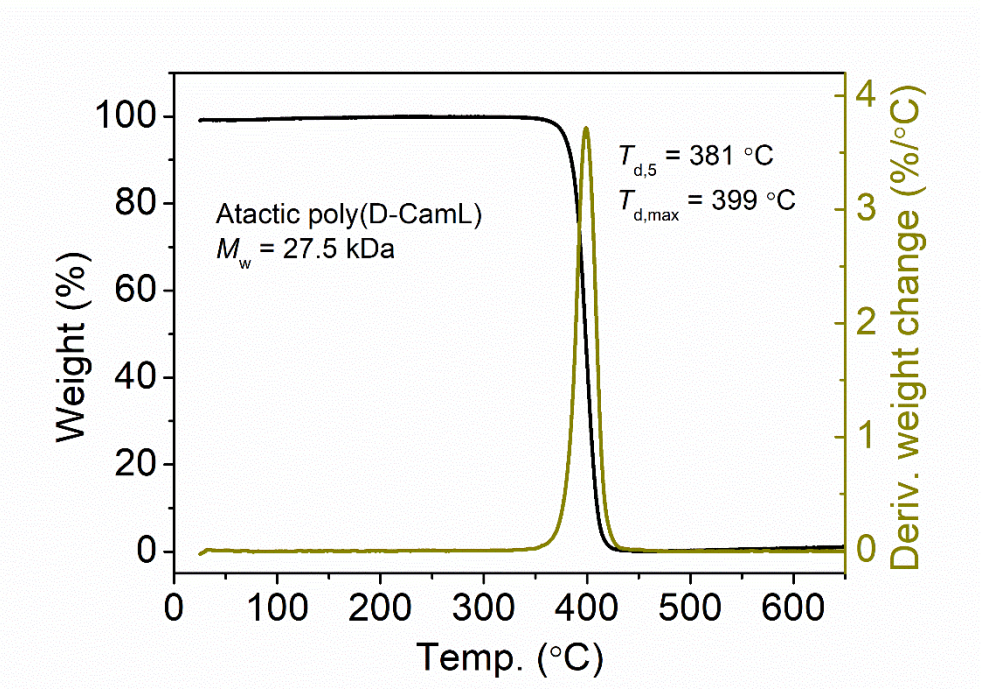

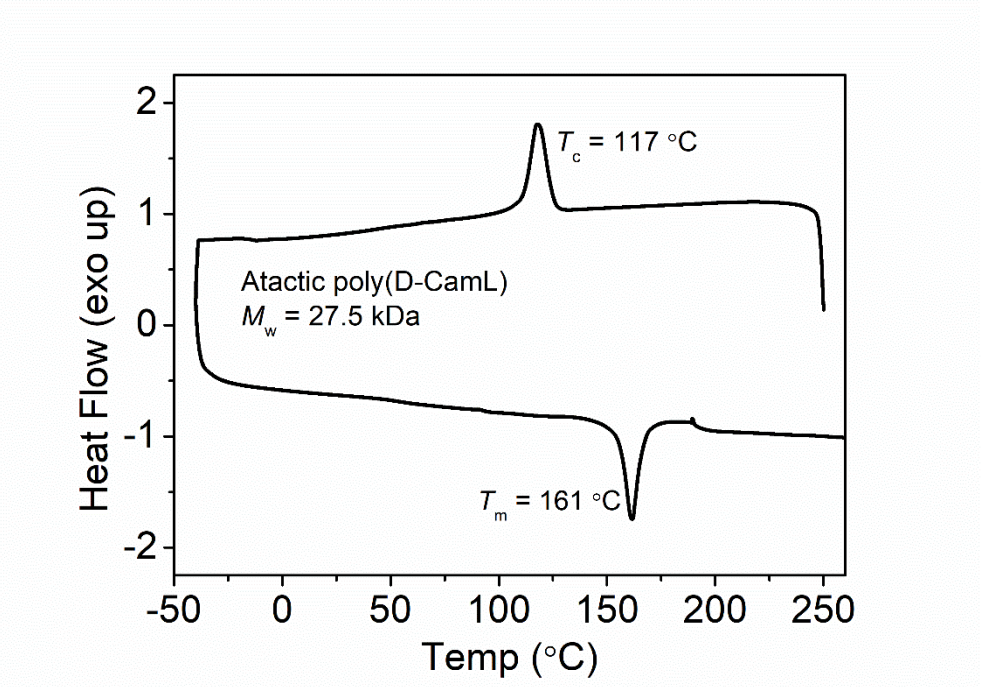

Figure S3.14. TGA curve (top) and DSC curve (bottom) of obtained atactic poly(D-CamL) (M_w = 27.5 kDa) from **Table 3.1**, **Run 6**. (1st cooling scan and 2nd heating scan, rates of heating: 10 °C/min).

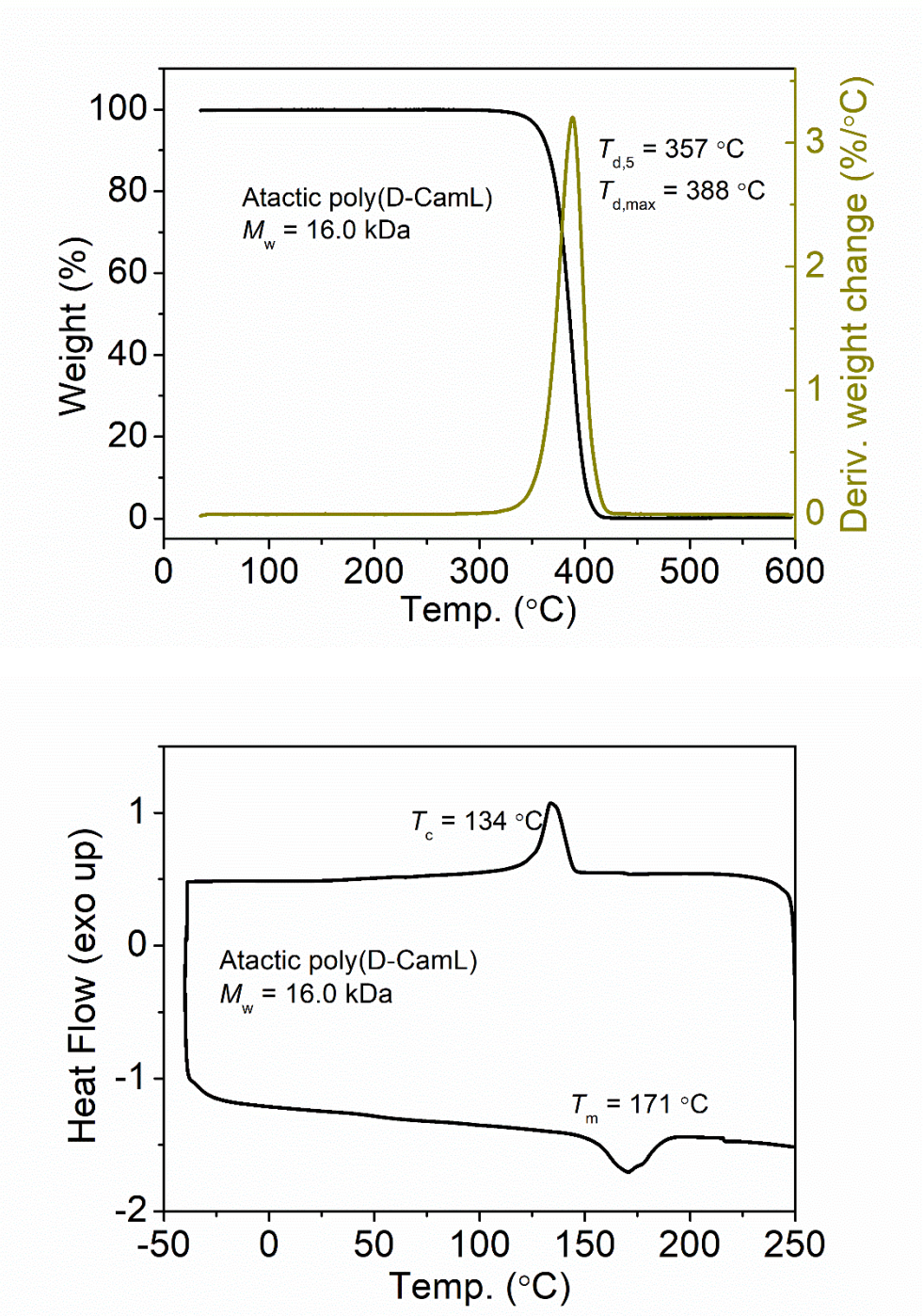

Figure S3.15. TGA curve (top) and DSC curve (bottom) of obtained atactic poly(D-CamL) (M_w = 16.0 kDa) from **Table 3.1**, **Run 7**. (1st cooling scan and 2nd heating scan, rates of heating: 10 °C/min).

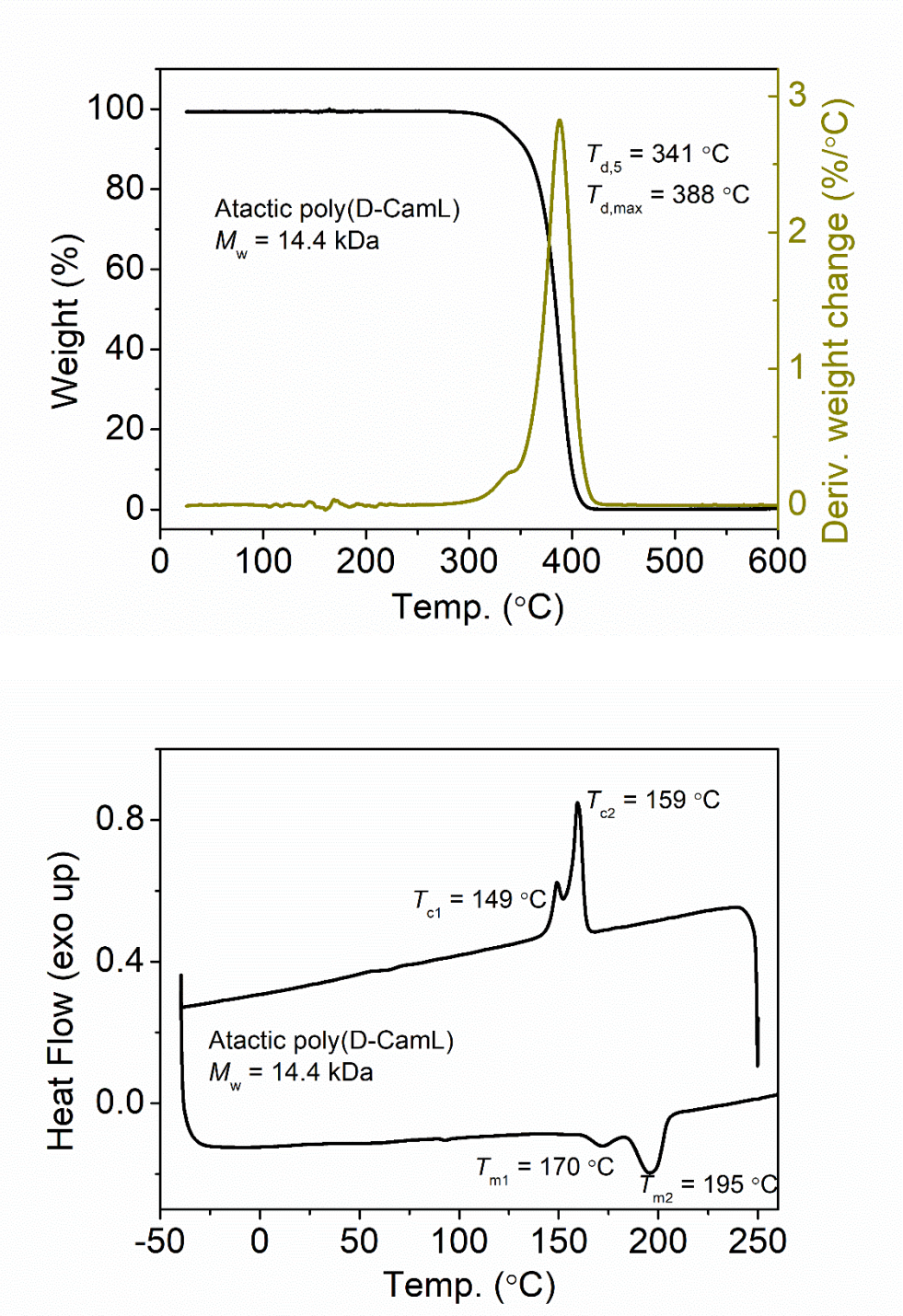

Figure S3.16. TGA curve (top) and DSC curve (bottom) of obtained atactic poly(D-CamL) (M_w = 14.4 kDa) from **Table 3.1**, **Run 8**. (1st cooling scan and 2nd heating scan, rates of heating: 10 °C/min).

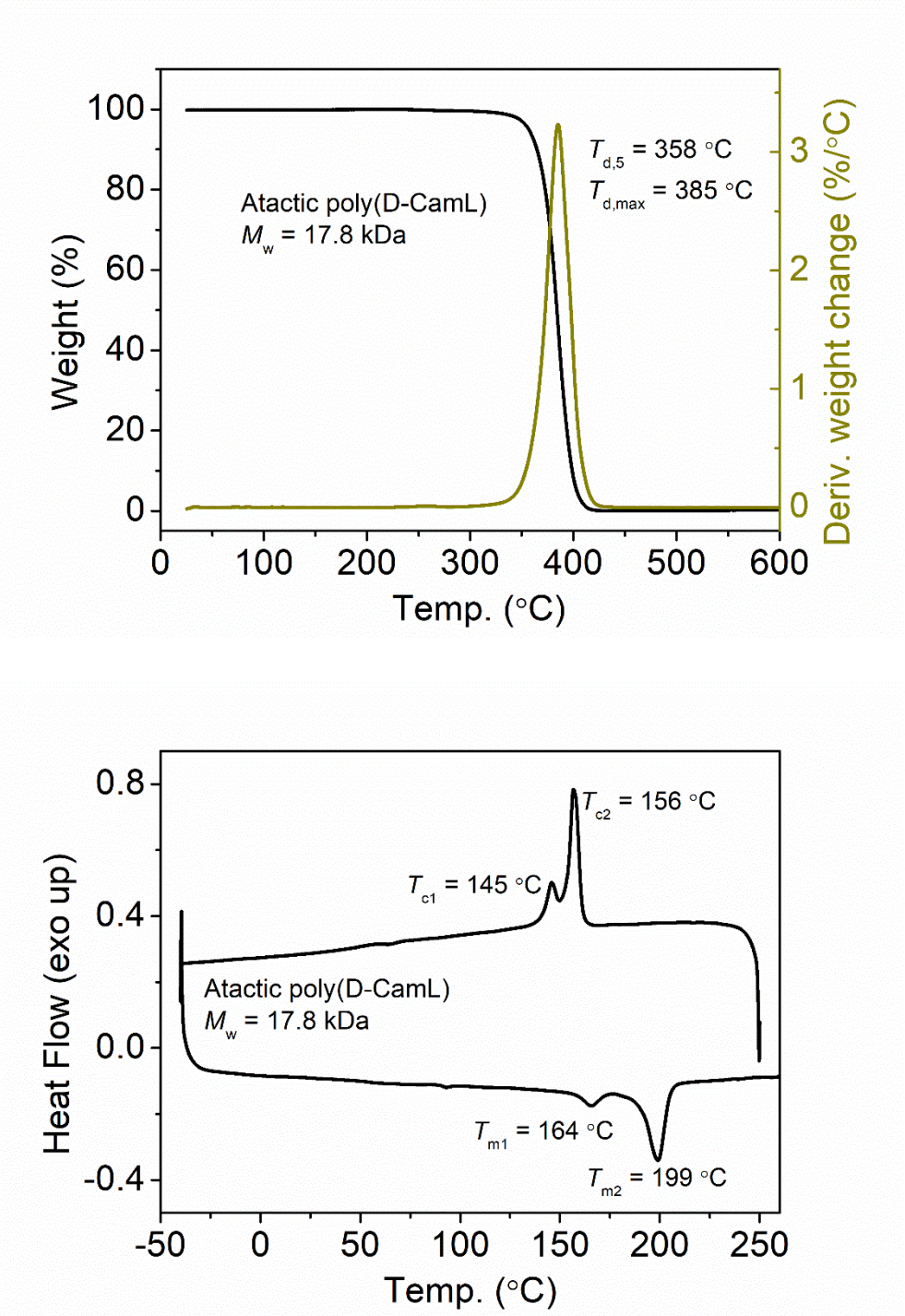

Figure S3.17. TGA curve (top) and DSC curve (bottom) of obtained atactic poly(D-CamL) (M_w = 17.8 kDa) from **Table 3.1**, **Run 9**. (1st cooling scan and 2nd heating scan, rates of heating: 10 °C/min).

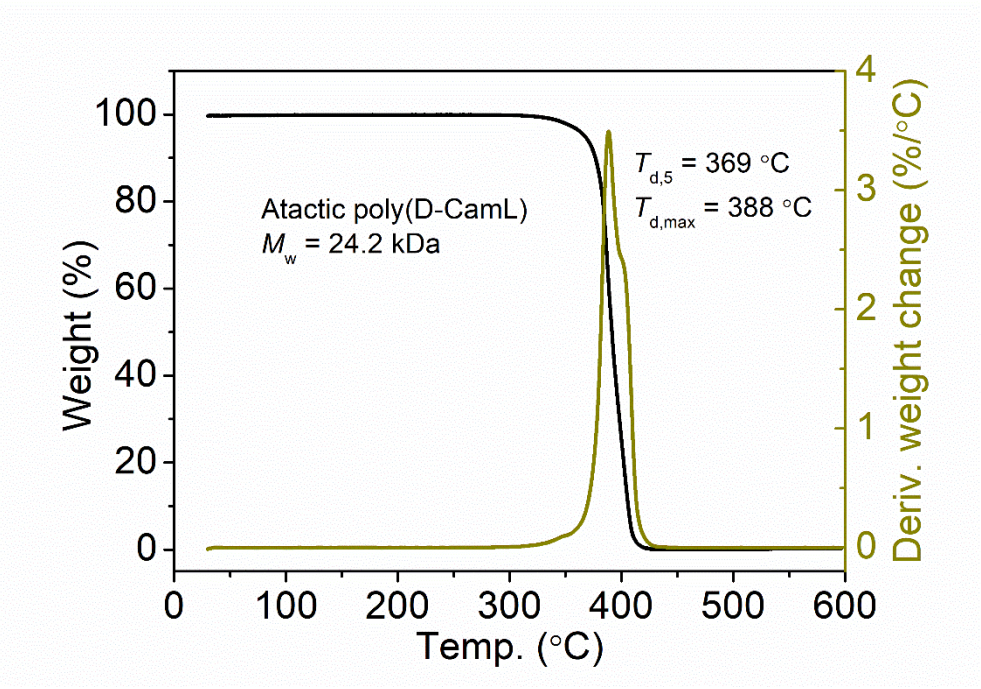

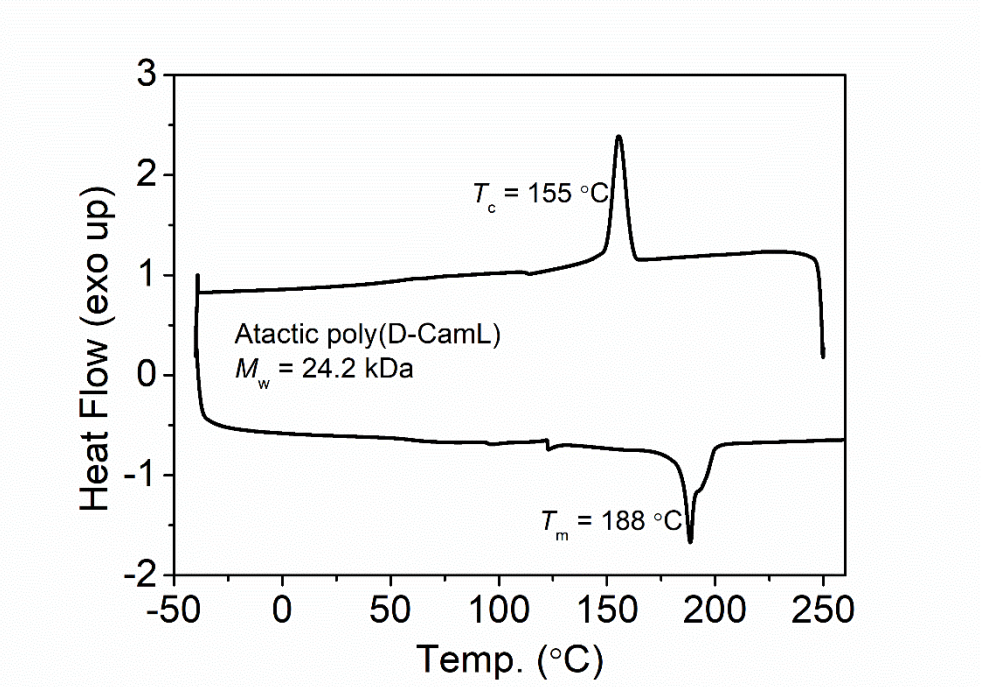

Figure S3.18. TGA curve (top) and DSC curve (bottom) of obtained atactic poly(D-CamL) (M_w = 24.2 kDa) from **Table 3.1**, **Run 10**. (1st cooling scan and 2nd heating scan, rates of heating: 10 °C/min).

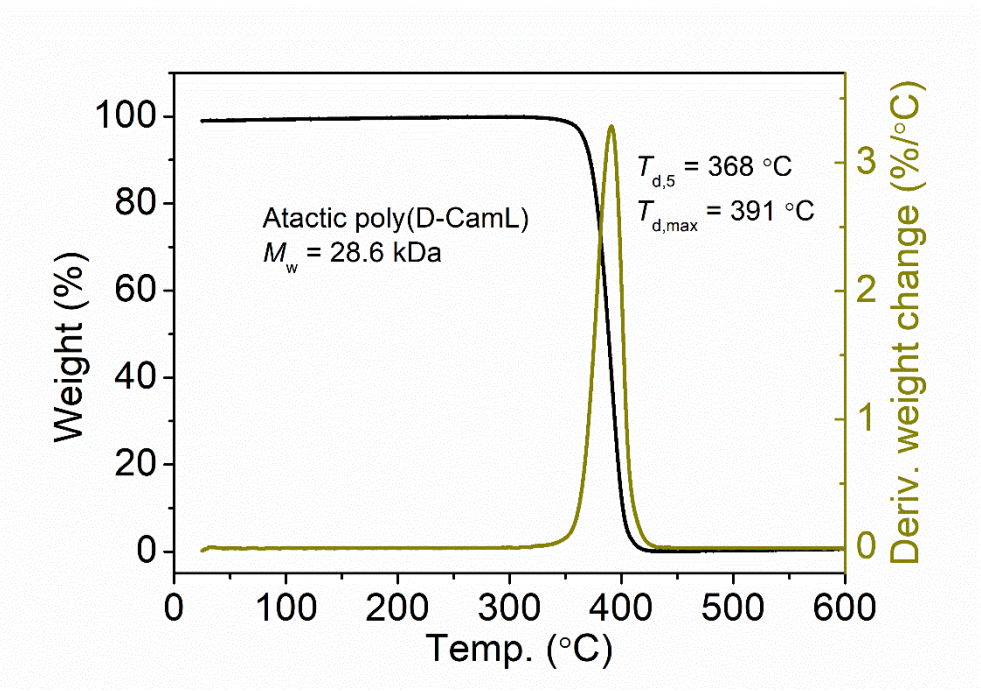

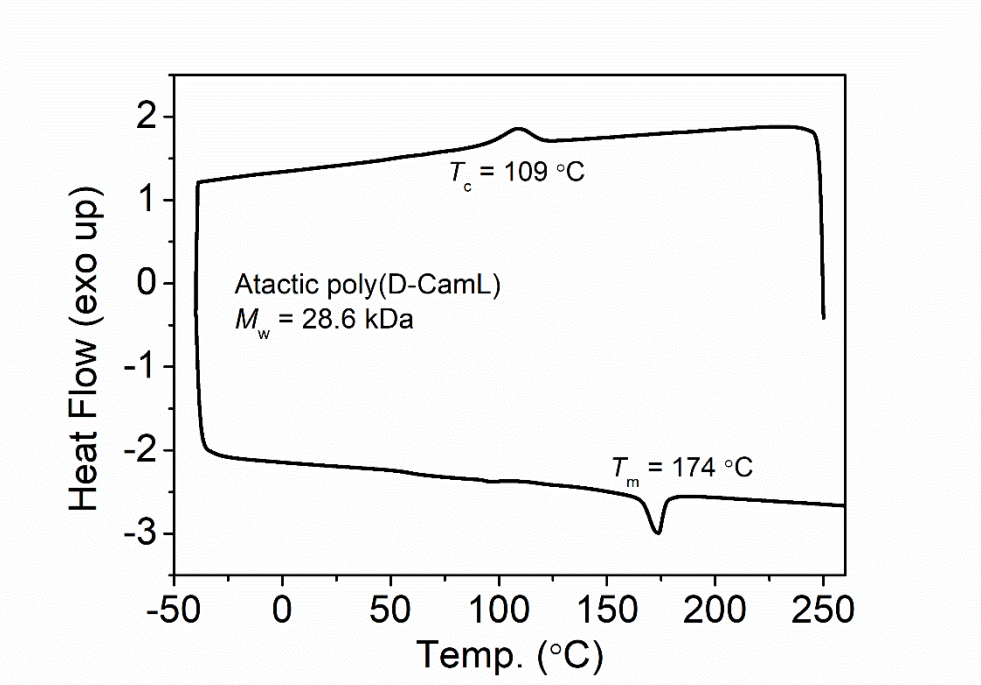

Figure S3.19. TGA curve (top) and DSC curve (bottom) of obtained atactic poly(D-CamL) (M_w = 28.6 kDa) from **Table 3.1**, **Run 11**. (1st cooling scan and 2nd heating scan, rates of heating: 10 °C/min).

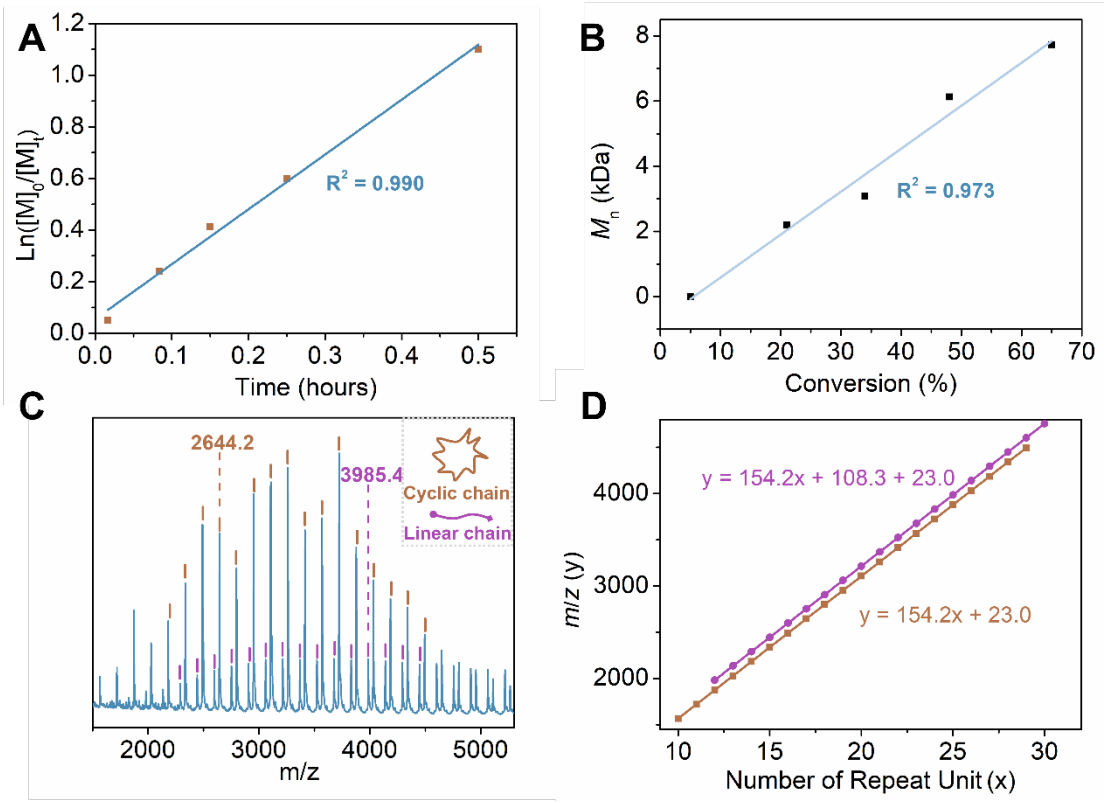

Figure S3.20. (A) pseudo-first-order kinetic plot. **(B)** evolution of polymer molecular weight as a function of monomer conversion of ^{t}BuP$_4$ catalyzed polymerization of D-CamL, [D-CamL]:[BnOH]:[^{t}BuP$_4$] = 100:1:1, concentration: 0.5 mg/μL. **(C) & (D)** MALDI-TOF mass spectrum of ^{t}BuP$_4$ catalyzed poly(D-CamL) from **Table 3.1**, **Run 3**, and **(D)** plots of *m*/*z* values (y) vs the number of D-CamL repeat units (x). (matrix: dithranol, salt: NaTFA). Note: The peaks height of cyclic chain is higher than linear chain can be attributed to the fact that low molecular weight polymers are more likely to show peak signals. Therefore, peaks height is not a reliable indicator of content.

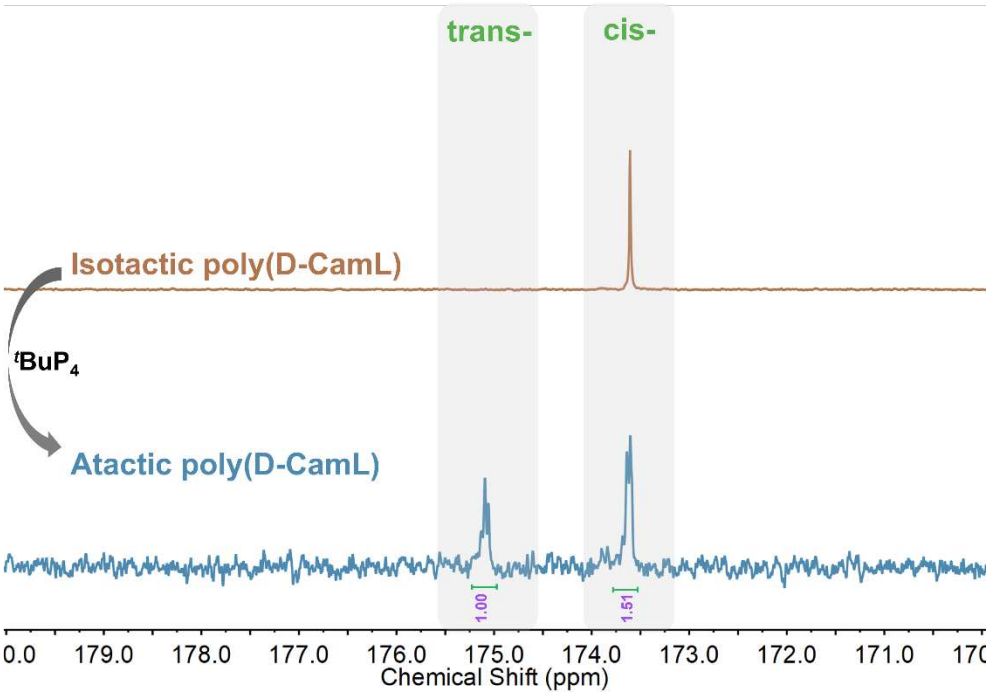

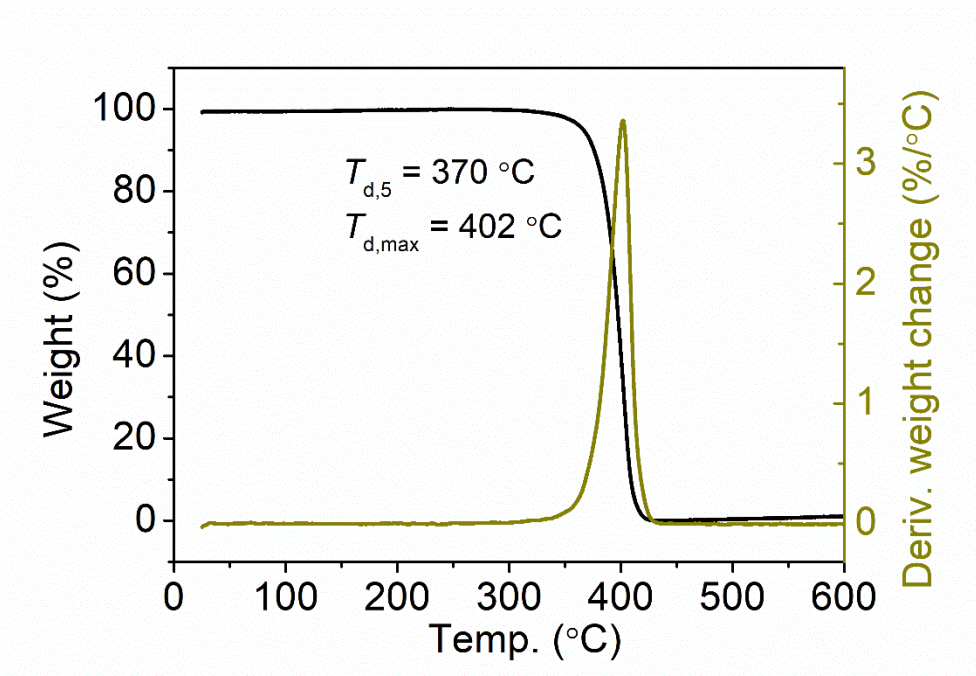

Figure S3.21. Plots of ^{13}C NMR ($CDCl_3$, 23 °C) spectra of isotactic poly(D-CamL) before (orange line) and after (blue line) epimerization by stirring with $^{t}BuP_4$ for 4.0 hours (top) and TGA experiment of epimerized poly(D-CamL) (bottom).

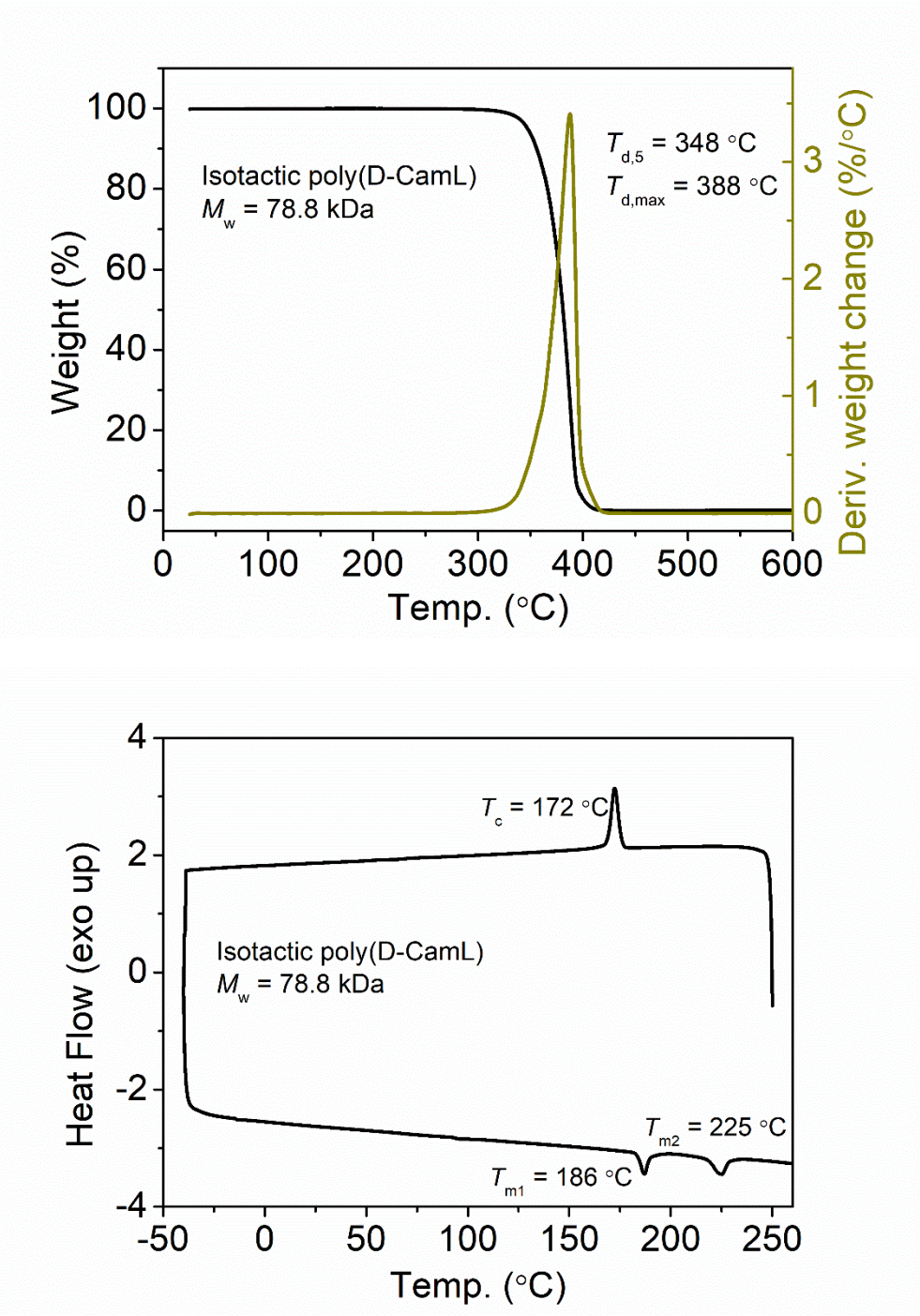

Figure S3.22. Plots of TGA experiment (top) and DSC experiment (bottom) of high molecular weight isotactic poly(D-CamL) (M_w = 78.8 kDa) from **Table 3.2**, **Run 1**. (1st cooling scan and 2nd heating scan, rates of heating: 10 °C/min).

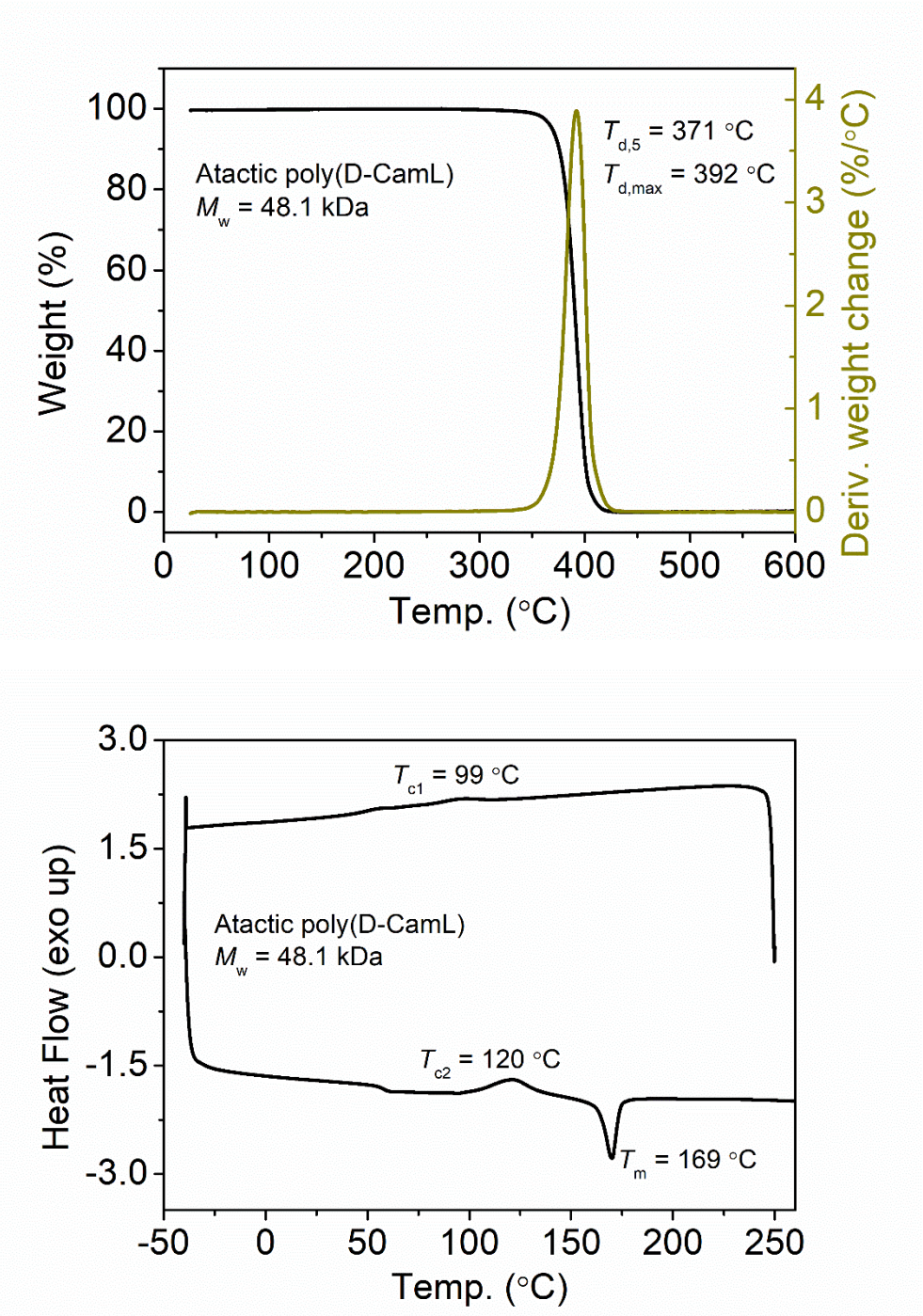

Figure S3.23. Plots of TGA experiment (top) and DSC experiment (bottom) of high molecular weight atactic poly(D-CamL) (M_w = 48.1 kDa) from **Table 3.2**, **Run 2**. (1st cooling scan and 2nd heating scan, rates of heating: 10 °C/min).

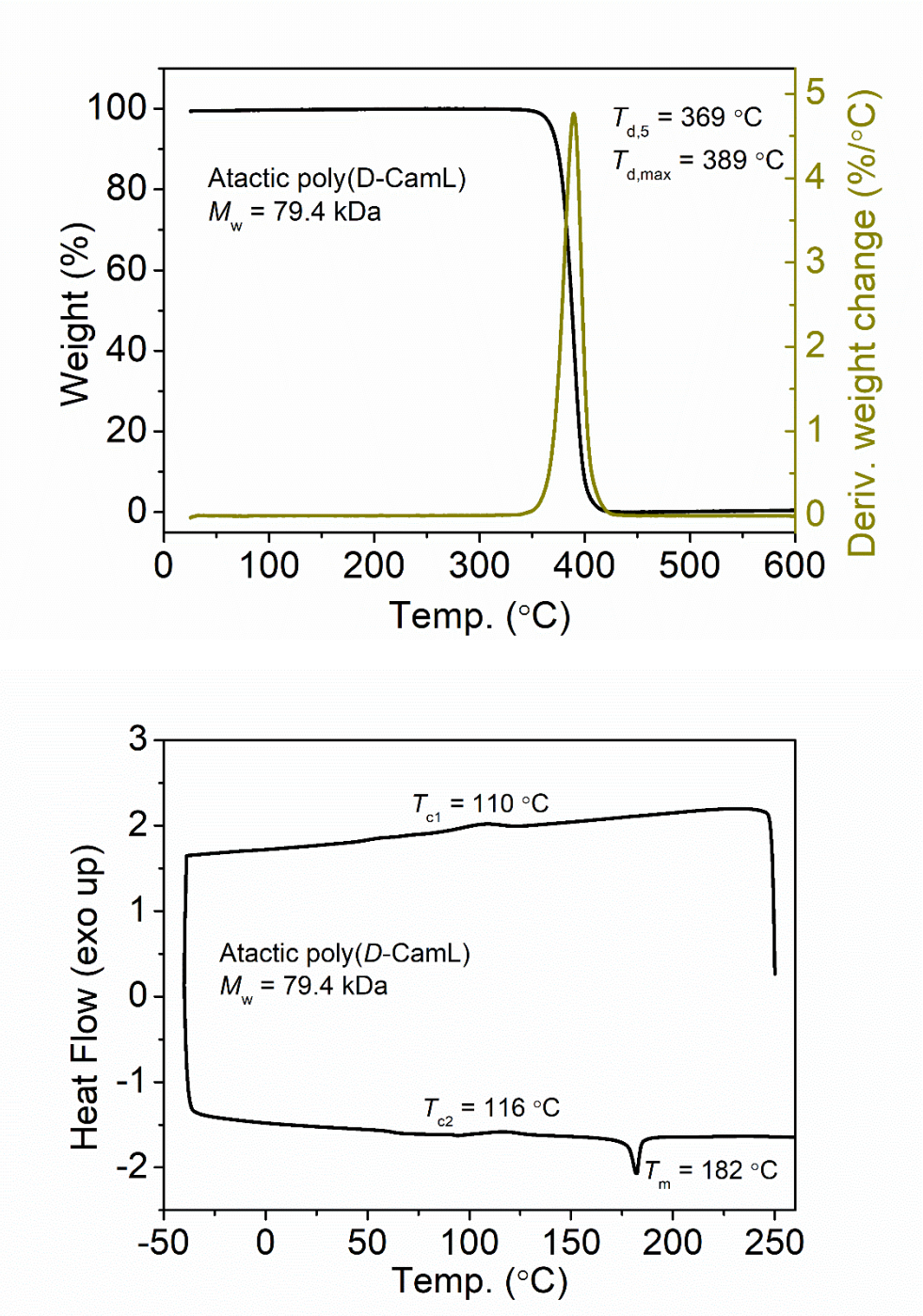

Figure S3.24. Plots of TGA experiment (top) and DSC experiment (bottom) of high molecular weight atactic poly(D-CamL) (M_w = 79.4 kDa) from **Table 3.2**, **Run 3**. (1st cooling scan and 2nd heating scan, rates of heating: 10 °C/min).

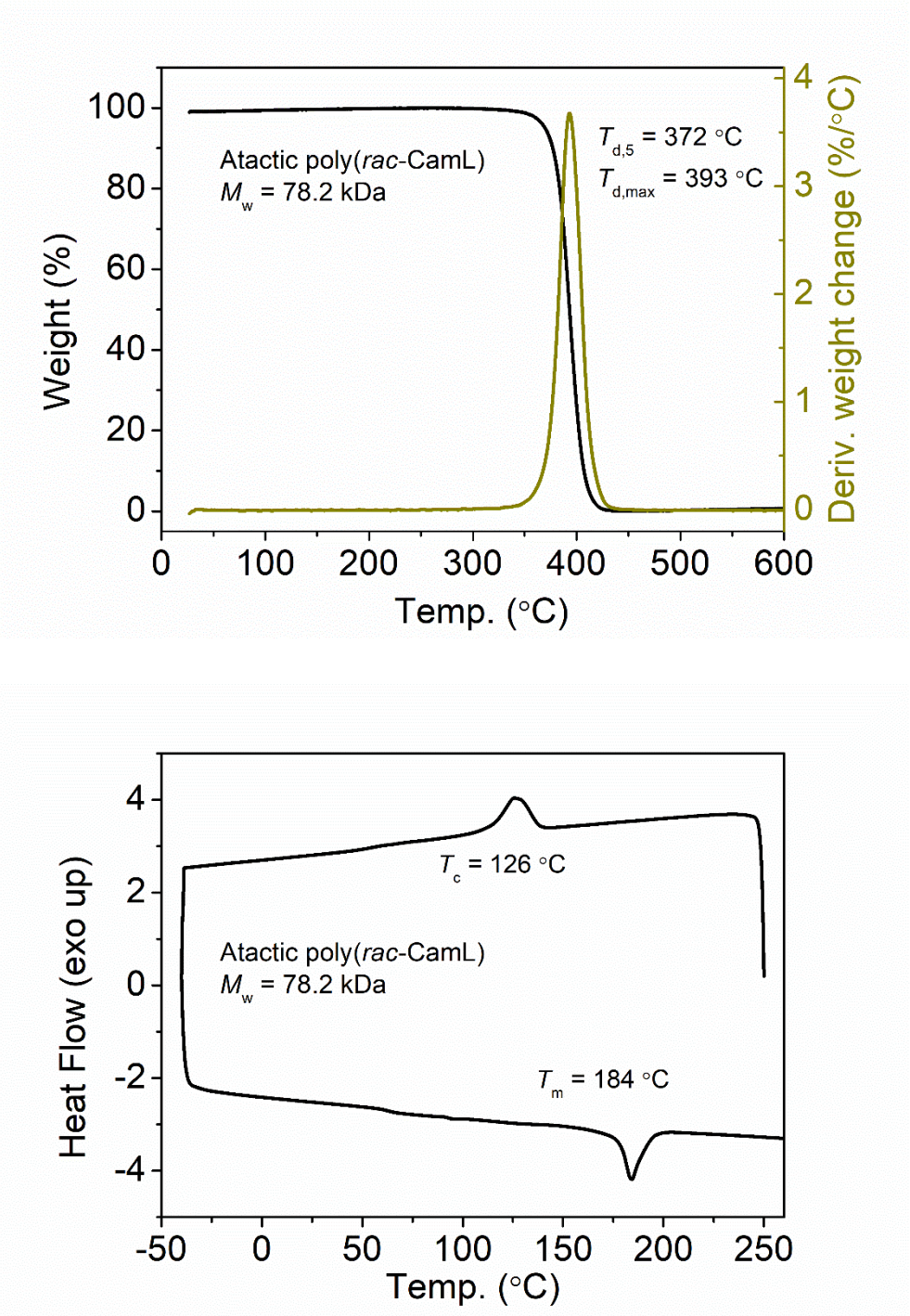

Figure S3.25. Plots of TGA experiment (top) and DSC experiment (bottom) of high molecular weight poly(*rac*-CamL) (M_w = 78.2 kDa) from **Table 3.2**, **Run 4**. (1st cooling scan and 2nd heating scan, rates of heating: 10 °C/min).

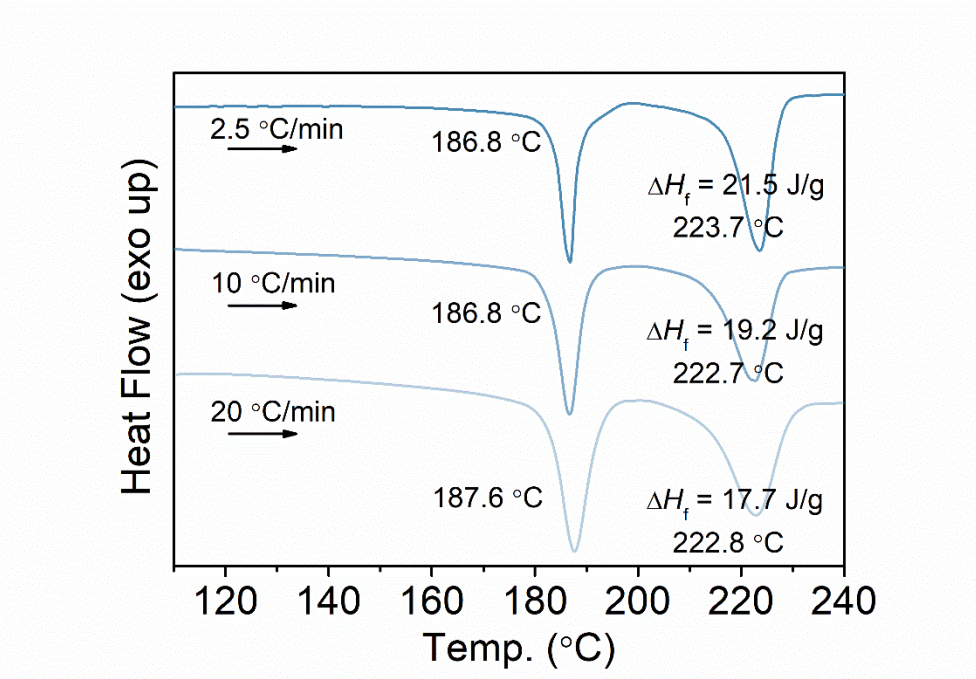

Figure S3.26. Plotted results from DSC experiments of isotactic poly(D-CamL) (**Table 3.2**, **Run 1**) at the indicated different heating rates (second heating scans). Each experiment consists of a first heating and a successive cooling at 10 °C/min. Then, the second heating scan of the melt-crystallized sample was performed at 2.5, 10, 20 and 30 °C/min.

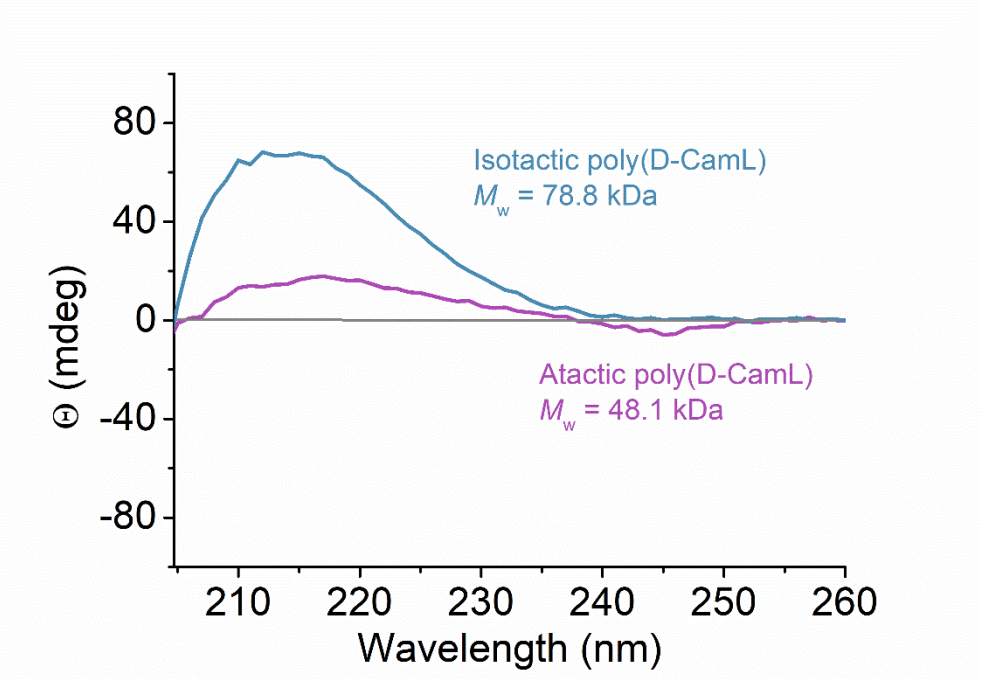

Figure S3.27. Plots of CD characterization of isotactic poly(D-CamL) (**Table 3.2**, **Run 1**) and atactic poly(D-CamL) (**Table 3.2**, **Run 2**), measured in HFIP (1.0 mg/mL).

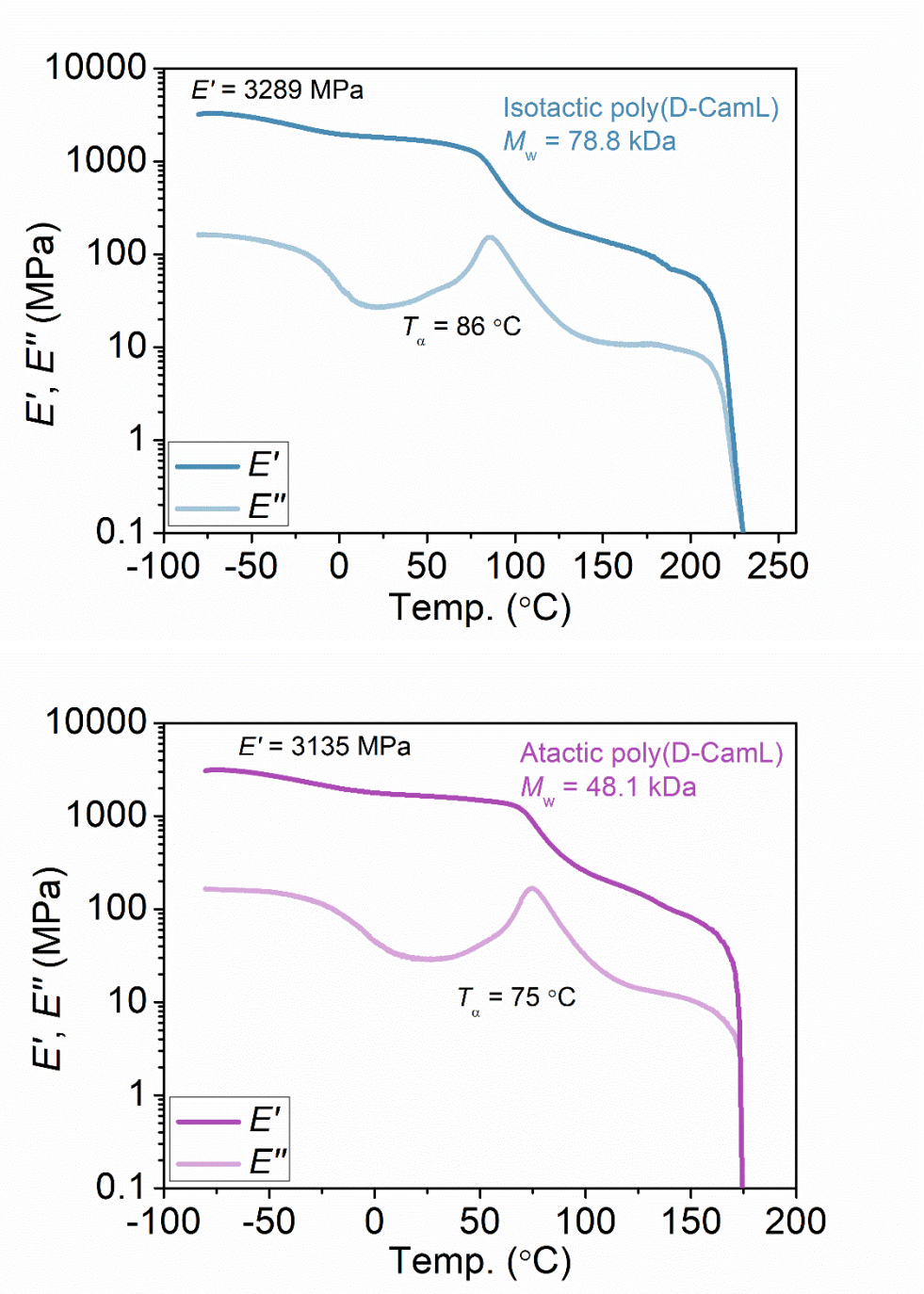

Figure S3.28. Plots of DMA characterization of isotactic poly(D-CamL) (**Table 3.2**, **Run 1**, top) and atactic poly(D-CamL) (**Table 3.2**, **Run 2**, bottom).

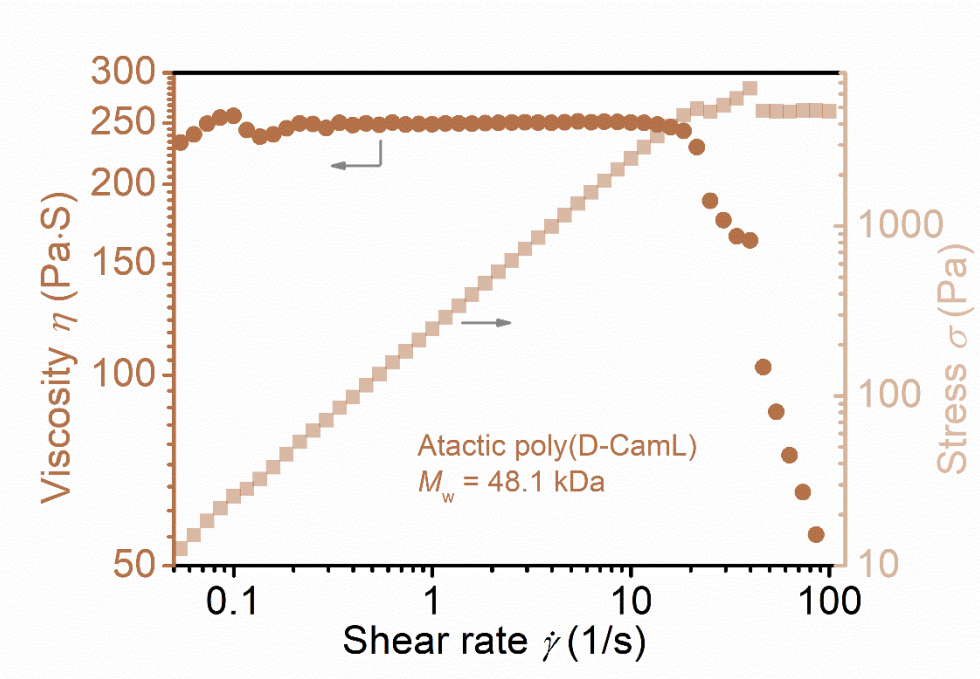

Figure S3.29. Plots of shear thinning experiment of atactic poly(D-CamL) (**Table 3.2**, **Run 2**, bottom).

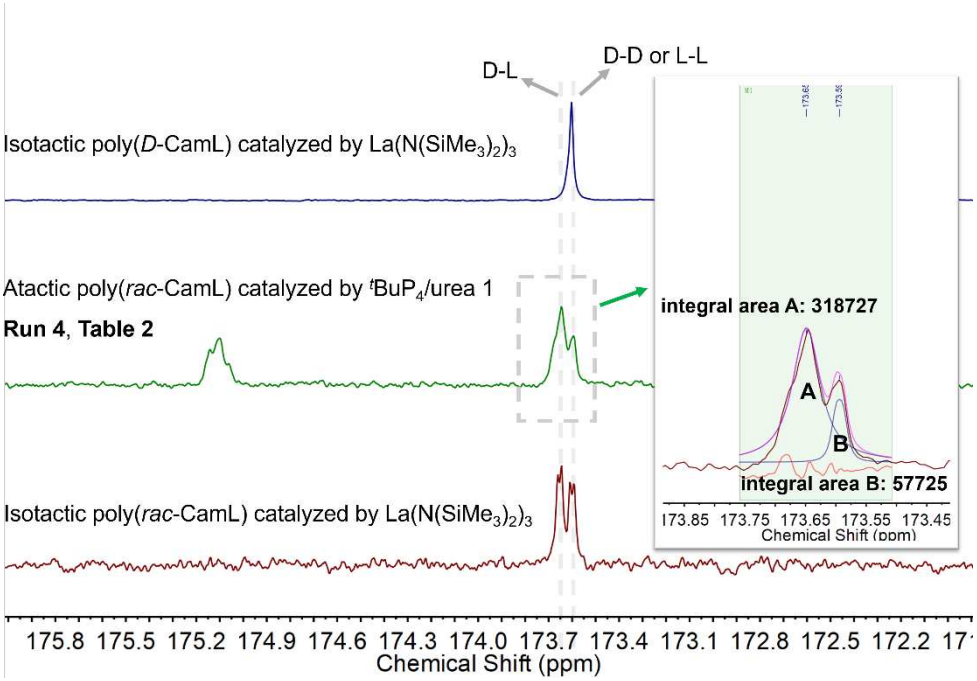

Figure S3.30. Plots of ^{13}C NMR ($CDCl_3$, 23 °C) spectra in the carbonyl region of isotactic poly(D-CamL) (top), high molecular weight poly(*rac*-CamL) (**Table 3.2**, **Run 4**, middle), and isotactic poly(*rac*-CamL) (bottom).

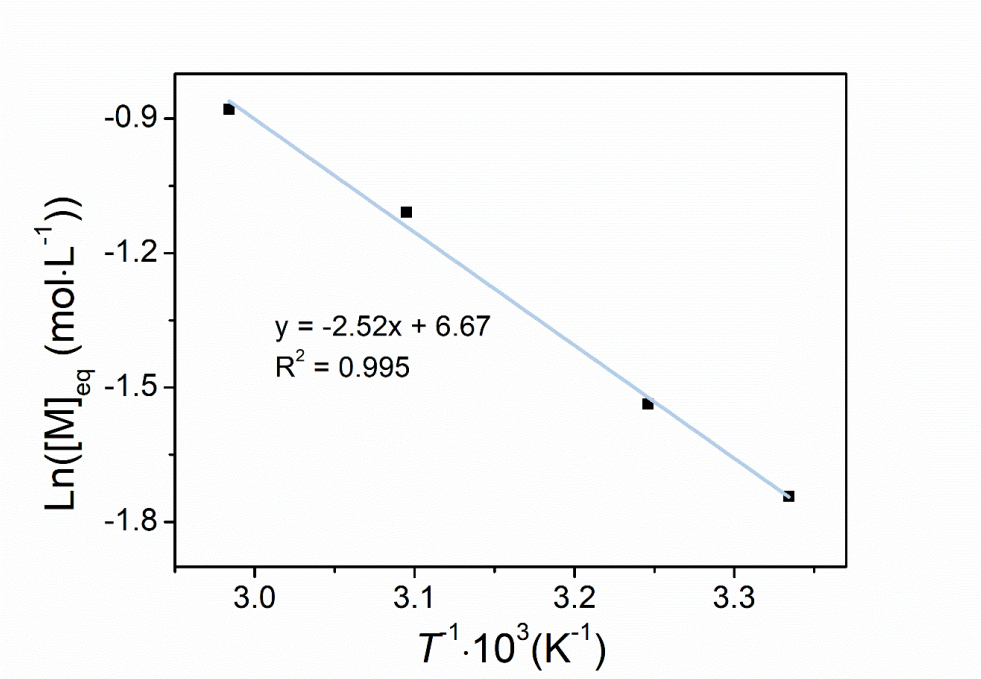

Figure S3.31. Van't Hoff plot of D-CamL polymerization under ^{t}BuP$_4$, [M]$_0$ = 1.0 M.

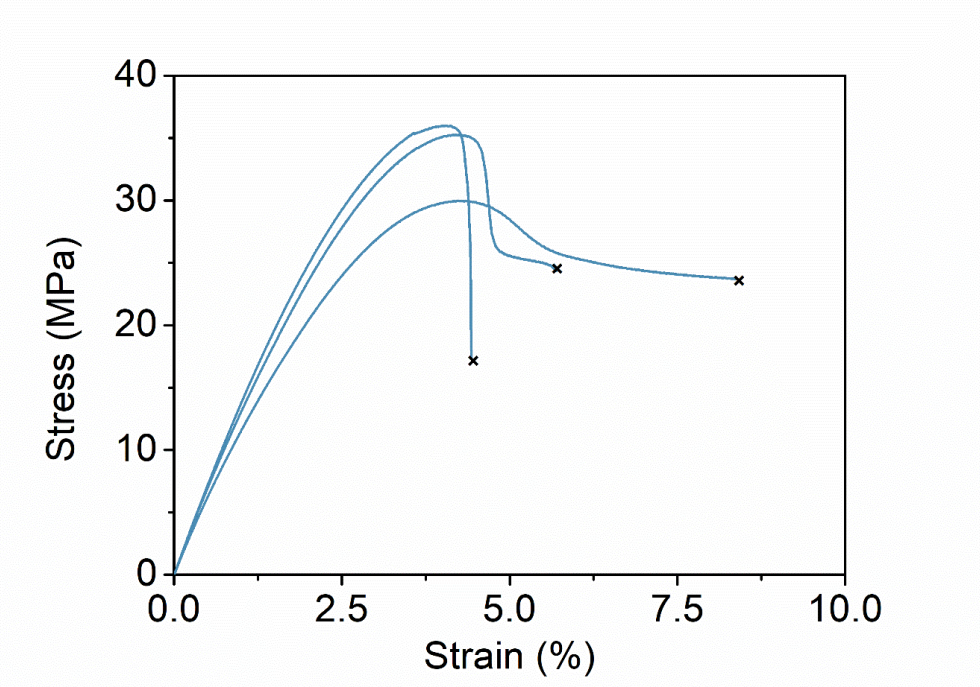

Figure S3.32. Plots of stress-strain experiments for isotactic poly(D-CamL) produced by a [D-CamL]:[La(N(SiMe$_3$)$_2$)$_3$]:[BnOH] ratio of 1000:2:1. M_w = 78.8 kDa, elongation rate = 5 mm/min, ambient conditions.

Table S3.3. Stress-strain data of isotactic poly(D-CamL) (M_w = 78.8 kDa).

Sample number	Yield stress (MPa)	ε_B (%)	E (GPa)
1	30.0	9	1.25
2	35.3	5	1.39
3	36.0	4	1.44
Average	33.8 ± 2.7	6 ± 2	1.36 ± 0.08

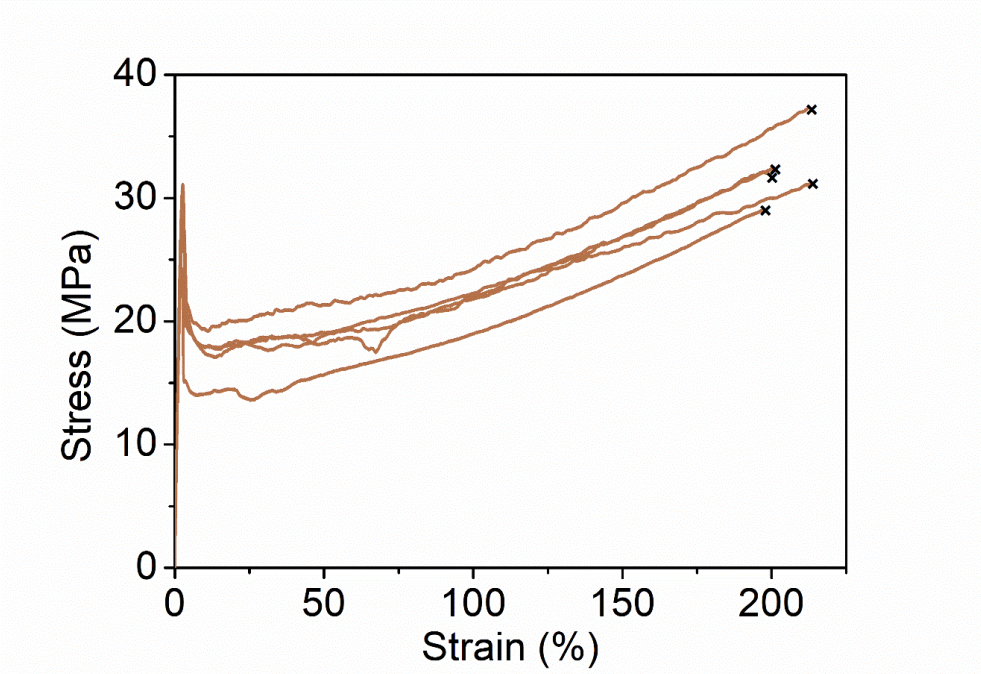

Figure S3.33. Plots of stress-strain experiments for atactic poly(D-CamL) produced by a [D-CamL]:[^{t}Bu-P$_4$]:[urea 1]:[BnOH] ratio of 1000:3:3:1. M_w = 48.1 kDa, elongation rate = 5 mm/min, ambient condition.

Table S3.4. Stress-strain data of atactic poly(D-CamL) (M_w = 48.1 kDa).

Sample number	Yield stress (MPa)	ε_B (%)	E (GPa)
1	28.5	201	1.61
2	28.0	262	1.51
3	31.1	229	1.76
4	24.3	198	1.66
5	28.3	202	1.67
Average	28.0 ± 2.2	218 ± 24	1.64 ± 0.08

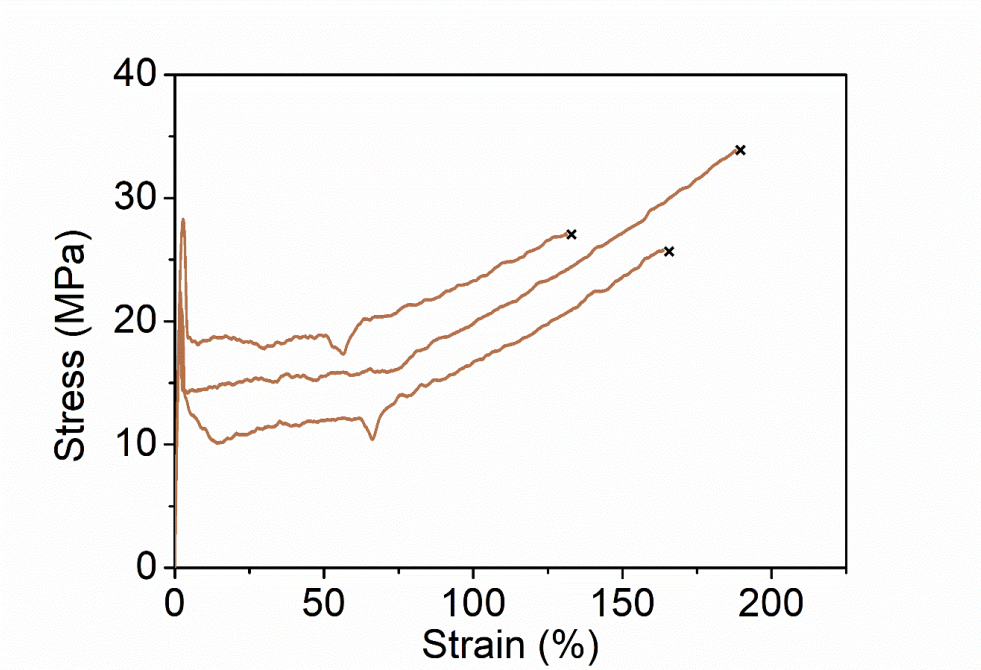

Figure S3.34. Plots of stress-strain experiments for atactic poly(D-C_{am}L) produced by a [D-CamL]:[^{t}Bu-P_4]:[urea 6]:[BnOH] ratio of 1000:3:3:1. M_w = 79.4 kDa, elongation rate = 5 mm/min, ambient condition.

Table S3.5. Stress-strain data of atactic poly(D-CamL) (M_w = 79.4 kDa).

Sample number	Yield stress (MPa)	ε_B (%)	E (GPa)
1	21.0	166	1.59
2	22.4	189	1.71
3	28.3	135	1.64
Average	23.9 ± 3.2	163 ± 22	1.65 ± 0.05

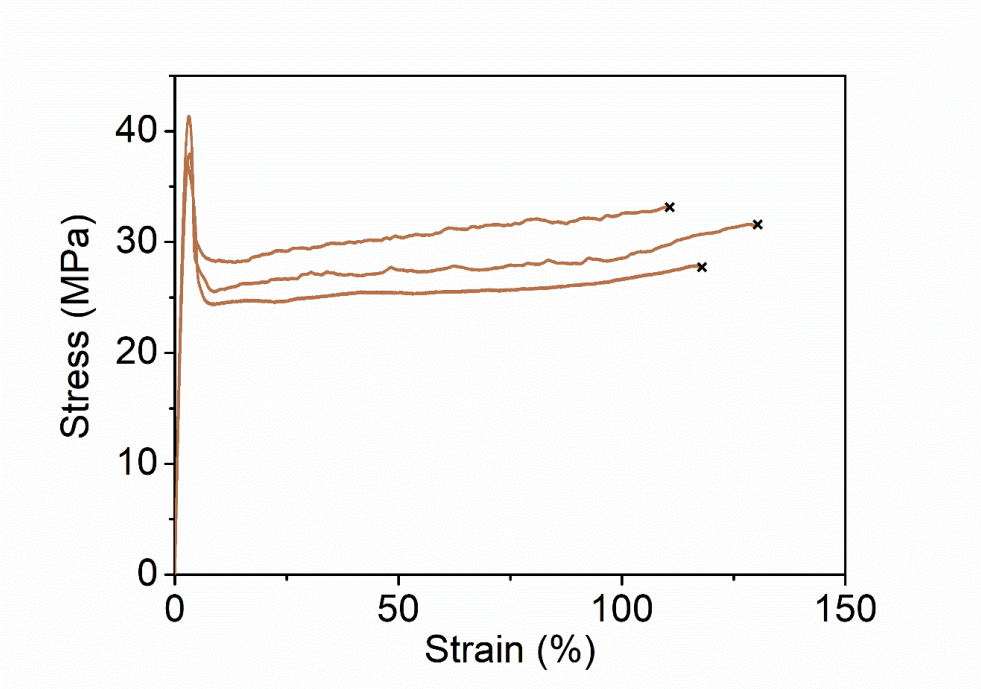

Figure S3.35. Plots of stress-strain experiments of atactic poly(*rac*-CamL) produced by a [*rac*-CamL]:[^{t}Bu-P$_4$]:[urea 1]:[BnOH] ratio of 1000:3:3:1. M_w = 78.2 kDa, elongation rate = 5 mm/min, ambient condition.

Table S3.6. Stress-strain data of atactic poly(*rac*-CamL) (M_w = 78.2 kDa).

Sample number	Yield stress (MPa)	ε_B (%)	E (GPa)
1	38.0	132	1.89
2	41.4	111	2.10
3	37.1	119	2.10
Average	38.8 ± 1.8	121 ± 9	2.00 ± 0.10

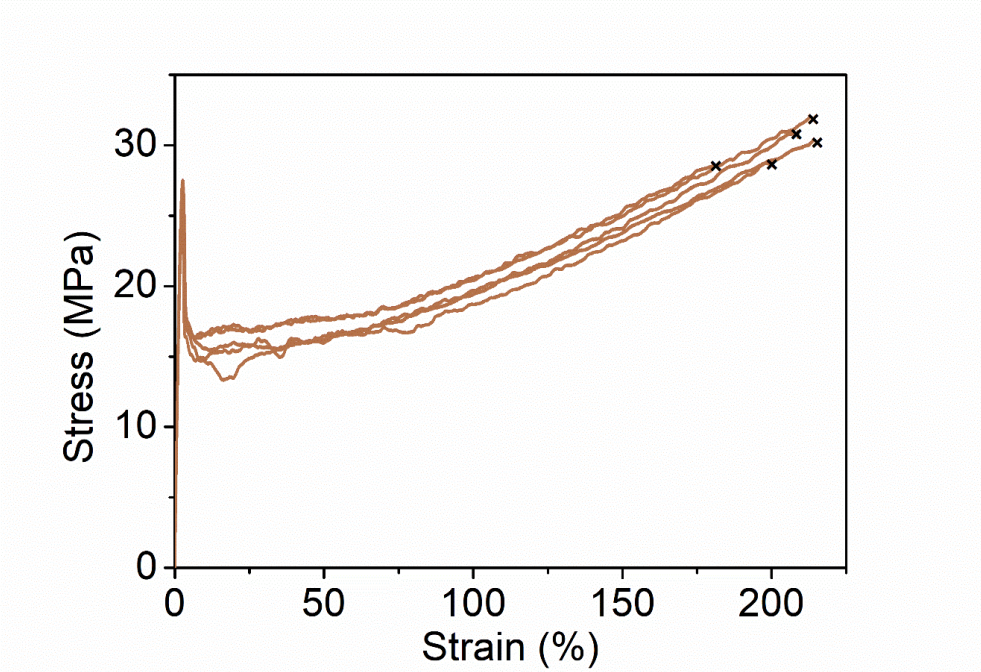

Figure S3.36. Plots of stress-strain experiments for repolymerized atactic poly(D-CamL) produced by a [D-CamL]:[^{t}Bu-P$_4$]:[urea 1]:[BnOH] ratio of 1000:3:3:1. M_w = 48.4 kDa, elongation rate = 5 mm/min, ambient condition.

Table S3.7. Stress-strain data of recycled atactic poly(D-CamL) (M_w = 48.4 kDa).

Sample number	Yield stress (MPa)	ε_B (%)	E (GPa)
1	26.5	180	1.64
2	25.0	200	1.59
3	27.5	213	1.62
4	24.9	214	1.46
5	26.4	208	1.65
Average	26.1 ± 1.0	203 ± 12	1.59 ± 0.07

REFERENCES

1. Munkuev, A.A., Dyrkheeva, N.S., Kornienko, T.E., Ilina, E.S., Ivankin, D.I., Suslov, E.V., Korchagina, D.V., Gatilov, Y.V., Zakharenko, A.L., Malakhova, A.A., et al. (2022). Adamantane-Monoterpenoid Conjugates Linked via Heterocyclic Linkers Enhance the Cytotoxic Effect of Topotecan. Molecules *27*.
2. McLean, E.B., Mooney, D.T., Burns, D.J., and Lee, A.-L. (2022). Direct Hydrodecarboxylation of Aliphatic Carboxylic Acids: Metal- and Light-Free. Organic Letters *24*, 686-691.
3. Lin, B., and Waymouth, R.M. (2017). Urea Anions: Simple, Fast, and Selective Catalysts for Ring-Opening Polymerizations. J Am Chem Soc *139*, 1645-1652.
4. Lin, L., Han, D., Qin, J., Wang, S., Xiao, M., Sun, L., and Meng, Y. (2018). Nonstrained γ-Butyrolactone to High-Molecular-Weight Poly(γ-butyrolactone): Facile Bulk Polymerization Using Economical Ureas/Alkoxides. Macromolecules *51*, 9317-9322.
5. Bordwell pK_a Table (https://organicchemistrydata.org/hansreich/resources/pka/).

APPENDIX C – SUPPLEMENTARY INFORMATION FOR CHAPTER 4

Materials and Methods:

Purchased Chemicals:

For the Synthesis of 2,7-bis(4-methoxyphenyl)-9,9-dimethyl-10-(4-cyanonaphthalen-1-yl)-9,10-dihydroacridine (PC1):

Buchwald Coupling: 9,9-Dimethyl-9,10-dihydroacridine was purchased from Ark Pharm. 1-Bromo-4-cyanonaphthalene was purchased from VWR. Bis(dibenzylideneacetone) palladium(0) and 1M tri-tert-butylphosphine in toluene were purchased from Sigma Aldrich. Sodium tert-butoxide was purchased from Sigma Aldrich. Anhydrous 99.8% toluene was purchased from Sigma Aldrich and kept under nitrogen atmosphere. **Bromination:** N-bromosuccinimide was purchased from VWR. HPLC grade THF was purchased from VWR. **Suzuki Coupling:** Tetrakis(triphenylphosphine) palladium(0) was purchased from Sigma Aldrich. Potassium carbonate was purchased from VWR. 4-Methoxyphenylboronic acid was purchased from Sigma Aldrich.

For the Synthesis of MVL:

δ-Valerolactone and anhydrous 99.5% ethanol were purchased from Thermo Scientific. Potassium carbonate was purchased from Sigma Aldrich. ACS grade 37% aqueous formaldehyde solution was purchased from RICCA Chemical. Diethyl oxalate was purchased from Alfa Aesar. Sodium hydride 60% dispersion in mineral oil was purchased from Oakwood Chemical. HPLC grade THF was purchased from VWR.

For the Synthesis of PMVL and PMBL by O-ATRP:

MBL was purchased from TCI chemicals. Extra dry 99.5% N,N-dimethylacetamide, dimethyl sulfoxide, and dimethylformamide over molecular sieves were purchased from Thermo Scientific. Diethyl 2-bromo-2-methylmalonate was purchased from MilliporeSigma.

For the Synthesis of PMVL and PMBL by RAFT:

MBL was purchased from TCI chemicals. Extra dry 99.5% N,N-dimethylacetamide over molecular sieves was purchased from Thermo Scientific. 2,2'-Azobis(isobutyronitrile) and 2-cyanopropan-2-yl benzodithioate were purchased from Sigma-Aldrich.

For the Synthesis of PMVL and PMBL by FRP:

MBL was purchased from TCI chemicals. Extra dry 99.5% N,N-dimethylacetamide over molecular sieves was purchased from Thermo Scientific. 2,2'-Azobis(isobutyronitrile) was purchased from Sigma-Aldrich.

Chemical Preparation and Storage:

Unless otherwise noted, chemicals and reagents were used as received from the manufacturer. For polymerizations, DBMM, MVL, and MBL were dried over calcium hydride, vacuum distilled, and degassed by three freeze-pump-thaw cycles, then stored in the freezer of a nitrogen-filled glove box at –38 °C until use.

Experimental Equipment:

Light beakers were composed of double-density white LED strips purchased from Creative Lighting Solutions (item no. CL-FRS1210-5M-12V-WH). The reactors were constructed by

covering a 400 mL beaker (height = 10.0 cm, diameter = 8.5 cm) with aluminum foil and wrapping the white LED strips (18 LED segments, 32” total) around the inside of the beaker.

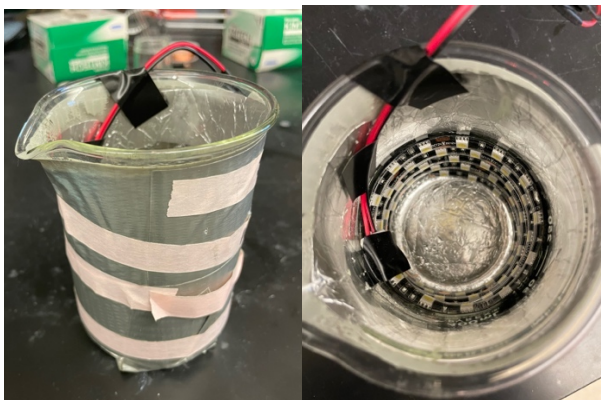

Figure S4.1: *photos of light beaker setup used in light-driven polymerizations*

Instrumentation:

Structural analysis was performed by a Bruker US 400 MHz NMR Spectrometer. Molecular weight analysis was performed using gel permeation chromatography (GPC) coupled with multi-angle light scattering (MALS) using an Agilent HPLC system fitted with one guard column and 3 PL-gel mixed C columns running DMF as eluent at 0.8 mL/minute. The detectors used for GPC were a Wyatt Technology Optilab differential refractometer (RI), a Wyatt Technology DAWN 8 light scattering detector (MALS), and an Agilent 1260 Infinity II Diode Array Detector WR for UV spectral detection. A dn/dc value of 0.0981 was used for all PMBL analyses, 0.0865 for PMVL analyses, and 0.1013 for PMVL-*co*-PMBL synthesized by simultaneous addition copolymerization. dn/dc values were determined through analysis with a known sample concentration assuming 100% mass recovery. PMVL-*co*-PMBL samples synthesized by sequential addition were analyzed by determining concentration and assuming 100% mass recovery.

Photocatalyst Synthesis

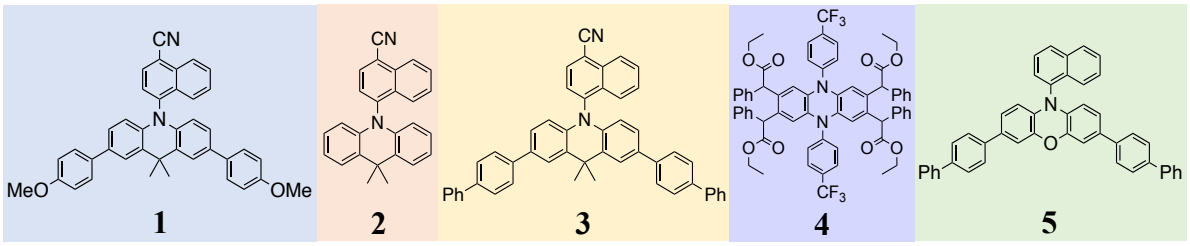

General Synthetic Scheme (PCs 1-3):

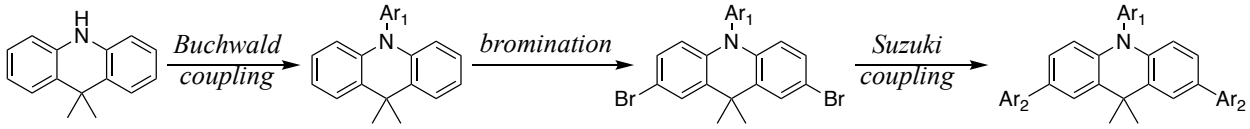

Synthesis of 2,7-bis(4-methoxyphenyl)-9,9-dimethyl-10-(4-cyanonaphthalen-1-yl)-9,10-dihydroacridine (PC 1):

Buchwald Coupling:

A storage tube was loaded with 0.5 g (2.39 mmol, 1 eq.) 9,10-Dihydro-9,9-dimethylacridine, 0.823 g 1-bromo-4-cyanonaphthalene (3.58 mmol, 1.5 eq.), 13.7 mg of bis(dibenzylideneacetone)palladium(0) (0.024 mmol, 1 mol%), 71.7 µL of 1M in toluene Tritert-butylphosphine (0.0717 mmol, 3 mol %), 0.69 g sodium tert-butoxide (7.17 mmol, 3.0 eq.), and 30 mL toluene under nitrogen atmosphere. The solution was heated to 115 ºC. After 24 hours, the red-brown solution was poured directly through a silica plug and rinsed with toluene. All blue fluorescent portions were collected and concentrated to via rotary evaporation to afford a yellow powder. The yellow powder was then recrystallized using DCM layered with methanol at -10 ºC overnight. The product, a yellow crystalline solid, was isolated by vacuum filtration and washed with methanol. The product was dried overnight under vacuum to yield 0.75 g (87.1% yield).

Bromination:

0.75 g of 9,10-dihydro-9,9-dimethyl-10-(4-cyanonapthalen-1-yl)-acridine (2.08 mmol, 1.0 eq.) was dissolved in 200 mL THF under ambient atmosphere. 0.926 g of N-bromosuccinimide

(5.20 mmol, 2.5 eq.) was slowly added to make a yellow solution. The reaction then stirred for 3 hours and 30 minutes. The solution was then concentrated via rotary evaporation. The afforded solid was re-dissolved in DCM, washed with water 3 times, and dried with magnesium sulfate. The organic layer was concentrated via rotary evaporation. The product was recrystallized using DCM layered with methanol at -10 ºC overnight. The product was isolated by filtration and dried under vacuum to give a yellow crystalline, which was used without further purification. Yield: 0.96 g (89.1%).

Suzuki Coupling:

0.40 g of 2,7-dibromo-9,10-dihydro-9,9-dimethyl-10-(4-cyanonapthalen-1-yl)-acridine (0.72 mmol, 1 eq.) was loaded into a storage tube. 0.47 g of 4-methoxyphenylboronic acid (3.09 mmol, 4 eq.) was added under ambient conditions. The flask was brought into a nitrogen-filled glovebox. Then, 89.2 mg tetrakis(triphenylphosphine)palladium(0) (0.077 mmol, 10 mol %) was added. Approximately 15 mL of THF was added to produce a yellow solution. The flask was taken out of the glovebox, where 8.5 mL of degassed 2M K_2CO_3 was added using a long needle and syringe. The biphasic solution was then sealed and heated to 110 ºC for 16 hours. At that time, the solution was cooled to room temperature and concentrated via rotary evaporation. The crude mixture was re-dissolved in toluene and then passed through a silica plug. The product was then recrystallized with DCM/MeOH at -10 ºC to yield an orange crystalline solid. ^{1}H NMR (400 MHz, chloroform-*d*) δ 8.45 – 8.43 (d, 1H), 8.19 – 8.17 (d, 1H), 7.89 – 7.86 (d, 1H), 7.80 – 7.76 (t, 1H), 7.73 (s, 2H), 7.66 – 7.64 (d, 1H), 7.58 – 7.54 (t, 1H), 7.49 – 7.46 (m, 4H), 7.08 – 7.05 (dd, 2H), 6.97 – 6.95 (d, 4H), 6.00 (s, 2H), 3.84 (s, 6H), 1.96 (s, 3H), 1.87 (s, 3H); 13C NMR (400 MHz, C_6D_6) δ 159.49, 142.84, 139.35, 134.82, 134.78, 134.27, 133.82, 132.19, 130.53, 129.52, 128.89, 128.82, 126.48, 125.75, 124.87, 124.75, 117.50, 115.02, 114.75, 111.56, 54.90, 36.67, 33.50, 32.15

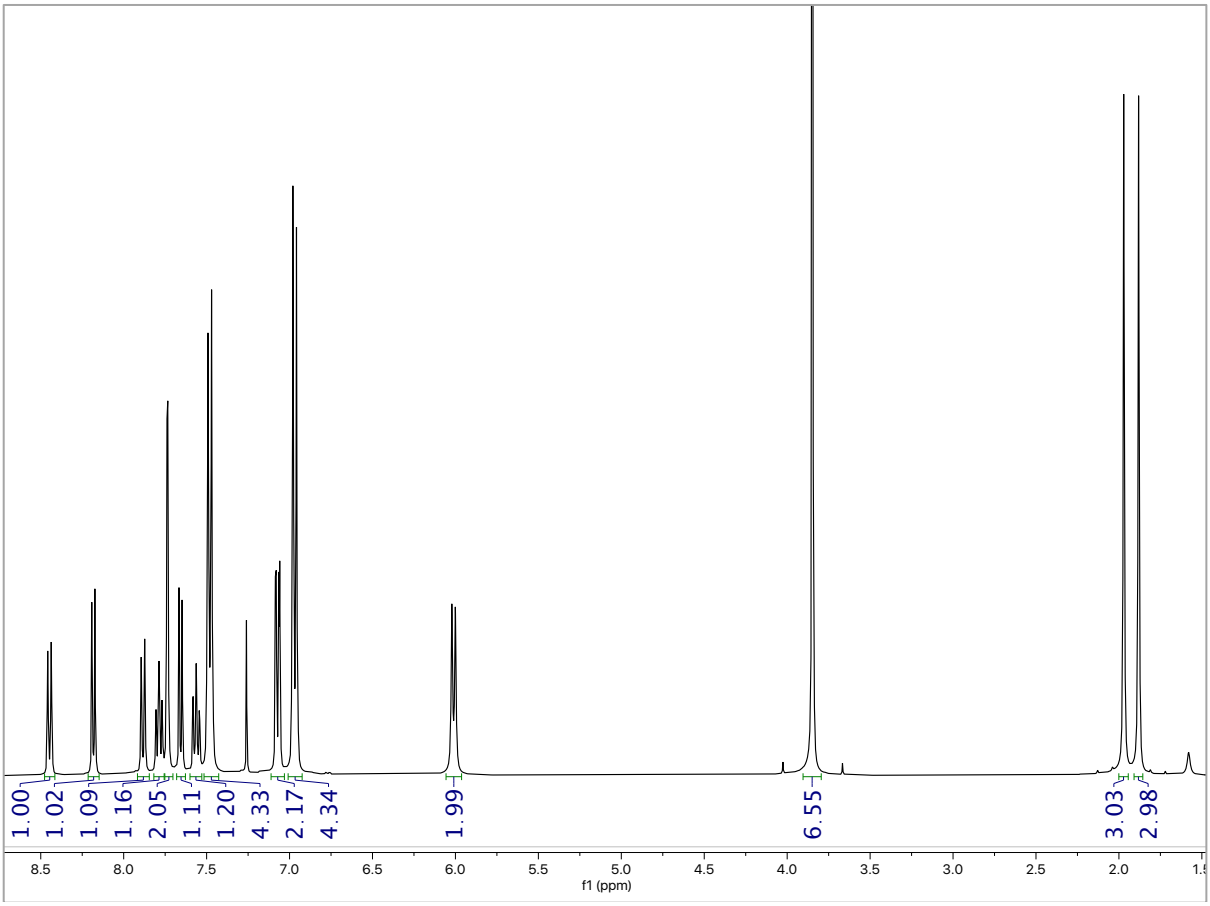

Figure S4.2: *^{1}H NMR of PC 1*

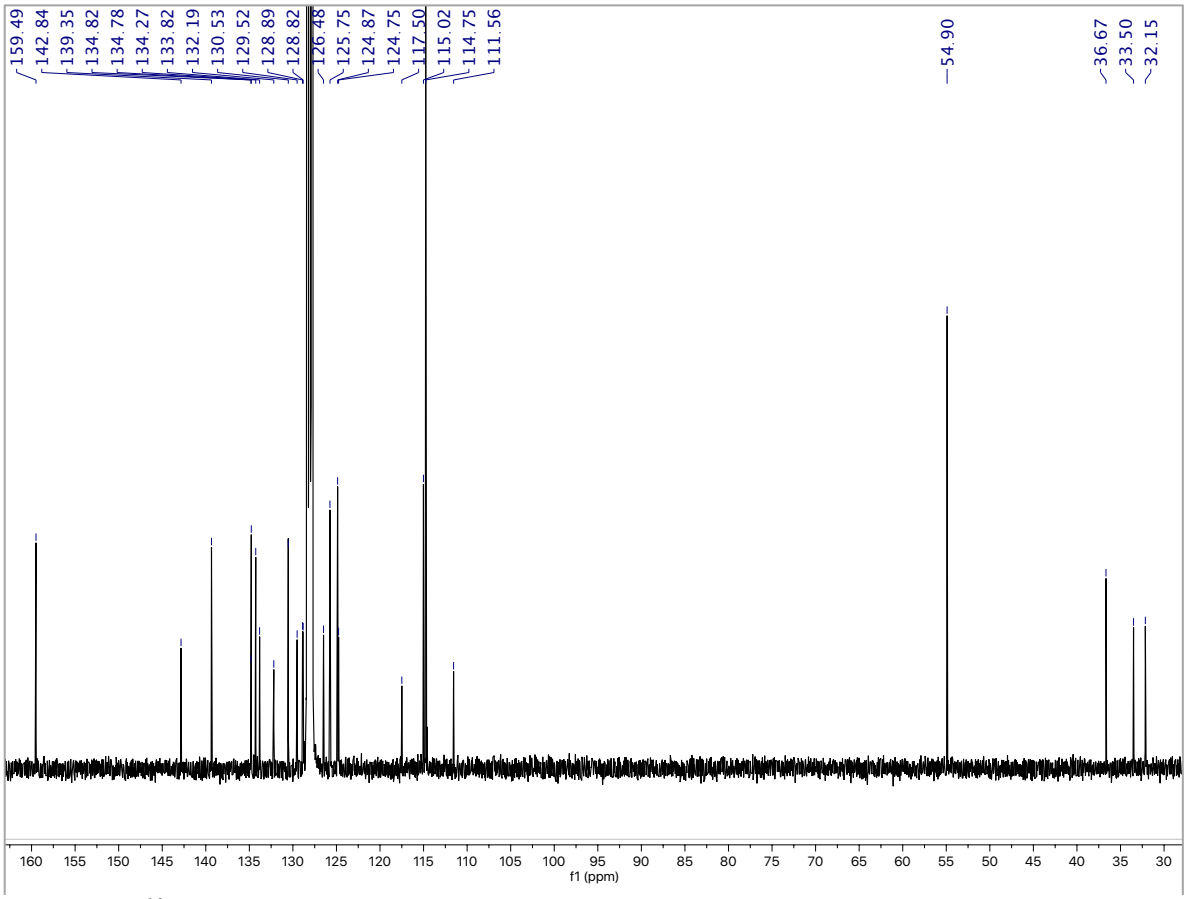

Figure S4.3: *^{13}C NMR of PC 1*

Synthesis of 9,9-dimethyl-10-(4-cyanonaphthalen-1-yl)-9,10- dihydroacridine (PC 2):

Buchwald Coupling:

A storage tube was loaded with 0.5 g (2.39 mmol, 1 eq.) 9,10-Dihydro-9,9-dimethylacridine, 0.823 g 1-bromo-4-cyanonaphthalene (3.58 mmol, 1.5 eq.), 13.7 mg of bis(dibenzylideneacetone)palladium(0) (0.024 mmol, 1 mol%), 71.7 µL of 1M in toluene Tritert-butylphosphine (0.0717 mmol, 3 mol %), 0.69 g sodium tert-butoxide (7.17 mmol, 3.0 eq.), and 30 mL toluene under nitrogen atmosphere. The solution was heated to 115 ºC. After 24 hours, the red-brown solution was poured directly through a silica plug and rinsed with toluene. All blue fluorescent portions were collected and concentrated to via rotary evaporation to afford a yellow powder. The yellow powder was then recrystallized using DCM layered with methanol at -10 ºC

overnight. The product, a yellow crystalline solid, was isolated by vacuum filtration and washed with methanol. The product was dried overnight under vacuum to yield 0.75 g (87.1% yield).

Bromination:

0.75 g of 9,10-dihydro-9,9-dimethyl-10-(4-cyanonapthalen-1-yl)-acridine (2.08 mmol, 1.0 eq.) was dissolved in 200 mL THF under ambient atmosphere. 0.926 g of N-bromosuccinimide (5.20 mmol, 2.5 eq.) was slowly added to make a yellow solution. The reaction then stirred for 3 hours and 30 minutes. The solution was then concentrated via rotary evaporation. The afforded solid was re-disolved in DCM, washed with water 3 times, and dried with magnesium sulfate. The organic layer was concentrated via rotary evaporation. The product was recrystallized using DCM layered with methanol at -10 ºC overnight. The product was isolated by filtration and dried under vacuum to give a yellow crystalline solid. Yield: 0.96 g (89.1%). ^{1}H NMR (400 MHz, chloroform-*d*) δ 8.42 – 8.40 (d, 1H), 8.16 – 8.14 (d, 1H), 7.81 – 7.73 (m, 2H), 7.61 – 7.59 (d, 1H), 7.53 – 7.50 (m, 3H), 6.96 – 6.84 (dt, 4H), 5.94 – 5.92 (d, 2H), 1.85 (s, 1H), 1.75 (s, 1H). 13C NMR (400 MHz, chloroform-*d*) δ 143.28, 140.04, 134.68, 133.92, 132.25, 130.01, 132.25, 130.01, 129.57, 128.96, 126.84, 126.33, 126.07, 124.82, 121.28, 117.54, 114.11, 111.11, 36.17, 33.10, 32.18.

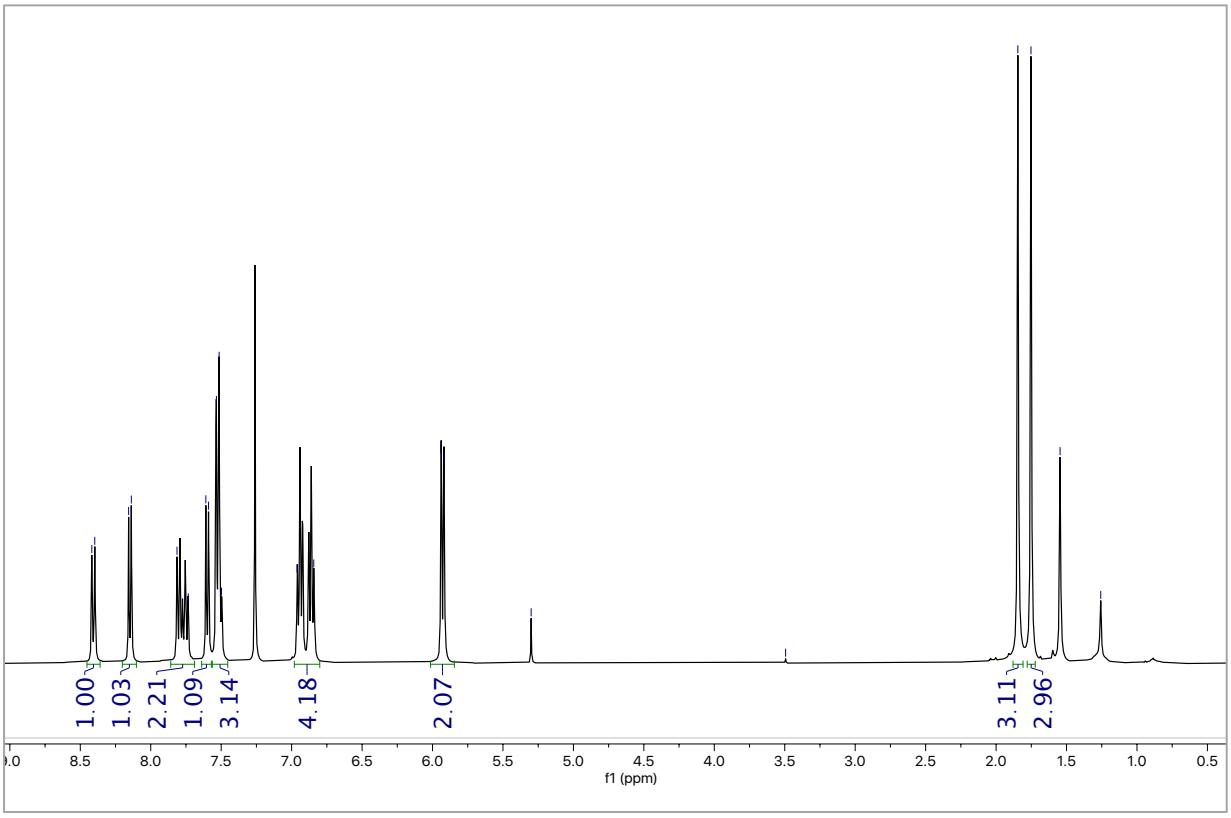

Figure S4.4: *^{1}H NMR of PC 2*

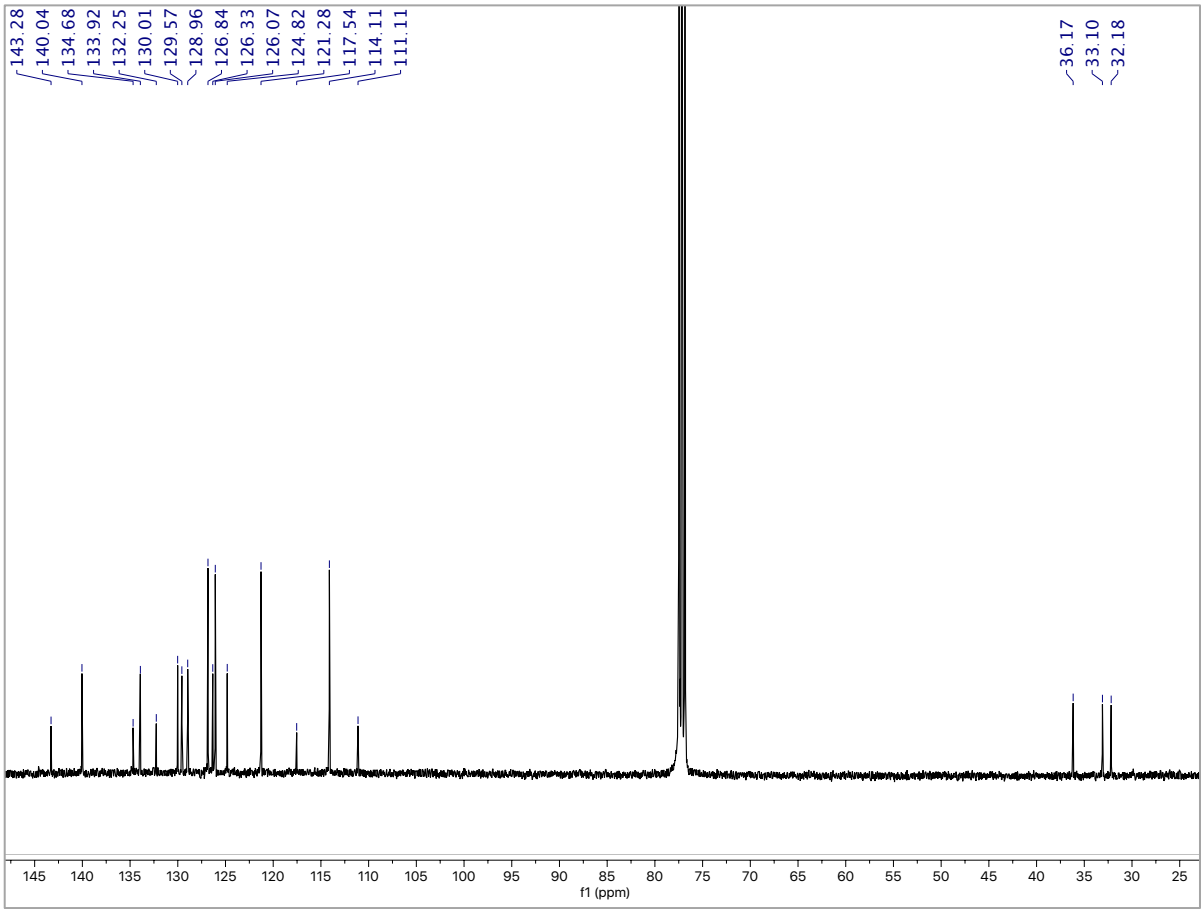

Figure S4.5: *^{13}C NMR of PC 2*

Synthesis of 2,7-bis(biphenyl)-9,9-dimethyl-10-(4-cyanonaphthalen-1-yl)-9,10-dihydroacridine (PC 3):

Buchwald Coupling:

A storage tube was loaded with 0.5 g (2.39 mmol, 1 eq.) 9,10-Dihydro-9,9-dimethylacridine, 0.823 g 1-bromo-4-cyanonaphthalene (3.58 mmol, 1.5 eq.), 13.7 mg of bis(dibenzylideneacetone)palladium(0) (0.024 mmol, 1 mol%), 71.7 µL of 1M in toluene Tritert-butylphosphine (0.0717 mmol, 3 mol %), 0.69 g sodium tert-butoxide (7.17 mmol, 3.0 eq.), and 30 mL toluene under nitrogen atmosphere. The solution was heated to 115 ºC. After 24 hours, the red-brown solution was poured directly through a silica plug and rinsed with toluene. All blue fluorescent portions were collected and concentrated to via rotary evaporation to afford a yellow

powder. The yellow powder was then recrystallized using DCM layered with methanol at -10 ºC overnight. The product, a yellow crystalline solid, was isolated by vacuum filtration and washed with methanol. The product was dried overnight under vacuum to yield 0.75 g (87.1% yield).

Bromination:

0.75 g of 9,10-dihydro-9,9-dimethyl-10-(4-cyanonapthalen-1-yl)-acridine (2.08 mmol, 1.0 eq.) was dissolved in 200 mL THF under ambient atmosphere. 0.926 g of N-bromosuccinimide (5.20 mmol, 2.5 eq.) was slowly added to make a yellow solution. The reaction then stirred for 3 hours and 30 minutes. The solution was then concentrated via rotary evaporation. The afforded solid was re-dissolved in DCM, washed with water 3 times, and dried with magnesium sulfate. The organic layer was concentrated via rotary evaporation. The product was recrystallized using DCM layered with methanol at -10 ºC overnight. The product was isolated by filtration and dried under vacuum to give a yellow crystalline solid, which was used without further purification. Yield: 0.96 g (89.1%).

Suzuki Coupling:

0.40 g of 2,7-dibromo-9,10-dihydro-9,9-dimethyl-10-(4-cyanonapthalen-1-yl)-acridine (0.72 mmol, 1 eq.) was loaded into a storage tube. 0.61 g of 4-biphenylboronic acid (3.09 mmol, 4 eq.) was added under ambient conditions. The flask was brought into a nitrogen-filled glovebox. Then, 89.2 mg tetrakis(triphenylphosphine)palladium(0) (0.077 mmol, 10 mol %) was added. Approximately 15 mL of THF was added to produce a yellow solution. The flask was taken out of the glovebox, where 8.5 mL of degassed 2M K_2CO_3 was added using a long needle and syringe. The biphasic solution was then sealed and heated to 110 ºC for 16 hours. At that time, the solution was cooled to room temperature and concentrated via rotary evaporation. The crude mixture was re-dissolved in toluene and then passed through a silica plug. The product was then recrystallized

with DCM/MeOH at -10 ºC to yield a yellow powder. ^{1}H NMR (400 MHz, benzene-d_6) δ 8.34 – 8.32 (d, 1H), 7.93 – 7.93 (d, 1H), 7.82 – 7.80 (d, 1H), 7.64 – 7.56 (m, 13H), 7.19 – 7.10 (m, 3H), 6.99 – 6.93 (m, 2H), 6.05 – 6.03 (d, 2H), 1.89 (s, 3H), 1.80 (s, 3H). ^{13}C NMR (400 MHz, benzene-d_6) δ 142.60, 141.33, 140.51, 140.19, 139.78, 134.83, 134.59, 132.09, 130.06, 129.61, 129.19, 128.93, 128.81, 127.57, 127.41, 127.38, 126.55, 126.07, 125.16, 124.66, 117.45, 115.16, 111.71, 36.71, 33.59, 32.17.

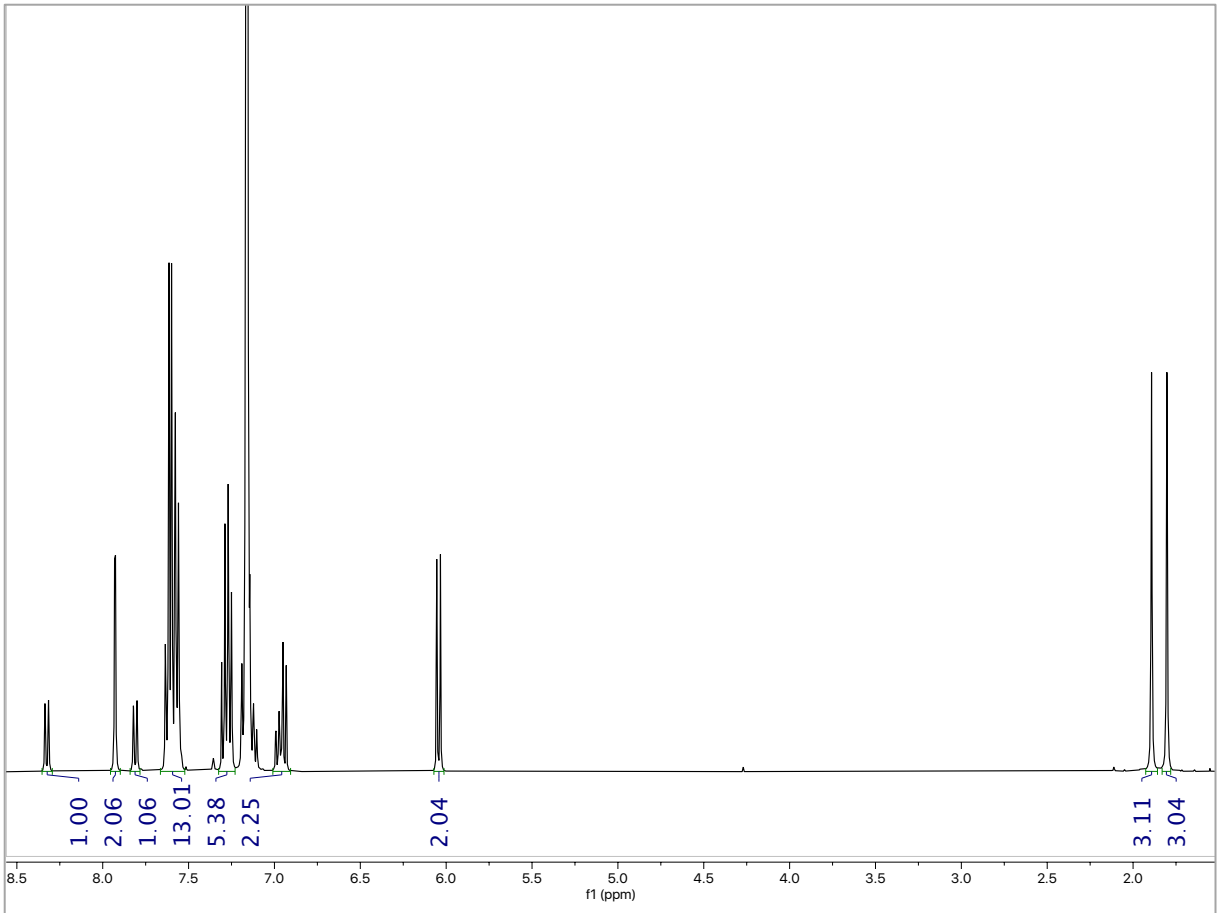

Figure S4.6: *^{1}H NMR of PC 3*

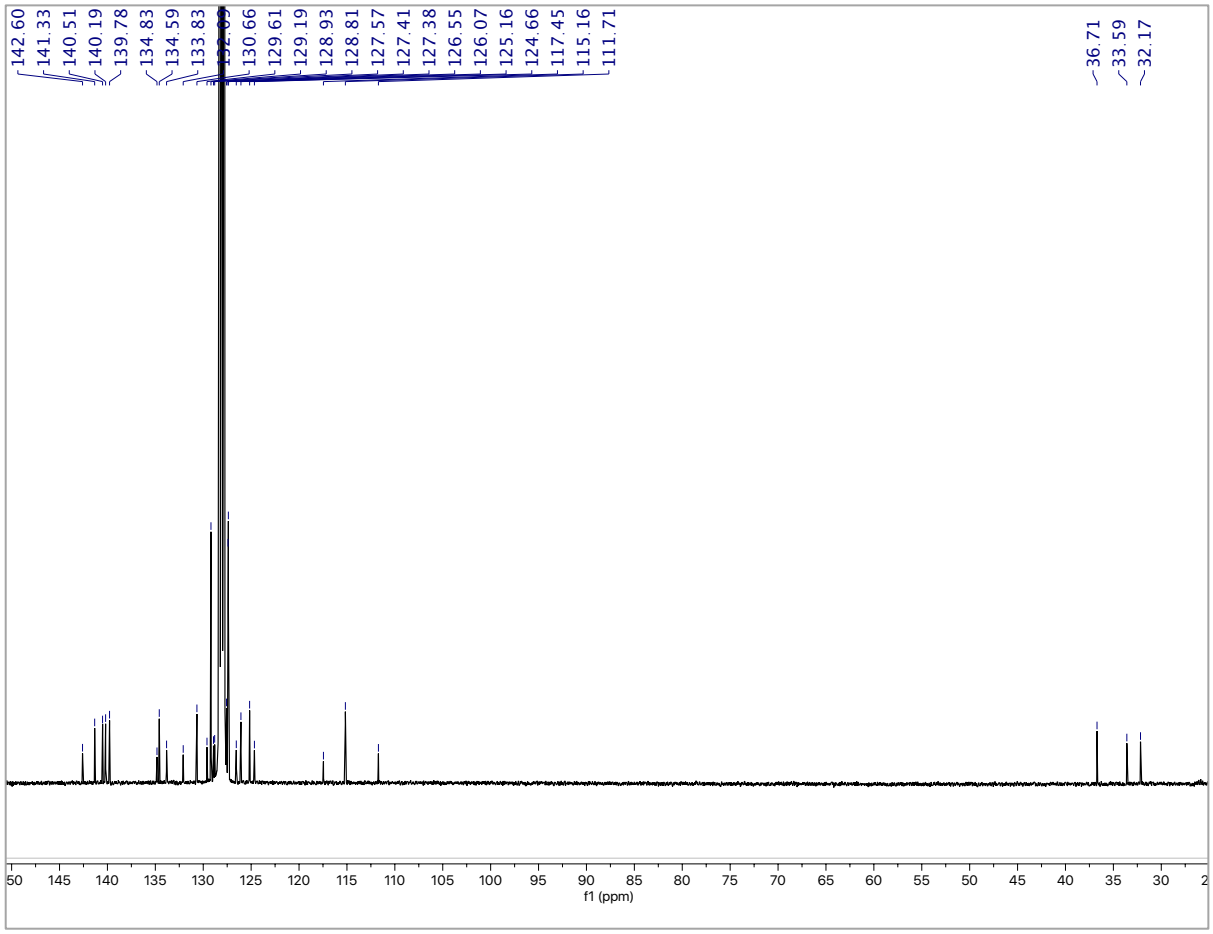

Figure S4.7: *^{13}C NMR of PC 3*

Synthesis of PCs 4 and 5:

PC 4 was synthesized according to literature procedure.[1] PC 5 was synthesized according to literature procedure.[2]

Monomer Synthesis

General Synthetic Scheme:

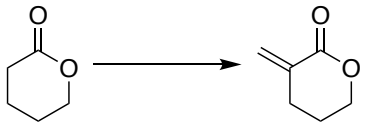

Synthesis of α-methylene-δ-valerolactone:

Sodium hydride (60% w/w dispersion in mineral oil; 340 mmol, 1.7 eq.) was added to a dry 1-liter Schlenk flask which was then sealed with a rubber septum. The reaction flask was evacuated and cycled with nitrogen three times and was then sealed under static vacuum. Air-free, anhydrous THF (approximately 250 mL) was added to the reaction flask via cannula needle, and the resulting mixture was stirred to create a suspension. The flask was then submerged in an ice/brine bath to reduce the temperature to between 0°C and -10°C. In a separate 500-mL Schlenk flask that had also been flame dried three times under vacuum, δ-valerolactone (18.5 mL, 200 mmol, 1.0 eq.), diethyl oxalate (27.4 mL, 202 mmol, 1.01 eq.), and THF (approximately 250 mL) were combined. The diethyl oxalate/ δ-valerolactone solution was added dropwise via cannula to the 1-liter Schlenk. After the addition was complete, anhydrous ethanol was added dropwise via syringe, and reaction was removed from ice bath and allowed to warm to room temperature. The reaction mixture was stirred under nitrogen at room temperature overnight (~16 hours). The reaction flask was then submerged into an ice/brine bath to lower the temperature to between 0°C and -10°C. Then, the reaction flask was opened to air and K_2CO_3 (aq.) (1.0 g/mL, 110 mL, 800 mmol, 4.0 eq.) and 37% aqueous formaldehyde (75.1 mL, 1.0 mol, 5.0 eq.) were added. The reaction mixture was allowed to stir for an additional hour at room temperature. Brine was added directly to the reaction flask to promote separation of layers, and the organic layer was decanted.

The remaining aqueous layer was extracted three times with diethyl ether. The combined organic layer was then washed with sodium thiosulfate until all color was removed, washed with brine, and dried over anhydrous sodium sulfate. The product was purified by silica plug followed by distillation. (Yield: 74%); 1H NMR (400 MHz, $CDCl_3$) δ (ppm): 1.87-1.93 (m, 2H), 2.59-2.63 (tt, 2H), 4.31-4.33 (t, 2H), 5.50-5.51 (q, 1H), 6.34-6.35 (m, 1H).

NMR Spectrum:

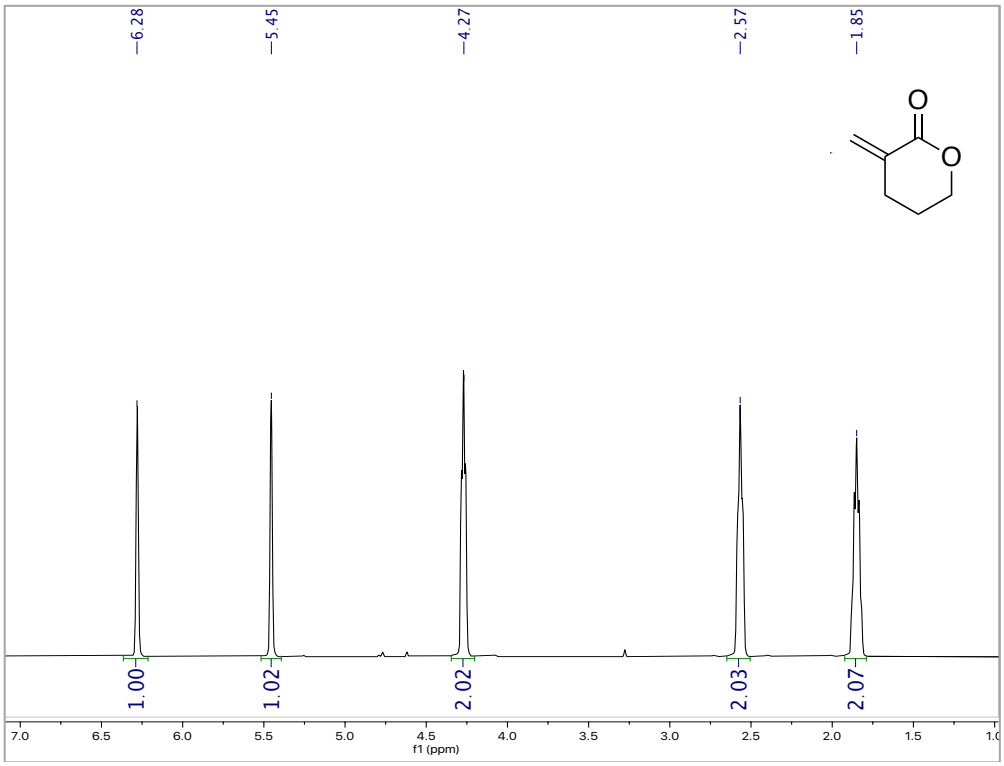

Figure S4.7: *1H NMR spectrum of α-methylene-δ-valerolactone in $CDCl_3$*

Polymerization

O-ATRP Synthetic Scheme:

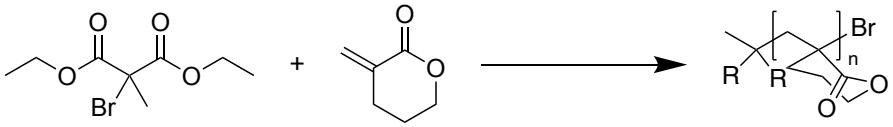

O-ATRP General Procedure:

A 20 mL scintillation vial was charged with photocatalyst (8.92 μmol, 1.0 eq) and equipped with a stir bar. The vial was brought into a nitrogen-filled glove box wherein DMAc (1:1 v/v of solvent:monomer) and MBL or MVL (8.92 mmol, 1000 eq) were added to the vial and allowed to stir for several minutes. Meanwhile, a beaker lined with foil and white-light LEDs (Figure S1, *Experimental Equipment*) was turned on. The vial was moved to the dark, and 17 μL of DBMM (89.2 μmol, 10.0 eq) was added using a micropipette. The reaction vial was then capped and introduced to the white-light LED beaker at which time the polymerization was considered to start (t = 0 for kinetic plots). A cooling fan was used to keep the reaction at room temperature.

Procedure for Analysis of Kinetics and Molecular Weight Growth:

The reaction setup proceeded according to *O-ATRP General Procedure*. To evaluate reaction kinetics and growth of polymer molecular weight as a function of monomer conversion for each reaction, an aliquot of ~0.10 mL of the reaction mixture was withdrawn and injected into a solution of deuterated chloroform containing butylated hydroxyl toluene as a radical inhibitor (BHT, 250 ppm) at predetermined times after the start of the polymerization (t = 0, as described in *O-ATRP General Procedure)*. The ^{1}H NMR spectrum of each aliquot was acquired and used to determine the percent conversion of monomer to polymer. After NMR analysis, each sample was

dried under reduced pressure, re-dissolved in HPLC-grade N,N-dimethylformamide, and analyzed by GPC.

Procedure for Simultaneous Addition Copolymerization by O-ATRP:

A 20 mL scintillation vial was charged with photocatalyst (8.92 μmol, 1.0 eq) and equipped with a stir bar. The vial was brought into a nitrogen-filled glove box wherein 0.88 mL of DMAc (1:1 v/v of solvent:monomer), 0.49 mL of MVL (4.46 mmol, 500 eq), and 0.39 mL of MBL (4.46 mmol, 500 eq) were added to the vial and allowed to stir for several minutes. Meanwhile, a beaker lined with foil and white-light LEDs (Figure S1, *Experimental Equipment*) was turned on. The vial was moved to the dark, and 17 μL of DBMM (89.2 μmol, 10.0 eq) was added using a micropipette. The reaction vial was then capped and introduced to the white-light LED beaker at which time the polymerization was considered to start (t = 0 for kinetic plots). A cooling fan was used to keep the reaction at room temperature.

Procedure for Sequential Addition Copolymerization by O-ATRP:

A 20 mL scintillation vial was charged with photocatalyst (8.92 μmol, 1.0 eq) and equipped with a stir bar. The vial was brought into a nitrogen-filled glove box wherein 0.88 mL of DMAc (1:1 v/v of solvent:monomer), and 0.49 mL of MVL (4.46 mmol, 500 eq) or 0.39 mL of MBL (4.46 mmol, 500 eq) were added to the vial and allowed to stir for several minutes. Meanwhile, a beaker lined with foil and white-light LEDs (Figure S1, *Experimental Equipment*) was turned on. The vial was moved to the dark, and 17 μL of DBMM (89.2 μmol, 10.0 eq) was added using a micropipette. The reaction vial was then capped and introduced to the white-light LED beaker at which time the polymerization was considered to start. A cooling fan was used to keep the reaction at room temperature. The monomer added first was allowed to polymerize for 24 hours, at which

point the second monomer was added. The copolymerization was allowed to proceed for an additional 24 hours and an aliquot (~0.10 mL) was taken at the end of the second 24 hour period.

RAFT Synthetic Scheme:

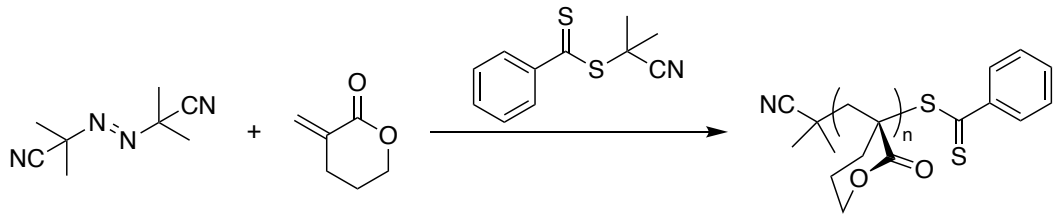

RAFT General Procedure:

A 10 mL Schlenk flask was charged with AIBN (44.6 μmol, 0.5 eq) and 2-cyanopropan-2-yl benzodithioate (89.2 μmol, 1.0 eq) and equipped with a stir bar. The flask was brought into a nitrogen-filled glove box wherein 0.98 mL of DMAc (1:1 v/v of solvent:monomer) and 0.98 mL of MVL (1.00 g, 8.92 mmol, 100 eq) were added to the flask. The flask was sealed with a septum and electrical tape and allowed to stir inside the glove box for several minutes. The reaction flask was then removed from the glove box and heated to 70 °C using an oil bath at which time the polymerization was considered to start (t = 0).

FRP Synthetic Scheme:

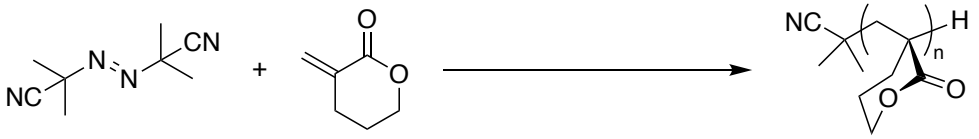

FRP General Procedure:

A 10 mL Schlenk flask was charged with AIBN (44.6 μmol, 0.5 eq) and equipped with a stir bar. The flask was brought into a nitrogen-filled glove box wherein 0.98 mL of DMAc (1:1 v/v of solvent:monomer) and 0.98 mL of MVL (1.00 g, 8.92 mmol, 100 eq) were added to the flask. The flask was sealed with a septum and electrical tape and allowed to stir inside the glove

box for several minutes. The reaction flask was then removed from the glove box and heated to 70 °C using an oil bath at which time the polymerization was considered to start (t = 0).

Supplemental Polymerization Data

O-ATRP of MVL

Table S4.1: *Results of O-ATRP of MVL with Varied PCs*[a]

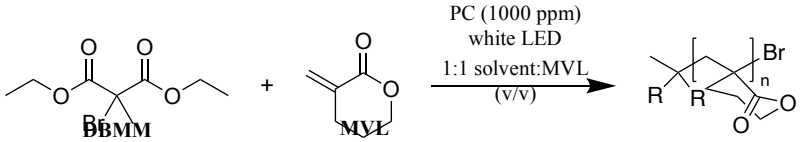

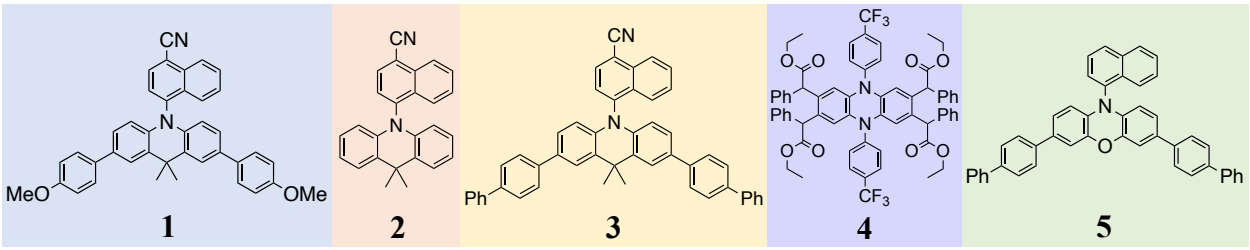

1 **2** **3** **4** **5**

Reaction #	PC	Time (hrs)	Conversion[b] (%)	M_w[c] (kDa)	M_n[c] (kDa)	$Đ$ (M_w/M_n)	I^* (%)[d]
SNB-4-74-A	1	1	13	8.19	6.20	1.32	25
		2	21	9.37	7.71	1.22	34
		4	37	9.98	7.44	1.34	58
		6	45	13.9	9.43	1.45	55
		8	52	17.5	9.94	1.76	61
		12	63	25.4	11.3	2.24	64
SNB-4-74-B	2	1	18	5.95	4.28	1.39	50
		2	26	8.26	6.21	1.33	49
		4	34	11.6	6.45	1.79	62
		6	41	13.9	7.36	1.89	65
		8	48	15.6	8.27	1.89	67
		12	61	16.8	7.83	2.14	90
SNB-4-74-C	3	1	17	5.19	3.90	1.33	54
		2	27	8.23	6.10	1.35	52
		4	35	14.3	6.65	2.16	62
		6	29	18.1	7.75	2.33	44
		8	48	20.1	7.22	2.79	77
		12	59	24.2	11.1	2.19	61
SNB-4-74-D	4	1	5	32.0	19.0	1.68	4
		2	8	30.3	20.4	1.49	5
		4	21	27.0	18.6	1.45	14
		6	29	24.5	14.8	1.66	23
		8	43	23.6	14.0	1.68	30
		12	68	21.3	13.9	1.53	36
SNB-4-74-E	5	2	12	9.21	8.14	1.13	18
		6	33	8.43	7.52	1.12	52
		8	43	10.8	6.77	1.59	74
		12	68	19.5	10.4	1.87	75

[a] Reaction scheme for the O-ATRP of MVL (top) catalyzed by PC 1, 2, 3, 4, or 5 (middle). O-ATRP was performed with a [1000]:[10]:[1] ratio of MVL:diethyl 2-bromo-2-methylmalonate (DBMM):PC using a 1:1 ratio of N,N-diemthylacetamide:MVL (v/v). A white-light LED beaker was used as the light source (see *O-ATRP General Procedure* for more details). [b]Conversion of monomer to polymer was determined by 1H NMR. [c] Values were measured using gel-permeation chromatography (GPC). [d] Initiator efficiency (I^*) was calculated using the equation $I^* = M_{n,theo}/M_n \times 100$ where $M_{n,theo}$ is the theoretical polymer molecular weight and M_n is the number-average polymer molecular weight measured using GPC.

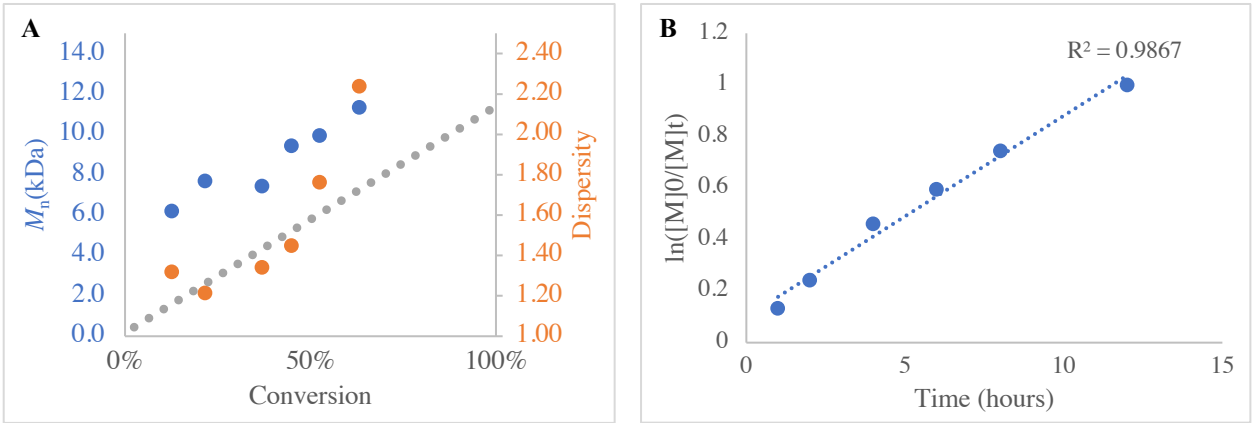

Figure S4.8: *Plots of polymerization data from run # SNB-4-74-A; A: plot of M_n (blue) and dispersity (orange) as a function of conversion, plotted against theoretical molecular weight (grey); B: first order kinetic plot*

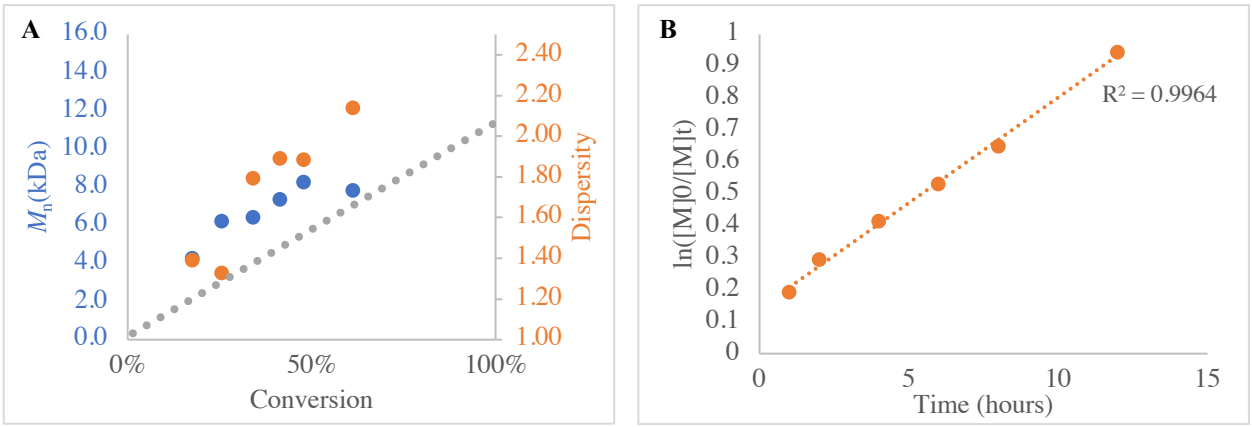

Figure S4.9: *Plots of polymerization data from run # SNB-4-74-B; A: plot of M_n (blue) and dispersity (orange) as a function of conversion, plotted against theoretical molecular weight (grey); B: first order kinetic plot*

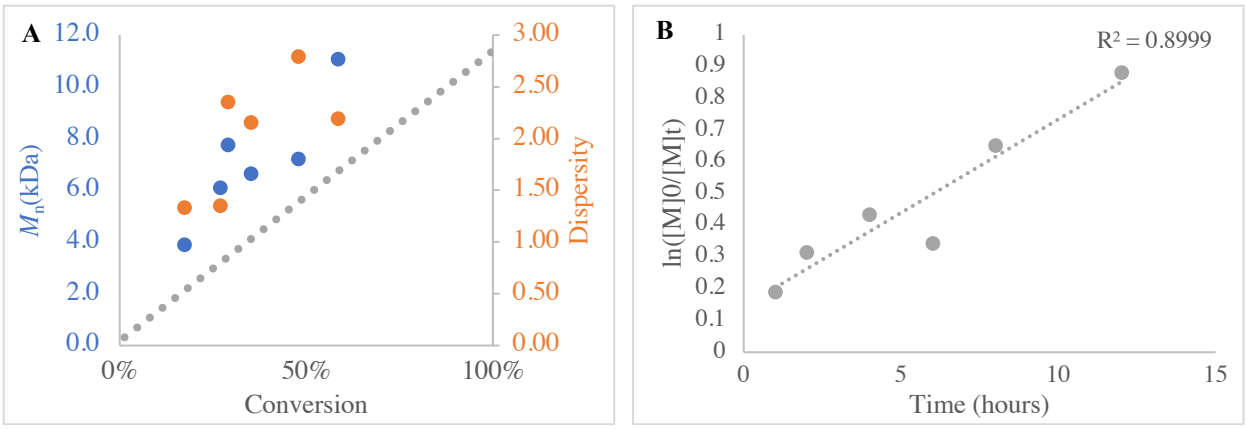

Figure S4.10: *Plots of polymerization data from run # SNB-4-74-C; A: plot of M_n (blue) and dispersity (orange) as a function of conversion, plotted against theoretical molecular weight (grey); B: first order kinetic plot*

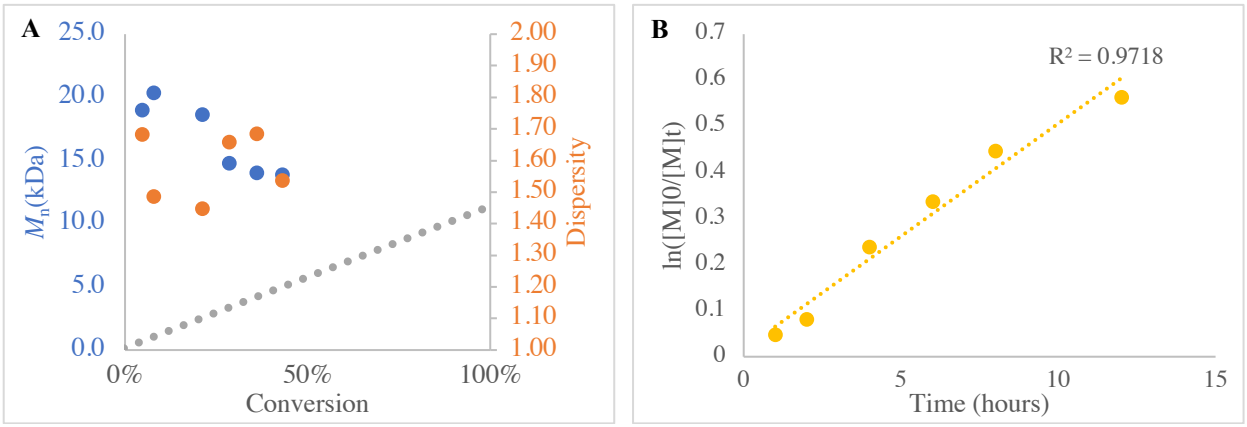

Figure S11: Plots of polymerization data from run # SNB-4-74-D; A: plot of M_n (blue) and dispersity (orange) as a function of conversion, plotted against theoretical molecular weight (grey); B: first order kinetic plot

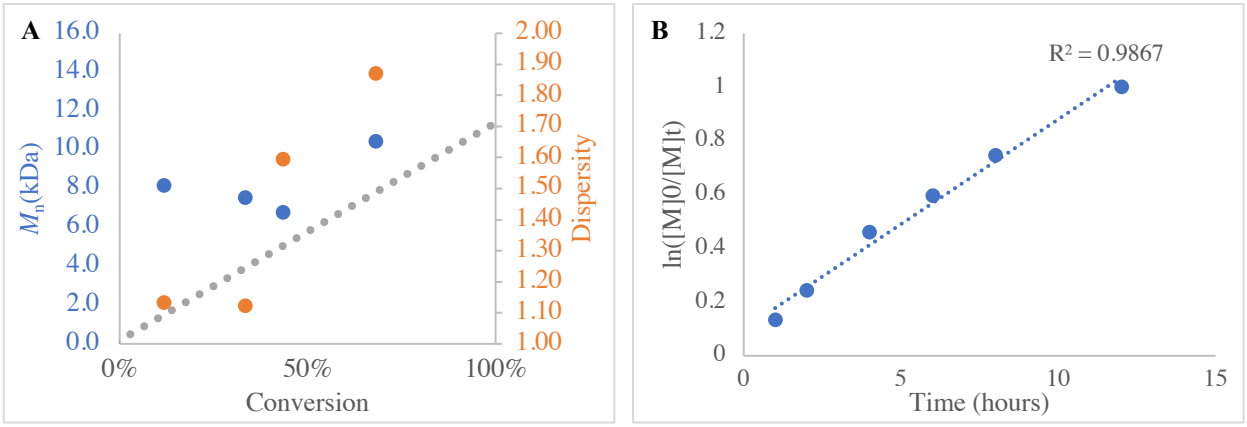

Figure S4.12: *Plots of polymerization data from run # SNB-4-74-E; A: plot of M_n (blue) and dispersity (orange) as a function of conversion, plotted against theoretical molecular weight (grey); B: first order kinetic plot*

Table S4.2: *Results of O-ATRP of MVL with Varied Solvents*[a]

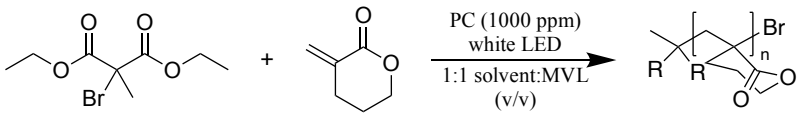

DBMM **MVL**

Reaction #	PC	Solvent	Time (hrs)	Conversion[b] (%)	M_w[c] (kDa)	M_n[c] (kDa)	$Đ$ (M_w/M_n)	I^* (%)[d]
SNB-4-76-A	1	DMSO	1	12	6.01	5.40	1.11	28
			1.67	18	6.26	5.73	1.09	37
			3	28	7.54	6.05	1.24	54
			5	39	10.1	7.20	1.40	64
			7	46	14.1	9.18	1.53	58
			9	53	16.0	10.0	1.59	61
			12	58	18.0	11.5	1.57	58
SNB-4-76-B	1	DMF	1	20	12.2	9.90	1.23	25
			1.67	30	12.6	10.2	1.24	35
			3	45	14.1	10.5	1.34	50
			5	54	17.8	12.8	1.38	49
			7	61	20.1	14.1	1.43	49
			9	70	22.0	14.0	1.57	57
			12	80	21.6	12.0	1.80	76
SNB-4-76-C	1	d-valerolactone	1	62	11.3	8.56	1.31	83
			1.67	67	13.1	9.85	1.35	78
			3	75	15.1	9.87	1.53	87
			5	86	24.6	12.2	2.02	81
			7	90	35.4	16.0	2.21	64
			9	93	38.7	15.5	2.50	68

[a] Reaction scheme for the O-ATRP of MVL (top) catalyzed by PC 1 (Table S1). O-ATRP was performed with a [1000]:[10]:[1] ratio of MVL:diethyl 2-bromo-2-methylmalonate (DBMM):PC using a 1:1 ratio of solvent:MVL (v/v). A white-light LED beaker was used as the light source (see *O-ATRP General Procedure* for more details). [b] Conversion of monomer to polymer was determined by 1H NMR. [c] Values were measured using gel-permeation chromatography (GPC). [d] Initiator efficiency (I^*) was calculated using the equation $I^* = M_{n,theo}/M_n \times 100$ where $M_{n,theo}$ is the theoretical polymer molecular weight and M_n is the number-average polymer molecular weight measured using GPC.

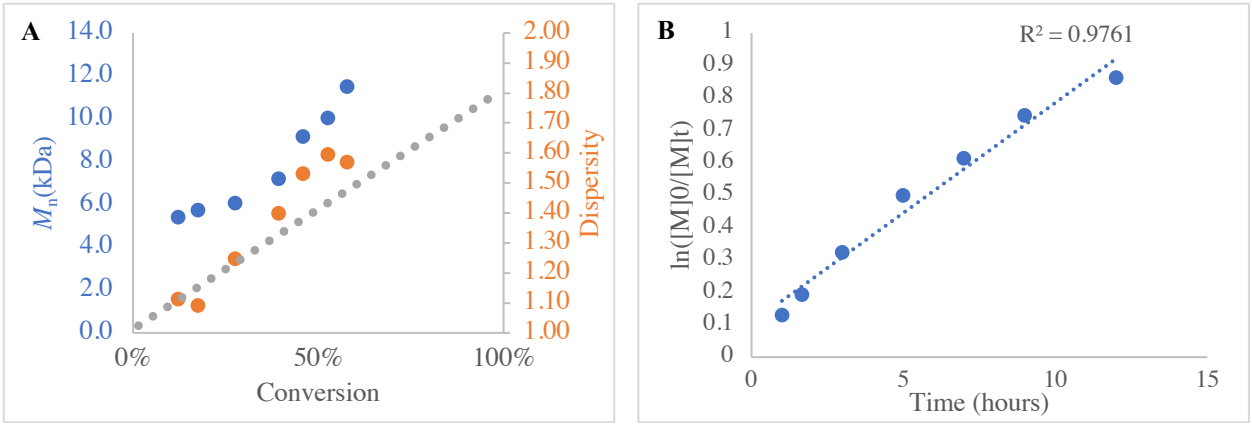

Figure S4.13: *Plots of polymerization data from run # SNB-4-76-A; A: plot of M_n (blue) and dispersity (orange) as a function of conversion, plotted against theoretical molecular weight (grey); B: first order kinetic plot*

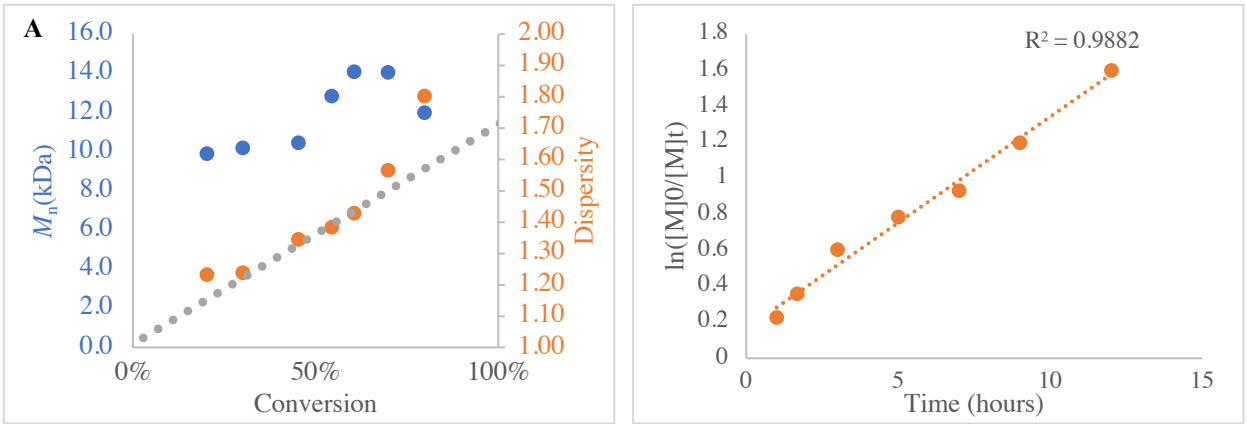

Figure S4.14: *Plots of polymerization data from run # SNB-4-76-B; A: plot of M_n (blue) and dispersity (orange) as a function of conversion, plotted against theoretical molecular weight (grey); B: first order kinetic plot*

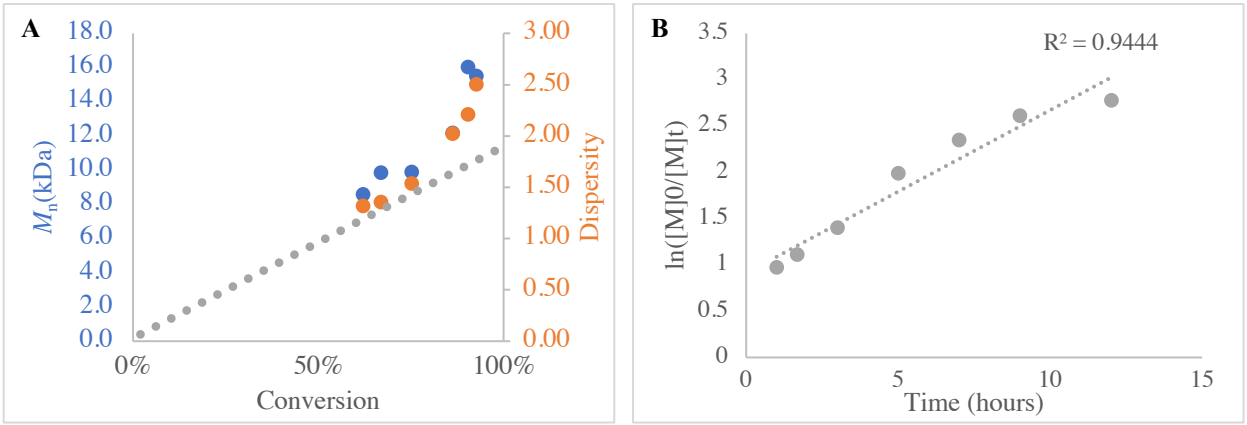

Figure S4.15: *Plots of polymerization data from run # SNB-4-76-C; A: plot of M_n (blue) and dispersity (orange) as a function of conversion, plotted against theoretical molecular weight (grey); B: first order kinetic plot*

Table S4.3: *Results of O-ATRP of MVL with Varied Initiators*[a]

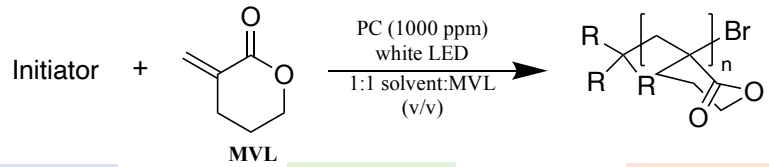

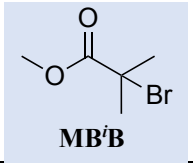

MB^{i}B

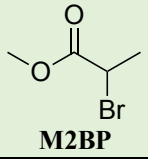

M2BP

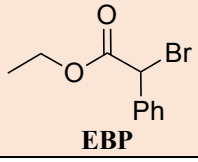

EBP

Reaction #	PC	Initiator	Time (hrs)	Conversion[b] (%)	M_w[c] (kDa)	M_n[c] (kDa)	$Đ$ (M_w/M_n)	I* (%)[d]
SNB-4-78-A	1	MBiB	1	4	60.3	39.2	1.54	2
			2	7	58.2	37.9	1.53	3
			4.33	18	56.9	38.1	1.49	6
			6	35	54.4	35.6	1.53	11
			8	49	52.1	36.8	1.41	15
			12	70	48.3	31.2	1.55	26
SNB-4-78-B	1	M2BP	1	3	78.5	49.7	1.58	1
			2	6	75.6	49.8	1.52	2
			4.33	20	69.3	45.0	1.54	5
			6	26	71.0	45.2	1.57	7
			12	59	68.6	46.4	1.48	15
SNB-4-78-C	1	EBP	1	18	11.1	9.5	1.17	23
			2	28	11.9	10.6	1.12	31
			4.33	42	14.0	11.5	1.21	42
			6	47	15.1	11.3	1.33	48
			8	53	16.5	12.7	1.30	48
			12	58	17.9	13.2	1.36	50

[a] Reaction scheme for the O-ATRP of MVL (top) catalyzed by PC 1 (Table S1) with varied initiators (middle). O-ATRP was performed with a [1000]:[10]:[1] ratio of MVL:initiator:PC using a 1:1 ratio of dimethyl sulfoxide:MVL (v/v). A white-light LED beaker was used as the light source (see *O-ATRP General Procedure* for more details). [b]Conversion of monomer to polymer was determined by 1H NMR. [c] Values were measured using gel-permeation chromatography (GPC). [d] Initiator efficiency (I*) was calculated using the equation $I^* = M_{n,theo}/M_n \times 100$ where $M_{n,theo}$ is the theoretical polymer molecular weight and M_n is the number-average polymer molecular weight measured using GPC.

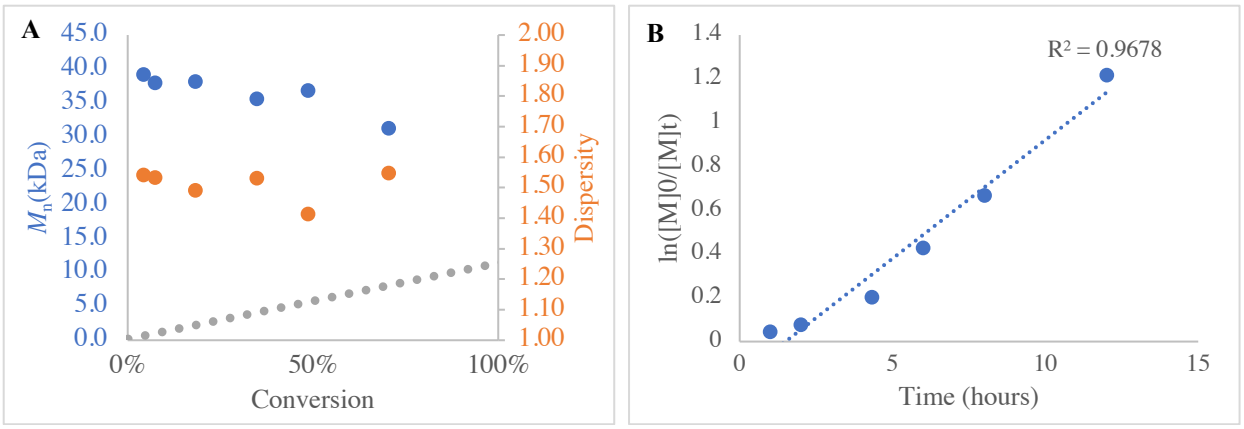

Figure S4.16: *Plots of polymerization data from run # SNB-4-78-A; A: plot of M_n (blue) and dispersity (orange) as a function of conversion, plotted against theoretical molecular weight (grey); B: first order kinetic plot*

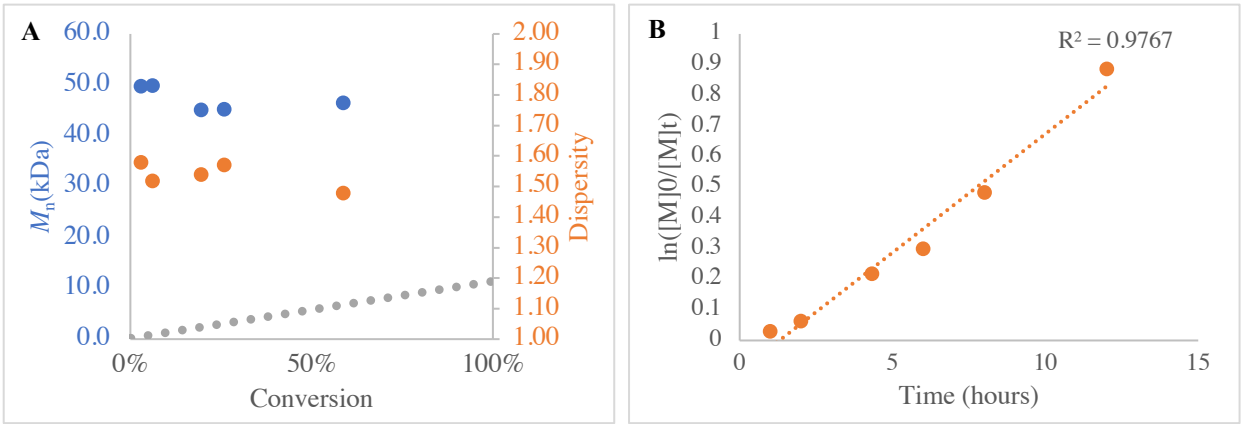

Figure S4.17: *Plots of polymerization data from run # SNB-4-78-B; A: plot of M_n (blue) and dispersity (orange) as a function of conversion, plotted against theoretical molecular weight (grey); B: first order kinetic plot*

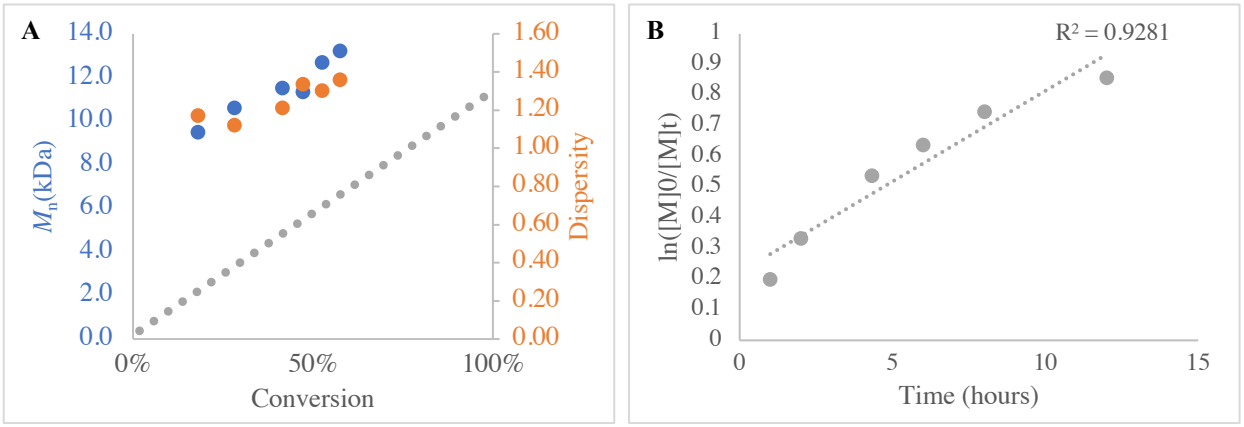

Figure S4.18: *Plots of polymerization data from run # SNB-4-78-C; A: plot of M_n (blue) and dispersity (orange) as a function of conversion, plotted against theoretical molecular weight (grey); B: first order kinetic plot*

Table S4.4: *Results of O-ATRP of MVL with Varied Feed Ratios*[a]

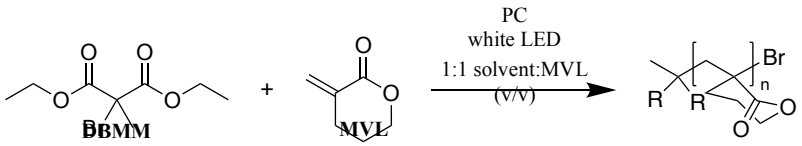

Reaction #	PC	Feed Ratio (MVL:DBMM:PC)	Time (hrs)	Conversion[b] (%)	M_w[c] (kDa)	M_n[c] (kDa)	$Đ$ (M_w/M_n)	I^* (%)[d]
SNB-4-80-A	1	1000:10:0.25	1	15				
			2	29	18.2	14.7	1.24	24
			4	48				
			6	61	19.3	15.5	1.25	45
			8	67	21.4	17.4	1.23	44
			12h7min	81	20.1	15.7	1.28	59
SNB-4-80-B	1	1000:10:0.5	1	11				
			2	26	22.2	17.8	1.25	17
			4	44	21.9	17.8	1.23	29
			6	56	22.6	18.6	1.22	35
			8	64	22.0	17.4	1.27	42
			12h7min	76	22.1	17.9	1.24	49
SNB-4-80-C	1	1000:1:0.1	1	5				
			2	9	61.2	40.7	1.50	25
			4	18	63.3	44.1	1.44	45
			6	27	66.7	41.5	1.61	72
			8	32	78.2	52.7	1.48	69
			12h7min	38	85.6	55.3	1.55	78

[a] Reaction scheme for the O-ATRP of MVL (top) catalyzed by PC 1 (Table S1). O-ATRP was performed with a varied ratio of MVL:diethyl 2-bromo-2-methylmalonate (DBMM):PC using a 1:1 ratio of dimethyl sulfoxide:MVL (v/v). A white-light LED beaker was used as the light source (see *O-ATRP General Procedure* for more details). [b] Conversion of monomer to polymer was determined by 1H NMR. [c] Values were measured using gel-permeation chromatography (GPC). [d] Initiator efficiency (I^*) was calculated using the equation $I^* = M_{n,theo}/M_n \times 100$ where $M_{n,theo}$ is the theoretical polymer molecular weight and M_n is the number-average polymer molecular weight measured using GPC.

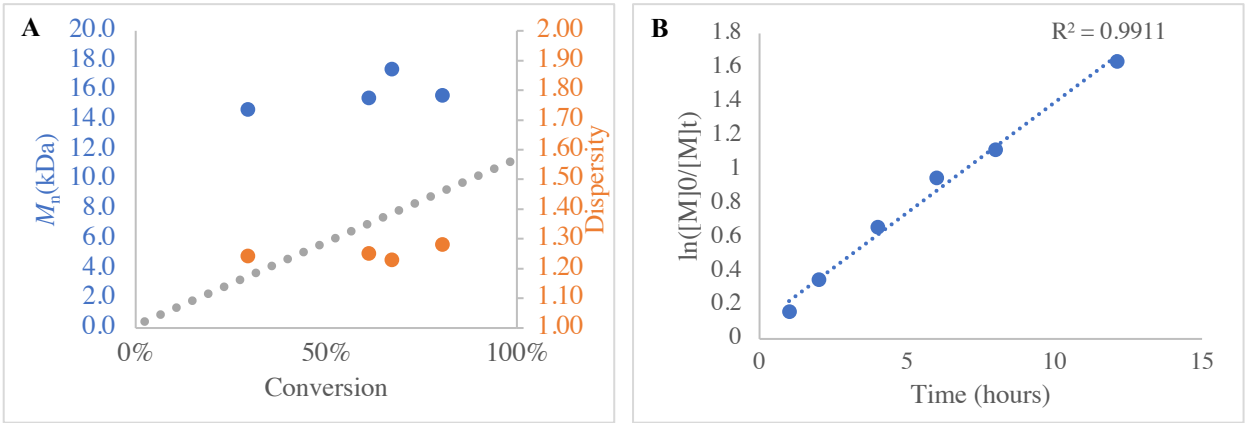

Figure S4.19: *Plots of polymerization data from run # SNB-4-80-A; A: plot of M_n (blue) and dispersity (orange) as a function of conversion, plotted against theoretical molecular weight (grey); B: first order kinetic plot*

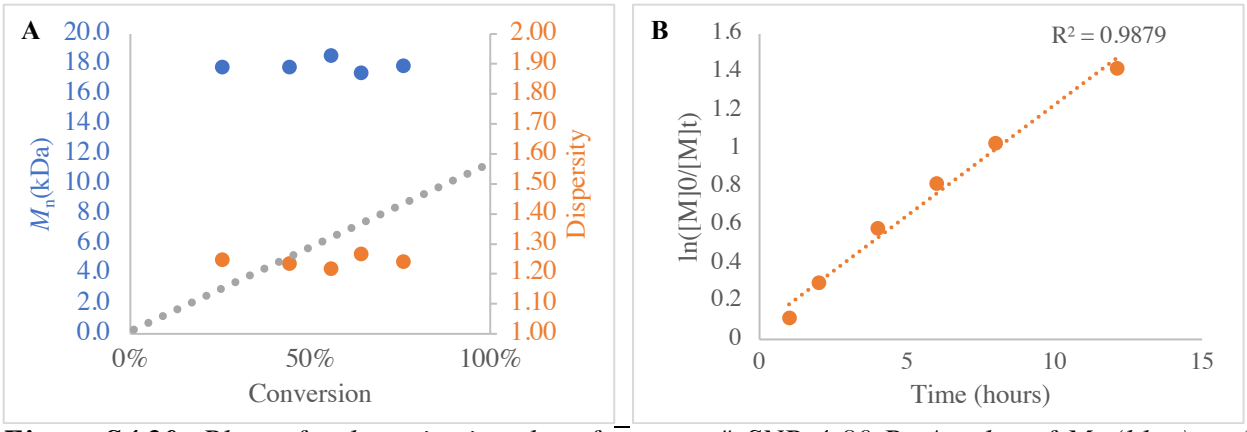

Figure S4.20: *Plots of polymerization data from run # SNB-4-80-B; A: plot of M_n (blue) and dispersity (orange) as a function of conversion, plotted against theoretical molecular weight (grey); B: first order kinetic plot*

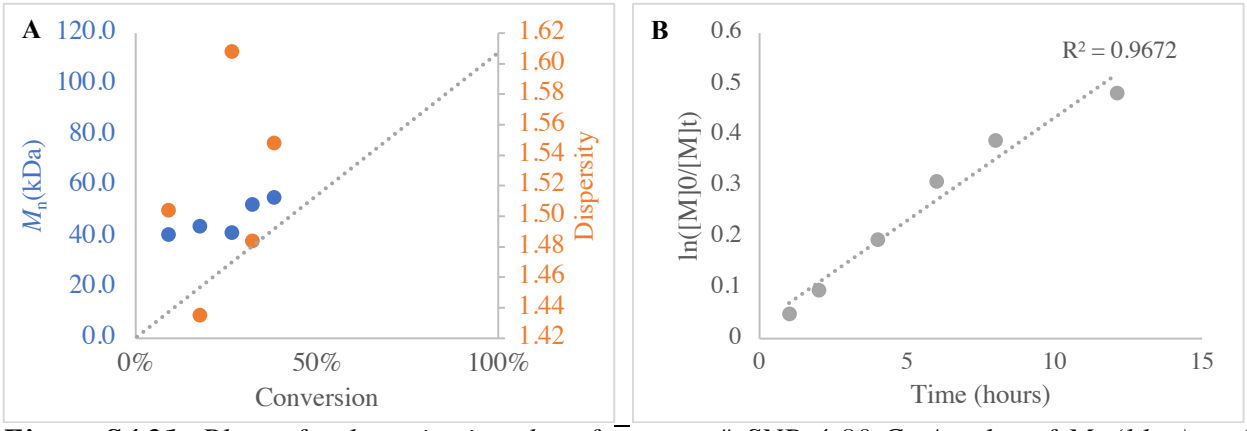

Figure S4.21: *Plots of polymerization data from run # SNB-4-80-C; A: plot of M_n (blue) and dispersity (orange) as a function of conversion, plotted against theoretical molecular weight (grey); B: first order kinetic plot*

Table S4.5: *Results of O-ATRP of MVL – controls*[a]

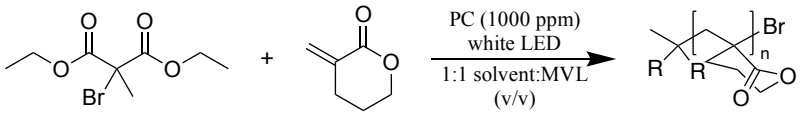

DBMM **MVL**

Reaction #	PC	Initiator	Time (hrs)	Conversion[b] (%)	M_w[c] (kDa)	M_n[c] (kDa)	$Đ$ (M_w/M_n)	I^* (%)[c]
SNB-4-74-F	none	DBMM	1	2	--	--	--	--
			2	1	--	--	--	--
			4	3	--	--	--	--
			6	3	--	--	--	--
			8	2	--	--	--	--
			12	3	--	--	--	--
SNB-4-78-D	1	none	1	0	--	--	--	--
			2	1	--	--	--	--
			4h20min	3	--	--	--	--
			6	4	--	--	--	--
			8	5	--	--	--	--
			12	7	--	--	--	--
SNB-4-80-D *no light*	1	DBMM	1	1	--	--	--	--
			2	0	--	--	--	--
			4h20min	0	--	--	--	--
			7	2	--	--	--	--
			12		--	--	--	--

[a] Reaction scheme for the O-ATRP of MVL (top) catalyzed by PC 1 (Table S1). O-ATRP was performed with a 1000:10:1 of MVL:diethyl 2-bromo-2-methylmalonate (DBMM):PC when applicable using a 1:1 ratio of N,N-diemthylacetamide:MVL (v/v). A white-light LED beaker was used as the light source when light was utilized (see *O-ATRP General Procedure* for more details). [b]Conversion of monomer to polymer was determined by 1H NMR. [c] Molecular weight analysis was not performed for these reactions due to insufficient quantity of polymer.

Table S4.6: *Results of FRP of MVL*[a]

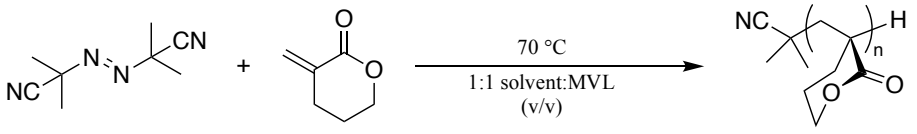

AIBN **MVL**

Reaction #	Solvent	Time (hrs)	Conversion[b] (%)	M_w[c] (kDa)	M_n[c] (kDa)	$Đ$ (M_w/M_n)	I^* (%)[d]
SNB-4-57-A	DMAc	5.5	58	53.2	52.9	1.01	13

[a] Reaction scheme for the FRP of MVL (top). FRP was performed with a 100:0.5 ratio of MVL: 2,2'-azobis(isobutyronitrile) (AIBN) using a 1:1 ratio of N,N-dimethylacetamide:MVL (v/v) (see *FRP General Procedure* for more details). [b] Conversion of monomer to polymer was determined by 1H NMR. [c] Values were measured using gel-permeation chromatography (GPC). [d] Initiator efficiency (I^*) was calculated using the equation $I^* = M_{n,theo}/M_n \times 100$ where $M_{n,theo}$ is the theoretical polymer molecular weight and M_n is the number-average polymer molecular weight measured using GPC.

Table S4.7: *Results of RAFT of MVL*[a]

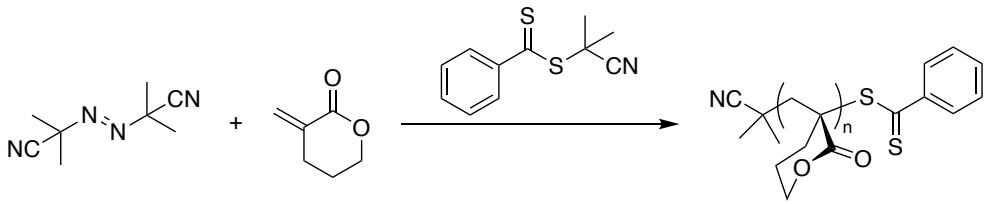

Reaction #	Solvent	Time (hrs)	Conversion[b] (%)	M_w[c] (kDa)	M_n[c] (kDa)	$Đ$ (M_w/M_n)	I^* (%)[d]
SNB-4-57-E	DMAc	6	70	11.8	10.9	1.08	73

[a] Reaction scheme for the RAFT of MVL (top). RAFT was performed with a 100:1:0.5 ratio of MVL : 2-cyanopropan-2-yl benzodithioate : 2,2'-azobis(isobutyronitrile) (AIBN) using a 1:1 ratio of N,N-dimethylacetamide:MVL (v/v) (see *RAFT General Procedure* for more details). [b] Conversion of monomer to polymer was determined by 1H NMR. [c] Values were measured using gel-permeation chromatography (GPC). [d] Initiator efficiency (I^*) was calculated using the equation $I^* = M_{n,theo}/M_n \times 100$ where $M_{n,theo}$ is the theoretical polymer molecular weight and M_n is the number-average polymer molecular weight measured using GPC.

O-ATRP of MBL

Table S4.8: *Results of O-ATRP of MBL with Varied PCs*[a]

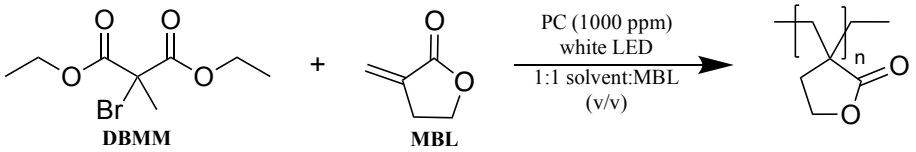

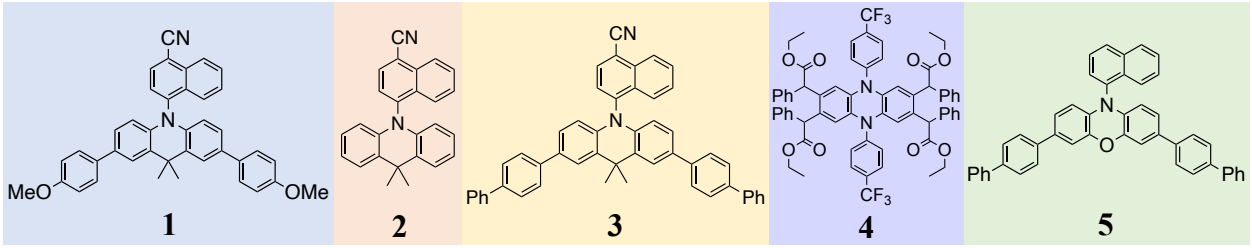

Reaction #	Catalyst	Time (hrs)	Conversion[b] (%)	M_w[c] (kDa)	M_n[c] (kDa)	$Đ$ (M_w/M_n)	I^* (%)[d]
SNB-4-73-A	1	0.25	13	11.8	6.50	1.81	23
		0.5	30	13.2	6.35	2.07	50
		1	52	14.4	7.85	1.84	68
		1.5	70	15.8	9.00	1.75	79
		2	86	16.1	9.28	1.74	94
		3	97	16.3	10.3	1.59	95
SNB-4-73-B	2	0.25	45	22.1	15.0	1.47	31
		0.5	76	21.8	11.3	1.92	68
		1	93	21.2	10.9	1.95	86
		1.5	97	21.7	12.3	1.76	79
		2	98	23.9	17.7	1.35	56
		3	100	21.4	12.4	1.72	81
SNB-4-73-C	3	0.25	32	13.6	8.10	1.68	41
		0.5	53	15.8	7.73	2.04	71
		1	86	17.1	9.54	1.80	91
		1.5	95	17.4	10.3	1.68	93
		2	97	17.1	9.94	1.72	98
		3	100	17.9	12.0	1.49	83
SNB-4-73-D	4	0.25	20	65.6	37.8	1.74	6
		0.5	34	63.6	37.5	1.70	9
		1	69	58.6	34.6	1.69	20
		1.5	86	54.2	33.8	1.60	26
		2	97	49.8	28.1	1.77	35
		3	98	51.0	22.8	2.24	43
SNB-4-73-E	5	0.25	21	9.55	5.15	1.86	45
		0.5	33	12.2	6.11	1.99	58
		1	51	15.2	7.46	2.03	71
		1.5	71	14.5	8.23	1.76	88
		2	89	14.8	9.12	1.63	99
		3	99	*needs redo			

[a] Reaction scheme for the O-ATRP of MBL (top) catalyzed by PC 1, 2, 3, 4, or 5 (middle). O-ATRP was performed with a [1000]:[10]:[1] ratio of MBL:diethyl 2-bromo-2-methylmalonate (DBMM):PC using a 1:1 ratio of N,N-diemthylacetamide:MBL (v/v). A white-light LED beaker was used as the light source (see *O-ATRP General Procedure* for more details). [b] Conversion of monomer to polymer was determined by 1H NMR. [c] Values were measured using gel-permeation chromatography (GPC). [d] Initiator efficiency (I^*) was calculated using the equation $I^* = M_{n,theo}/M_n \times 100$ where $M_{n,theo}$ is the theoretical polymer molecular weight and M_n is the number-average polymer molecular weight measured using GPC.

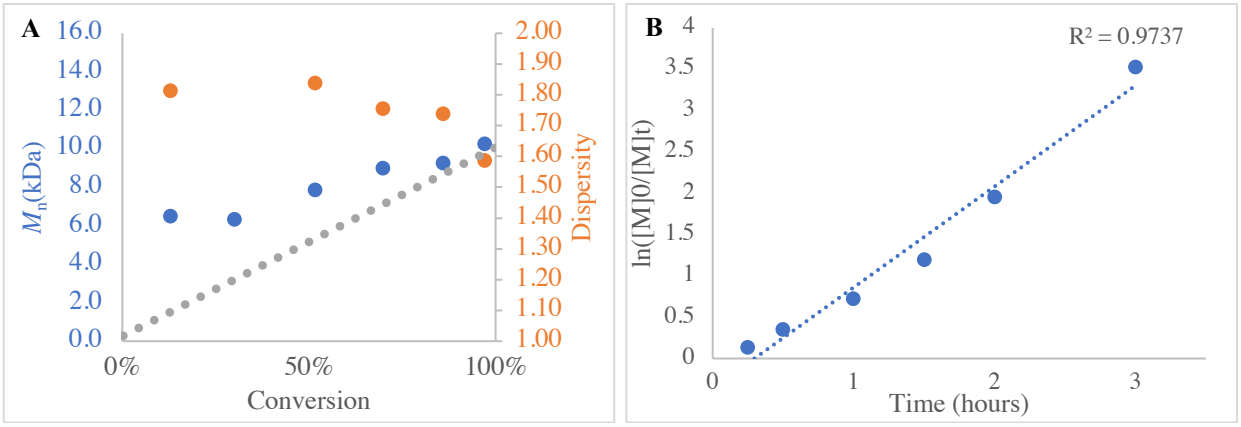

Figure S4.22: *Plots of polymerization data from run # SNB-4-73-A; A: plot of M_n (blue) and dispersity (orange) as a function of conversion, plotted against theoretical molecular weight (grey); B: first order kinetic plot*

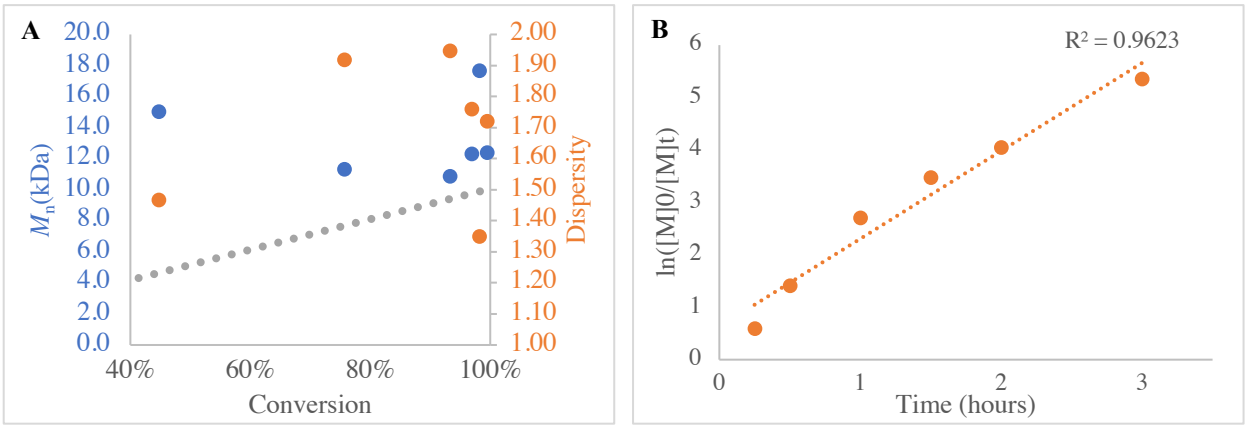

Figure S4.23: *Plots of polymerization data from run # SNB-4-73-B; A: plot of M_n (blue) and dispersity (orange) as a function of conversion, plotted against theoretical molecular weight (grey); B: first order kinetic plot*

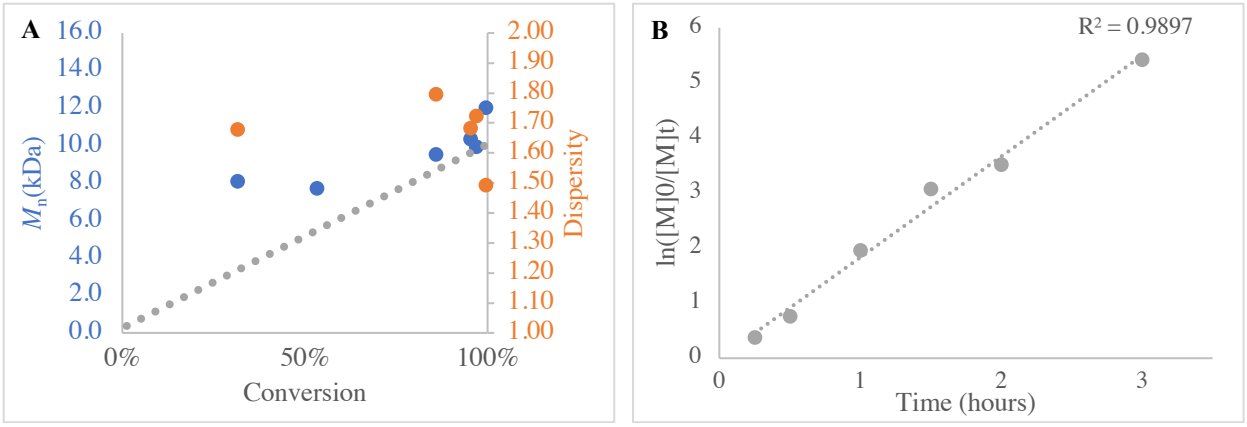

Figure S4.24: *Plots of polymerization data from run # SNB-4-73-C; A: plot of M_n (blue) and dispersity (orange) as a function of conversion, plotted against theoretical molecular weight (grey); B: first order kinetic plot*

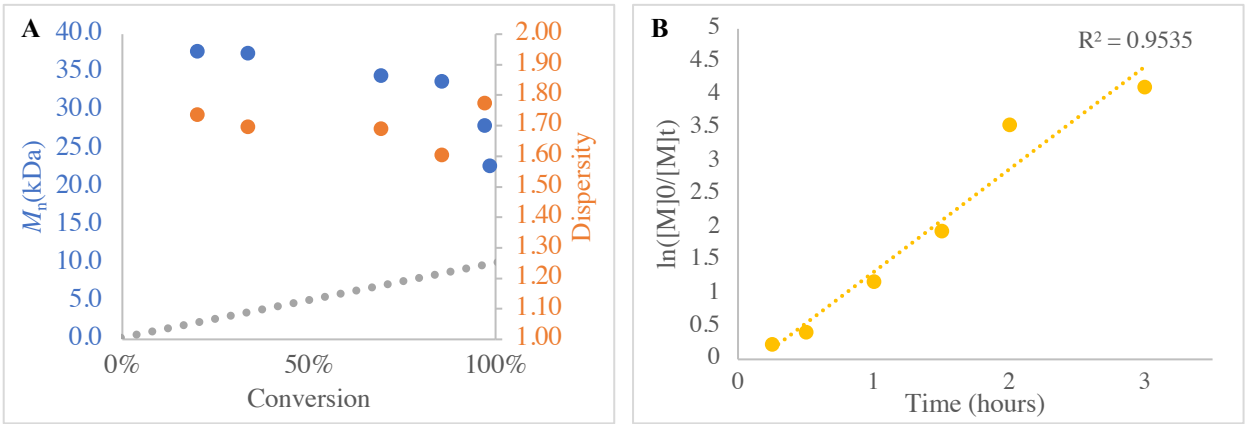

Figure S4.25: *Plots of polymerization data from run # SNB-4-73-D; A: plot of M_n (blue) and dispersity (orange) as a function of conversion, plotted against theoretical molecular weight (grey); B: first order kinetic plot*

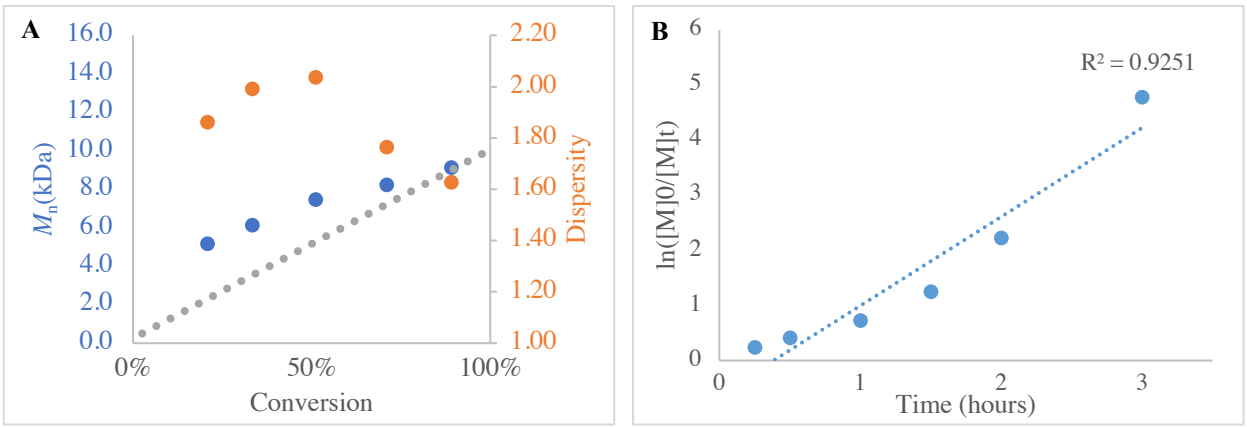

Figure S4.26: *Plots of polymerization data from run # SNB-4-73-E; A: plot of M_n (blue) and dispersity (orange) as a function of conversion, plotted against theoretical molecular weight (grey); B: first order kinetic plot*

Table S4.9: *Results of O-ATRP of MBL with Varied Solvents*[a]

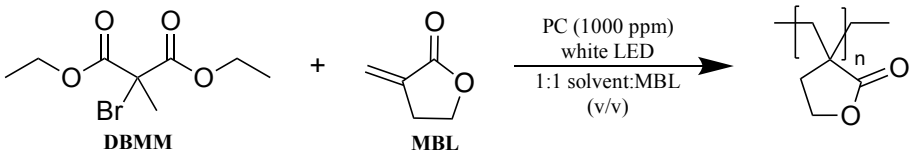

Reaction #	PC	Solvent	Time (hrs)	Conversion[b] (%)	M_w[c] (kDa)	M_n[c] (kDa)	$Đ$ (M_w/M_n)	I^* (%)[d]
SNB-4-75-A	1	DMSO	0.25	14	7.87	3.02	2.60	53
			0.5	23	11.2	6.51	1.72	39
			1	39	19.6	9.32	2.10	43
			1.5	55	12.8	8.38	1.52	67
			2	64	13.2	8.73	1.51	75
			3	92				
SNB-4-75-B	1	DMF	0.25	28	31.5	18.9	1.66	16
			0.5	57	32.2	19.8	1.63	30
			1	87	27.7	15.5	1.79	57
			1.5	93	28.0	14.3	1.95	66
			2	95	29.5	15.0	1.97	64
			3	96				

[a] Reaction scheme for the O-ATRP of MBL (top) catalyzed by PC 1 (Table S6). O-ATRP was performed with a [1000]:[10]:[1] ratio of MBL:diethyl 2-bromo-2-methylmalonate (DBMM):PC using a 1:1 ratio of solvent:MBL (v/v). A white-light LED beaker was used as the light source (see *O-ATRP General Procedure* for more details). [b] Conversion of monomer to polymer was determined by 1H NMR. [c] Values were measured using gel-permeation chromatography (GPC). [d] Initiator efficiency (I^*) was calculated using the equation $I^* = M_{n,theo}/M_n \times 100$ where $M_{n,theo}$ is the theoretical polymer molecular weight and M_n is the number-average polymer molecular weight measured using GPC.

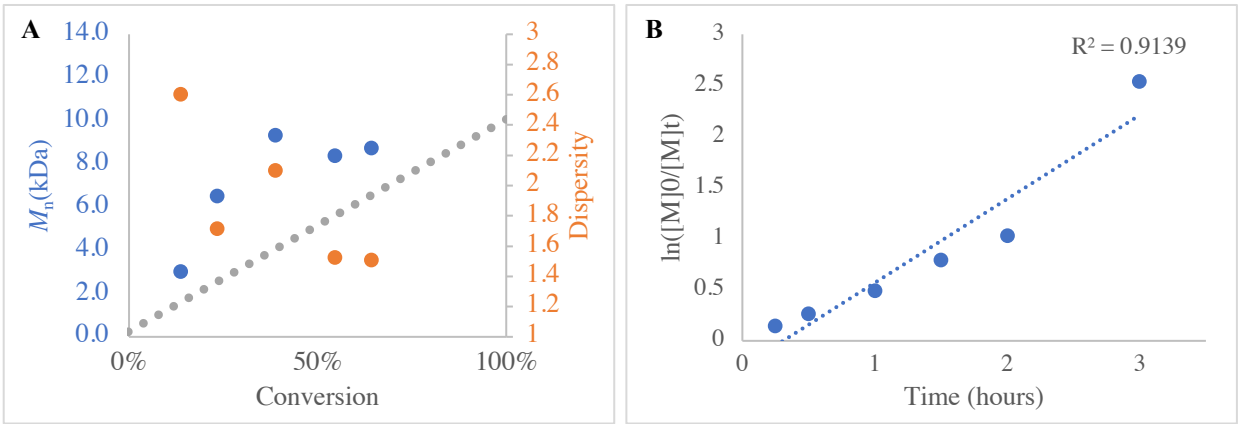

Figure S4.27: *Plots of polymerization data from run # SNB-4-75-A; A: plot of M_n (blue) and dispersity (orange) as a function of conversion, plotted against theoretical molecular weight (grey); B: first order kinetic plot*

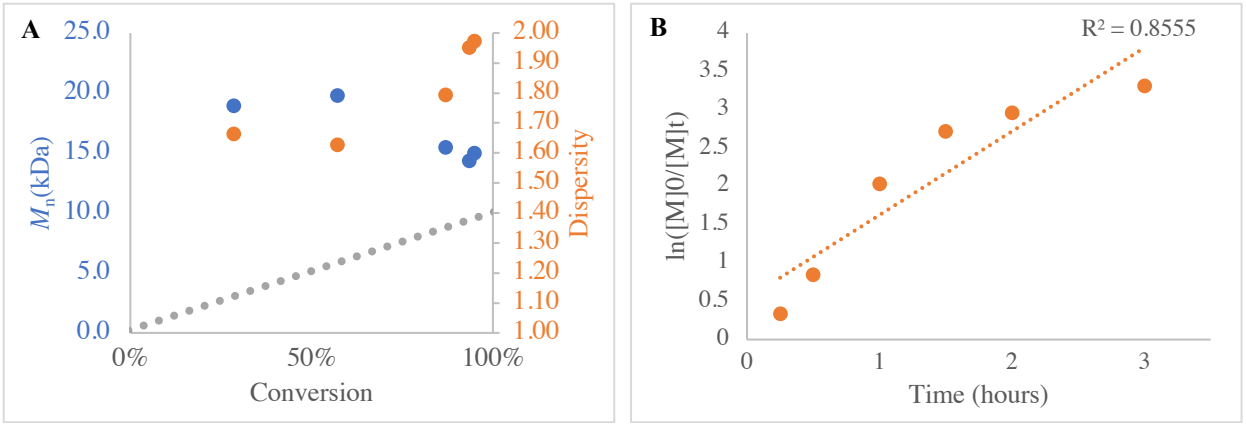

Figure S4.28: *Plots of polymerization data from run # SNB-4-75-B; A: plot of M_n (blue) and dispersity (orange) as a function of conversion, plotted against theoretical molecular weight (grey); B: first order kinetic plot*

Table S10: *Results of O-ATRP of MBL with Varied Initiators*[a]

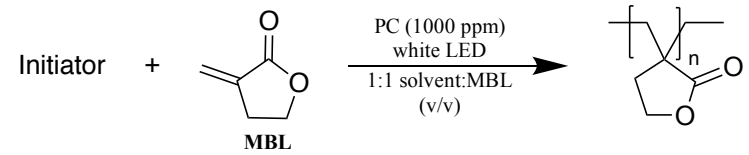

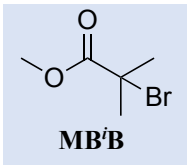

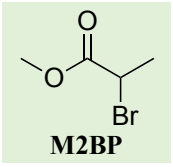

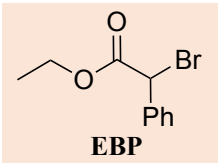

Reaction #	PC	Initiator	Time (hrs)	Conversion[b] (%)	M_w[c] (kDa)	M_n[c] (kDa)	$Đ$ (M_w/M_n)	I^* (%)[d]
SNB-4-77-A	1	MBiB	0.25	2	21.6	15.6	1.39	3
			0.5	3	24.1	15.3	1.58	4
			1	error	27.7	17.0	1.62	
			1.5	6	31.2	17.7	1.76	5
			2	8	37.3	20.6	1.81	5
			3h10min	12	69.6	43.8	1.59	3
SNB-4-77-B	1	M2BP	0.25	3	18.5	12.8	1.45	5
			0.5	3	21.0	12.4	1.69	4
			1.5	7	25.7	16.0	1.60	6
			2	6	26.1	15.0	1.74	6
			3h10min	6	23.1	12.4	1.86	7
SNB-4-77-C	1	EBP	0.25	13	27.0	15.2	1.78	10
			0.5	28	34.8	23.0	1.52	13
			1	55	29.1	17.9	1.62	32
			1.5	67	30.8	19.0	1.62	36
			2	84	27.6	17.4	1.59	49
			3h10min	92	29.9	17.6	1.70	53

[a] Reaction scheme for the O-ATRP of MBL (top) catalyzed by PC 1 (Table S1) with varied initiators (middle). O-ATRP was performed with a [1000]:[10]:[1] ratio of MBL:initiator:PC using a 1:1 ratio of dimethyl sulfoxide:MBL (v/v). A white-light LED beaker was used as the light source (see *O-ATRP General Procedure* for more details). [b] Conversion of monomer to polymer was determined by 1H NMR. [c] Values were measured using gel-permeation chromatography (GPC). [d] Initiator efficiency (I^*) was calculated using the equation $I^* = M_{n,theo}/M_n \times 100$ where $M_{n,theo}$ is the theoretical polymer molecular weight and M_n is the number-average polymer molecular weight measured using GPC.

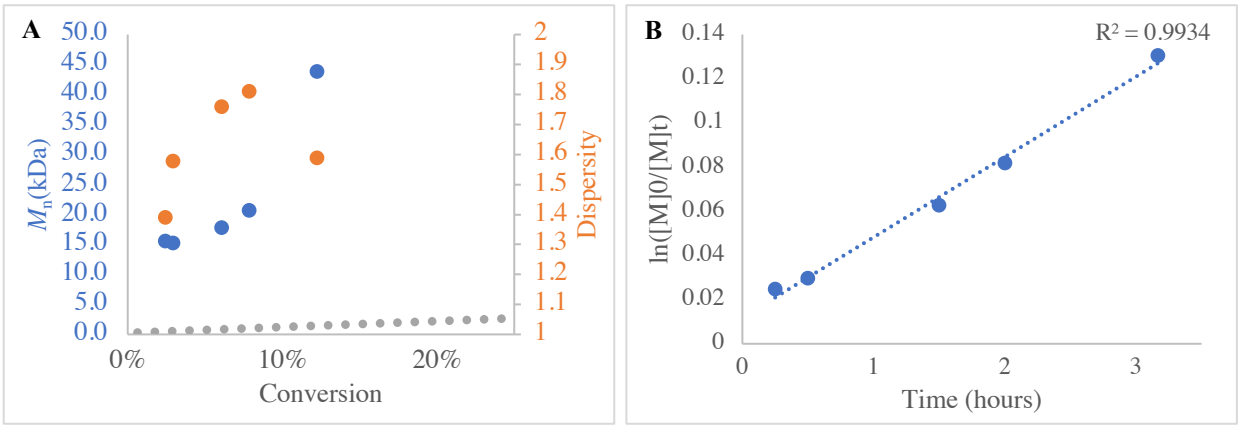

Figure S4.29: *Plots of polymerization data from run # SNB-4-77-A; A: plot of M_n (blue) and dispersity (orange) as a function of conversion, plotted against theoretical molecular weight (grey); B: first order kinetic plot*

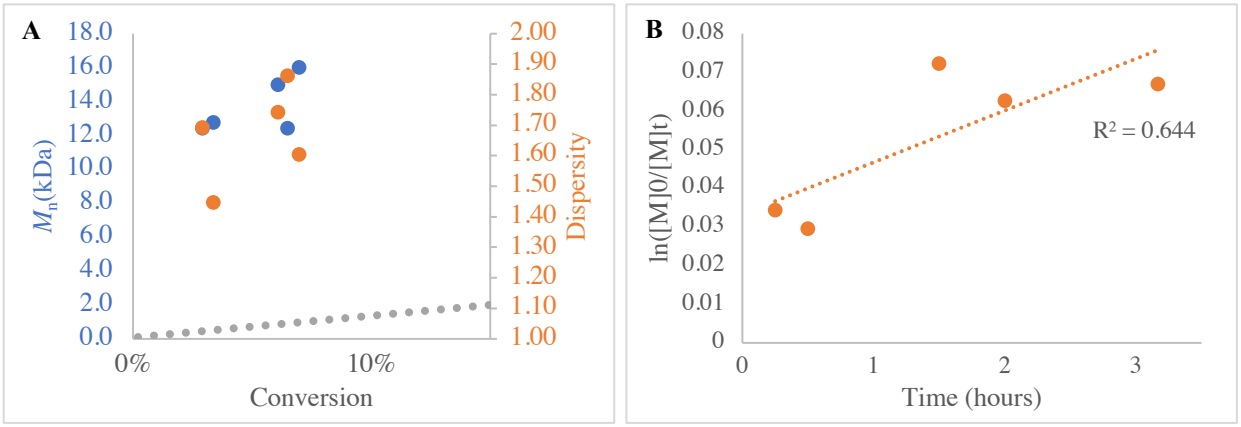

Figure S4.30: *Plots of polymerization data from run # SNB-4-77-B; A: plot of M_n (blue) and dispersity (orange) as a function of conversion, plotted against theoretical molecular weight (grey); B: first order kinetic plot*

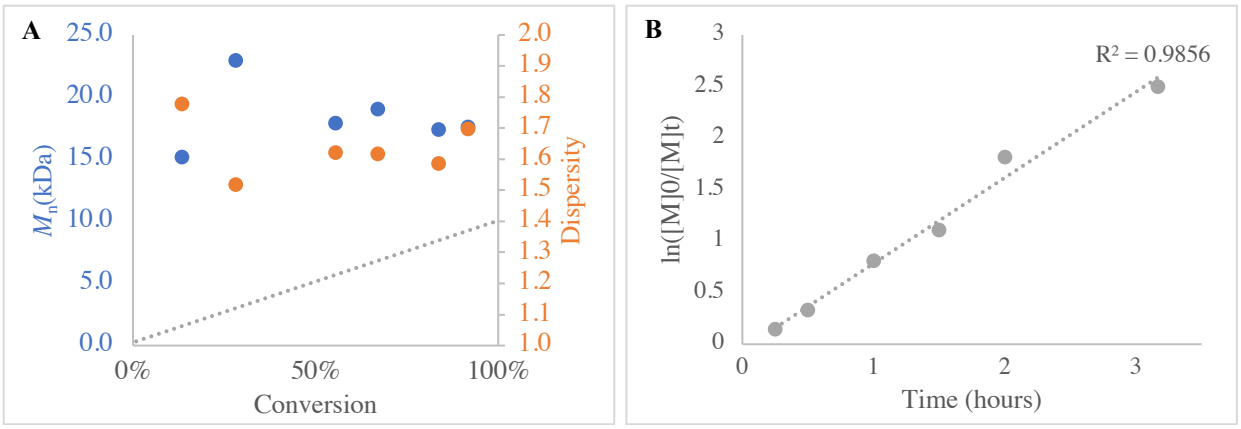

Figure S4.31: *Plots of polymerization data from run # SNB-4-77-C; A: plot of M_n (blue) and dispersity (orange) as a function of conversion, plotted against theoretical molecular weight (grey); B: first order kinetic plot*

Table S4.11: *Results of O-ATRP of MBL with Varied Feed Ratios*[a]

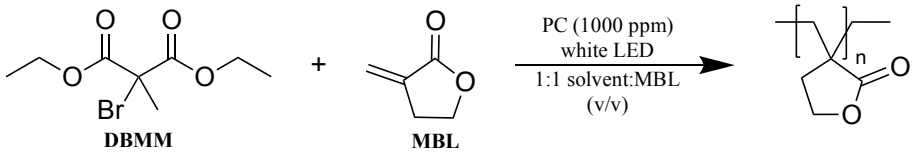

Reaction #	PC	Feed Ratio (MBL:DBMM:PC)	Time (hrs)	Conversion[b] (%)	M_w[c] (kDa)	M_n[c] (kDa)	$Đ$ (M_w/M_n)	I^* (%)[d]
SNB-4-82-A	1	1000:10:0.25	0.25	23	193.1	42.3	4.57	6
			0.5	45	128.0	49.0	2.61	9
			1	79	609.3	39.1	1.56	21
			1.5	97	56.4	32.6	1.73	30
			2	99	52.5	30.2	1.74	33
			3	99	58.7	36.2	1.62	27
SNB-4-82-B	1	1000:10:0.5	0.25	18	105.6	32.8	3.22	6
			0.5	42	74.2	30.9	2.40	14
			1	75	42.2	26.5	1.59	29
			1.5	93	41.2	23.8	1.73	39
			2	96	39.5	23.3	1.70	41
			3	97	40.7	24.6	1.65	40
SNB-4-82-C	1	1000:1:0.1	0.25	5	13.9	9.98	1.39	54
			0.5	5	24.0	11.6	2.07	46
			1	10	72.9	39.5	1.84	26
			1.5	14	95.2	53.0	1.80	26
			2	20	103	61.1	1.69	32
			3	30	139	100	1.39	30

[a] Reaction scheme for the O-ATRP of MBL (top) catalyzed by PC 1 (Table S1) with varied initiators (middle). O-ATRP was performed with a [1000]:[10]:[1] ratio of MBL:initiator:PC using a 1:1 ratio of dimethyl sulfoxide:MBL (v/v). A white-light LED beaker was used as the light source (see *O-ATRP General Procedure* for more details). [b] Conversion of monomer to polymer was determined by 1H NMR. [c] Values were measured using gel-permeation chromatography (GPC). [d] Initiator efficiency (I^*) was calculated using the equation $I^* = M_{n,theo}/M_n \times 100$ where $M_{n,theo}$

is the theoretical polymer molecular weight and M_n is the number-average polymer molecular weight measured using GPC.

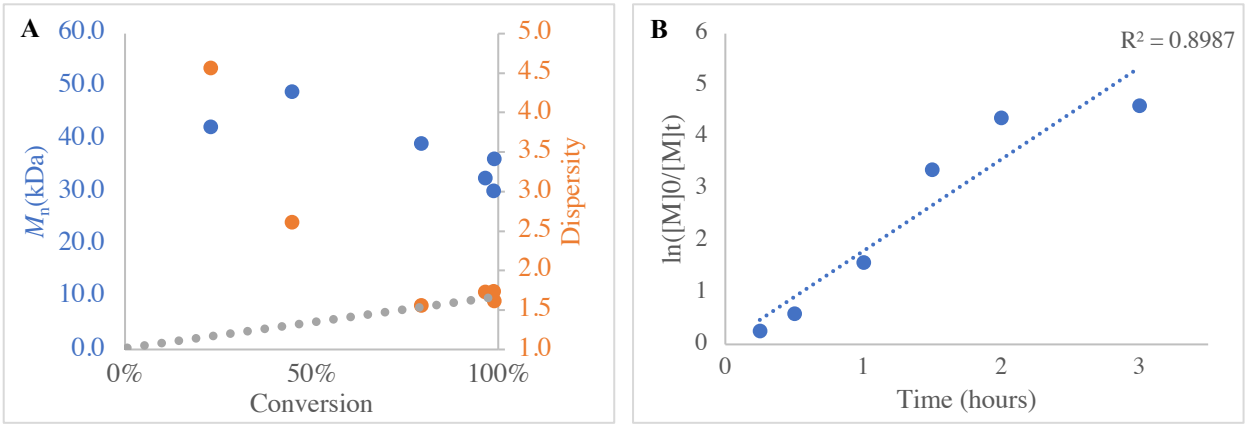

Figure S4.32: *Plots of polymerization data from run # SNB-4-82-A; A: plot of M_n (blue) and dispersity (orange) as a function of conversion, plotted against theoretical molecular weight (grey); B: first order kinetic plot*

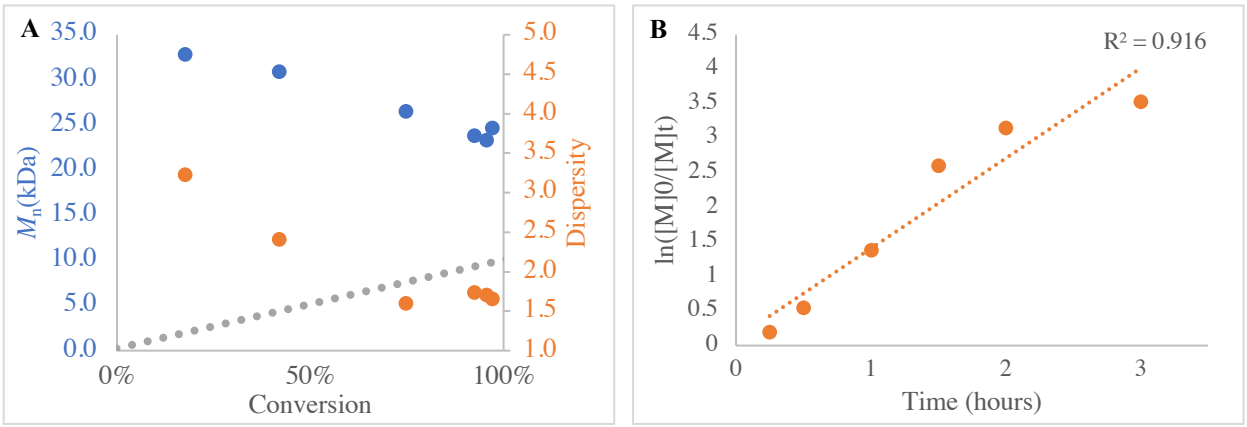

Figure S4.33: *Plots of polymerization data from run # SNB-4-82-B; A: plot of M_n (blue) and dispersity (orange) as a function of conversion, plotted against theoretical molecular weight (grey); B: first order kinetic plot*

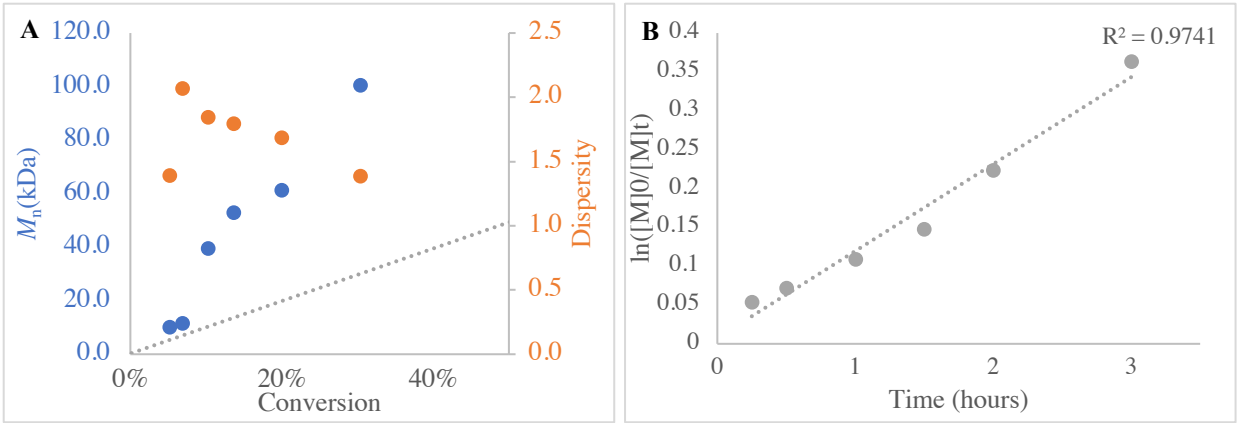

Figure S4.34: *Plots of polymerization data from run # SNB-4-82-C; A: plot of M_n (blue) and dispersity (orange) as a function of conversion, plotted against theoretical molecular weight (grey); B: first order kinetic plot*

Table S4.12: *Results of O-ATRP of MBL – Controls*[a]

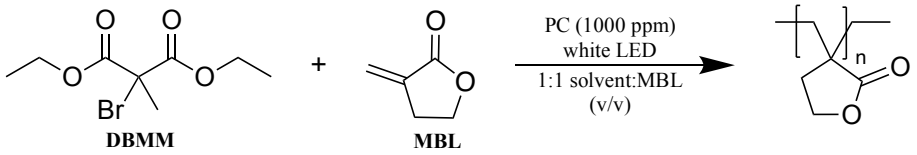

Reaction #	PC	Initiator	Time (hrs)	Conversion[b] (%)	M_w[c] (kDa)	M_n[c] (kDa)	$Đ$ (M_w/M_n)	I* (%)[d]
SNB-4-73-F	None	DBMM	0.25	2	--	--	--	--
			0.5	3	--	--	--	--
			1	2	--	--	--	--
			1.5	1	--	--	--	--
			2	2	--	--	--	--
			3h10min	2	--	--	--	--
SNB-4-77-D	1	None	0.25	2	--	--	--	--
			1	4	--	--	--	--
			1.5	6	--	--	--	--
			2	5	--	--	--	--
			3h40min	4	--	--	--	--
SNB-4-82-D *no light*	1	DBMM	0.25	6	--	--	--	--
			0.5	5	--	--	--	--
			1	5	--	--	--	--
			1.5	4	--	--	--	--
			2	4	--	--	--	--
			3	4	--	--	--	--

[a] Reaction scheme for the O-ATRP of MBL (top) catalyzed by PC 1 (Table S1). O-ATRP was performed with a 1000:10:1 of MBL:diethyl 2-bromo-2-methylmalonate (DBMM):PC when applicable using a 1:1 ratio of N,N-diemthylacetamide:MBL (v/v). A white-light LED beaker was used as the light source when light was utilized (see *O-ATRP General Procedure* for more details). [b]Conversion of monomer to polymer was determined by 1H NMR. [c] Molecular weight analysis was not performed for these reactions due to insufficient quantity of polymer.

Table S4.13: *Results of MBL/MVL Copolymerization via O-ATRP*[a]

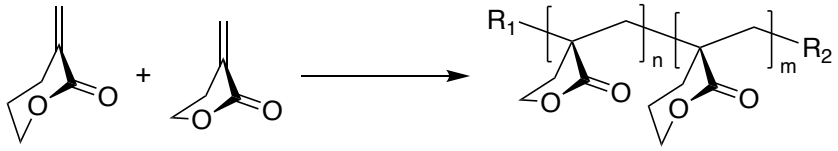

Reaction #	PC	Addition Order	Time (hrs)	Conversion[b] (%)	MBL/MVL Ratio[c]	M_w[d] (kDa)	M_n[d] (kDa)	$Đ$ (M_w/M_n)
			0.25	6	1.00	4.59	2.27	2.02
			0.5	54	1.01	5.74	4.68	1.23
			1	56	1.03	6.05	5.01	1.21
			2	61	1.09	6.79	5.60	1.21
SNB-4-81-A	1	Simultaneous	4	70	1.23	8.77	7.24	1.21
			6	79	1.47	11.3	9.68	1.17
			8	89	1.93	14.5	11.3	1.29
			12	97	4.99	17.2	10.7	1.61
			24	100	100% MBL	19.6	13.9	1.41
SNB-4-81-B	1	MBL then MVL	48	99	0.03			
SNB-4-81-C	1	MVL then MBL	48	84	4.38			

[a] Reaction scheme for the co-O-ATRP of MBL and MVL (top) catalyzed by PC 1 (Table S1). O-ATRP was performed with a 500:500:10:1 ratio of MVL:MBL:diethyl 2-bromo-2-methylmalonate (DBMM):PC using a 2:1 ratio of N,N-diemthylacetamide:MBL (v/v). A white-light LED beaker was used as the light source when light was utilized (see *Procedure for Simultaneous Addition Copolymerization by O-ATRP* and *Procedure for Sequential Addition Copolymerization by O-ATRP* for more details). [b] Conversion reported as an average of both monomers, determined by ^{1}H NMR. [c] MBL/MVL ratios determined by ^{1}H NMR. [d] Values were measured using gel-permeation chromatography (GPC).

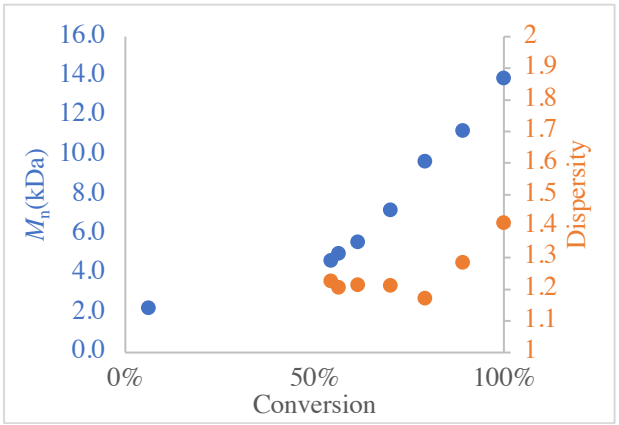

Figure S4.35: *Plot of polymerization data from run # SNB-4-81-A including M_n (blue) and dispersity (orange) as a function of average conversion of the two monomers*

REFERENCES

1. D. A. Corbin, K. O. Puffer, K. A. Chism, J. P. Cole, J. C. Theriot, B. G. McCarthy, B. L. Buss, C.-H. Lim, S. R. Lincoln, B. S. Newell, G. M. Miyake, *Macromol*. **2021**, *54*, 4507–4516.
2. B. G. McCarthy, R. M. Pearson, C.-H. Lim, S. M. Sartor, N. H. Damrauer, G. M. Miyake, *J. Am. Chem. Soc*. **2018**, *140*, 5088–5101.